



UNIVERSITÀ DEGLI STUDI
DI MILANO

UNIVERSITA' DEGLI STUDI DI MILANO
PHD in TRANSLATIONAL MEDICINE

CYCLE XXXIV

DOCTORAL THESIS

BIO/13

Activation of defective WNT pathway in Cornelia de
Lange Syndrome in *in vitro* models

PhD Student: Chiara PARODI

Matricola N° R12169

Tutor: Prof.ssa Valentina MASSA

PhD Coordinator: Prof.ssa Chiarella SFORZA

A.A. 2020/2021

"Mastering others is strength, mastering yourself is true power"

TABLE OF CONTENTS

ABSTRACT	2
LIST OF ABBREVIATIONS.....	3
RESEARCH INTEGRITY STATEMENT	4
1. INTRODUCTION.....	5
1.1 HISTORICAL NOTES.....	5
1.2 EPIDEMIOLOGY	5
1.3 CLINICAL FEATURES OF CDLS	6
1.4 PRENATAL ASPECTS	11
1.5 FACIAL FEATURES	14
1.6 CLINICAL ASPECTS.....	15
1.7 GENETICS OF CDLS.....	20
1.8 CDLS CAUSATIVE GENES.....	24
1.9 COHESIN COMPLEX	30
1.10 WNT PATHWAY.....	35
2. AIM	41
3 MATERIALS AND METHODS	43
3.1 LYMPHOBLASTOID IMMORTALIZED CELL LINES	43
3.2 FUCCI2 MURINE PRIMARY CULTURES	46
3.3 DATA ANALYSIS AND STATISTICS	48
3.4 SALIVA MOLECULAR TESTING FOR SARS-COV-2 INFECTION	50
4. RESULTS	53
4.1 LITHIUM RESTORES PROLIFERATION RATE IN CDLS LYMPHOBLASTOID CELL LINES.....	53
4.2 WNT ACTIVATORS RESTORES PROLIFERATION IN CDLS LINES	57
4.3 LITHIUM RESTORES NEURONAL RATE DIFFERENTIATION IN FUCCI2 PRIMARY CULTURES...	60
4.4 CLINICAL TRIAL DESIGN	63
4.5 PROTOCOL TO DETECT SARS-COV-2 INFECTION	69
5. DISCUSSION.....	71
6. CONCLUSIONS	78
7. REFERENCES.....	79
APPENDIX 1. List of Publications.....	107
ACKNOWLEDGMENTS.....	

Abstract

Background: Cornelia de Lange Syndrome (CdLS) is a rare genetic disease caused by *de novo* mutations in cohesin genes. CdLS phenotypic features vary from mild to severe and is characterized by an array of congenital malformations, neurodevelopmental delay, and autism-spectrum disorder. Current hypothesis is that CdLS clinical signs arise from deregulation of developmental molecular pathways, and we have previously shown that canonical WNT pathway is perturbed. In this study, our goal was assessing possible ameliorative effects of canonical WNT pathway chemical activation in Lymphoblastoid cell lines (LCLs) from CdLS patients and *ex vivo* FUCCI2 murine neurons.

Methods: LCLs from CdLS patients (6) and from healthy donors (4) were exposed to different concentrations of WNT pathway activators: lithium chloride (LiCl), BIO, IQ-1, DCA, CHIR99021 or vehicle for 24h. Proliferation/death rate were measured using Tripan blue staining, TUNEL and Ki67 assays. *CyclinD1* gene expression was analysed by qPCR. Primary cultures of murine neurons from day2 pups (FUCCI2) harvested from cerebellum were cultured and treated with PCI34051 (HDAC8 inhibitor) and LiCl for 13 days. Immunostaining for Tuj1 was performed.

Results: Upon WNT activation, proliferation rate is restored and *CyclinD1* gene expression increased, rescuing physiological levels. Immunostaining for Tuj1 on FUCCI2 primary cultures, markers of neurons, demonstrated that LiCl treatment increases the rate of neuronal differentiation.

Conclusions and Perspectives: I confirmed the impairment of WNT canonical pathway in CdLS models and described that WNT activators such as lithium are capable of rescuing adverse phenotype. Due to SARS-CoV-2 pandemic, clinical trial for lithium in CdLS patients is still under development. During this period, I was part of the team that worked for optimization of a new device for saliva collection and molecular testing to detect SARS-CoV-2 RNA – an exceptional tool for fragile patients such as CdLS. When enrolment begins, I plan to use the new device for COVID-19 surveillance in CdLS patients enrolled in the trial.

List of Abbreviations

ABC – Aberrant Behavior Checklist
ANKRD11 – Ankyrin Repeat Domain 11
ASD – Autism Spectrum Disorder
BdLS – Brachmann-de Lange syndrome
BRD4 – Bromodomain Containing 4
CdLS – Cornelia de Lange Syndrome
CNS – Central Nervous System
CRF – Case Report Form
CTCF – CCCTC-binding Factor
DCA – Deoxycholic Acid
DPBS – Dulbecco's Phosphate-Buffered Saline
FUCCI2 – Fluorescence Ubiquitin Cell Cycle Indicator
GAPDH – Glyceraldehyde 3-Phosphate Dehydrogenase
GFP – Green Fluorescent Protein
GSK3 β – Glycogen Synthase Kinase 3 β
HBSS – Hanks' Balanced Salt Solution
HDAC8 – Histone Deacetylase 8
ID – Intellectual disability
LCL – Lymphoblastoid cell lines
LRP5/6 – Low-density-lipoprotein-Related Protein 5/6
MB – Mushroom Bodies
MTD – Maximum Tolerated Dose
NGS – Next Generation Sequencing
NIPBL – Nipped-B Like Protein
NMR – Nuclear Magnetic Resonance
PEI – polyethyleneimine
PBS – Phosphate-Buffered Saline
PBT – Phosphate-Buffered Saline + Triton X-100
PFA – Paraformaldehyde
RAD21 - RAD21 Cohesin Complex Component
SDT – Start Drug Treatment
SMC1A – Structural Maintenance of Chromosomes 1A
SMC3 – Structural Maintenance of Chromosomes 3
TBARS - thiobarbituric acid reactive substance assay
WES – Whole Exome Sequencing
WNT – Wingless-related integration site

Research Integrity Statement

This PhD project contains data that were produced and analysed according to the principles of “The European Code of Conduct for Research Integrity” (ALLEA - All European Academies, Berlin 2018):

RELIABILITY in ensuring the quality of research, reflected in the design, the methodology, the analysis and the use of resources.

HONESTY in developing, undertaking, reviewing, reporting and communicating research in a transparent, fair, full and unbiased way.

RESPECT for colleagues, research participants, society, ecosystems, cultural heritage and the environment.

ACCOUNTABILITY for the research from idea to publication, for its management and organisation, for training, supervision and mentoring, and for its wider impacts.

This PhD project respects the open access key: research results have been and will be presented to conferences to establish an open dialogue with other researchers.

1. Introduction

1.1 HISTORICAL NOTES

Cornelia De Lange Syndrome (CdLS) [OMIM #122470, #300590, #610759, #614701, #300882] is a rare genetic disorder well-characterized at physical, auxological, cognitive and behavioural level, affecting almost any organ, including the Central Nervous System (CNS). CdLS is a genetically heterogeneous disorder mainly caused by dominant autosomal or X-linked *de novo* mutations (Kline et al., 2018). The syndrome takes its name from Cornelia de Lange (1871-1950), the Dutch paediatrician who first described the clinical presentation of two girls from Amsterdam in 1933. Clinical manifestations shared by the two patients were growth failure with proportional microcephaly, feeding difficulties and distinctive facial features, overall defined as "*Typus Degenerativus Amstelodamensis*" (De Lange, 1933). Following studies described the clinical differences among patients highlighting the wide spectrum of the phenotype presentation (Brachmann, 1916; Eekelen and Hennekam, 1994; JM, 1994).

1.2 EPIDEMIOLOGY

The real incidence of this syndrome is difficult to estimate both due to a high number of misdiagnoses and a fair number of inappropriate diagnoses (Beck, 1976).

In 1967, with the first epidemiological data Pearce defined the prevalence of CdLS as 1:100,000 (Pearce and Pitt, 1967). Years later, the incidence of CdLS was still estimated to be 1:100,000 new-borns (Beck, 1976; Beck and Fenger, 1985) then corrected to 1:10,000-30,000 (Kline et al., 2007) probably due to an underestimation of milder cases (Barisic et al., 2008). Indeed, diagnosis of CdLS might be arduous because of the mild presentation of several patients and the discordance cases between molecular diagnosis and clinical evaluation.

Others provided to assess the incidence of this syndrome: an important contribution was offered by Beck and Fenger who estimated the incidence of CdLS around one per 50,000 new-borns (Beck and Fenger, 1985). In the same year, in an "Editorial Comment" published in "American journal of Medical Genetics", Opitz proposed an incidence of 1: 10,000 (Opitz, 1985). A more recent study (Allanson et al., 1997), in which the characteristics of patients with a classical phenotype were compared to those with a mild one, suggested an incidence of about 1: 40,000. In the same year, Ireland and colleagues argued that cases with a milder phenotype represented about 20-30% of all affected subjects, thus assuming a higher incidence of the condition (Allanson et al., 1997). On the contrary, in 2008 a prevalence of the classical form of CdLS of 1: 81,000 births was proposed and an overall prevalence of CdLS of 1: 45,450-62,500 (Barisic et al., 2008).

Currently, according to data both collected in public Databases (OMIM, GeneReviews and GeneticsHomeReference) and reported by the most recent clinical reviews (Dorsett, 2007b; Kline et al., 2007), the incidence can be estimated around 1: 10,000.

1.3 CLINICAL FEATURES OF CdLS

The features of this disorder vary widely among affected individuals in a range from relatively mild to severe. CdLS is characterized by the simultaneous presence of specific dysmorphisms, pre- and post-natal growth retardation, microcephaly, psychomotor and intellectual development delay, hirsutism, abnormalities of bones in the arms, hands and fingers, and disorders in gastrointestinal tract. Associated major malformations may be present in any organ and system, although the presence/absence of these anomalies is not an indispensable element for clinical diagnosis. Both in childhood and in adulthood,

medical complications and behavioural problems can frequently arise. About one third of patients have upper limbs reduction defects.

Cardinal Features	Score
Synophrys (HP:0000664) and/or thick eyebrows (HP:0000574)	2
Short nose (HP:0003196), concave nasal ridge (HP:0011120) and/or upturned nasal tip (HP:0000463)	2
Long (HP:0000343) and/or smooth philtrum (HP:0000319)	2
Thin upper lip vermilion (HP:0000219) and/or downturned corners of mouth (HP:0002714)	2
Hand oligodactyly (HP:0001180) and/or adactyly (HP:0009776)	2
Congenital diaphragmatic hernia (HP:0000776)	2
Suggestive Features	
Global developmental delay (HP:0001263) and/or intellectual disability (HP:0001249)	1
Prenatal growth retardation (<2 SD) (HP:0001511)	1
Postnatal growth retardation (<2 SD) (HP:0008897)	1
Microcephaly (prenatally and/or postnatally) (HP:0000252)	1
Small hands (HP:0200055) and/or feet (HP:0001773)	1
Short fifth finger (HP:0009237)	1
Hirsutism (HP:0001007)	1
Interpretation of the Score	
Score \geq 11 points, of which at least 3 are cardinal features	classical CdLS
Score between 9 or 10 points, of which at least 2 are cardinal features	non-classical CdLS
Score between 4-8 points, of which at least 1 is cardinal feature	molecular testing for CdLS indicated
Score <4 points	Insufficient to indicate molecular testing for CdLS indicated

Table 1. Diagnostic algorithm modified from the Consensus Statement

(Selicorni et al., 2021)

Patients present distinctive facial features, including arched eyebrows, long eyelashes, low-set ears, small and widely spaced teeth, and a small and upturned nose. CdLS patients present intellectual disability (ID) and autism-like behaviour (Deardorff et al., 1993, 2007; Avagliano et al., 2017).

In general, individuals with CdLS have a growth-weight deficit: growth retardation is often evident in the prenatal period (IUGR) and it is maintained in the post-natal period (PNGF) (Bruner and Hsia YE, 1990; Kline et al., 1993; Kousseff et al., 1993; Boog et al., 1999). This aspect is often related to the presence of gastroesophageal reflux and difficulty in sucking/swallowing which, in some cases, can make enteral nutrition via a nasogastric tube or gastrostomy necessary. These difficulties are usually transient as in later life most patients acquire the ability to feed orally without any problems. In contrast, overweight or obesity are rather common in young adults, often due to a high-calories diet and low physical activity (Mariani et al., 2016).

Due to phenotypic variability of CdLS, a *consensus* statement was drawn up by an international group (Kline et al., 2018) to help physicians for addressing clinical diagnosis. In this huge work authors drafted a diagnostic algorithm represented in Table 1 (Selicorni et al., 2021), which is made up of “cardinal” and “suggestive” features of CdLS. After establishing a specific score for every clinical sign, the final sum of all scores reached by the patient can discriminate the spectrum of belonging (classical or non-classical CdLS). Specific growth curves, which run parallel to those of the general population, have been generated but fall below the fifth centile during early childhood. The use of these curves monitoring growth is therefore fundamental, especially in the neonatal and infantile period (Fig. 1 and 2) (Kline et al., 1993). However, it should be noted that the curves available today were generated by the auxological trend of subjects diagnosed in the pre-molecular era, in which the diagnosis was made only on a clinical basis. On the other hand, growth curves divided by genotype

are not available. This information is important because growth is influenced by the genetic variant type and causative gene: growth trend is less impaired in individuals with mutations in the *SMC1A* gene than in those with mutations in *NIPBL* (Kline et al., 1993).

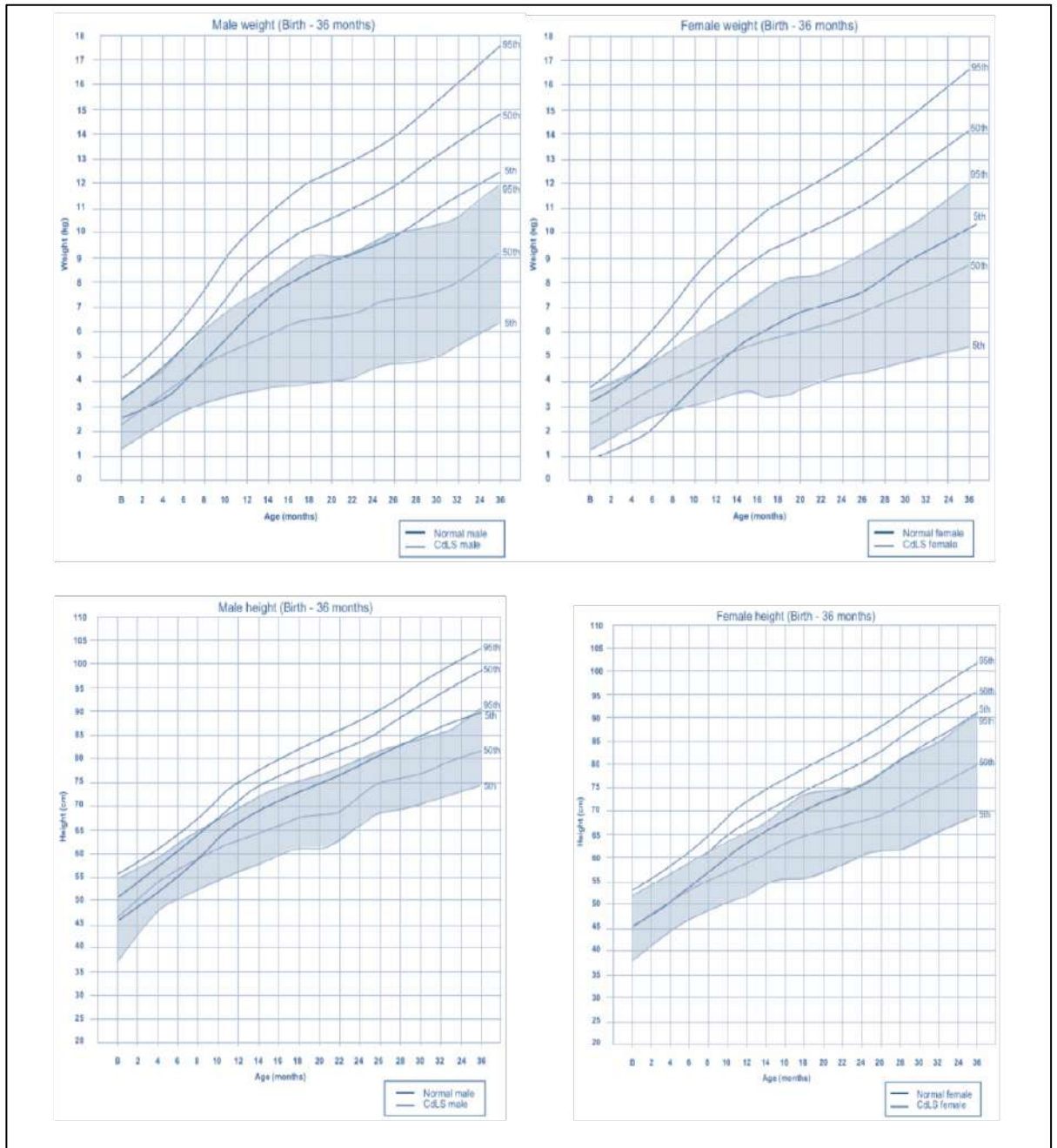


Figure 1: Growth curves for weight (top) and height (bottom) in males (left) and females (right) from birth to 36 months (Kline et al., 1993)

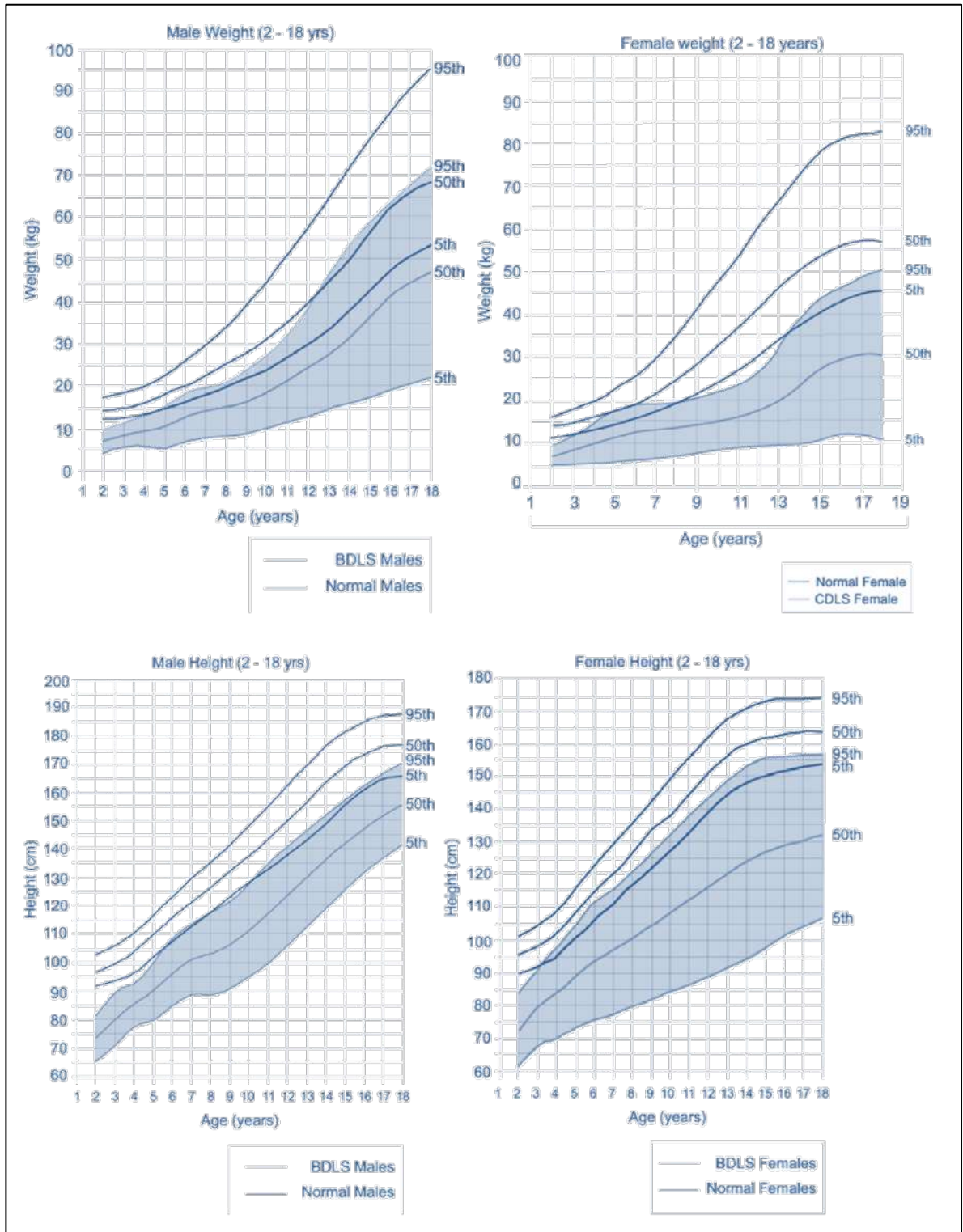


Figure 2. Growth curves for weight (top) and height (bottom) in males (left) and females (right) aged 2 to 18 (Kline et al., 1993)

1.4 PRENATAL ASPECTS

Few data in literature report CNS malformations in CdLS. Neurulation is the known process that leads to the formation of the human CNS and occurs between the 20th and 27th day after fertilization. During the previous phase of development, called gastrulation, the ectoderm is formed through the response to molecular signals from the underlying notochord, which originates from the neural plate. This layer of ectodermal cells will form the neural tube by merging along the midline across its anterior-posterior axis (Nikolopoulou et al., 2017). During gastrulation, neural crest cells are organized at the edges of the neural plate (Fernández-Garre et al., 2002). The cells of the neural crest are initially located on the dorsal part of the neural tube: during the closure of the tube, cells migrate along the embryonic axis differentiating into different neuronal cell types and other structures (Mishina and Snider, 2014; Noisa and Raivio, 2014).

Before the neural tube closes, the anterior end of the tube begins to expand, forming the three primitive cerebral vesicles: forebrain, midbrain and hindbrain (Stiles and Jernigan, 2010). The forebrain and hindbrain soon divide to form secondary cerebral vesicles (telencephalon and diencephalon rostrally and metencephalon and myelencephalon caudally). All these structures are visible from the 49th day after fertilization (Stiles and Jernigan, 2010). At 9 weeks of gestation the encephalic lobes are formed and the formation of the corpus callosum begins, which represents the interhemispheric connection point (Stiles and Jernigan, 2010). To ensure adequate formation and function of the CNS, the complex development process must be coordinated by the activity of a large number of genes and proteins, including the cohesion complex (D'Mello, 2019).

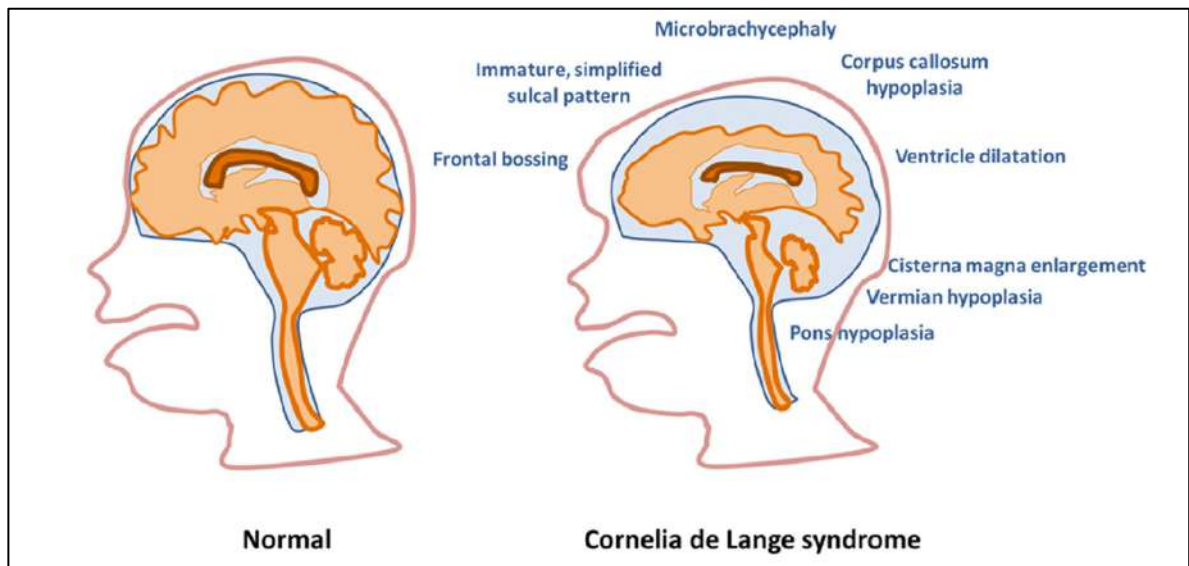


Figure 3. Brain abnormalities in CdLS. Comparison between sagittal section of normal brain (on the left) with the sagittal section of affected brain (on the right) (Avagliano et al., 2017)

To date, published data agree on excluding that the age of the parents is a predisposing factor for this syndrome (Opitz, 1985), with the only exception of X-linked forms. Generally, pregnancy has a regular course without significant complications. A higher incidence of premature birth is reported than in the general population (Jackson et al., 1993). Diagnosing CdLS in the prenatal period is very difficult, especially in the first and second trimester. Non-specific plasma markers (beta-HCG and pregnancy-associated plasma protein A, PAPP-A) and ultrasound (to see nuchal translucency) are used: some studies have reported PAPP-A values below normal in pregnancies with fetuses affected by CdLS (Westergaard et al., 1983; Aitken et al., 1999; Arbuzova et al., 2003; Chong et al., 2009; Avagliano et al., 2017) and increased nuchal translucency in 51% of cases (Sekimoto et al., 2000; Huang and Porto, 2002). However, it is not clear whether the decrease in PAPP-A values is specifically related to CdLS.

The most frequently encountered ultrasound features are intrauterine growth retardation, upper limb malformations (visible in 66% of foetuses), diaphragmatic hernia (28%), cardiac anomalies (15%) and characteristic facial profile (small nose, anteverted nostrils, protruded upper lip, micro-retrognathia) evident in about 50% of cases (Jackson et al., 1993; MA et al., 1993; S et al., 1996; Marino et al., 2002; Vaillant et al., 2004; Gregori et al., 2007; Chong et al., 2009; Sepulveda et al., 2009; Wilmink et al., 2009; Pajkrt et al., 2010). Manifestation of ultrasound abnormalities in the second and third trimesters leads to a suspected diagnosis only in a small proportion of patients (less than 30%).

Some parameters are therefore detectable in the prenatal period in a few patients, but currently the definitive diagnosis is almost always given at birth (Pajkrt et al., 2010). In case of known familiarity and increased risk of recurrence, it would be possible to carry out research for specific mutation on foetal DNA obtained from chorionic villus sampling or amniocytes or by analysing embryonic cells obtained by *in vitro* fertilization. The use of non-invasive screening tests on free circulating foetal DNA of gene panels, which also include CdLS genes, is currently not an applicable approach in clinical practice, due to the complexity of interpreting the results of molecular investigations. The validity and informative value of the results of prenatal analyses and the possible ethical implications for family choices must be considered and deeply discussed with couples before engaging on the prenatal diagnosis process (Avagliano et al., 2017).

1.5 FACIAL FEATURES

The peculiar dysmorphisms represent the most specific aspects of the syndrome and are present in all individuals with CdLS.

The face is characterized by a low and narrow forehead and frequent frontal lanugo. The ears may appear with the pavilion dislocated downwards and/or rotated backwards and externally thickened. In about 98% of cases the eyebrows, well drawn and arched, join on the median line (synophrys), giving an arched conformation which can also be accentuated by a marked eyelid ptosis. Lashes are typically long, thick and very curved both upwards, starting from the upper edge, and downwards, from the lower one (Kline et al., 1993). The central portion of the face is flattened, the root of the nose is depressed and enlarged, with a saddle-like conformation, while the nostrils are anteverted in 85% of patients and the tip of the nose is slightly triangular (Jackson et al., 1993). In most cases (94%), the lips are thin, especially the upper lip, and terminate in downward-oriented commissures; the upper lip has a median prominence which corresponds to a sort of hollow at the level of the lower lip. In some cases, cleft lip and palate may be present and dental malposition and excessive tooth spacing may be found, which can cause malocclusion in several patients (Jackson et al., 1993). The neck is generally short (Fig. 4).

One of the peculiar elements of the clinical picture is represented by hirsutism. Typically, there is a hair increase on the forehead, on the back, in particular at the level of the lumbo-sacral region, and on the forearms.

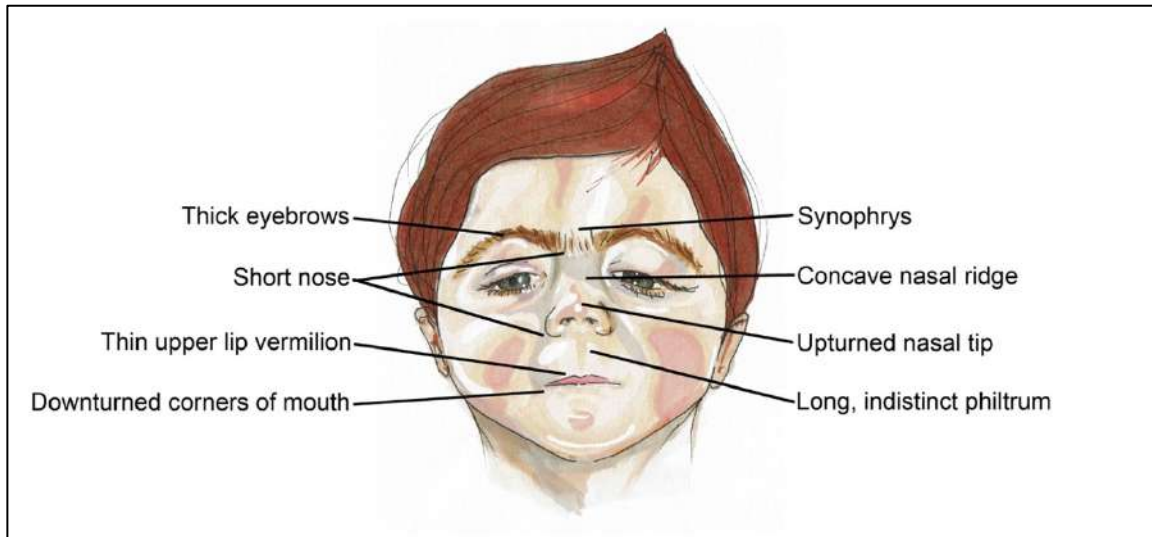


Figure 4. Typical facial features of a CdLS patient carrying a mutation in NIPBL gene, modified from (Avagliano et al., 2020)

1.6 CLINICAL ASPECTS

In CdLS one or more major malformations and medical problems are usually present (Table 2 and 3). From an early age, subjects with CdLS can also have a wide range of associated medical problems (Jackson et al., 1993; Kline et al., 2007; Ayerza Casas et al., 2017). It is important to provide careful monitoring as many of these complications if not diagnosed and treated adequately, can cause chronic pain and thus contribute to behavioural problems (hyperactivity, agitation, self and hetero aggression).

The most frequent gastrointestinal malformations in CdLS are the annular pancreas, duodenal atresia, Meckel's diverticulum, imperforate anus and congenital diaphragmatic hernia. Pyloric stenosis is reported in more than 7% of patients and inguinal hernia is common in children. Two papers described a certain frequency of intestinal malrotation with acute presentation as caecal volvulus (Kline et al., 2007; Mariani et al., 2016). Bowel malrotation is an atypical symptom and can be difficult to diagnose due to the communication difficulties of affected individuals. However, it can be recurrent and can present as a surgical

emergency at any age. Complications related to the presence of intestinal malrotation are the first cause of death in CdLS subjects after the second year of life. This malformation causes significant mortality – due to intestinal obstruction, often not recognized also due to high pain threshold and communication difficulties – which is why it should be sought in all patients with CdLS by performing an X-ray of the digestive system with contrast medium (Jackson et al., 1993; Masumoto et al., 2001; Kline et al., 2007, 2018b; Schrier et al., 2011). Eating difficulties are reported in 70-100% of the subjects observed. Structural abnormalities of the digestive tract or functional abnormalities are common. The most important medical complication is represented by gastroesophageal reflux, which is present among 70-90% of patients (Cates et al., 1989; Jackson et al., 1993; Luzzani et al., 2003; Kline et al., 2007; Macchini et al., 2018). This condition can lead to severe lung infections which are one of the most frequent causes of death in CdLS subjects (Schrier et al., 2011). The presence of reflux can be complicated in young adulthood by the early onset of metaplasia of the oesophageal mucosa (Barrett's esophagus) in about 10% of cases (Luzzani et al., 2003; Kline et al., 2007; Macchini et al., 2018). This condition can develop as malignant degeneration into oesophageal adenocarcinoma (DuVall and Walden, 1996; Fitzgerald et al., 2014).

Malformation	Prevalence
Heart malformations (no specific defect)	25%
Palate	20%
Eyes	
Unilateral or bilateral nasolacrimal duct obstruction	60-80%
Central Nervous System	47% (in the wider cohort reported)
Limb defects	About one third
Urinary tract	10%
Genitalia	
Cryptorchidism	80%
Micropenis	37%
Hypospadias	9%
Bicornuate uterus	19%
Gastrointestinal system	
Intestinal malrotation	5-10%
Pyloric stenosis	7%
Diaphragmatic Hernia	rare

Table 2. CdLS major malformations modified from Selicorni et al. (Kline et al., 2018b; Selicorni et al., 2021)

An Italian study reports clinical symptoms referable to gastroesophageal reflux in 71% of individuals with CdLS, only partially confirmed from a molecular point of view (Mariani et al., 2016). A genotype-phenotype correlation work showed that gastroesophageal reflux is more frequent in individuals with variants in *NIPBL* (71%) than in *SMC1A* (60%) (Huisman et al., 2017).

Other studies report a high prevalence in individuals with classical phenotype variants (usually associated with variants in *NIPBL*) and it is evidenced by a positive endoscopic examination for esophagitis (Luzzani et al., 2003; Nizon et

al., 2016). This disorder may not manifest itself with the classical symptoms - vomiting, regurgitation, poor growth - but can express itself with atypical symptoms characterized by nocturnal agitation, recurrent infections of the upper and lower respiratory tract, hyperactivity, self-aggression and Sandifer-like dystonic events (Luzzani et al., 2003; Macchini et al., 2018)(Bull et al., 1993; Sommer et al., 1993). Luzzani and colleagues (2003) suggested a gastrointestinal evaluation in all subjects with CdLS and in patients being treated for esophagitis, the behavioural evaluation as a clinical indicator of the evolution of oesophageal lesions. They observed that a partial or total regression of the oesophageal lesions in response to treatment (medical or surgical therapy) leads to a corresponding important improvement in the patient's behaviour.

The *consensus* work on CdLS shows that the first-line treatment involves a dietary approach and therapy with proton pump inhibitors (Kline et al., 2018b). Surgery is performed only on individuals who do not respond satisfactorily to nutritional and pharmacological treatments or individuals at risk of inhalation. Other gastrointestinal aspects found in 10-15% of adults with CdLS are constipation and rumination, diarrhoea (18%), bloating (48%) and lactose intolerance (18%). An increased prevalence for celiac disease is not reported (Macchini et al., 2007). About 10% of CdLS patients have palate malformations (cleft palate or submucosal cleft of the palate) (Jackson et al., 1993; Kline et al., 2007).

Medical Problem	Prevalence
Gastrointestinal problems	
-Feeding problems	Frequent
-Enteral nutrition	40%
-Gastro oesophageal reflux	60-75%
-Batter oesophagus	9%
-Eosinophilic esophagitis	16%
-Constipation	10-15%
Neurology	
-Seizures	45% (<i>SMC1A</i> gene) 15% (<i>NIPBL</i> gene)
-Autonomic nervous system dysfunction	81% (mild) 26%(severe)
-Sleep problems	12-72%
Orthopaedics	
- Perthes disease	4%
-Leg length differences	46%
-Congenital hip dislocation	10%
-Scoliosis	One third of patients after 10 years
-Kyphosis	A quarter of patients
-Joint contractures	18-25%
-Bunions	75%
Visual problems	
-Palpebral ptosis	37% (unilateral) 44%(bilateral)
-Blepharitis	25%
-Nystagmus	14-17%
-Strabismus	16-26%
-Visual impairment	44-53%
-Pigmented peripapillary ring	83%
Hearing problems	
-Conductive hearing loss	75%
-Neurosensorial hearing loss	25%
-Otitis media with effusion	80-85%
Immunological defects	33% (only one specific report)
Thrombocytopenia	rare
Cancer	No increase of risk

Table 3. Medical problems in CdLS from Selicorni et al 2021(Kline et al., 2018b; Selicorni et al., 2021)

1.7 GENETICS OF CdLS

The first hypothesis of the CdLS genetic aetiology was formulated by Opitz in a Letter to Editor published by Lancet in 1964 (Opitz et al., 1964), in which he suggested autosomal recessive transmission. Subsequently, over thirty chromosomal anomalies involving different chromosomes were associated with the CdLS phenotype (Broholm et al., 1968; Borck et al., 2004; Gervasini et al., 2008).

However, the diagnosis of CdLS in patients with chromosomal abnormalities is hampered either by the rarity of familial cases and by the presence of chromosome abnormalities also in healthy individuals (Beratis et al., 1971).

Boue and colleagues in 1974 highlighted the phenotypic similarity between CdLS and the *3q duplication syndrome*, suggesting chromosomal partial aneuploidy as a possible cause of CdLS (A and J, 1974). A family, whose components were previously described as CdLS patients (Falek et al., 1966), was later shown to carry a partial duplication of the long arm of chromosome 3 (Wilson et al., 1985). However, these patients reported important differences compared to the typical CdLS phenotype i.e. mild growth retardation, absence of synophrys and anteversion of the nostrils, normal pronation and supination of the elbow, convulsions. Considering these differences, the CdLS diagnosis was contested by Opitz and Smith in a Letter to Editor at Paediatrics. The description of anomalies on the long arm of chromosome 3– in particular 3q26.3 – in patients with classical form of CdLS lead to an in-depth genetic investigation aimed both at balanced translocation identification and at phenotypic similarity between 3q

duplication syndrome and CdLS assessment (Holder et al., 1994; Tonkin et al., 2004); Steinbach et al., 1981; Wilson et al., 1985; Ireland et al., 1991).

Russell and co-authors (2001) studied family cases contributing to the analysis of the transmission modalities of CdLS (Fig.5) (Russell et al., 2001). 25 families were examined: 60% suggested an autosomal dominant transmission, while 40% was compatible with a recessive transmission. More rarely, a X-linked, mitochondrial modality or the presence of germinal mosaicism was hypothesized. However, the most quoted hypothesis was that the disease transmission occurred in an autosomal dominant manner since 99% of the cases described were sporadic. Further, any consanguineous parents or a more susceptible population for CdLS were identified.

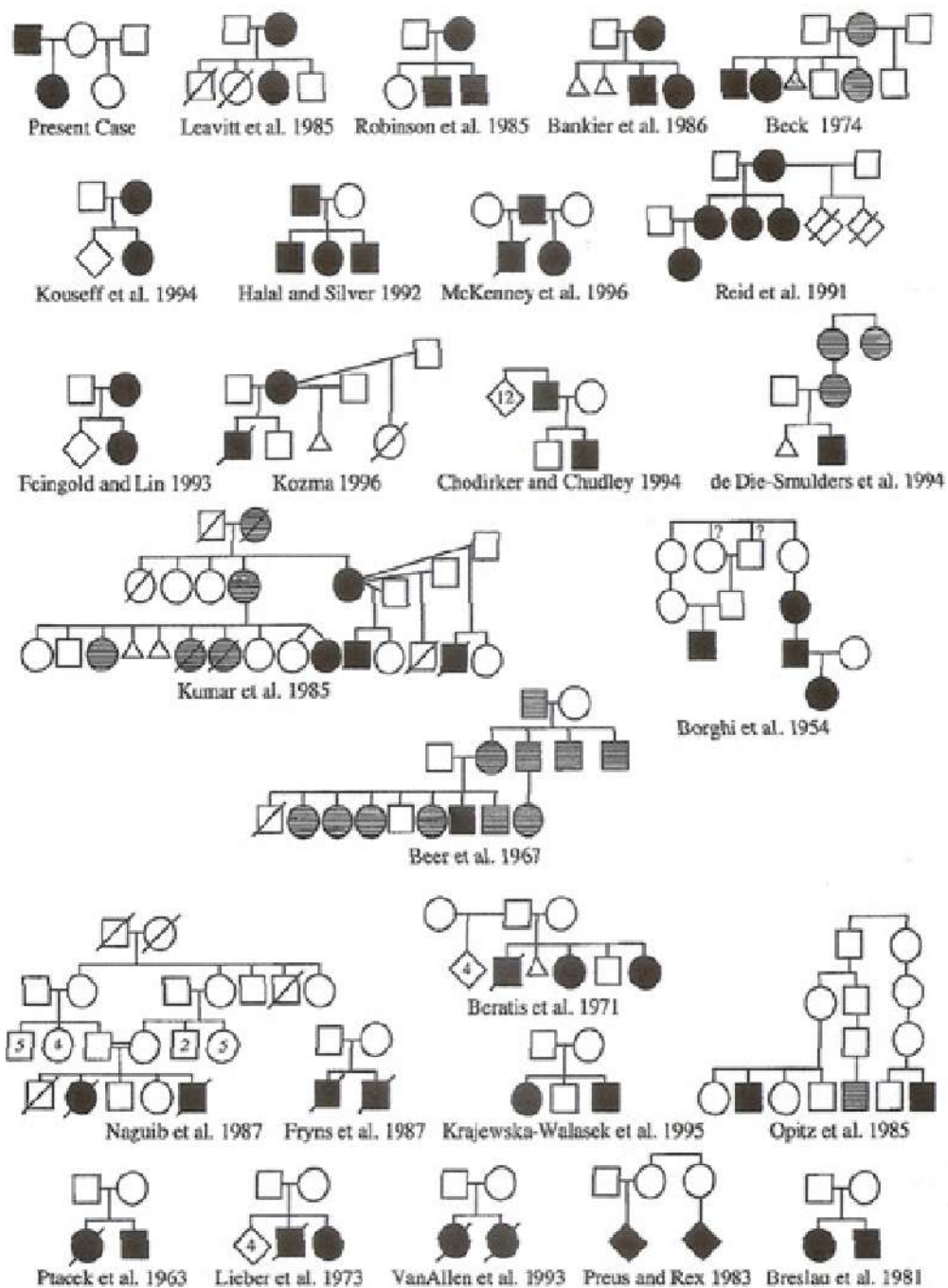


Figure 5. Family cases identified up to 2001 (Russell et al., 2001)

Considering the observed phenotypic variability, the hypothesis that CdLS could be subjected to the phenomenon of genetic heterogeneity, i.e. the disease can be caused by different mutations in the same gene or different genes, could not

be excluded (Allanson et al., 1997; Russell et al., 2001). In 2004 two independent groups identified *NIPBL* as the first causative gene: Emma Tonkin and her collaborators, analysing the breakpoint region of the translocation t (5; 13) (p13.1; q12.1) found in a child with classical signs of CdLS (Tonkin et al., 2004), and Ian Krantz's team, through a genome-wide linkage analysis in nine CdLS affected families with more than one family member affected (Krantz et al., 2004). In 2006 *SMC1A* was identified as the second causative gene of CdLS, responsible for almost 5% of cases at present day and for a milder phenotype than the one associated to *NIPBL* mutations (Musio et al., 2006), and one year later, mutations in *SMC3* were also linked to CdLS (Deardorff et al., 2007).

The advent of next generation sequencing (NGS) techniques led to a more precise definition of the transmission process. In fact, from 2018 CdLS spectrum could account on other four causative genes thanks to the identification of *RAD21* (Deardorff et al., 2012), *HDAC8* (Deardorff et al., 2012), *ANKRD11* (Ansari et al., 2014) and *BRD4* (Kline et al., 2018a), confirming the genetic heterogeneity hypothesized for this syndrome (Fig. 6 and 7).

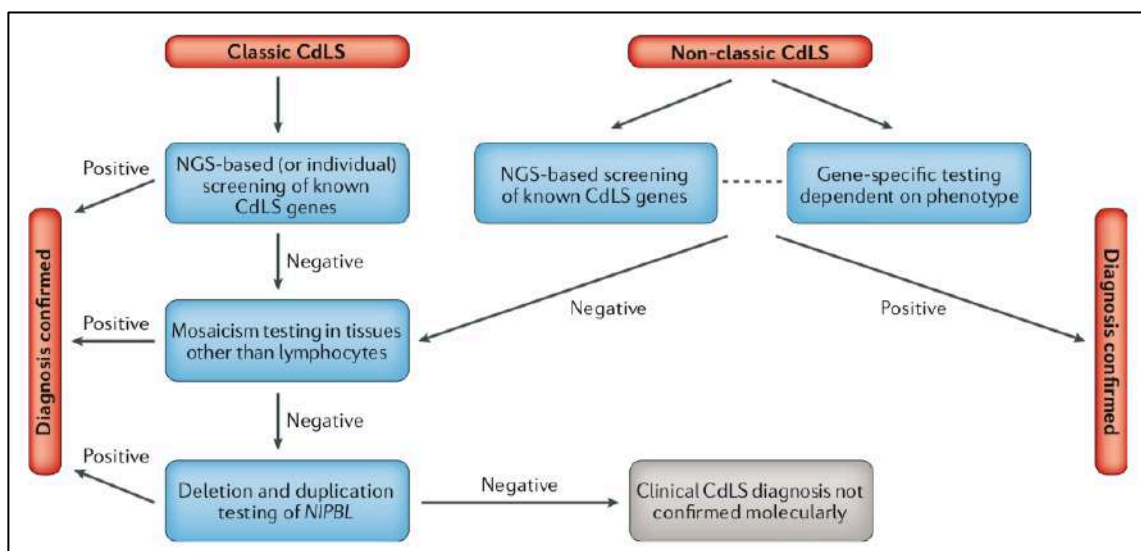


Figure 6. Molecular diagnostic pathways for the identification of CdLS (Kline et al., 2018).

1.8 CdLS CAUSATIVE GENES

NIPBL

NIPBL (Nipped-B like) is the commonest gene mutated in CdLS. About 70% of CdLS patients carry a mutation on this gene (OMIM #608667 – CDLS1). Human *NIPBL* is located on chromosome 5p13.2, occupies a region of 188 kb and consists of 47 exons; whose coding sequence comprehends exon 2-47. *NIPBL* encodes a protein called delangin which belongs to a family of evolutionarily conserved proteins known as adherins, involved in chromosomal cohesion and in the loading of the cohesive complex at the chromosomal level (Rollins et al., 2004).

The *NIPBL* gene presents homology with the *Nipped-B* gene of *Drosophila melanogaster* and its homologues have also been identified in worms (*Caenorhabditis elegans*) and in yeast (*Saccharomyces cerevisiae*, with the name of *Scs2*) (Tonkin et al., 2004). This gene encodes for the homolog protein Nipped-B in the *Drosophila melanogaster* and cohesion proteins of fungal *Scs2*-type sister chromatid.

NIPBL forms a heterodimeric complex – cohesin loading complex – with MAU2/SCC4 which mediates the loading of the cohesin core onto chromatin (Bermudez et al., 2012; Rhodes et al., 2017). *NIPBL* plays a fundamental role in the loading of the cohesin complex onto the DNA and it has a role in cohesin loading at sites of DNA damage (Bot et al., 2017).

Analysis showed that *NIPBL* expression is ubiquitous, although variable among different tissues. Expression is higher in the heart and skeletal muscle, and is very low in the brain, lungs, colon and intestine (Krantz et al., 2004; Tonkin et al., 2004; Bettini et al., 2018). Interestingly, a major level of expression is required in some tissues for the regulation of embryonic development (Strachan, 2005). In fact, the embryonic expression of *NIPBL* correlates with the pathogenesis of

CdLS: it is expressed in the limbs, craniofacial bones and muscles, in the craniofacial mesenchyme, in the respiratory, gastrointestinal and genitourinary systems, in the renal tubules and, finally, in the heart (Tonkin et al., 2004) which are compromised tissues and organs in CdLS (Fig. 7).

The role of *NIPBL* in regulating the cohesion of sister chromatids pushed the search for the other causative genes towards the components of the cohesin complex.

SMC1A

2006 was the year of the discovery of the second CdLS causative gene, *SMC1A* (Structural Maintenance of Chromosomes 1A) (OMIM #300040 – CDLS2), currently identified in about 5% of CdLS individuals (Borck et al., 2004; Musio et al., 2006; Deardorff et al., 2007; Mannini et al., 2010; Huisman et al., 2017). *SMC1A* is localized at the level of chromosome Xp11.22, a region that partially escapes inactivation (Brown et al., 1995). In fact, in seven out of nine cases the allele located on the inactive X chromosome is expressed, while expression levels of the inactivated allele range from 15 to 30% (Carrel and Willard, 2005).

The protein product *SMC1A* is one of the core proteins of the cohesin complex. Heterozygous missense or ins/del in frame mutations in *SMC1A* interfere with the structure of the cohesin complex subunits and its function, thus causing CdLS (Deardorff et al., 2007; Revenkova et al., 2009).

Patients with mutations in the *SMC1A* gene usually show milder symptoms and fewer structural abnormalities than those with the *NIPBL* mutation. However, all patients manifest some degree of cognitive defect (Deardorff et al., 2007; Rohatgi et al., 2010), suggesting that *SMC1A* plays a crucial role during brain development in the embryo. In some cases, it has been reported that females

are less affected than males (Musio et al., 2006; Huisman et al., 2017) because of *SMC1A* X-chromosome inactivation escape (Carrel and Willard, 2005).

SMC3

Mutations in *SMC3* (Structural Maintenance of Chromosomes 3) (OMIM # 606062 - CDLS3) are present in approximately 2% of patients with CdLS. *SMC3* gene pathogenetic variant was reported by Deardorff et al. (2007) in a patient with a clinical diagnosis of CdLS. Missense or in-frame ins/del variants usually occur (Gil-Rodríguez et al., 2015), but nonsense mutations have also been reported (Gil-Rodríguez et al., 2015). The *SMC3* gene, located at chromosome 10q25, encodes a protein that is a central component of the cohesin complex. With *SMC1A*, *SMC3* forms a ring and mediates the cohesion of sister chromatids. *SMC3* mutations were also identified in patients with similar clinical features to CdLS (short stature and ID) but did not fully meet the clinical diagnostic criteria of non-classical CdLS (Ansari et al., 2014; Gil-Rodríguez et al., 2015).

RAD21

CdLS can also be caused by mutations in a gene encoding for another structural protein of the cohesin complex, *RAD21* (*RAD21* Cohesin Complex Component) (OMIM # 606462 - CDLS4), including heterozygous deletions and missense mutations (Deardorff et al., 2012). *RAD21* is located on chromosome 8q24.11. Deardorff and colleagues first described mutations on six patients resulted negative for *NIPBL*, *SMC1A* and *SMC3*, and who were characterized by slow growth, minor skeletal anomalies, and other features similar to CdLS. Patients with these pathogenetic variants have even milder symptoms (Deardorff et al., 2012). The *RAD21* protein is encoded by a highly conserved gene which was

also found in the yeast *Schizosaccharomyces pombe*. The RAD21 protein is a nuclear phospho-protein that becomes hyperphosphorylated during the M phase of the cell cycle, showing a strong specific association in the centromere region, and it is part of the main nucleus of the cohesin complex. It is involved both in the repair of DNA double strand breaks and in the cohesion of chromatids (Nasmyth and Haering, 2009). Cultured cells from patients showed high sensitivity to radiation, consistent with its important role in the response to DNA damage (Deardorff et al., 2012). To date, *RAD21* mutations represent only a small percentage of CdLS causes (about 1%) in fact only 23 patients have *RAD21* variants and usually show a non-classical CdLS phenotype (Deardorff et al., 2012; Ansari et al., 2014; Boyle et al., 2017).

HDAC8

Individuals with *HDAC8* (Histone Deacetylase 8) pathogenetic variants (OMIM # 300882 - CDLS5) (Deardorff et al., 2012; Harakalova et al., 2012; Ansari et al., 2014; Feng et al., 2014; Kaiser et al., 2014; Parenti et al., 2016) account for approximately 5% of CdLS cases. Mutations in the *HDAC8* gene are currently described in more than 60 individuals with a wide variability of clinical expression (Deardorff et al., 2012; Harakalova et al., 2012; Feng et al., 2014; Kaiser et al., 2014; Parenti et al., 2016).

The *HDAC8* gene is located on the X chromosome (Xq13.1) and encodes a protein responsible for the deacetylation of lysine residues on the N-terminal part of the core histones (H2A, H2B, H3 and H4). Contrary to *SMC1A*, *HDAC8* may be inactivated (Kaiser et al., 2014) and female carriers of the mutated alleles may be affected or be completely healthy.

HDAC8 regulates epigenetic repression and plays an important role in transcriptional regulation, cell cycle progression and developmental events.

Furthermore, it is involved in the deacetylation of non-histone proteins such as SMC3, which regulates the release of cohesin complexes from chromatin (Fazio et al., 2016). Interestingly, patients phenotype associated to *HDAC8* mutations is typically non-classical and can vary widely.

BRD4

BRD4 (Bromodomain Containing 4), whose chromosomal localisation is at 19p13.12, has recently been described as a causative gene of CdLS (Kline et al., 2018b). It was identified in an individual with a non-classical CdLS phenotype where a *de novo* mutation (deletion that included *BRD4*) was found (Olley et al., 2018) (Fig. 7). Subsequently, the specific sequencing of *BRD4* allowed to identify *de novo* intragenic variants and demonstrate molecular association with NIPBL (Alesi et al., 2019; Luna-Peláez et al., 2019). *BRD4* encodes a protein with a chromatin reader function and plays a key role in the transmission of epigenetic memory through cell division and transcription regulation by recognizing and binding acetylated histones (Mochizuki et al. 2008). NIPBL was identified as the predominant interacting protein with *BRD4* by mass-spectrometry and it was shown that mutations in *BRD4* decreased its interaction with acetylated histone while maintaining NIPBL (Olley et al., 2018). Therefore, this mechanism suggests that *NIPBL* capture could underlie the pathogenic mechanism.

ANKRD11

ANKRD11 (Ankyrin Repeat Domain 11) has been recently classified among the causative genes of CdLS. To date, only five *ANKRD11 de novo* variants have been described in patients with a non-classical CdLS phenotype (Ansari et al., 2014; Parenti et al., 2016a) and some additional variants have been identified in research cohorts (Kline et al., 2018b). *ANKRD11* (16q24.3) is a chromatin

regulator, which modulates histone acetylation and gene expression in neural precursor cells. It inhibits ligand-dependent transactivation by interacting with HDACs to the p160 coactivator/nuclear receptor complex (Zhang et al., 2004) and also plays a role in the proliferation and development of cortical neural precursors (Gallagher et al., 2015). Mutations in *ANKRD11* are usually related to KBG syndrome, another rare genetic disorder, whose name is due to the initials of the surnames of the first three families identified in 1975 (Herrmann et al., 1975). KBG syndrome has features partially overlapping with CdLS: short stature, developmental anomalies of the limbs, vertebrae, extremities and/or underdevelopment of the skeletal bones and possible craniofacial dysmorphism (Fig. 7). Most patients have some degree of ID and developmental delay (Morel Swols et al., 2017).

In recent years, thanks to NGS techniques and the use of Whole Exome Sequencing (WES), pathogenetic variants in several additional genes have been identified in patients with non-classical CdLS phenotype. These patients showed some features overlapping with the ones of other chromatinopathies (disorders whose causative genes belong to the epigenetic machinery) (Fahrner and Bjornsson, 2014), but they still exhibited a CdLS-like phenotype which however did not fulfil all clinical diagnostic criteria (Izumi, 2016). It has been reported that patients diagnosed with a chromatinopathies - e.g. Rubinstein-Taybi syndrome (#180849), Wiedemann-Steiner syndrome (#605130), Coffin-Siris syndrome (#135900) - may show clinical signs common to CdLS (Woods et al., 2014; Yuan et al., 2015; Parenti et al., 2017). It is hypothesized that this clinical overlap may be due to the functional network shared between the complexes associated with chromatin and the complex of cohesin. *AFF4* (Izumi et al., 2015), *EP300* (Woods et al., 2014), *KMT2A* (Yuan et al., 2015; Parenti et al., 2017), *NAA10* (Saunier et al., 2016), *SETD5* (Parenti et al., 2017), *SWI/SNF* complex genes (Parenti et al.,

2017), TAF6 (Yuan et al., 2015) are the new candidate genes which however require further studies to be associated with CdLS (Avagliano et al., 2020) (Fig. 7).

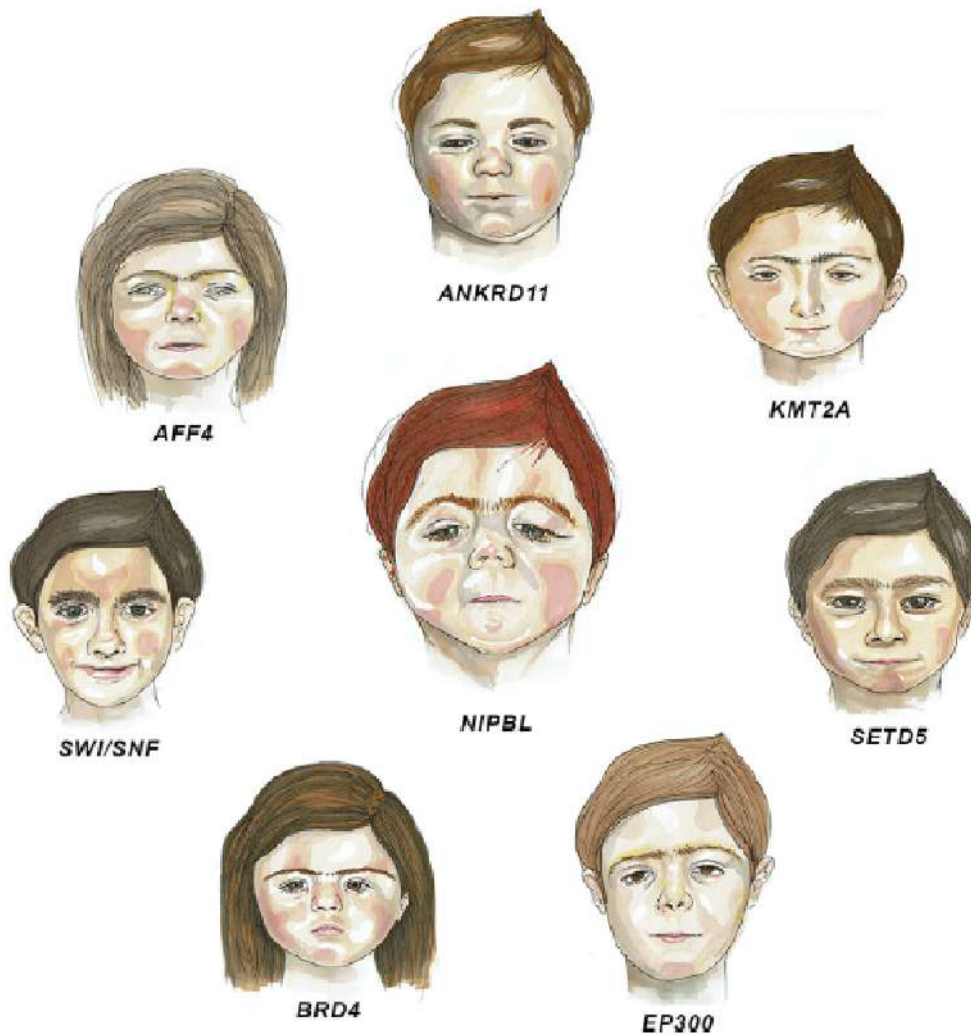


Figure 7. CdLS differential diagnosis (Avagliano et al., 2020)

1.9 COHESIN COMPLEX

The genes encoding for proteins of the cohesin complex (i.e. *NIPBL*, *SMC1A*, *SMC3*, *RAD21*, *HDAC8*, *BRD4* and *ANKRD11*), a multimeric system highly conserved across species, from the most primitive life forms to human cells (Haering et al., 2002; Nasmyth, 2011; Deardorff et al., 2012; Banerji et al., 2017), have been found to be implicated in the pathogenesis of CdLS.

Genetic variants causing functional alterations of this complex underly a broad group of congenital pathologies named "cohesinopathies", and Cornelia de Lange Syndrome is the most common among them (Liu and Krantz, 2009).

Cohesins are essential Structural Maintenance of Chromosomes (SMC) protein-containing complexes that interact with chromatin modulating its organization.

The components of the cohesin complex form a ring-like multimeric structure (Fig. 8) responsible for holding sister chromatids together (Nasmyth and Haering, 2009). Specifically, the different subunits forming the complex are SMC1, SMC3, STAG1/STAG2 (or STAG3 in germ cells) and RAD21, and other factors (PSD5, WAPL) (Onn et al., 2008; Nasmyth, 2011). In addition, NIPBL with its partner MAU2 is involved in the loading of the cohesin complex onto chromatin during S-phase, while HDAC8 regulates the deacetylation of SMC3 following its removal from chromatin in both prophase and anaphase to allow a correct mechanism up to the following cell cycle (Deardorff et al., 2012). The cohesin complex is fundamental for chromosomal segregation, regulation of gene expression, maintenance of genome stability, chromatin structure and genome organization, thus regulating most aspects of cell biology (Michaelis et al., 1997; Kagey et al., 2010; Watrin et al., 2016; Kamada and Barillà, 2018). Particularly, thanks to the interaction with the adherins, at the beginning of the cycle, the cohesins are loaded on the chromatin and, with the help of factors such as PDS5 and ESCO2, keep the sister chromatids stabilized together after the duplication of the genome. Subsequently, with the onset of mitosis and meiosis processes, the cohesins are concentrated at the centromere for compacting the structure. Finally, the proteolytic cleavage of the cohesin ring in anaphase allows the segregation of chromatids (Nasmyth and Haering, 2005).

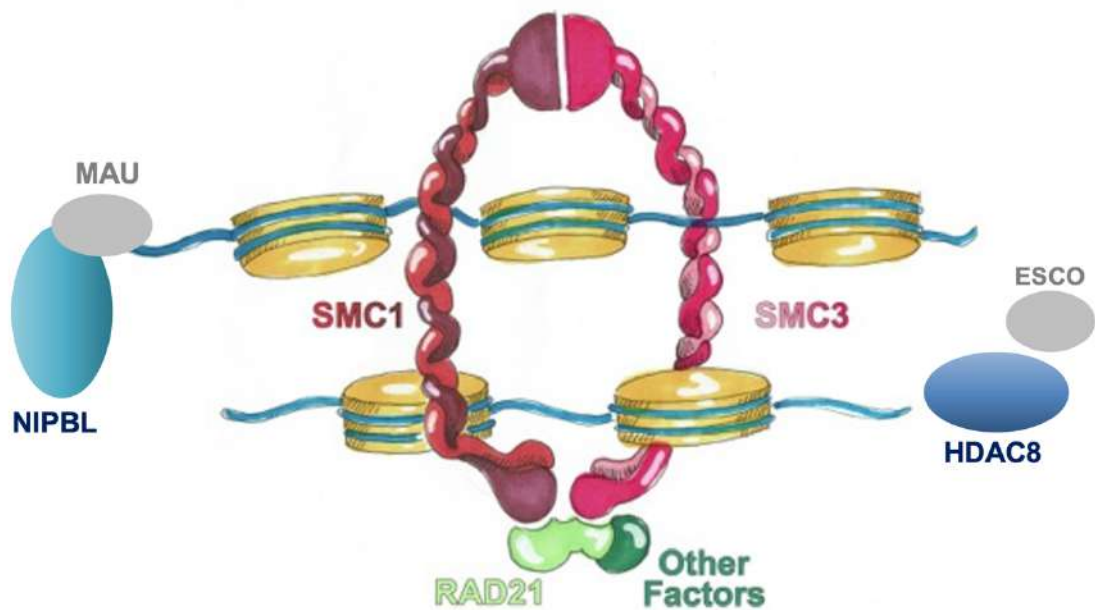


Figure 8. Cohesin Complex modified from (Selicorni et al., 2021)

Furthermore, this complex acts – in its non-canonical role – as one of the many players involved in transcriptional regulation: the cohesin complex is important for controlling gene expression together with tissue specific transcription factors and/or in combination with the CCCTC-binding factor (CTCF) insulator protein (Kagey et al., 2010; Zuin et al., 2014; Bettini et al., 2018).

To date, several genes have been associated with chromatinopathies classified as “Cornelia de Lange Syndrome-like”. It is known that the phenotype of these patients can overlap with characteristic features of other syndromes caused by genetic variants that affect different regulators of chromatin structure and function.

Interestingly, it has been observed that the cell lines of CdLS patients, although presenting mutations affecting the cohesins, do not show cohesin defects (Castronovo et al., 2009; Dorsett and Krantz, 2009). It may depend on the alteration of the role of cohesins and their regulators in the balancing of gene expression, rather than by the alteration of the cohesion activity of sister

chromatids (Liu and Krantz, 2009), a function probably maintained by compensatory factors and altered only in homozygosity.

An analysis of the binding sites of cohesins to chromatin showed that these sites are overrepresented for many gene promoters (Pichè et al 2019). This suggests that cohesins can regulate gene expression by acting directly as transcription factors. However, most of the expressed genes do not appear to have any cohesin binding sites in their intragenic region, indicating that most genes in the human genome could be regulated in a cohesin-independent manner, or that cohesins could be involved in the regulation of such genes with different mechanisms, or that only some specific genes are regulated by cohesins.

Molecular bases of CdLS are still not fully understood, but it is known that the cohesin complex has a fundamental role in CdLS pathogenesis due to its non-canonical role in gene expression regulation.

The canonical role of cohesins

The DNA damage repair capacity of the cohesin complex is the philologically preserved function inherited from the proteins responsible for maintaining the chromosome structure (SMC) of bacteria (Dorsett and Ström, 2012). In eukaryotes, this activity was identified in a model of *Schizosaccharomyces pombe*, when it was observed that a mutation of *Rad21* gave the cells a particular sensitivity to γ radiation, making DNA repair mechanisms ineffective (Birkenbihl and Subramani, 1992).

Later it was shown that this function is maintained even in more complex organisms. Cohesins are involved in DNA damage through the cohesion of chromatids during the S and G2 phases of the cell cycle (Schmitz et al., 2007); the recruitment of cohesins at the DNA breakpoints, regardless of the cohesion of sister chromatids (Potts et al., 2006) and the correct activation of the cell cycle

checkpoints, which have the role of delaying the progression of the cell cycle, until the integrity of the double strand is restored. Also in the latter case, the action is mediated by the cohesins themselves, regardless of the cohesion of the sister chromatids (Callegari and Kelly, 2007; Watrin and Peters, 2009).

The second canonical role of cohesins consists in keeping the sister chromatids adherent during cell division, arranging themselves to form a ring structure that surrounds the two DNA molecules. As previously mentioned, these proteins bind to DNA during interphase and the complex is firmly stabilized during the S phase, while cell replication takes place (Moldovan et al., 2006). From phase G2 onwards, the complex responsible for stabilizing cohesins on DNA (Esco1/2) and those that promote their removal (PDS5 and Wapl) compete until the PDS5 and Wapl complex prevails. At metaphase, almost all the cohesins are removed from the chromatids, except for those located in the centromeric region, which will be removed during the anaphase (Horsfield et al, 2012).

The non-canonical role

The non-canonical role concerns the regulation of gene expression, in particular during embryonic development (Dorsett, 2007). This is a very complex function and the mechanisms through which it works is not yet fully elucidated. It is known that this function is independent from the role that cohesins play in the cohesion of sister chromatids (Pauli et al., 2010). The first data derived from studies on *D. melanogaster* which proved that *Nipped-b*, *NIPBL* homolog, activates the expression of the *ultrabithorax* gene, while *Smc3* inhibits the *cut* genes (Dorsett, 2009). From several studies on *Drosophila* cell lines, in *Drosophila* salivary gland cells, HeLa cells, human lymphocytes, murine embryonic stem cells and partly also in human thymocytes and murine B lymphocytes, it was found that cohesins and *NIPBL* bind to different DNA sites scattered throughout the genome –

particularly in the proximity of the transcription initiation sites of active genes (Misulovin et al., 2008; Liu et al., 2009; Wendt and Peters, 2009). In human lymphoblastoid cells, an overlap has been observed between the bonds of the cohesive protein complex and the CCCTC binding sites (CTCF), a protein that promotes bonds between enhancers and promoters, through the formation of chromatin loops (Göndör and Ohlsson, 2008). In recent years, several studies have highlighted the role of cohesins and CTCF in controlling the expression of genes involved in the maturation of the immune system, in maintaining the stem cell and germ cell pool (Rubio et al., 2008; Wendt and Peters, 2009)

Several studies have highlighted a direct role of cohesins in the formation of loops of chromatin portions of different gene loci (Hadjur et al., 2009). Therefore, it is believed that these proteins regulate gene expression in synergy with other gene transcription factors (Dorsett et al., 2011).

Cohesins regulate other genes involved in maintenance of neuronal identity such as genes that encode for protocadherins, proteins capable of "building" synaptic connections. Even the processes of neuronal migration and axonal development appear to be regulated by the cohesin complex (Pauli et al., 2008, 2010; Mönnich et al., 2009, 2011).

Both the canonical and non-canonical role of the cohesin complex are based on the ability to create topological links between two segments of the chromatin fiber (Watrín et al., 2016).

1.10 WNT PATHWAY

A signalling pathway involved in all steps of CNS development is the WNT pathway (Mulligan and Cheyette, 2012). WNT signals are involved in the genesis and migration of neural crest cells (Lee et al., 2004; Brugmann et al., 2007;

Mishina and Snider, 2014; Noisa and Raivio, 2014), and are implicated in craniofacial development (Geetha-Loganathan et al., 2009; Song et al., 2009; Fu et al., 2011). WNT proteins provide information for the arrangement of the neural plate along the embryonic axis (Klecker et al., 2001), regulating the morphogenesis of the neural tube (Pinson et al., 2000; Kokubu et al., 2004; Carter et al., 2005) (Fig. 9).

WNT signalling is involved in numerous events of animal development and in the maintenance of adult tissue homeostasis. It participates in the formation of neurons from neuronal stem cells, neuronal proliferation, neuron migration and maturation (including axon growth), dendrite formation and synaptogenesis, differentiation (including the proliferation of stem cells and the specification of the neural crest), migration, genetic stability and apoptosis (Mulligan and Cheyette, 2012; Inestrosa and Varela-Nallar, 2015), as well as being involved in the maintenance of adult stem cells in a pluripotent state (Kahn, 2015).

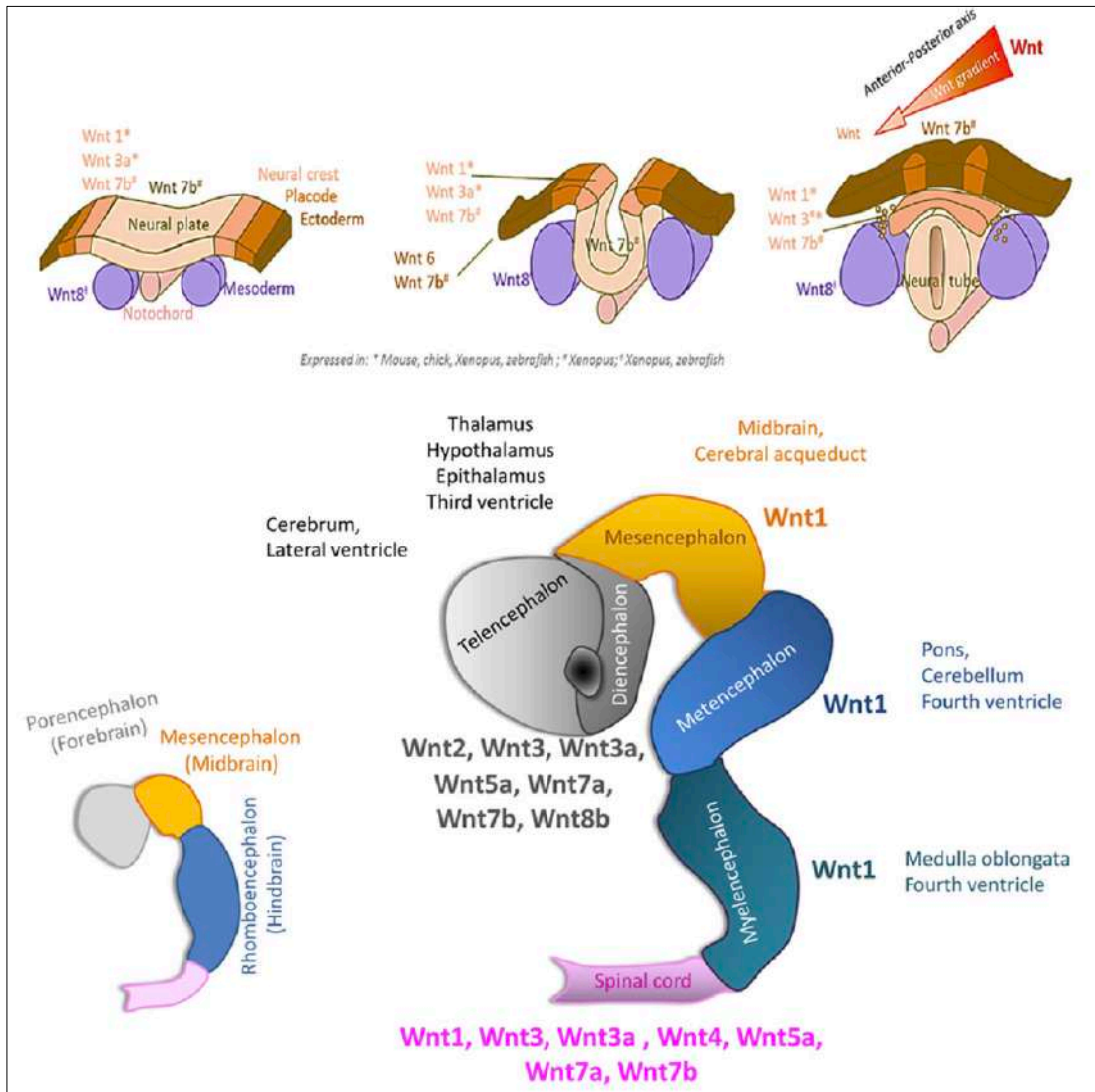


Figure 9. Expression of WNT genes during the brain development process with space-time overlapping of the gene expression pattern (Avagliano et al., 2017).

Our current hypothesis is that CdLS malformations arise from a deregulation of developmental molecular pathways and in this context, our and others previous studies have shown that canonical WNT pathway is perturbed (Pistocchi et al., 2013; Avagliano et al., 2017; Bottai et al., 2019; Grazioli et al., 2021).

WNT intracellular pathway plays a fundamental role in all steps of development of the CNS, and in fact, its alterations have been associated to a plethora of CNS abnormalities (Avagliano et al., 2017).

WNT pathway enclose two categories that differ for the mechanism of the intracellular cascade (Florian et al., 2013; Thrasivoulou et al., 2013): the canonical WNT pathway (Wnt/ β -catenin dependent pathway) and the non-canonical WNT pathway (β -catenin independent pathway). The non-canonical pathway has been further divided into additional branches: the planar cell polarity (PCP) and the Wnt/calcium pathways (Komiya and Habas, 2008).

WNT consists in a group of proteins that pass signals into a cell through cell surface receptors. WNT-proteins bind to a frizzled family receptor (GPCR), which passes the biological signal to the dishevelled protein inside the cell. This leads to β -catenin translocation in the nucleus which in turn regulates key developmental genes expression (Miyabayashi et al., 2007). The non-canonical pathway of WNT (or β -catenin-independent pathway) is known to regulate both cell polarity and movements of dorsal mesodermal cells during convergent extension and later during neural tube closure in vertebrates (Komiya and Habas, 2008; De, 2011).

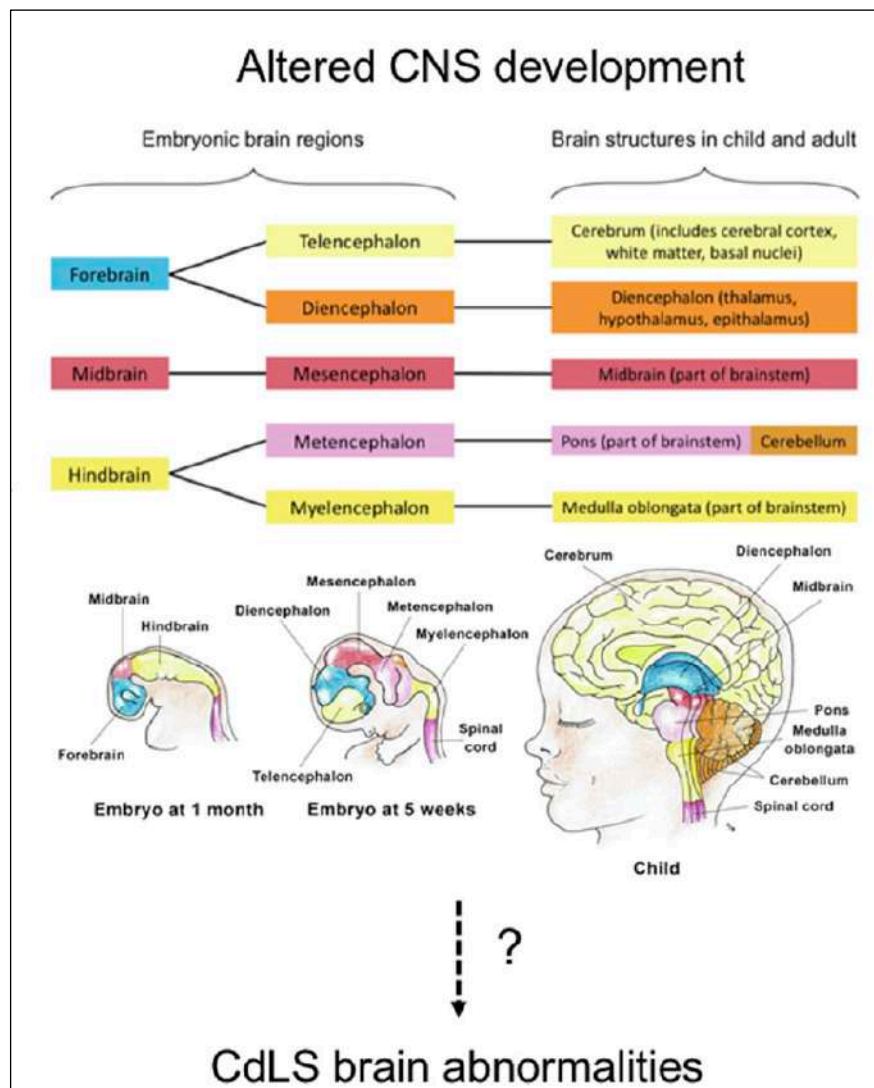
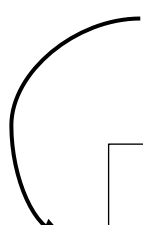
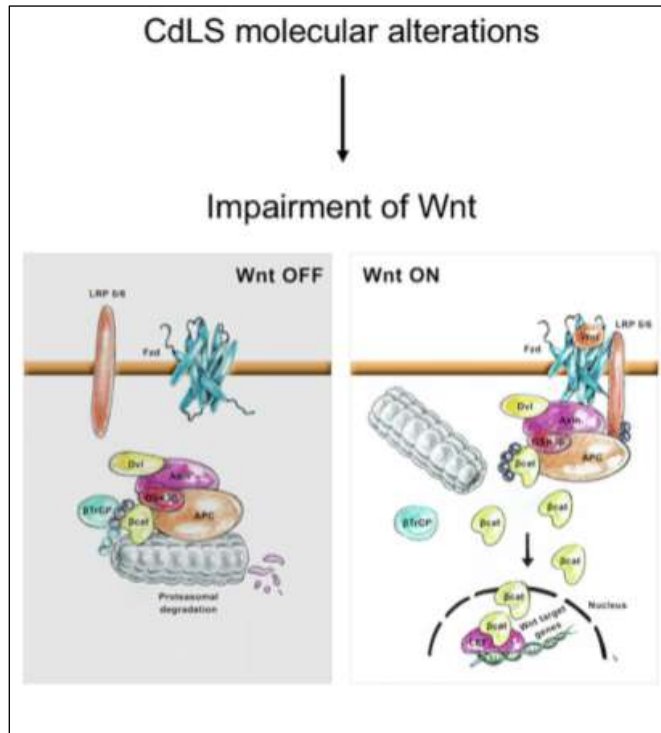


Figure 10. Mutations effects in CdLS genes on the WNT pathway and brain development. WNT pathway consists in a group of proteins that binds to a membrane receptors family known as GPCRs, which pass the biological signal inside the cell, determining the passage of β -catenin in the nucleus and the consequent expression of key developmental genes. The independent β -catenin WNT pathway regulates cell polarity and movements of mesodermal cells, first during extension and then, closure of the neural tube in vertebrates.

Modified from (Avagliano et al., 2017)

β -catenin is a fundamental player of the canonical WNT pathway. When WNT ligands are not bound to the membrane frizzled family receptor, the intracellular level of β -catenin decreases because this protein undergoes proteasomal degradation by the "destruction complex"(Jackstadt et al., 2020). When this situation happens, the mechanism does not allow the nuclear translocation of the β -catenin which finally ends with gene transcription inhibition (MacDonald et al., 2009) (Fig.10).

2. AIM

Pathogenetic variants affecting cohesin complex cause functional alterations and induce an array of congenital pathologies named "cohesinopathies", Cornelia de Lange Syndrome being the commonest among them.

CdLS is a rare condition that leads to multiple malformations with wide variability of expression. CdLS phenotypic features vary from mild to severe and is characterized by different malformations, neurodevelopmental delay and behavior of the autism-spectrum disorder (ASD). The prevalence of specific anomalies affecting the different organs is not well defined yet. The molecular mechanisms underlying the etiopathogenesis are not fully elucidated and this represents one of the main problems that hinder the progress of a possible therapeutic approach, as for many Mendelian genetic conditions. Thus, a deeper understanding of the biology of CdLS is urgently needed to develop much essential targeted therapies.

From a biological point of view, our working hypothesis is that an haploinsufficiency of the cohesins, genetic basis of the syndrome, can lead to a downregulation of the canonical WNT pathway. This alteration can cause a drop of *CylinD1* expression which leads to an increase in cell death at specific times in specific tissues in embryos.

WNT pathway plays a fundamental role in all the steps necessary for the development of the CNS and, has been associated with several brain anomalies, in particular involving structures derived from the hindbrain. WNT signalling is involved in a plethora of developmental events and in the maintenance of homeostasis of adult tissues by regulating cell proliferation, differentiation, cell migration, stability and apoptosis as well as the maintenance of adult stem cells in the state of pluripotency.

Previous studies performed in our laboratories using *in vivo* models of CdLS – *Danio rerio* and *Drosophila melanogaster* – have shown that an alteration of the development of the CNS is correlated to a defective WNT pathway. The results have been confirmed by *in vitro* studies on fibroblasts from CdLS patients.

My PhD project aimed at validating the relevance of canonical WNT pathway and assess possible ameliorative effects of its chemical activation in Lymphoblastoid cell lines from CdLS patients and in an *ex vivo* murine model.

3 Materials and Methods

3.1 Lymphoblastoid immortalized cell lines

Cell culturing

Lymphoblastoid lines (LCL) from patients with different mutations were used: 6 lines from CdLS patients carrying mutations in *NIPBL* (3), *HDAC8* (1) or *SMC1A* (2) (Gervasini et al., 2013)(Table4) and 4 lines from healthy donors (HD) serving as controls. The cell lines were developed in specialized and authorized biobanks (the Gaslini Genetic Bank service - Telethon Network of Genetic Biobanks, Genoa). After immortalization process, mutations were confirmed in Medical Genetic laboratory in collaboration with professor Gervasini, DiSS – Università degli Studi di Milano. Cells were cultured using 25ml flasks in suspension in RPMI-1640 medium supplemented with 20% foetal bovine serum (FBS), 1% penicillin/streptomycin and were maintained at 37°C in a humidified incubator with 5% CO₂. The cells were checked daily and divided as needed (depending on the rate of proliferation) until the exponential growth phase.

<i>Lines</i>	<i>Gene</i>	<i>Exon</i>	<i>Gene mutation</i>	<i>Protein mutation</i>
<i>Sp47</i>	<i>NIPBL</i>	-	<i>t(5;15);inv(5p)</i>	-
<i>Sp11</i>	<i>NIPBL</i>	19	<i>c.4253G>A</i>	<i>p.(Gly1418Glu)</i>
<i>Sp12</i>	<i>NIPBL</i>	4	<i>c.231-2_231-1delAG</i>	<i>p.(Glu78Valfs*4)</i>
<i>Sp35</i>	<i>SMC1A</i>	2	<i>c.173del15</i>	<i>p.(Val58-Arg62)</i>
<i>202</i>	<i>SMC1A</i>	15	<i>c.T2351C</i>	<i>p.(Ile784Thr)</i>
<i>Sp59</i>	<i>HDAC8</i>	10	<i>c.1022delG</i>	<i>p.(Gly341Valfs*33)</i>

Table 4. Patients lines and related mutations (CE approval number 99/20)

Lithium exposure and additional compounds

Cells were exposed to a canonical WNT pathway activator, lithium chloride (LiCl, PM 42.39 g/mol). I used three different concentrations: 1 mM, 2.5 mM, and 5 mM (Abu-Baker et al., 2013) or water (vehicle) as control. Lithium solution was freshly prepared for use. In addition, we used 4 other WNT activators compounds: BIO (6-bromoindirubin-3'-oxime) (0.1 μ M, 0.5 μ M, and 1 μ M); IQ-1 (5 μ M, 10 μ M, and 20 μ M); Deoxycholic acid (DCA) (5 μ M, 100 μ M, and 250 μ M); and CHIR99021 (1 μ M, 5 μ M, and 10 μ M) (Pai et al., 2004b; Naujok et al., 2014a; Rieger et al., 2016) or water/DMSO (vehicle) as control. Cells were treated for 24 hours during exponential phase of growth and counted at 2 different timepoints: before and after chemical exposure (0, 24 hours). Proliferation/death rates were measured counting cells upon trypan blue staining ($cells\ n^{\circ} \times dilution\ (2) \times ml \times 10^4$) using Bürker chamber to evaluate compounds' effects on viability and cytotoxicity (Fig. 11).

TUNEL assay

Apoptosis rate in LCLs was evaluated using terminal deoxynucleotidyl transferase (TdT) dUTP Nick-End Labeling (TUNEL) assay, designed to detect apoptotic cells during the late stages of apoptosis, as previously described (Bottai et al., 2019). Cells were cytopinned on glass slides (50 μ l per field) and then fixed with 4% paraformaldehyde PFA for 10 minutes at room temperature (RT) and washed three times in phosphate buffer saline (PBS) for 5 minutes. Staining for apoptotic cells was performed using the AP-*In situ* Cell Death Detection Kit (Roche Diagnostics, Penzberg, Germany) following manufacturer's protocol. Slides were mounted for microscope imaging with homemade glycerol based mounting media with DABCO (1,4-diazabicyclo [2.2.2]octane) as anti-fading compound. Apoptotic cells were detected with NanoZoomer-XR Digital slide scanner (Hamamatsu, Japan) for counting.

Immunofluorescence assay

For assessing cell proliferation rate, Ki67 immunoassay (Gerdes et al., 1984) was used. Cells were cytopinned on glass slides (50µl per field) and then fixed with 4% paraformaldehyde PFA for 10 minutes at RT and washed three times in PBS for 5 minutes. Cells were permeabilized using PBS Triton X-100 (PBT) 0,5 % for 15 minutes and then aspecific sites were blocked with PBT 0,25 % + Foetal Bovine Serum (FBS) 10%, for 1 hour at RT. Slides were stained with anti-Ki-67 primary antibody (1:250, #9129 (D3B5), Cell Signaling) overnight at 4°C, followed by 3 washes and then incubation with Alexa-488 anti-rabbit secondary antibody (1:1000, #6441-30 SouthernBiotech) for 2 hours. Slides were mounted for microscope imaging with EverBrite Hardset Mounting Medium with DAPI (#23004, Biotium) and positive cells were detected and acquired with NanoZoomer-XR Digital slide scanner (Hamamatsu, Japan) for counting.

qPCR analysis

RNA was extracted with Trizol (Sigma Aldrich, Italy) following the manufacturer's protocol. First strand cDNA was synthesized using SensiFAST™ cDNA Synthesis Kit (#BIO-65054, Bioline, Italy) following manufacturer's protocol. qPCR was carried out using *TB Green* Premix Ex Taq (Tli RNase H Plus) (#RR420A, Takara Bio Inc., Kusatsu, Japan) and the *Applied Biosystems StepOnePlus™ Real-Time* PCR System (Thermo Fisher Scientific, Waltham, MA, United States). Primers used are reported in (Table 5). Each sample was assayed in technical triplicates and *CCND1* levels were quantified relatively to the expression of *GAPDH* gene. Data are shown as fold change, calculated as $2^{-\Delta\Delta Ct}$.

<i>Homo sapiens</i> qPCR primers	
<i>CCND1_Fw</i>	CTGGAGGTCTGCGAGGAA
<i>CCND1_Rv</i>	GGGGATGGTCTCCTTCATCT
<i>GAPDH_Fw</i>	GAGTCAACGGATTTGGTCGT
<i>GAPDH_Rv</i>	TTGATTTTGGAGGGATCTCG

Table 5. Primers used for *Homo sapiens* qPCR analyses.

3.2 FUCCI2 murine primary cultures

For modelling CdLS in primary neurons from mouse cerebellum, neurons from day2 transgenic mice pups FUCCI2 (Fluorescence Ubiquitin Cell Cycle Indicator) were harvested from cerebellum and cultured in collaboration with professor Bollini, DIMES – Università degli Studi di Genova. FUCCI2 technology makes possible the distinction between live cells in the G(1) and S/G(2)/M phases by dual-colour imaging. Cells were cultured in adhesion, first using Neurobasal Plating Media (Neurobasal Media containing B27 Supplement, 0.5 mM Glutamine Solution, 25 µM Glutamate, Penicillin (10,000 units/ml)/Streptomycin (10,000 µg/ml), 1mM HEPES, 10% Heat Inactivated Donor Horse Serum) and then using Neurobasal Feeding Media (Neurobasal Media containing B27 Supplement, 0.5 mM Glutamine Solution, Penicillin (10,000 units/ml)/Streptomycin (10,000 µg/ml), 1 mM HEPES). Cells were maintained at 37°C in a humidified incubator with 5% CO₂ (Fig. 11).

Brain dissection and cell culturing

Neurons from day2 FUCCI2 pups were harvested from cerebellum and cultured. The cerebellum from different pups was first isolated, then they were pooled in

a 1.5ml vial with cold Hanks' Balanced Salt Solution (HBSS) and kept on ice. Collected all the organs, HBSS was removed and a solution with 500µl of HBSS and 200µl of trypsin was added. After an incubation for 15 minutes at 37°C, a cold HBSS wash was performed and then added the plating medium. Finally, tissue was mechanically disrupted to single cells, which were placed in a coated polyethyleneimine (PEI) support using the plating medium. After at least 3 days – only checking daily – half volume of culture medium was changed with neurobasal feeding medium and the process was repeated twice a week.

Then, cells were exposed to different conditions:

1. FUCCI2
2. FUCCI2 + 5 µl of DMSO (PCI-34051 vehicle)
3. FUCCI2 + PCI-34051 5 µM
4. FUCCI2 + PCI-34051 5 µM + LiCl 3 mM

Drugs were added after 2-3 days, when cells were attached.

Immunohistochemistry assay

Following 18-20 days of culture, to evaluate presence of neuronal marker, DAB (3,3'-Diaminobenzidine) (Vector Laboratories, Inc., Burlingame, VCA 94010) assay was performed. Slides were stained with anti-*Tuj1* primary antibody (neuron-specific class III beta-tubulin) (1:1000) overnight, followed by incubation with ABC solution (avidin-biotin complex) (Vectastain ABC kit) for 1 hour. After 3 washes, slides were incubated in a peroxidase substrate solution (DAB, Vector Laboratories, Inc., Burlingame, VCA 94010) for a maximum of 20 minutes. Slides were mounted for microscope imaging.

Immunofluorescence assay

For assessing cell differentiation rate, immunoassay was performed. Slides were stained with primary antibody anti-*Tuj1* (1:1000) and anti-GFP (1:500) overnight,

followed by incubation with anti-mouse Alexa555 and anti-rabbit Alexa488 secondary antibodies (1:1000) for 2 hours. Slides were mounted for microscopic imaging with EverBrite Hardset Mounting Medium with DAPI and positive cells were detected and acquired with Confocal Microscope (Nikon A1R).

3.3 Data analysis and statistics

LCL counting were made picking three randomly selected fields per experimental group (20X magnification), and positive cells were calculated by counting within the three fields, by two operators blinded to experimental groups. Sample size was determined considering two independent study groups, with primary end point continuous (mean), with α error: 0.05, β error 0.2 and power: 0.8. MRI data from CdLS patients were analysed using Fisher test. For all the analyses, $p \leq 0.05$ (*) was set as statistically significant, $p \leq 0.01$ (**), $p \leq 0.005$ (***). Graphs were made using GraphPad Prism 7 and figures were assembled using either GIMP-2.1 or Adobe Photoshop CC. qPCR data for LCL were analysed with student's unpaired t-test.

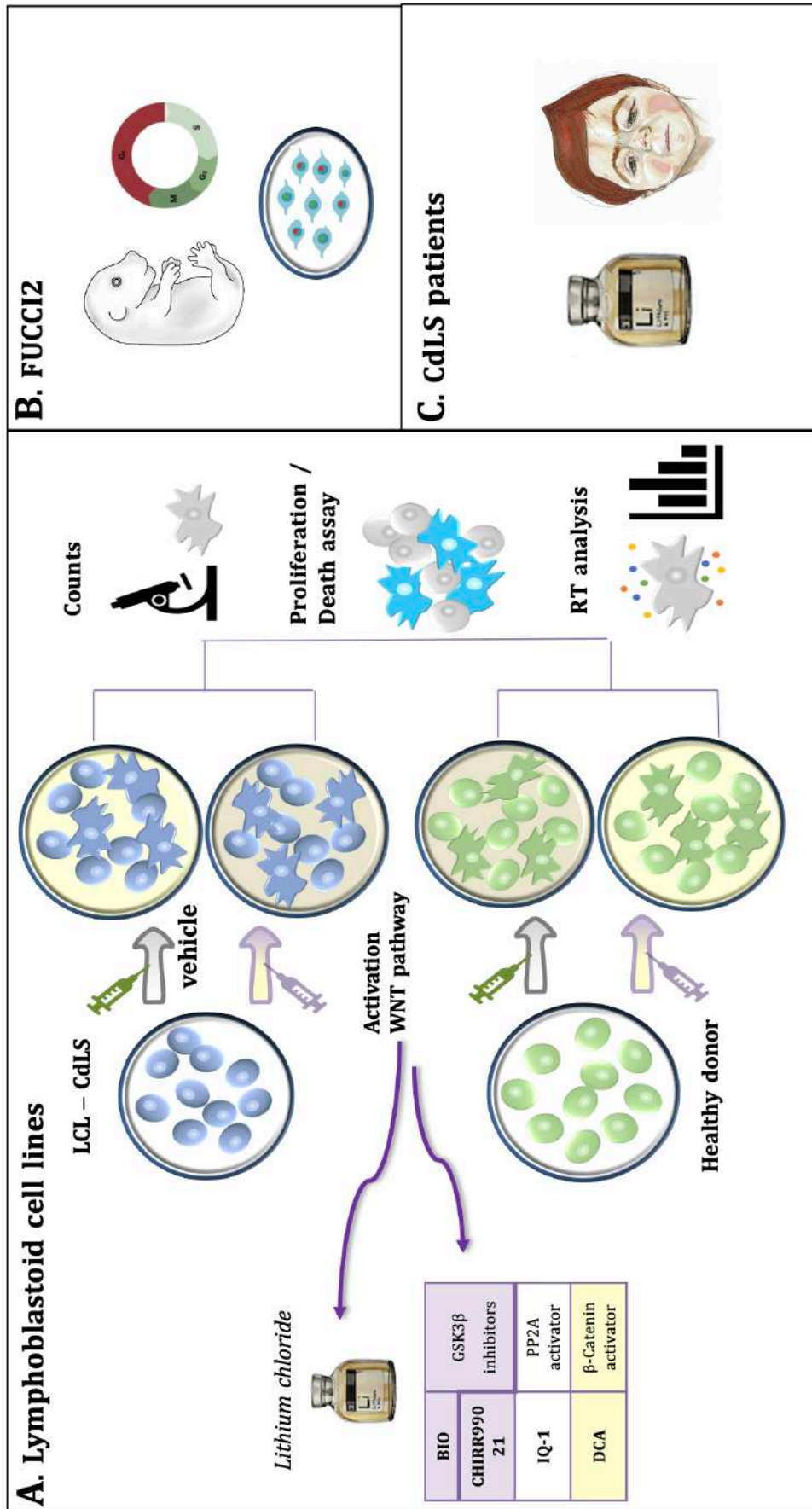


Figure 11. Materials and Methods

(A) LCL-CdLS and HD lines were cultured and exposed to different doses of lithium chloride (LiCl), and other known WNT modulating compounds (BIO, IQ-1, DCA and CHIR99021) for rescuing pathway downregulation. Cells were treated for 24 hours during exponential phase of growth and counted before and after chemical exposure. Cell death and proliferation assays (TUNEL test and Ki67 immunostaining) were performed. qPCR real-time gene expression analysis has been assessed to quantify the downstream targets of the WNT pathway. (B) Neuronal primary cell cultures derived from 2days pups of Fucci2 transgenic mouse model have been evaluated. (C) The ultimate aim is the clinical trial with CdLS patients.

3.4 SALIVA MOLECULAR TESTING FOR SARS-CoV-2 INFECTION

Protocol to detect SARS-CoV-2 infection

To detect severe acute respiratory syndrome coronavirus 2 (SARS-CoV-2), saliva sampling was used. Saliva was collected with two methods.

1. a sterile dental cotton roll was used and it was kept for at least one minute next to lower premolar-molar area in the vestibular space (Fig. 12). Once properly soaked in saliva, the dental roll was stored in a sterile 50 ml tube, at RT until analysis process (stable up to 7 days).

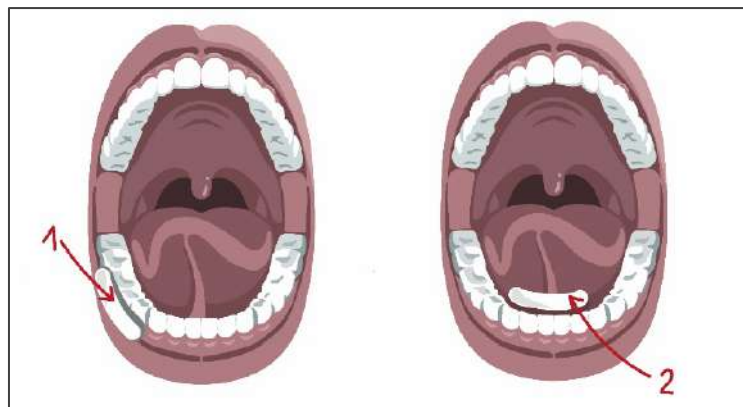


Figure 12 - Cotton dental roll for saliva self-collection (Borghini et al., 2021)

Saliva was processed under sterile conditions and recovered by using a 10 ml syringe for squeezing the cotton roll.

2. LolliSponge™ device was used and it was held in the mouth allowing the sponge to soak the saliva for a minute. The device could be safely stored in a collection tube and the contact between the hands and the sponge was avoided. Saliva sample could be kept at RT and being the saliva self-preserving, without the aid of a transport medium. LolliSponge™ was centrifuged for 1 min at 500 × g and saliva was recovered.

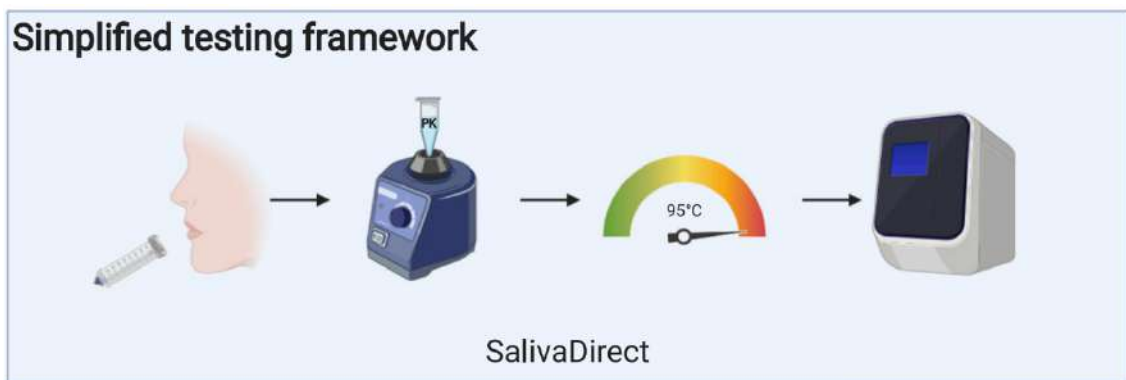


Figure 13. Saliva Direct Protocol (modified from Vogels et al. 2020)

The saliva collected was processed as recommended by Vogels et al (Vogels et al., 2020), making a modification of the thermocycler profile which foresees a passage of 5' at 95 ° C followed by 5' at 4 ° C (Fig.13). After inactivation in pk, 5µl of saliva were used for RT-qPCR for simultaneous detection of N1 (FAM probe), N2 (SUN) and human RNase P genes (RP, ATTO647) (Table 6) using the protocol published by the Centers for Disease Control (Real-time RT-PCR Primers and Probes for COVID-19 | CDC)(Borghi et al., 2021). The sample in which N1 and / or N2 is detected (Ct <40) are positive. Invalid samples were evaluated by RP (Ct > 35).

Description	Oligonucleotide Sequence (5'>3')
2019-nCoV_N1 Forward Primer	GAC CCC AAA ATC AGC GAA AT
2019-nCoV_N1 Reverse Primer	TCT GGT TAC TGC CAG TTG AAT CTG
2019-nCoV_N1 Probe	FAM-ACC CCG CAT TAC GTT TGG TGG ACC-BHQ1
2019-nCoV_N1 Probe	FAM-ACC CCG CAT /ZEN/ TAC GTT TGG TGG ACC-3IABkFQ
2019-nCoV_N2 Forward Primer	TTA CAA ACA TTG GCC GCA AA
2019-nCoV_N2 Reverse Primer	GCG CGA CAT TCC GAA GAA
2019-nCoV_N2 Probe	FAM-ACA ATT TGC CCC CAG CGC TTC AG-BHQ1
2019-nCoV_N2 Probe	FAM-ACA ATT TGC /ZEN/ CCC CAG CGC TTC AG-3IABkF
RNase P Forward Primer	AGA TTT GGA CCT GCG AGC G
RNase P Reverse Primer	GAG CGG CTG TCT CCA CAA GT
RNase P Probe	FAM – TTC TGA CCT GAA GGC TCT GCG CG – BHQ-1
RNase P Probe	FAM-TTC TGA CCT /ZEN/ GAA GGC TCT GCG CG-3IABkFQ

Table 6 . (Real-time RT-PCR Primers and Probes for COVID-19 | CDC).

4. Results

4.1 Lithium restores proliferation rate in CdLS lymphoblastoid cell lines

I studied lymphoblastoid cell lines from CdLS patients and healthy donors to evaluate possible ameliorative effects of lithium treatment in patients *in vitro*. As expected (Yuen et al., 2016), I observed, when compared to control lines, a reduced proliferation rate in CdLS patient-derived cells (Kline et al., 2017). Interestingly, proliferation of CdLS cells was significantly increased upon lithium exposure (Fig. 14, 15A and 16A, B).

CdLS lines were exposed to different concentrations of lithium chloride (LiCl, 1 mM, 2.5 mM, and 5 mM). Interestingly, upon LiCl exposure, proliferation in CdLS cells was increased (Fig. 14, 15A and 16A, B). Very intriguingly, patient-derived cells - light blue bars - showed a significant increase in proliferation after exposure to LiCl compared to the untreated cells, and also compared to lithium-exposed healthy donor lines (HD) (Fig. 14, 15A and 16A, B).

Such ameliorative effects mediated by WNT activation was confirmed evaluating *Cyclin D1* expression. *Cyclin D1* is a well-known gene target of WNT canonical pathway and is required for progression through the G1 phase of the cell cycle, regulating proliferation. *Cyclin D1* showed a trend of increased expression following lithium exposure in CdLS cell lines (Fig. 15C).

Cyclin D1 expression increased with a significant p-value ≤ 0.01 in both lines with mutation in *SMC1A*. Similarly, *Cyclin D1* expression significantly increased in all three lines with mutation in *NIPBL*: we observed a significant increase in p-value ≤ 0.05 in two lines and in p-value ≤ 0.005 in the third cell line derived from the patient. The *HDAC8* did not show statistical significance.

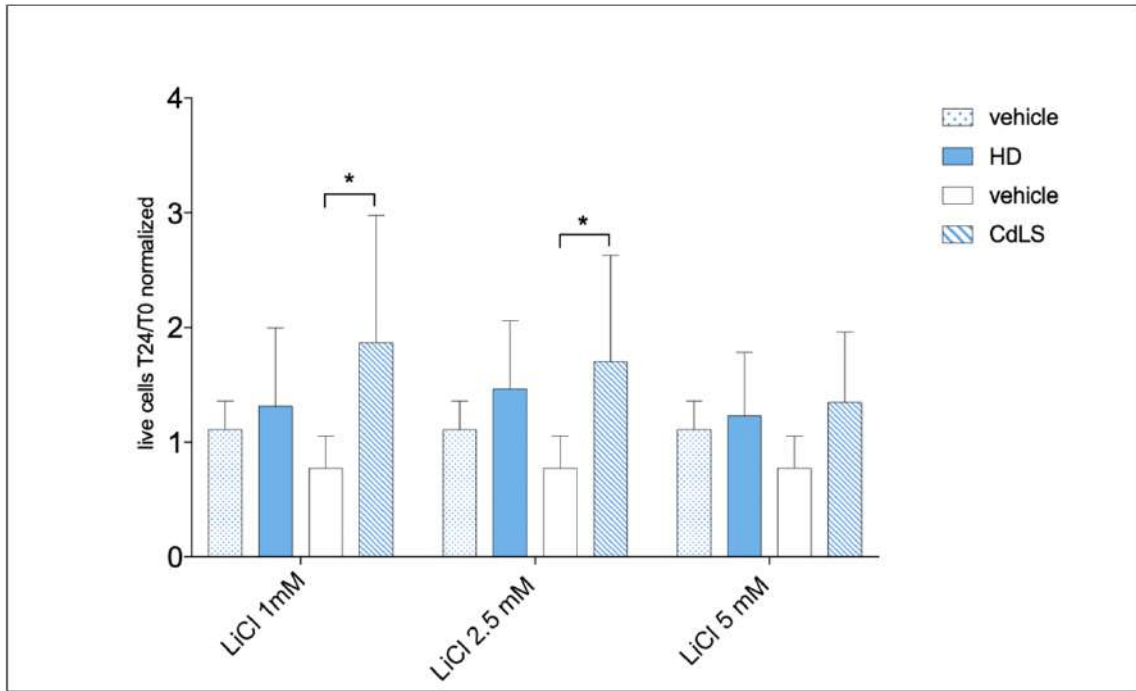


Figure 14. Lithium rescues cell survival in CdLS LCLs through WNT activation using different concentrations

(A) Proliferation of patient-derived cells (CdLS H₂O, white bar) is reduced compared to the proliferation rate of controls (HD H₂O, dots white bar). All CdLS lines (striped bar) exposed to lithium chloride (1mM, 2.5 mM and 5mM) showed increased proliferation compared to untreated CdLS cells (CdLS H₂O, white bar) and compared to treated HD cells (solid blue bar). Data are shown as fold change, calculated as $2^{-\Delta\Delta Ct} \pm SD$. $p \leq 0.05$ (*), $p \leq 0.01$ (**), $p \leq 0.005$ (***)

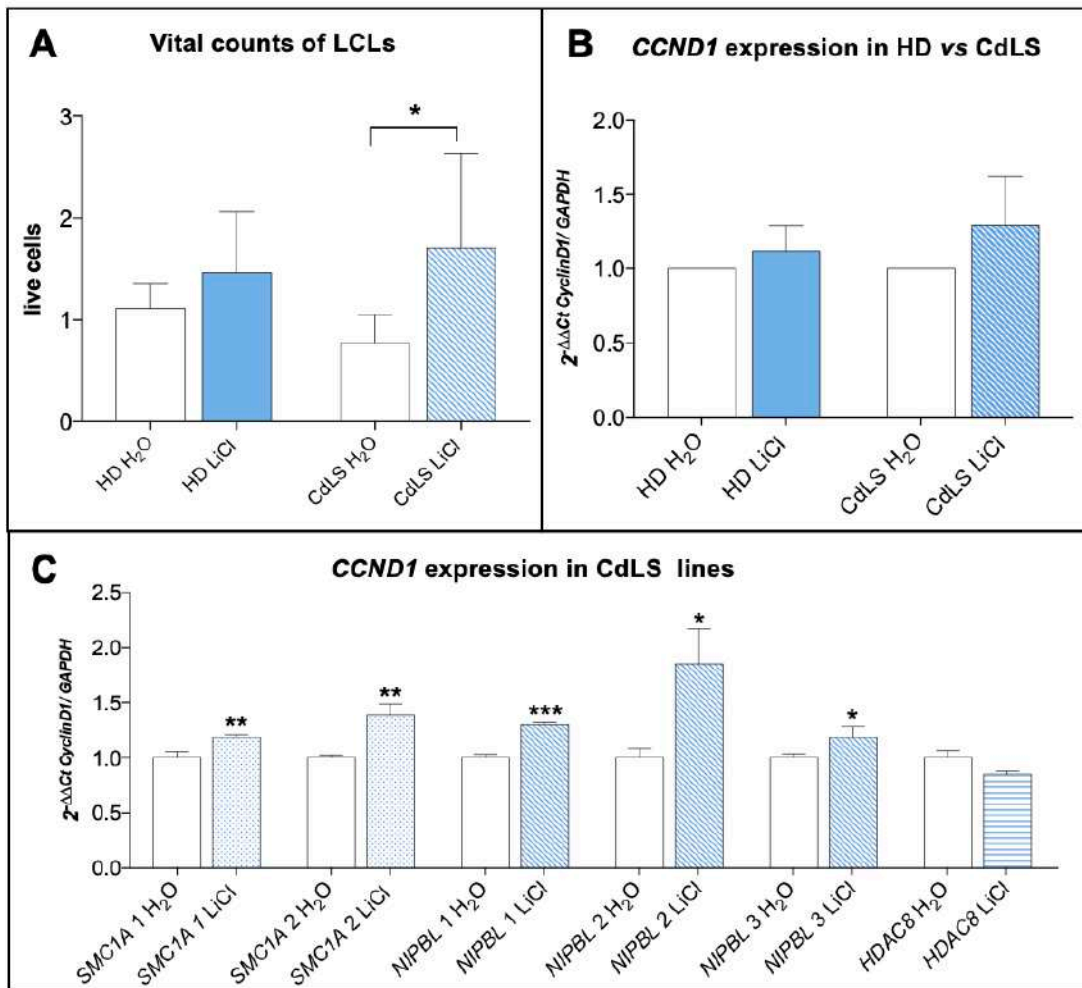


Figure 15. Lithium rescues cell survival in CdLS LCLs through WNT activation

(A) Proliferation of patient-derived cells (CdLS H₂O, white bar) is reduced compared to the proliferation rate of controls (HD H₂O, white bar). All CdLS lines (striped bar) exposed to lithium chloride (2.5 mM) showed increased proliferation compared to untreated CdLS cells (CdLS H₂O, white bar) and compared to treated HD cells (solid blue bar). (B-C) CyclinD1 gene expression was significantly increased upon lithium exposure (2.5 mM) in LCLs, especially in CdLS lines (SMC1A: blue dotted bars, NIPBL: blue oblique bars) except for HDAC8 (blue horizontal bar). (B) In pulled CdLS lines (blue striped bar) CyclinD1 gene expression was increased upon lithium exposure (2.5 mM) compared to controls (blue solid bar). (C) CdLS lines are shown separately. Data are shown as fold change, calculated as $2^{-\Delta\Delta Ct} \pm SD$. $p \leq 0.05$ (*), $p \leq 0.01$ (**), $p \leq 0.005$ (***)

Importantly, these effects on proliferation rate were associated with changes in cell death and assay analyses showed a decrease in death in cells derived from patients treated with lithium (Fig. 16C-D). Remarkably, lithium exposure showed an increase in proliferation in vital count mirrored by a trend in decrease of cell death in patient-derived cells, both compared to untreated cells or to HD control lines.

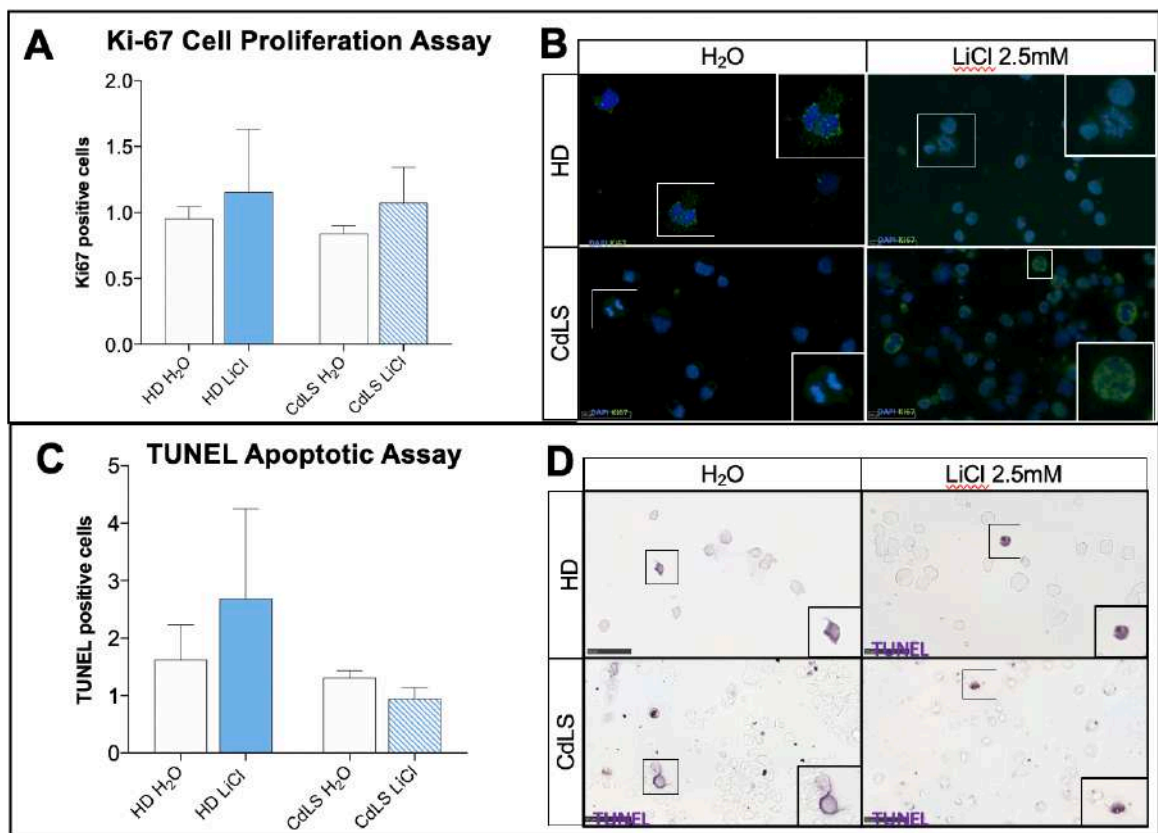


Figure 16. Viability in CdLS LCLs through WNT activation

(A, B) Proliferation assay using Ki-67 was performed to evaluate the viability in CdLS LCLs compared to healthy donors (HD). (A) In standard conditions, the proliferation of patient-derived cells (CdLS H₂O, white bar) is reduced compared to the proliferation rate of healthy donors (HD H₂O, white bar). CdLS cell lines (blue striped bar) exposed to LiCl (2.5mM) have an increased proliferation compared with untreated CdLS cells (CdLS H₂O, white bar) and treated HD cells

(blue solid bar). On the axis are reported: the experimental groups (x-axis), and numbers of cells in proliferation at 24 hours of lithium exposure, normalized on water/vehicle (y-axis). Bars express mean \pm SEM. (B) Examples of cells in proliferation following Ki-67 immunoassay. Images were taken at 40X, while insets display magnification of the white square (80X). (C, D) TUNEL assay was used to evaluate cytotoxicity in CdLS LCLs compared to healthy donors (HD). (C) Upon lithium exposure, CdLS cell lines (blue striped bar) show a decrease in cell death compared to untreated CdLS cells (CdLS H₂O, white bar) and treated HD cells (blue solid bar). On the axis are reported: the experimental groups (x-axis), and numbers of TUNEL positive cells at 24hours of lithium exposure, normalized on water/vehicle (y-axis). Bars express mean \pm SEM. (C) Examples of positive TUNEL cells. Images were taken at 40X, while insets display magnification of the white square (80X). Scale bar represents 50 μ m.

4.2 Wnt activators restores proliferation in CdLS lines

The same positive effects on proliferation rate were observed exposing the cell lines to other chemical compounds such as BIO, IQ-1 (Rieger et al., 2016), DCA (Pai et al., 2004a) and CHIR99021 (Naujok et al., 2014b) with known WNT-activation effects (Fig. 17A-D).

These chemical compounds activate the canonical WNT pathway on different levels (Table 7) and we can observe a significantly increase in proliferation using different concentrations.

BIO and CHIR99021 are GSK3 β inhibitors. When chemical inhibition of GSK3 β occurs, it leads to a pharmacological activation of the canonical WNT signalling pathway. However, the compound to be used in a study must be carefully selected as small molecules can exhibit cytotoxicity, side effects and differ in activity. DCA increase tyrosine phosphorylation of β -Catenin. IQ-1 is a cell-

permeable compound that works as specific inhibitor of p300/ β -Catenin interaction: IQ-1 modulates Wnt/ β -catenin signalling by targeting a subunit of PP2A and thereby blocking PP2A/Nkd complex formation, resulting in diminished β -catenin/p300 interaction.

BIO showed a significance of $p \leq 0.05$ in increased cell proliferation in CdLS patient-derived lines after exposure, using different concentrations: 0.1uM, 0.5uM and 1uM. Likewise, CHIR99021 exhibited the same significance (≤ 0.05) with all three concentrations – 1uM, 5uM and 10uM.

Upon cells exposure to DCA 5uM concentration, we observed a higher significant increase equal to $p\text{-value} \leq 0.01$. Exposure to a concentration of 100uM lead to a significance equal to $p\text{-value} \leq 0.05$. We did not find a significant increase in proliferation rate using 250uM concentration.

IQ-1 showed a similar trend with the other activator compounds. We observed an increase in cell proliferation using different concentrations (1uM, 10uM and 20uM) compared to untreated patients-derived lines.

Compound	Level of action
BIO	GSK3 β inhibitors
CHIR99021	GSK3 β inhibitors
IQ-1	PP2A activator
DCA	β -Catenin activator

Table 7. WNT activators compounds.

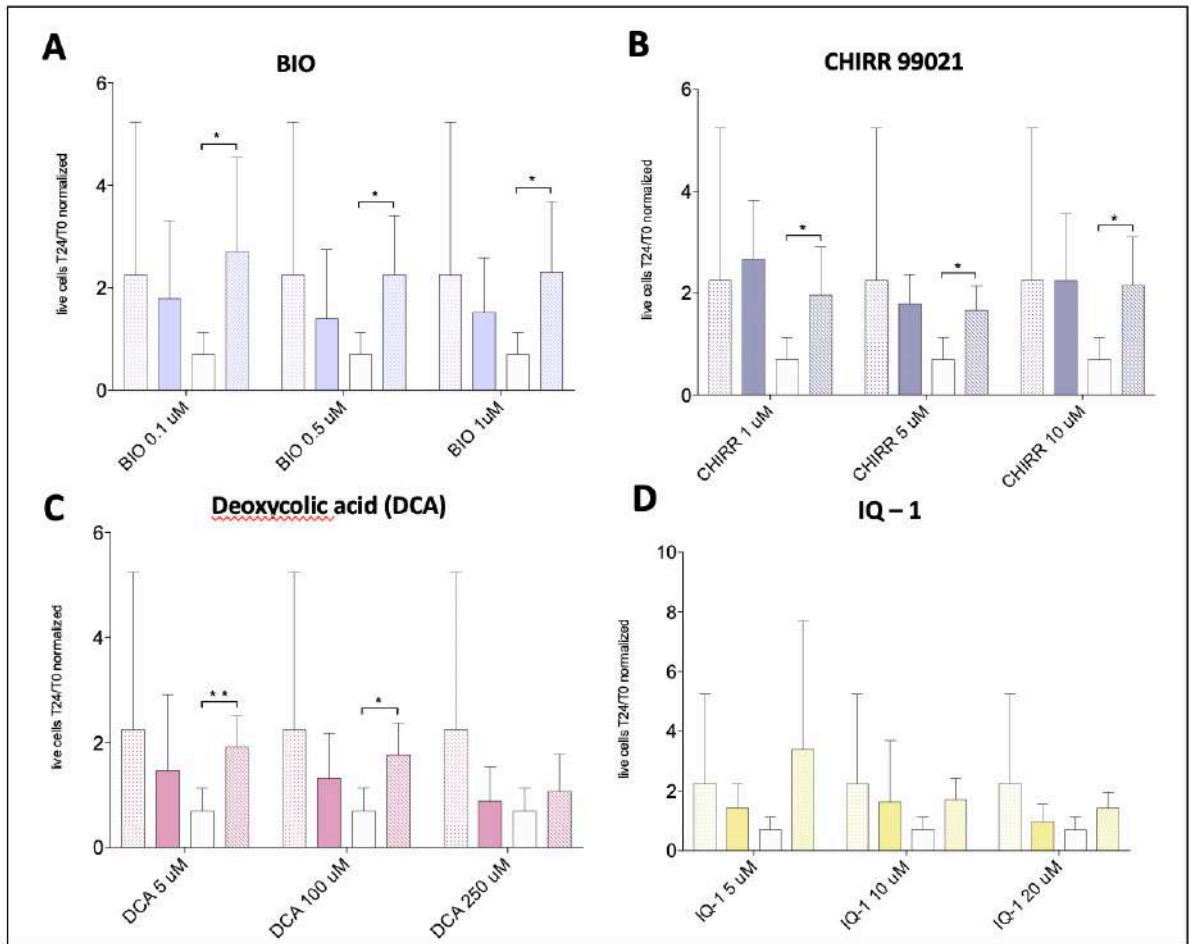


Figure 17. Vital counts of LCLs.

(A-D) Treatments with others WNT pathway activators are shown (HD untreated: dotted bars; treated HD: solid-colored bars). Untreated CdLS cells (white bars) are exposed to different concentrations of the compounds (oblique striped bars). Treatments with (A) BIO 0.1 μM , 0.5 μM , 1 μM ; (B) CHIR99021 1 μM , 5 μM , 10 μM ; (C) Deoxycolic acid 5 μM , 100 μM , 250 μM (D) IQ-1 5 μM , 10 μM , 20 μM are represented. On the axis are reported: the experimental groups (x-axis), and numbers of number of live cells at 24 hours of exposure divided by number of live cells at T0, normalized on water/vehicle (y-axis). * $p < 0.05$, ** $p < 0.01$.

4.3 Lithium restores neuronal rate differentiation in Fucci2 primary cultures

Performing immunostaining for neuron-specific class III beta-tubulin (*Tuj1*) on Fucci2 primary cultures, I confirmed that LiCl treatment restores the rate of neuronal differentiation, compared to where the HDAC8 inhibitor was present – mimicking CdLS (Fig. 18).

Beta-tubulins are one of two structural components that form microtubule network. Beta tubulin III is specifically localized to neurons and beta III tubulin's expression correlates with the earliest phases of neuronal differentiation. For this reason, we used beta tubulin III that has implications in neurogenesis, axon guidance and maintenance.

Immunofluorescence showed a normal neuronal rate in Fucci2 when not treated (Fig 18 A, B). The presence of the vehicle did not interfere with the neurons capability to differentiate (Fig. 18 C, D). Instead, we observed a reduced neuronal differentiation with *HDAC8* inhibitor.

Upon PCI-34051 (5uM) treatment we observed an inhibition effect on neuronal differentiation (Fig. 18 E,F).

Remarkably, rate of neuronal differentiation rescue following exposure to lithium (3mM) in combination with PCI-34051 (Fig. 18 G,H).

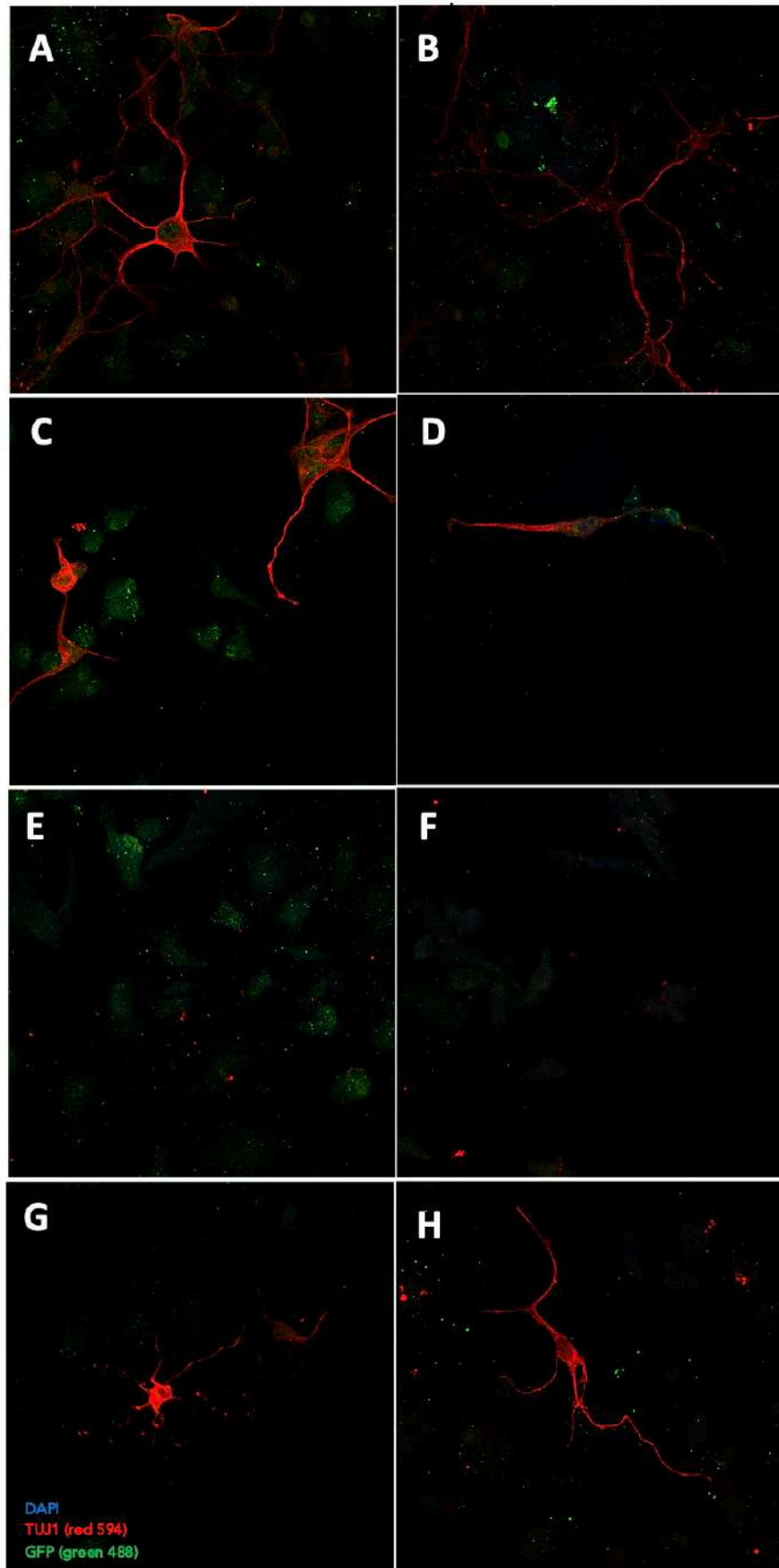


Figure 18. Immunostaining for Tuj1 on FUCCI2 primary cultures

(E-H) Treatments with PCI-34051 and lithium. Examples of cells in neuronal differentiation following Tuj1 immunoassay. (A,B) FUCCI2, (C,D) FUCCI2 + DMSO, (E,F) FUCCI2 + PCI-34051 5 μ M and (G,H) FUCCI2 + PCI-34051 5 μ M + LiCl 3 mM. (A-H) Cell nuclei are displayed in blue (DAPI); neurons in red (TUJ1); green signal is present during S and G2 phases and it disappears rapidly in M phase (GFP). Images were acquired at 63X.

CdLS patients

Considering the results obtained in our previous studies, with our clinical collaborators we decided to evaluate the presence of malformations in the CNS in a cohort of CdLS patients. Correlations between CNS malformations and clinical symptoms, such as severity of intellectual disability, presence of epilepsy, behavioural problems or other major malformations, in particular reducing defects in the limbs, were evaluated.

Analysis of the cases showed a statistically significant correlation between CNS anomalies, in particular of the structures of the posterior cranial fossa of rhombencephalic derivation, and the presence of autistic traits.

These findings represent an element in support of the potential relationship between cerebellar anomalies and behavioural issues in CdLS patients. They further support that brain malformations in CdLS subjects are secondary to an abnormal expression of the WNT pathway. It is known that WNT plays a fundamental role in the development of the CNS but in particular of the hindbrain (Avagliano et al., 2017).

4.4 CLINICAL TRIAL DESIGN

Cornelia de Lange Syndrome: assessing positive effects of Lithium treatment – CloSER

The purpose of this study is to evaluate the effectiveness of lithium carbonate therapy on behavioural modifications in patients with CdLS (Fig. 19). The proposal is to perform a multicentre, non-commercial pilot clinical study. The specific objectives are as follows:

Primary outcomes

Improvement in the following parameters:

- ◆ Behaviour assessed using *the Aberrant Behavior Checklist* (ABC scale1) which measures psychiatric symptoms and behavioural disorders even in patients with intellectual disabilities;
- ◆ *SCQ questionnaire* (SCQ; Rutter, Bailey & Lord, 20032) to assess communication skills and social functioning;
- ◆ *Childhood Autism Rating Scale* (CARS 2 -T3) for the assessment of autistic behaviour;
- ◆ Cognitive Performance through the *Leiter scale* (Leiter-R, Roid & Miller, 19974), a non-verbal scale that can be used for subjects between 2 and 20 years of age.
- ◆ *Vineland Adaptive Behavior Scales 2* to also evaluate the adaptive functioning in the different areas (motor, communication, autonomy, socialization). Furthermore, for very serious patients, for whom a direct evaluation with the Leiter might be insignificant or impossible, it would allow to have adaptation quotient (QD).

Secondary outcomes

To evaluate improvement of the following parameters:

- ◆ Sleep quality through the Sleep disturbances scale for children (SDSC5), to be administered to parents; there are two versions, one for subjects between 6-16 years, the other for children 3-6 years;
- ◆ Impression of Change Clinical Global Impression of Change (CGI-C) filled in by the clinician at each visit;
- ◆ Improvement of the quality of life through Pediatric Quality of Life Inventory (PedsQL6);
- ◆ Specific biomarkers (TBARS - thiobarbituric acid reactive substance assay) used to measure lipid peroxidation in cell, tissue, and biological fluid extracts.

Study centres and number of subjects

It is planned to enrol at least 15 subjects affected by CdLS, belonging to the Childhood Epilepsy-Neuropsychiatry Center of the A.O. San Paolo ASST-Santi Paolo e Carlo of Milan, at the U.O. Department of Pediatrics of the ASST Lariana and the Child and Adolescent Neuropsychiatry Operating Unit (UONPIA) IRCSS Ca 'Granda Foundation Ospedale Maggiore Policlinico di Milano. The laboratory analysis will be carried out at the ASST-Santi Paolo e Carlo laboratories in Milan and the Applied Biology laboratories of Prof. Valentina Massa at the Department of Health Sciences, Università degli Studi di Milano.

Inclusion criteria

The patient must meet all the following inclusion criteria to be eligible for study participation:

- ◇ Age > 4 years
- ◇ Body weight within the normal range in the reference range for CdLS, based on age and height;

- ◇ Diagnosis of CdLS based on consensual clinical criteria and a confirmed mutation in the *NIPBL* gene;
- ◇ Stable medication treatment for 4 weeks before starting the study;
- ◇ Written consent signed by the parent / legal guardian / representative prior to the screening visit;
- ◇ Ability to take study drug provided in capsules or drops (for younger patients and those with swallowing difficulties) or combined with food / drink
- ◇ The caregiver must be able to understand the instructions and consciously participate in the study.

Exclusion criteria

The presence of one of the following cases excludes a patient from participation in the study:

- ◇ The patient is participating in another clinical trial;
- ◇ QT interval prolongation, thyroid dysfunction, renal or hepatic insufficiency, leukopenia or other currently clinically significant medical disorders (determined by the investigator), in addition to those directly related to CdLS;
- ◇ QTcF interval on ECG greater than 450 msec;
- ◇ Severe diabetes mellitus or hereditary metabolic dysfunction.

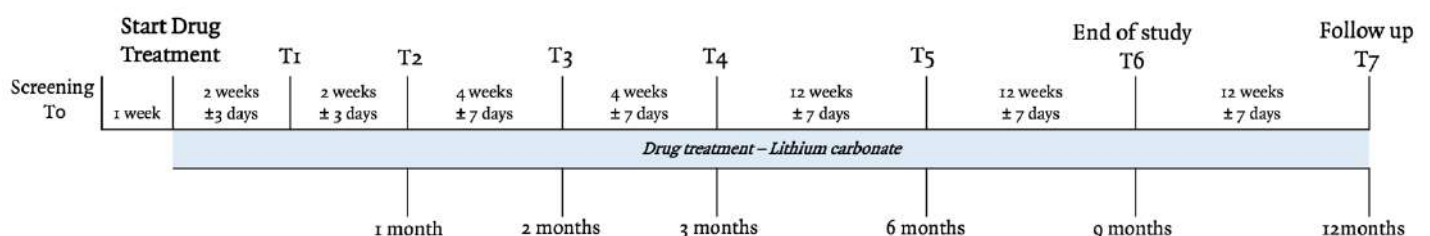


Figure 19. Study design: 52-week prospective treatment study to evaluate the efficacy of lithium carbonate in CdLS.

Patients will receive a drug supply at T0 for the following 2–4-week period. Dose titration to dose level 2 should be completed by day 15. If there are no tolerability issues, patients will continue with the maximum tolerated dose (MTD) even if it represents the final dose. Patients will receive a supply of study drugs at each visit. The date, time and number of capsules administered by the caregiver will be recorded on the Case Report Form (CRF). If intolerance develops at any time during the study, the investigator can reduce the patient's dose by interrupting the single dose and dosing every other day. Patient unable to tolerate treatment even after dose interruption should be discontinued from the study.

Whenever the patient access to the hospital for a visit, a saliva collection for SARS-CoV-2 detection using LolliSponge™ will be performed, if pandemic is still ongoing.

Sample size

The study foresees the enrolment of at least 15 patients. The sample was calculated based on the expected changes in the Biomarker levels (5% difference on the average of the general population 0.374 StDev 0.02, alpha 0.05, power 80%, n = 9) and the expected changes in the scales used (15% mean difference general (80 ± 5), alpha 0.05, power 80%, n = 12), also taking into account the expected size of treatment effects.

Patients will be considered to have completed the study after conducting the last follow-up visit. Patients can withdraw from the study at any time according to their decision or the investigator can decide to leave the study for lack of compliance or safety reasons.

The study aims to evaluate whether lithium treatment may represent a valid option for improving behaviour and cognitive performance in CdLS patients.

Study protocol

The study will include the following phases:

- ◇ Screening / Baseline (T0): Subjects will be considered for the study if they meet the inclusion criteria. This phase includes medical history, including drug history in treated patients and evaluation of concomitant medications, and clinical evaluation.

Each subject will undergo cognitive assessment (Leiter-R scale and Vineland Adaptive Behavior Scales 2), behavioral scales (ABC and CARS-T) communication and social function scales (SCQ), sleep quality scales (SDSC) and quality of vita (PedsQL) in collaboration with Dr. Ajmone of the UO of Childhood and Adolescent Neuropsychiatry (UONPIA) IRCSS Ca 'Granda Foundation Ospedale Maggiore Policlinico of Milan. Laboratory tests (hematology, biochemistry, urinalysis, serum pregnancy test for post-pubertal women and thyroid function tests) and 12-lead ECG will be performed at the Epilepsy Center, ASST Santi Paolo Carlo in Milan. Plasma levels of TBARS, known to be associated with lithium treatment, will be evaluated.

Written informed consent will be collected from the parents / legal representative of eligible CdLS patients willing to participate in the study.

- ◇ Start Drug Treatment (SDT, 1 week after T0): Patients included in the study begin taking the drug after the clinical evaluation of the tests performed at T0. A blood sample will be taken for the preparation of lymphoblastoid lines derived from patients by immortalizing lymphocytes with Epstein-barr virus (EBV) at the "Istituto Giannina Gaslini" in Genoa and the mutation of the immortalized cell lines will be confirmed thanks to the use of molecular genetics techniques such as PCR and Sanger sequencing at the Medical Genetics laboratory of the University of Milan. The preparation of the lines

guarantees genetically characterized material on which to carry out molecular and cytotoxicity tests.

- ◇ T1 (2 weeks \pm 3 days after SDT): clinical evaluation, laboratory tests including serum lithium levels, renal and thyroid function, and ECG. Any adverse events will be recorded and concomitant medications evaluated.
- ◇ T2 (2 weeks \pm 3 days after T1): clinical evaluation, blood tests including serum lithium levels, renal and thyroid function and ECG, as well as safety concerns.
- ◇ T3 (1 month \pm 1 week after T2): clinical evaluation, laboratory tests (haematology, biochemistry, urinalysis, serum pregnancy test for post-pubertal women and thyroid function tests) and ECG. Plasma levels of TBARS will be evaluated.
- ◇ T4 (1 month \pm 1 week after T3): clinical evaluation, blood tests including serum lithium level, renal and thyroid function and ECG, as well as safety concerns.
- ◇ T5 (3 months \pm 1 week after T4) - Laboratory tests (haematology, biochemistry, serum lithium level, urinalysis, serum pregnancy test for post-pubertal women and thyroid function tests) and 12-lead ECG will be performed. Plasma levels of TBARS will be evaluated.
- ◇ T6 (3 months \pm 1 week after T5): end of the first study period: Laboratory tests (haematology, biochemistry, serum lithium level, urinalysis, serum pregnancy test for post-pubertal women and thyroid function tests will be performed) and '12-lead ECG.
- ◇ Follow-up T7 (3 months \pm 1 week after T6): all patients will return for final evaluations. A final safety level (laboratory tests, ECG, vital signs) and efficacy evaluation will be performed. The scales and tests carried out at the baseline will be repeated.

Patients benefiting from lithium therapy will be guaranteed the continuation of the treatment and the relative controls relating to the tolerability / safety of the drug.

The other analyses are part of the clinical practice of managing the CdLS patient.

Statistical analysis

Clinical, demographic, and biochemical data will be presented as mean and standard deviation, if normally distributed, otherwise as median and interquartile range for continuous variables, and as percentages for categorical variables. For pre / post comparisons the differences in continuous variables will be analysed by t-test for paired data (or non-parametric equivalent - Wilcoxon test-) or McNemar's test for qualitative variables; the Chi-square test or Fisher's exact test, as appropriate, will instead be used for categorical variables. Specific statistical tests and corrections can be used where necessary.

4.5 Protocol to detect SARS-CoV-2 infection

During the SARS-CoV-2 pandemic, I was part of the team who worked on a new tool for SARS-CoV-2 infection. We started from the *SalivaDirect*TM protocol of Yale University (Vogels et al., 2020) – FDA emergency approved – and we optimized a saliva collection method able to guarantee a correct self-sampling or caregiver-guided sampling.

The following months, a new device for saliva collection was developed and optimized thanks to the collaboration between Prof. Elisa Borghi of Medical Microbiology laboratory and Professor Valentina Massa of Applied Biology laboratory, University of Milan, and Copan Italia S.p.A. (same manufacturer of nasopharyngeal swabs) – called LolliSpongeTM (Fig. 20).

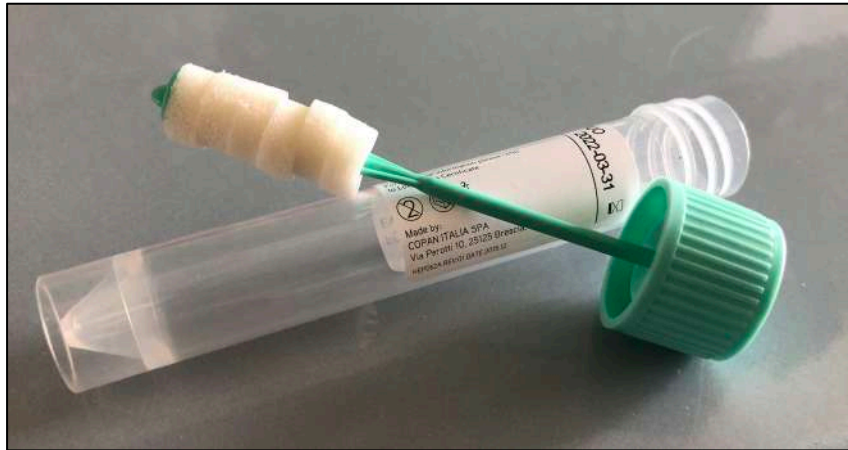


Figure 20. (Self - Lollisponge™ buccal sponge and swabs | Copan).

(Ottaviano et al., 2021)

This tool represents a possible advantage of an active saliva sample surveillance for early detection of SARS-CoV-2 (Wyllie et al., 2020). Viral replication in saliva begins in the very early stages of SARS-CoV-2 infection and the viral load is independent of symptoms severity (O'Donnell et al., 2020), thus allowing to identify the (even asymptomatic) infected subjects in a timely manner (Wang et al., 2004).

5. Discussion

CdLS is a rare genetic disorder characterized by growth retardation, mental delay, peculiar facial dysmorphism and, in most cases, by abnormalities of the upper limbs. The causative genes known for this syndrome encode proteins that belong to the cohesin protein complex. The basic research on cohesins had a growing interest in recent years since the "non-canonical" role of cohesin was identified, i.e. control of gene expression by the complex (Horsfield et al., 2012). Several studies tried to clarify which role was involved in cohesinopathies and in particular in the CdLS, and thanks to *in vitro* and *in vivo* experimental studies, it is currently believed that the "non-canonical" role is the main altered as a result of mutations underlying this condition (Dorsett, 2007; Horsfield et al., 2012).

In several works, researchers found that inactivating somatic mutations in genes that encode for cohesin subunits were a major cause of human cancer. These mutations (genes encoding SMC1A, SMC3, and the nipped-B-like protein) were heterozygous missense mutations of unknown functional significance. Subsequent sequencing of the cancer genome demonstrated that mutations in genes encoding the cohesin subunits (most commonly truncating mutations in STAG2, but also heterozygous missense mutations in RAD21, SMC1A, SMC3 and NIPBL) were present in bladder cancer, myeloid leukaemia, brain tumours, other types of cancer. That cohesin genes were involved in tumorigenesis was an unexpected discover. Cohesins are fundamental component of the basic cellular machinery that controls mitosis (Guacci et al., 1997; Michaelis et al., 1997; Losada et al., 1998) and their inactivation was expected to be incompatible with cellular proliferation. This may help explain why many tumour-derived mutations of these genes are heterozygous missense mutations that not completely inactivate functions of the encoded protein. Furthermore, it was already known that hereditary heterozygous mutations in the *NIPBL* gene were responsible for an inherited neurodevelopmental syndrome which is not known

to be a cancer predisposition syndrome: Cornelia de Lange syndrome (Nasmyth, 2002; Krantz et al., 2004).

The control and regulation of different gene pathways could be responsible for the heterogeneity of the clinical involvement of CdLS patients. Experiments here discussed further demonstrate how the WNT pathway - which plays a crucial role in the development of the central nervous system - is altered in CdLS. The canonical WNT pathway is mediated by the activation of β -catenin, which translocates to the nucleus where it binds DNA for the regulation of gene expression. In several studies this mechanism has been observed to be defective and reduced in CdLS models (Clevers et al., 2000; Tortelote et al., 2017).

Our previous studies focused on central nervous system development, here we aimed at studying modelling cells response to a possible chemical treatment.

Lymphoblastoid cell lines (LCLs) have been selected for our set of experiments, considering the nature of this cell type which allows abundant repetitive experiments compared to primary cultures. We used LCLs derived from CdLS patients with pathogenic variants in several causative genes. LCLs represent a useful cohesin-defective *in vitro* system, because of their role in the bone marrow structure and development (Bettini et al., 2018; Fazio et al., 2019; Mazzola et al., 2020). Despite it would be interesting to have data on prolonged treatments, the effect was evaluated only after 24h, that might probably explain the modest effects observed and represent. In the future, we plan to evaluate the impact of WNT modulation on gene expression and/or 3D chromatin organization in patients' cells.

Studies on CdLS *in vivo* models have shown an increase in cell death in the developing brain (Horsfield et al., 2007; Pistocchi et al., 2013; Fazio et al., 2016) associated with a reduced activation of the canonical WNT pathway further demonstrating that its chemical activation is able to rescue the affected

phenotype in *nipbl* and *smac1a* knocked-down *D. rerio* (Avagliano L. et al 2017). Interestingly we showed that WNT activators, such as lithium chloride (LiCl), induce an increase in proliferation, especially in cell lines that normally grow slowly compared to controls (i.e., CdLS LCLs). This significant boost has been also observed when cell lines have been exposed to other WNT compound activators (BIO, IQ-, DCA and CHIR99021). At the same time, we further investigated cell viability, appreciating a reduction in cell death after LiCl exposure in patient-derived cells.

Among the known targets of WNT canonical pathway, *Cyclin D1* (CCND1) is the most widely described (Shtutman et al., 1999). In particular, *CCND1* is known to play a pivotal role during neurogenesis, and it is required for progression through the G1 phase of the cell cycle. Reduced regulation of *Cyclin D1* and increased apoptosis are common features of cohesinopathies (Fazio et al. 2016). The importance of the balance of apoptosis levels of CNS modelling in model systems are extensively described (Hayashi et al., 1996; Massa et al., 2009). Our group demonstrated that cohesins are highly expressed in the cerebellum (Bettini et al., 2018) accordingly, zebrafish CdLS models displayed aberrant structure in the hindbrain region (Fazio et al., 2016). Furthermore, a mouse model study of neurological damage and cerebellar hypoplasia suggests a direct correlation between reduced levels of *CCND1*, increased apoptosis and morphological abnormalities in the developing cerebellum. In our experiments, *Cyclin D1* expression significant increases after exposure to lithium, in most of CdLS lines. Interestingly, the activation of WNT pathway (although it is not yet understood the underlying mechanism) seems to rescue *in vitro* the expression of genes involved in CdLS pathogenesis and in pathway sensitive to a cohesins haploinsufficiency.

We confirm our data mimicking CdLS in CNS *ex vivo* model exploiting FUCCI2 technology (Sakaue-Sawano et al., 2008), that provides a powerful model system

to study the coordination of the cell cycle and development. FUCCI2 emits a detectable *mCherry* signal during the G1 phase of the cell cycle, but decreases upon entry into the S phase, while the *mVenus* signal is present during the S and G2 phases. Both *mCherry* and *mVenus* are absent during the advanced M phase, therefore no fluorescence signal is detected. During the transition from G1 phase to S phase, cells emit both red and green fluorescence appearing yellow. This tool allows us to study death and proliferation at the level of the CNS, an extremely complex system.

Some studies performed by our group on an *in vitro* model of hiPSCs (useful tool for studying neural development through its lineage differentiation) revealed concordant results. Cells were treated with PCI-34051, a specific *HDAC8* inhibitor, implicated in the pathogenesis of CdLS, (Bottai et al., 2019) and the dynamics with which an impairment of the cohesin complex could be reflected in a human cell model was observed. At the same time, the canonical WNT pathway was activated chemically. Downstream analyses showed that the differentiation capabilities of cells, in which *HDAC8* was inhibited, were improved and the activation of the WNT pathway reflected on the hiPSC phenotype. By treating hiPSCs during the neuronal differentiation process, we highlighted that *HDAC8* inhibition interfered with the correct neuronal differentiation process. Curiously, this damage appeared to be recovered by activating the canonical pathway of the WNT through exposure to LiCl.

These data are in line with previous results, using murine neural stem cells (Bottai et al., 2019). Moreover, using *in vitro* CdLS model, we further demonstrated how cohesin genes, through the WNT pathway, play a determining role compared to the maintenance of the CNS and how the chemical activation of the pathway could rescue the normal functionality of the mechanism.

Studying *Drosophila melanogaster* it has been shown that, through the administration of LiCl, the canonical activation of the WNT pathway results in a

morphological improvement in mushroom bodies (MB) in adult flies. MB are a symmetrical CNS structures involved in olfactory learning and memory.

*Nipped-B*⁴⁰⁷ CdLS flies showed abnormal morphology of MB. After breeding parental flies on LiCl, the rescue of MB morphology was observed in a significant percentage of mutants. Treatment with lithium succeeded in improving the phenotype not only in the embryo, but also in adult animals of the F1 generation. So, it was shown that a molecular improvement resulted in a macroscopic structural recovery.

Wnt1^{-/-} embryos show severe malformations with no midbrain and cerebellum originating from the anterior metencephalon (McMahon et al., 1990; Thomas et al., 1990). In addition, it has been shown that β -catenin inactivation caused by WNT1 deletion results in severe brain malformations and craniofacial failure (Brault et al., 2001). In CdLS patients, the most frequently reported anomaly is microcephaly.

Kline and colleagues published a series that includes 15 clinically diagnosed individuals with CdLS, describing them from a neuroradiological point of view. Authors failed to demonstrate a significant correlation between brain abnormalities observed on MRI and the behavioural aspects of the investigated patients (Roshan Lal et al., 2016).

Nonetheless, the limited number of neuropathological studies available confirm these anomalies. The 2018 *Consensus* highlights the indication to perform an MRI scan for individuals suffering from CdLS with neurological manifestations. In fact, the mere presence of microcephaly in an individual with CdLS with molecular confirmation does not in itself constitute an indication to perform neuroradiological investigations (Kline et al., 2018).

Our collaborators obtained clinical data on the largest cohort (n=155) of CdLS patients ever published (Grazioli et al., 2021). In particular, CdLS patients have

been analysed evaluating the type and the prevalence of anomalies affecting the central nervous system. Prior to that, studies describing CNS abnormalities of CdLS patients were performed by Whitehead (Whitehead et al., 2015), who compared the neuroradiological characteristics of 8 CdLS patients, and by Roshan Lal (Roshan Lal et al., 2016) who obtained data from 15 CdLS patients by nuclear magnetic resonance (NMR), but most information was reported in individual case reports.

CdLS patient data analysis has highlighted a statistically significant correlation between CNS anomalies and clinical-neurological variables, such as autism and severe cognitive retardation.

With this work we demonstrated – using *in vivo* and *in vitro* CdLS models – how the cohesin genes, through the WNT pathway, have a determining role with respect to the structure of the CNS. The comparison with clinic showed a higher prevalence of CNS anomalies of hindbrain derivation, in full consistency with the data of the experimental models.

To date, only medical and surgical therapeutic interventions aimed at improving the quality of life are recommended for these patients. No drug therapy is validated for cognitive / behavioural disorders.

Lithium is already widely used in psychiatry and has a long history of clinical efficacy as the first drug used in the treatment of mental illness. This drug is approved for the treatment of bipolar disorder due to its ability to stabilize mania and depression. Its use must be properly monitored so that ideal blood concentrations (0.4-1.2 mequiv / L) are maintained and to monitor possible side effects.

Currently, some studies are evaluating the effects of lithium in non CdLS patients which however present overlapping features to CdLS. A clinical trial has proposed lithium therapy for treatment of Fragile X Syndrome showing

promising results (Liu and Smith, 2014). These patients share phenotypic characteristics with CdLS patients, in particular intellectual disability and a character profile that includes the autism spectrum disorder. Another work demonstrated the efficacy of lithium treatment as a mood stabilizer in two patients with mutations in *SHANK3* gene who were diagnosed with autism spectrum disorder in childhood (Serret et al., 2015).

The project we present intends to transfer the preliminary data obtained from *in vitro* and *in vivo* studies to patients with CdLS (Deardorff et al., 2012; Barbero, 2013; Fazio et al., 2016; Bettini et al., 2018; Bottai et al., 2019; Luna-Peláez et al., 2019; Grazioli et al., 2021). Given the currently untreatable nature of the syndrome, this treatment could represent a possible therapeutic strategy aimed at improving the behavioural and intellectual disabilities typical of CdLS. The study aims at evaluating whether lithium treatment may represent a valid option for improving behaviour and cognitive performance in CdLS patients.

In the contest of fragile individuals and in children, LolliSponge™ represents a simple tool for testing for SARS-CoV-2 infection. Italy was the first European Country to be involved in the COVID-19 pandemic and Lombardy region was the epicenter (first pandemic spread in spring 2020). During the first wave peak of SARS-CoV-2, there was a particular risk in specific fragile populations for severe COVID-19. LolliSponge™ allows an active and simple surveillance on patients who refer to medical examinations, moreover without specialized staff for sampling.

6. Conclusions

My data on LCLs confirm the impairment of WNT canonical pathway in CdLS. Importantly, based on my *in vitro* and *ex vivo* studies and complementary studies in animal models – which do not include mouse model as it does not recapitulate CdLS phenotype as well – WNT activators such as lithium can rescue adverse phenotype.

Because of pandemic, the planned clinical trial for treating CdLS patients with lithium was delayed, however the study design has been completed and ready to start.

The purpose of this study will be to evaluate the effectiveness of lithium therapy on behavioural modifications, communication skills and social functioning sleep quality and other different areas in patients with Cornelia de Lange syndrome. Specific biomarkers (TBARS - thiobarbituric acid reactive substance assay) will be used to measure lipid peroxidation in cell, tissue, and biological fluid extracts.

Moreover, should the pandemic still be undergoing, I plan to use a new method for molecular testing to detect SARS-CoV-2 RNA when such clinical trial starts. Indeed, I was part of the team to develop a new device for saliva collection and molecular testing to detect SARS-CoV-2 RNA. Starting from the FDA emergency approved *SalivaDirect™* protocol of Yale University, we optimized a saliva collection method able to guarantee a correct self-sampling or caregiver-guided sampling. In the contest of fragile individuals, like CdLS patients, this tool can be the breakthrough for infection surveillance.

7. References

- A, B., and J, B. (1974). Chromosome abnormalities and abortion. *Basic Life Sci.* 4, 317–339. doi:10.1007/978-1-4684-2892-6_22.
- Abu-Baker, A., Laganriere, J., Gaudet, R., Rochefort, D., Brais, B., Neri, C., et al. (2013). Lithium chloride attenuates cell death in oculopharyngeal muscular dystrophy by perturbing Wnt/ β -catenin pathway. *Cell Death Dis.* 4. doi:10.1038/cddis.2013.342.
- Aitken, D. A., Ireland, M., Berry, E., Crossley, J. A., Macri, J. N., Burn, J., et al. (1999). Second-trimester pregnancy associated plasma protein-A levels are reduced in Cornelia de Lange syndrome pregnancies - Aitken - 1999 - Prenatal Diagnosis - Wiley Online Library. *Prenat. Diagn.* Available at: [https://obgyn.onlinelibrary.wiley.com/doi/abs/10.1002/\(SICI\)1097-0223\(199908\)19:8%3C706::AID-PD613%3E3.0.CO;2-W](https://obgyn.onlinelibrary.wiley.com/doi/abs/10.1002/(SICI)1097-0223(199908)19:8%3C706::AID-PD613%3E3.0.CO;2-W) [Accessed September 19, 2021].
- Alesi, V., Dentici, M. L., Loddo, S., Genovese, S., Orlando, V., Calacci, C., et al. (2019). Confirmation of BRD4 haploinsufficiency role in Cornelia de Lange–like phenotype and delineation of a 19p13.12p13.11 gene contiguous syndrome. *Ann. Hum. Genet.* 83, 100–109. doi:10.1111/AHG.12289.
- Allanson, J. E., Hennekam, R. C., and Ireland, M. (1997). De Lange syndrome: subjective and objective comparison of the classical and mild phenotypes. *J. Med. Genet.* 34, 645. doi:10.1136/JMG.34.8.645.
- Ansari, M., Poke, G., Ferry, Q., Williamson, K., Aldridge, R., Meynert, A. M., et al. (2014). Genetic heterogeneity in Cornelia de Lange syndrome (CdLS) and CdLS-like phenotypes with observed and predicted levels of mosaicism. *J. Med. Genet.* doi:10.1136/jmedgenet-2014-102573.
- Arbuzova, S., Nikolenko, M., Krantz, D., Hallahan, T., and Macri, J. (2003). Low

- first-trimester pregnancy-associated plasma protein-A and Cornelia de Lange syndrome [3]. *Prenat. Diagn.* 23, 864. doi:10.1002/PD.690.
- Avagliano, L., Bulfamante, G. Pietro, and Massa, V. (2017a). Cornelia de lange syndrome: To diagnose or not to diagnose in utero? *Birth Defects Res.* 109, 771–777. doi:10.1002/bdr2.1045.
- Avagliano, L., Grazioli, P., Mariani, M., Bulfamante, G. P., Selicorni, A., and Massa, V. (2017c). Integrating molecular and structural findings: Wnt as a possible actor in shaping cognitive impairment in Cornelia de Lange syndrome. *Orphanet J. Rare Dis.* 12. doi:10.1186/s13023-017-0723-0.
- Avagliano, L., Parenti, I., Grazioli, P., Di Fede, E., Parodi, C., Mariani, M., et al. (2020a). Chromatinopathies: A focus on Cornelia de Lange syndrome. *Clin.*
- Ayerza Casas, A., Puisac Uriol, B., Teresa Rodrigo, M. E., Hernández Marcos, M., Ramos Fuentes, F. J., and Pie Juste, J. (2017). Cornelia de Lange syndrome: Congenital heart disease in 149 patients. *Med. Clínica (English Ed.* 149, 300–302. doi:10.1016/J.MEDCLE.2017.03.024.
- Banerji, R., Skibbens, R. V., and Iovine, M. K. (2017). How many roads lead to cohesinopathies? *Dev. Dyn.* 246, 881–888. doi:10.1002/dvdy.24510.
- Barbero, J. L. (2013). Genetic basis of cohesinopathies. *Appl. Clin. Genet.* 6, 15. doi:10.2147/TACG.S34457.
- Barisic, I., Tokic, V., Loane, M., Bianchi, F., Calzolari, E., Garne, E., et al. (2008a). Descriptive epidemiology of Cornelia de Lange syndrome in Europe. *Am. J. Med. Genet. Part A* 146A, 51–59. doi:10.1002/ajmg.a.32016.
- Beck, B. (1976). Epidemiology of Cornelia De Lange Syndrome. *Acta Pædiatrica* 65, 631–638. doi:10.1111/j.1651-2227.1976.tb04943.x.
- Beck, B., and Fenger, K. (1985). Mortality, Pathological Findings and Causes of

- Death in the de Lange Syndrome. *Acta Pædiatrica* 74, 765–769.
doi:10.1111/j.1651-2227.1985.tb10028.x.
- Beratis, N. G., Hsu, L. Y. F., and Hirschhorn, K. (1971). Familial de Lange syndrome. *Clin. Genet.* 2, 170–176. doi:10.1111/J.1399-0004.1971.TB00274.X.
- Bermudez, V. P., Farina, A., Higashi, T. L., Du, F., Tappin, I., Takahashi, T. S., et al. (2012). In vitro loading of human cohesin on DNA by the human Scc2-Scc4 loader complex. *Proc. Natl. Acad. Sci. U. S. A.* 109, 9366–71. doi:10.1073/pnas.1206840109.
- Bettini, L. R., Graziola, F., Fazio, G., Grazioli, P., Scagliotti, V., Pasquini, M., et al. (2018a). Rings and bricks: Expression of cohesin components is dynamic during development and adult life. *Int. J. Mol. Sci.* 19. doi:10.3390/ijms19020438.
- Birkenbihl, R. P., and Subramani, S. (1992). Cloning and characterization of rad21 an essential gene of *Schizosaccharomyces pombe* involved in DNA double-strand-break repair. *Nucleic Acids Res.* doi:10.1093/nar/20.24.6605.
- Boog, G., Sagot, F., Winer, N., David, A., and Nomballais, M. (1999). Brachmann-de Lange syndrome: a cause of early symmetric fetal growth delay. *Eur. J. Obstet. Gynecol. Reprod. Biol.* 85, 173–177. doi:10.1016/S0301-2115(99)00021-4.
- Borck, G., Redon, R., Sanlaville, D., Rio, M., Prieur, M., Lyonnet, S., et al. (2004). NIPBL mutations and genetic heterogeneity in Cornelia de Lange syndrome. *J. Med. Genet.* 41, e128. doi:10.1136/JMG.2004.026666.
- Borghi, E., Massa, V., Carmagnola, D., Dellavia, C., Parodi, C., Ottaviano, E., et al. (2021a). Saliva sampling for chasing SARS-CoV-2: A Game-changing

- strategy. *Pharmacol. Res.* 165, 105380. doi:10.1016/J.PHRS.2020.105380.
- Bot, C., Pfeiffer, A., Giordano, F., Manjeera, D. E., Dantuma, N. P., and Ström, L. (2017). Independent mechanisms recruit the cohesin loader protein NIPBL to sites of DNA damage. *J. Cell Sci.* 130, 1134–1146. doi:10.1242/jcs.197236.
- Bottai, D., Spreafico, M., Pistocchi, A., Fazio, G., Adami, R., Grazioli, P., et al. (2019). Modeling Cornelia de Lange syndrome in vitro and in vivo reveals a role for cohesin complex in neuronal survival and differentiation. *Hum. Mol. Genet.* 28, 64–73. doi:10.1093/hmg/ddy329.
- Boyle, M. I., Jespersgaard, C., Nazaryan, L., Bisgaard, A. M., and Tümer, Z. (2017). A novel RAD21 variant associated with intrafamilial phenotypic variation in Cornelia de Lange syndrome – review of the literature. *Clin. Genet.* doi:10.1111/cge.12863.
- Brachmann, W. R. C. (1916). Ein Fall von symmetrischer Monodaktylie durch Ulnadefekt, mit symmetrischer Flughautbildung in den Ellenbeugen, sowie anderen Abnormitäten (Zwerghaftigkeit, Halsrippen, Behaarung): Aus d. Inn. Abt. d. Kinderheilanst. in Dresden ; Leiter: Brückner. *Jarb Kinder Phys Erzie*, 225–35. Available at: <https://books.google.it/books?id=MFjIQAAACAAJ>.
- Broholm, K., Eeg-Olofsson, O., and Hall, B. (1968). An inherited chromosome aberration in a girl with signs of de Lange syndrome. *Acta Paediatr. Scand.* 57, 547–552. doi:10.1111/J.1651-2227.1968.TB06978.X.
- Brugmann, S. A., Goodnough, L. H., Gregorieff, A., Leucht, P., ten Berge, D., Fuerer, C., et al. (2007). Wnt signaling mediates regional specification in the vertebrate face. *Development* 134, 3283–3295. doi:10.1242/DEV.005132.

- Bruner, J., and Hsia YE (1990). Prenatal findings in Brachmann-de Lange syndrome - PubMed. *Obs. Gynecol .*, 76(5 Pt 2):966--8. Available at: <https://pubmed.ncbi.nlm.nih.gov/1699187/> [Accessed September 19, 2021].
- Callegari, A. J., and Kelly, T. J. (2007). Shedding Light on the DNA Damage Checkpoint. <http://dx.doi.org/10.4161/cc.6.6.3984> 6, 660–666. doi:10.4161/CC.6.6.3984.
- Carrel, L., and Willard, H. F. (2005). X-inactivation profile reveals extensive variability in X-linked gene expression in females. *Nature* 434, 400–404. doi:10.1038/nature03479.
- Carter, M., Chen, X., Slowinska, B., Minnerath, S., Glickstein, S., Shi, L., et al. (2005). Crooked tail (Cd) model of human folate-responsive neural tube defects is mutated in Wnt coreceptor lipoprotein receptor-related protein 6. *Proc. Natl. Acad. Sci. U. S. A.* 102, 12843. doi:10.1073/PNAS.0501963102.
- Castronovo, P., Gervasini, C., Cereda, A., Masciadri, M., Milani, D., Russo, S., et al. (2009). Premature chromatid separation is not a useful diagnostic marker for Cornelia de Lange syndrome. *Chromosom. Res.* 2009 176 17, 763–771. doi:10.1007/S10577-009-9066-6.
- Cates, M., Billmire, D., Bull, M., and Grosfeld, J. (1989). Gastroesophageal dysfunction in Cornelia de Lange syndrome. *J. Pediatr. Surg.* 24, 248–250. doi:10.1016/S0022-3468(89)80004-1.
- Chong, K., Keating, S., Hurst, S., Summers, A., Berger, H., Seaward, G., et al. (2009). Cornelia de Lange syndrome (CdLS): prenatal and autopsy findings. *Prenat. Diagn.* 29, 489–494. doi:10.1002/PD.2228.
- Clevers, H., Barker, N., and Morin, P. J. (2000). The Yin-Yang of TCF/beta-

- catenin signaling. *Adv. Cancer Res.* 77, 1–24. doi:10549354.
- D’Mello, S. R. (2019). Regulation of CNS Development by Class I HDACs. *Dev. Neurosci.* 41, 149. doi:10.1159/000505535.
- De, A. (2011). Wnt / Ca signaling pathway : a brief overview The Non-canonical Wnt Signaling Cascade. 43, 745–756. doi:10.1093/abbs/gmr079.Advance.
- De Lange, C. C. (1933). Sur un type nouveau de degenerescence (typus Amstelodamensis). *Arch Med Enfants*, 713–719.
- Deardorff, M. A., Bando, M., Nakato, R., Watrin, E., Itoh, T., Minamino, M., et al. (2012a). HDAC8 mutations in Cornelia de Lange syndrome affect the cohesin acetylation cycle. *Nature* 489, 313–317. doi:10.1038/nature11316.
- Deardorff, M. A., Clark, D. M., and Krantz, I. D. (1993). Cornelia de Lange Syndrome. *GeneReviews(R)*, 3–7. Available at: <http://www.ncbi.nlm.nih.gov/pubmed/20301283>.
- Deardorff, M. A., Kaur, M., Yaeger, D., Rampuria, A., Korolev, S., Pie, J., et al. (2007a). Mutations in cohesin complex members SMC3 and SMC1A cause a mild variant of cornelia de Lange syndrome with predominant mental retardation. *Am. J. Hum. Genet.* 80, 485–94. doi:10.1086/511888.
- Deardorff, M. A., Wilde, J. J., Albrecht, M., Dickinson, E., Tennstedt, S., Braunholz, D., et al. (2012c). RAD21 mutations cause a human cohesinopathy. *Am. J. Hum. Genet.* 90, 1014–1027. doi:10.1016/j.ajhg.2012.04.019.
- Dorsett, D. (2007a). Roles of the sister chromatid cohesion apparatus in gene expression, development, and human syndromes. *Chromosoma* 116, 1–13. doi:10.1007/s00412-006-0072-6.
- Dorsett, D. (2009). Cohesin, gene expression and development: lessons from *Drosophila*. *Chromosome Res.* 17, 185–200. doi:10.1007/s10577-009-

9022-5.

- Dorsett, D., and Krantz, I. D. (2009). On the Molecular Etiology of Cornelia de Lange Syndrome. *Ann. N. Y. Acad. Sci.* 1151, 22. doi:10.1111/J.1749-6632.2008.03450.X.
- Dorsett, D., and Ström, L. (2012). The ancient and evolving roles of cohesin in DNA repair and gene expression. *Curr. Biol.* 22, R240. doi:10.1016/J.CUB.2012.02.046.
- DuVall, G., and Walden, D. (1996). Adenocarcinoma of the esophagus complicating Cornelia de Lange syndrome. *J. Clin. Gastroenterol.* 22, 131–133. doi:10.1097/00004836-199603000-00012.
- Eekelen, A. de K., and Hennekam, R. C. M. (1994). Historical study: Cornelia C. de Lange (1871–1950)—a pioneer in clinical genetics. *Am. J. Med. Genet.* 52, 257–266. doi:10.1002/AJMG.1320520302.
- Fahrner, J. A., and Bjornsson, H. T. (2014). Mendelian disorders of the epigenetic machinery: Tipping the balance of chromatin States. *Annu. Rev. Genomics Hum. Genet.* 15, 269–293. doi:10.1146/annurev-genom-090613-094245.
- Falek, A., Schmidt, R., and Jervis, G. A. (1966). FAMILIAL DE LANGE SYNDROME WITH CHROMOSOME ABNORMALITIES. *Pediatrics* 37.
- Fazio, G., Gaston-Massuet, C., Bettini, L. R., Graziola, F., Scagliotti, V., Cereda, A., et al. (2016a). CyclinD1 Down-Regulation and Increased Apoptosis Are Common Features of Cohesinopathies. *J Cell Physiol* 231, 613–622. doi:10.1002/jcp.25106.
- Fazio, G., Massa, V., Grioni, A., Bystry, V., Rigamonti, S., Saitta, C., et al. (2019). First evidence of a paediatric patient with Cornelia de Lange syndrome with acute lymphoblastic leukaemia. *J. Clin. Pathol.* 72, 558–561.

doi:10.1136/jclinpath-2019-205707.

Feng, L., Zhou, D., Zhang, Z., Liu, Y., and Yang, Y. (2014). Exome sequencing identifies a de novo mutation in HDAC8 associated with Cornelia de Lange syndrome. *J. Hum. Genet.* doi:10.1038/jhg.2014.60.

Fernández-Garre, P., Rodríguez-Gallardo, L., Gallego-Díaz, V., Alvarez, I., and Puellas, L. (2002). Fate map of the chicken neural plate at stage 4. *Development* 129, 2807–2822. Available at: <https://pubmed.ncbi.nlm.nih.gov/12050131/> [Accessed September 27, 2021].

Fitzgerald, R. C., Pietro, M. di, Ragnath, K., Ang, Y., Kang, J.-Y., Watson, P., et al. (2014). British Society of Gastroenterology guidelines on the diagnosis and management of Barrett's oesophagus. *Gut* 63, 7–42. doi:10.1136/GUTJNL-2013-305372.

Florian, M. C., Nattamai, K. J., Dörr, K., Marka, G., Uberle, B., Vas, V., et al. (2013). A canonical to non-canonical Wnt signalling switch in haematopoietic stem-cell ageing. *Nature* 503, 392–6. doi:10.1038/nature12631.

Fu, J., Yu, H.-M. I., Maruyama, T., Mirando, A. J., and Hsu, W. (2011). Gpr177/mouse Wntless is essential for Wnt-mediated craniofacial and brain development. *Dev. Dyn.* 240, 365. doi:10.1002/DVDY.22541.

Gallagher, D., Voronova, A., Zander, M. A., Cancino, G. I., Bramall, A., Krause, M. P., et al. (2015). Ankrd11 is a chromatin regulator involved in autism that is essential for neural development. *Dev. Cell* 32, 31–42. doi:10.1016/j.devcel.2014.11.031.

Geetha-Loganathan, P., Nimmagadda, S., Antoni, L., Fu, K., Whiting, C. J., Francis-West, P., et al. (2009). Expression of WNT signalling pathway

- genes during chicken craniofacial development. *Dev. Dyn.* 238, 1150–1165. doi:10.1002/DVDY.21934.
- Gerdes, J., Lemke, H., Baisch, H., Wacker, H. H., Schwab, U., and Stein, H. (1984). Cell cycle analysis of a cell proliferation-associated human nuclear antigen defined by the monoclonal antibody Ki-67. *J. Immunol.* 133, 1710–5. Available at: <http://www.ncbi.nlm.nih.gov/pubmed/6206131> [Accessed June 11, 2020].
- Gervasini, C., Pfundt, R., Castronovo, P., Russo, S., Roversi, G., Masciadri, M., et al. (2008). Search for genomic imbalances in a cohort of 24 Cornelia de Lange patients negative for mutations in the NIPBL and SMC1L1 genes. *Clin. Genet.* 74, 531–538. doi:10.1111/J.1399-0004.2008.01086.X.
- Gervasini, C., Russo, S., Cereda, A., Parenti, I., Masciadri, M., Azzollini, J., et al. (2013). Cornelia de Lange individuals with new and recurrent SMC1A mutations enhance delineation of mutation repertoire and phenotypic spectrum. *Am. J. Med. Genet. A* 161A, 2909–19. doi:10.1002/ajmg.a.36252.
- Gil-Rodríguez, M. C., Deardorff, M. A., Ansari, M., Tan, C. A., Parenti, I., Baquero-Montoya, C., et al. (2015). De novo heterozygous mutations in SMC3 cause a range of cornelia de lange syndrome-overlapping phenotypes. *Hum. Mutat.* doi:10.1002/humu.22761.
- Göndör, A., and Ohlsson, R. (2008). Chromatin insulators and cohesins. *EMBO Rep.* 9, 327. doi:10.1038/EMBOR.2008.46.
- Goodenough, S., Schäfer, M., and Behl, C. (2003). Estrogen-induced cell signalling in a cellular model of Alzheimer's disease. *J. Steroid Biochem. Mol. Biol.* 84, 301–305. doi:10.1016/S0960-0760(03)00043-8.
- Grazioli, P., Parodi, C., Mariani, M., Bottai, D., Di Fede, E., Zulueta, A., et al.

- (2021). Lithium as a possible therapeutic strategy for Cornelia de Lange syndrome. *Cell Death Discov.* 2021 71 7, 1–11. doi:10.1038/s41420-021-00414-2.
- Gregori, M. De, Ciccone, R., Magini, P., Pramparo, T., Gimelli, S., Messa, J., et al. (2007). Cryptic deletions are a common finding in “balanced” reciprocal and complex chromosome rearrangements: a study of 59 patients. *J. Med. Genet.* 44, 750. doi:10.1136/JMG.2007.052787.
- Guacci, V., Koshland, D., and Strunnikov, A. (1997). A Direct Link between Sister Chromatid Cohesion and Chromosome Condensation Revealed through the Analysis of MCD1 in *S. cerevisiae*. *Cell* 91, 47. Available at: [/pmc/articles/PMC2670185/](https://pubmed.ncbi.nlm.nih.gov/10800000/) [Accessed September 27, 2021].
- Haering, C. H., Löwe, J., Hochwagen, A., and Nasmyth, K. (2002). Molecular architecture of SMC proteins and the yeast cohesin complex. *Mol. Cell* 9, 773–788. doi:10.1016/S1097-2765(02)00515-4.
- Harakalova, M., van den Boogaard, M. J., Sinke, R., van Lieshout, S., van Tuil, M. C., Duran, K., et al. (2012). X-exome sequencing identifies a HDAC8 variant in a large pedigree with X-linked intellectual disability, truncal obesity, gynaecomastia, hypogonadism and unusual face. *J. Med. Genet.* doi:10.1136/jmedgenet-2012-100921.
- Hayashi, M., Sakamoto, K., Kurata, K., Nagata, J., Satoh, J., and Morimatsu, Y. (1996). Septo-optic dysplasia with cerebellar hypoplasia in Cornelia de Lange syndrome. *Acta Neuropathol.* 92, 625–30. doi:10.1007/s004010050571.
- Herrmann, J., Pallister, P. D., Tiddy, W., and Opitz, J. M. (1975). The KBG syndrome—a syndrome of short stature, characteristic facies, mental retardation, macrodontia and skeletal anomalies. *Birth Defects Orig Artic Ser* 11, 7–18.

- Holder, S. E., Grimsley, L. M., Palmer, R. W., Butler, L. J., and Baraitser, M. (1994). Partial trisomy 3q causing mild Cornelia de Lange phenotype. *J. Med. Genet.* 31, 150. doi:10.1136/JMG.31.2.150.
- Horsfield, J. A., Anagnostou, S. H., Hu, J. K.-H., Cho, K. H. Y., Geisler, R., Lieschke, G., et al. (2007). Cohesin-dependent regulation of Runx genes. *Development* 134, 2639–2649. doi:10.1242/dev.002485.
- Horsfield, J. A., Print, C. G., and Mönnich, M. (2012). Diverse developmental disorders from the one ring: distinct molecular pathways underlie the cohesinopathies. *Front. Genet.* 3, 171. doi:10.3389/fgene.2012.00171.
- Huang, W., and Porto, M. (2002). Abnormal first-trimester fetal nuchal translucency and Cornelia De Lange syndrome. *Obstet. Gynecol.* 99, 956–958. doi:10.1016/S0029-7844(02)01982-8.
- Huisman, S., Mulder, P. A., Redeker, E., Bader, I., Bisgaard, A. M., Brooks, A., et al. (2017). Phenotypes and genotypes in individuals with SMC1A variants. *Am. J. Med. Genet. Part A* 173, 2108–2125. doi:10.1002/ajmg.a.38279.
- Inestrosa, N., and Varela-Nallar, L. (2015). Wnt signalling in neuronal differentiation and development. *Cell Tissue Res.* 359, 215–223. doi:10.1007/S00441-014-1996-4.
- Izumi, K. (2016). Disorders of Transcriptional Regulation: An Emerging Category of Multiple Malformation Syndromes. *Mol. Syndromol.* doi:10.1159/000448747.
- Izumi, K., Nakato, R., Zhang, Z., Edmondson, A. C., Noon, S., Dulik, M. C., et al. (2015). Germline gain-of-function mutations in AFF4 cause a developmental syndrome functionally linking the super elongation complex and cohesin. *Nat. Genet.* doi:10.1038/ng.3229.

- Jackson, L., Kline, A., Barr, M., and Koch, S. (1993). de Lange syndrome: a clinical review of 310 individuals. *Am. J. Med. Genet.* 47, 940–946. doi:10.1002/AJMG.1320470703.
- Jackstadt, R., Hodder, M. C., and Sansom, O. J. (2020). WNT and β -Catenin in Cancer: Genes and Therapy. *Annu. Rev. Cancer Biol.* 4, 177–196. doi:10.1146/annurev-cancerbio-030419-033628.
- JM, O. (1994). RSH/SLO (“Smith-Lemli-Opitz”) syndrome: historical, genetic, and developmental considerations. *Am. J. Med. Genet.* 50, 344–346. doi:10.1002/AJMG.1320500408.
- Kagey, M. H., Newman, J. J., Bilodeau, S., Zhan, Y., Orlando, D. A., Van Berkum, N. L., et al. (2010). Mediator and cohesin connect gene expression and chromatin architecture. *Nature* 467, 430–435. doi:10.1038/nature09380.
- Kahn, M. (2015). HHS Public Access. 13, 513–532. doi:10.1038/nrd4233.Can.
- Kaiser, F. J., Ansari, M., Braunholz, D., Gil-Rodríguez, M. C., Decroos, C., Wilde, J. J., et al. (2014). Loss-of-function HDAC8 mutations cause a phenotypic spectrum of Cornelia de Lange syndrome-like features, ocular hypertelorism, large fontanelle and X-linked inheritance. *Hum. Mol. Genet.* 23, 2888–2900. doi:10.1093/hmg/ddu002.
- Kamada, K., and Barillà, D. (2018). Combing Chromosomal DNA Mediated by the SMC Complex: Structure and Mechanisms. *BioEssays.* doi:10.1002/bies.201700166.
- Kline, A. D., Barr, M., and Jackson, L. (1993). Growth manifestations in the Brachmann-de Lange syndrome. *Am. J. Med. Genet.* 47, 1042–1049. doi:10.1002/AJMG.1320470722.
- Kline, A. D., Grados, M., Sponseller, P., Levy, H. P., Blagowidow, N., Schoedel,

- C., et al. (2007). Natural history of aging in Cornelia de Lange syndrome. *Am. J. Med. Genet. Part C Semin. Med. Genet.* 145, 248–260. doi:10.1002/ajmg.c.30137.
- Kline, A. D., Krantz, I. D., Deardorff, M. A., Shirahige, K., Dorsett, D., Gerton, J. L., et al. (2017). Cornelia de Lange syndrome and molecular implications of the cohesin complex: Abstracts from the 7th biennial scientific and educational symposium 2016. *Am. J. Med. Genet. Part A* 173, 1172–1185. doi:10.1002/ajmg.a.38161.
- Kline, A. D., Moss, J. F., Selicorni, A., Bisgaard, A.-M., Deardorff, M. A., Gillett, P. M., et al. (2018a). Diagnosis and management of Cornelia de Lange syndrome: first international consensus statement. *Nat. Rev. Genet.* doi:10.1038/s41576-018-0031-0.
- Kokubu, C., Heinzmann, U., Kokubu, T., Sakai, N., Kubota, T., Kawai, M., et al. (2004). Skeletal defects in ringelschwanz mutant mice reveal that Lrp6 is required for proper somitogenesis and osteogenesis. *Development* 131, 5469–5480. doi:10.1242/DEV.01405.
- Komiya, Y., and Habas, R. (2008a). Wnt signal transduction pathways. *Organogenesis* 4, 68–75. doi:10.4161/org.4.2.5851.
- Kousseff, B., J, T.-M., P, N., and AW, R. (1993). Physical growth in Brachmann-de Lange syndrome. *Am. J. Med. Genet.* 47, 1050–1052. doi:10.1002/AJMG.1320470723.
- Krantz, I. D., McCallum, J., DeScipio, C., Kaur, M., Gillis, L. A., Yaeger, D., et al. (2004). Cornelia de Lange syndrome is caused by mutations in NIPBL, the human homolog of *Drosophila melanogaster* Nipped-B. *Nat. Genet.* 36, 631–635. doi:10.1038/ng1364.
- Lee, H. Y., Kléber, M., Hari, L., Brault, V., Suter, U., Taketo, M. M., et al. (2004).

- Instructive Role of Wnt/ β -Catenin in Sensory Fate Specification in Neural Crest Stem Cells. *Science* (80-.). 303, 1020–1023.
doi:10.1126/SCIENCE.1091611.
- Liu, J., and Krantz, I. (2009a). Cornelia de Lange syndrome, cohesin, and beyond. *Clin. Genet.* 76, 303–314. doi:10.1111/j.1399-0004.2009.01271.x.
- Liu, J., Zhang, Z., Bando, M., Itoh, T., Deardorff, M. A., Clark, D., et al. (2009). Transcriptional Dysregulation in NIPBL and Cohesin Mutant Human Cells. *PLoS Biol.* 7. doi:10.1371/JOURNAL.PBIO.1000119.
- Liu, Z., and Smith, C. B. (2014). Lithium: A promising treatment for fragile X syndrome. *ACS Chem. Neurosci.* 5, 477–483. doi:10.1021/cn500077p.
- Losada, A., Hirano, M., and Hirano, T. (1998). Identification of Xenopus SMC protein complexes required for sister chromatid cohesion. *Genes Dev.* 12, 1986. doi:10.1101/GAD.12.13.1986.
- Luna-Peláez, N., March-Díaz, R., Ceballos-Chávez, M., Guerrero-Martínez, J. A., Grazioli, P., García-Gutiérrez, P., et al. (2019). The Cornelia de Lange Syndrome-associated factor NIPBL interacts with BRD4 ET domain for transcription control of a common set of genes. *Cell Death Dis.*
doi:10.1038/s41419-019-1792-x.
- Luzzani, S., Macchini, F., Valadè, A., Milani, D., and Selicorni, A. (2003). Gastroesophageal reflux and Cornelia de Lange syndrome: Typical and atypical symptoms. *Am. J. Med. Genet. Part A* 119A, 283–287.
doi:10.1002/AJMG.A.20191.
- MA, K., SG, K., BS, H., and JD, B. (1993). Fetal biometry in the Brachmann-de Lange syndrome. *Am. J. Med. Genet.* 47, 1035–1041.
doi:10.1002/AJMG.1320470721.
- Macchini, F., Selicorni, A., Luzzani, S., Milani, D., Roggero, P., and Valadè, A.

- (2007). Coeliac disease and cornelia de Lange Syndrome: lack of association. *Acta Pædiatrica* 96, 1518–1520. doi:10.1111/J.1651-2227.2007.00468.X.
- Macchini, F., Zanini, A., Farris, G., Morandi, A., Brisighelli, G., Gentilino, V., et al. (2018). Infant Percutaneous Endoscopic Gastrostomy: Risks or Benefits? *Clin. Endosc.* 51, 260. doi:10.5946/CE.2017.137.
- MacDonald, B. T., Tamai, K., and He, X. (2009). Wnt/ β -Catenin Signaling: Components, Mechanisms, and Diseases. *Dev. Cell* 17, 9–26. doi:10.1016/j.devcel.2009.06.016.
- Mannini, L., Liu, J., Krantz, I. D., and Musio, A. (2010). Spectrum and consequences of SMC1A mutations: The unexpected involvement of a core component of cohesin in human disease. *Hum. Mutat.* 31, 5–10. doi:10.1002/humu.21129.
- Mariani, M., Decimi, V., Bettini, L., Maitz, S., Gervasini, C., Masciadri, M., et al. (2016). Adolescents and adults affected by Cornelia de Lange syndrome: A report of 73 Italian patients. *Am. J. Med. Genet. C. Semin. Med. Genet.* 172, 206–213. doi:10.1002/AJMG.C.31502.
- Marino, T., Wheeler, P. G., Simpson, L. L., Craigo, S. D., and Bianchi, D. W. (2002). Fetal diaphragmatic hernia and upper limb anomalies suggest Brachmann-de Lange syndrome. *Prenat. Diagn.* 22, 144–147. doi:10.1002/PD.281.
- Massa, V., Savery, D., Ybot-Gonzalez, P., Ferraro, E., Rongvaux, A., Cecconi, F., et al. (2009). Apoptosis is not required for mammalian neural tube closure. *Proc. Natl. Acad. Sci. U. S. A.* 106, 8233–8. doi:10.1073/pnas.0900333106.
- Masumoto, K., Izaki, T., and Arima, T. (2001). Cornelia de Lange syndrome associated with cecal volvulus: Report of a case. *Acta Paediatr. Int. J.*

- Paediatr.* 90, 701–703. doi:10.1111/J.1651-2227.2001.TB02437.X.
- Mazzola, M., Pezzotta, A., Fazio, G., Rigamonti, A., Bresciani, E., Gaudenzi, G., et al. (2020). Dysregulation of NIPBL leads to impaired RUNX1 expression and haematopoietic defects. *J. Cell. Mol. Med.* 24, 6272–6282. doi:10.1111/jcmm.15269.
- Michaelis, C., Ciosk, R., and Nasmyth, K. (1997). Cohesins: Chromosomal proteins that prevent premature separation of sister chromatids. *Cell.* doi:10.1016/S0092-8674(01)80007-6.
- Mishina, Y., and Snider, T. N. (2014). Neural crest cell signaling pathways critical to cranial bone development and pathology. *Exp. Cell Res.* 325, 138. doi:10.1016/J.YEXCR.2014.01.019.
- Misulovin, Z., Schwartz, Y. B., Li, X.-Y., Kahn, T. G., Gause, M., MacArthur, S., et al. (2008). Association of cohesin and Nipped-B with transcriptionally active regions of the *Drosophila melanogaster* genome. *Chromosoma* 117, 89. doi:10.1007/S00412-007-0129-1.
- Miyabayashi, T., Teo, J.-L., Yamamoto, M., McMillan, M., Nguyen, C., and Kahn, M. (2007). Wnt/beta-catenin/CBP signaling maintains long-term murine embryonic stem cell pluripotency. *Proc. Natl. Acad. Sci.* 104, 5668–5673. doi:10.1073/pnas.0701331104.
- Mönnich, M., Banks, S., Eccles, M., Dickinson, E., and Horsfield, J. (2009). Expression of cohesin and condensin genes during zebrafish development supports a non-proliferative role for cohesin. *Gene Expr. Patterns* 9, 586–594. doi:10.1016/J.GEP.2009.08.004.
- Mönnich, M., Kuriger, Z., Print, C. G., and Horsfield, J. A. (2011). A Zebrafish Model of Roberts Syndrome Reveals That Esco2 Depletion Interferes with Development by Disrupting the Cell Cycle. *PLoS One* 6, e20051.

doi:10.1371/JOURNAL.PONE.0020051.

Morel Swols, D., Foster, J., and Tekin, M. (2017). KBG syndrome. *Orphanet J. Rare Dis.* 12. doi:10.1186/s13023-017-0736-8.

Mulligan, K. A., and Cheyette, B. N. R. (2012). Wnt Signaling in Vertebrate Neural Development and Function. *J. Neuroimmune Pharmacol.* 7, 774. doi:10.1007/S11481-012-9404-X.

Musio, A., Selicorni, A., Focarelli, M. L., Gervasini, C., Milani, D., Russo, S., et al. (2006). X-linked Cornelia de Lange syndrome owing to SMC1L1 mutations. *Nat. Genet.* 38, 528–530. doi:10.1038/ng1779.

Nasmyth, K. (2002). Segregating Sister Genomes: The Molecular Biology of Chromosome Separation. *Science (80-.).* 297, 559–565. doi:10.1126/SCIENCE.1074757.

Nasmyth, K. (2011a). Cohesin: a catenase with separate entry and exit gates? *Nat. Cell Biol.* 13, 1170–1177. doi:10.1038/ncb2349.

Nasmyth, K., and Haering, C. H. (2005). THE STRUCTURE AND FUNCTION OF SMC AND KLEISIN COMPLEXES. <http://dx.doi.org/10.1146/annurev.biochem.74.082803.133219> 74, 595–648. doi:10.1146/ANNUREV.BIOCHEM.74.082803.133219.

Nasmyth, K., and Haering, C. H. (2009). Cohesin: Its roles and mechanisms. *Annu. Rev. Genet.* 43, 525–558. doi:10.1146/annurev-genet-102108-134233.

Naujok, O., Lentjes, J., Diekmann, U., Davenport, C., and Lenzen, S. (2014a). Cytotoxicity and activation of the Wnt/beta-catenin pathway in mouse embryonic stem cells treated with four GSK3 inhibitors. *BMC Res. Notes* 7. doi:10.1186/1756-0500-7-273.

Naujok, O., Lentjes, J., Diekmann, U., Davenport, C., and Lenzen, S. (2014b).

- Cytotoxicity and activation of the Wnt/beta-catenin pathway in mouse embryonic stem cells treated with four GSK3 inhibitors. *BMC Res. Notes* 7, 1–8. doi:10.1186/1756-0500-7-273.
- Nikolopoulou, E., Galea, G. L., Rolo, A., Greene, N. D. E., and Copp, A. J. (2017). Neural tube closure: cellular, molecular and biomechanical mechanisms. *Development* 144, 552–566. doi:10.1242/dev.145904.
- Nizon, M., Henry, M., Michot, C., Baumann, C., Bazin, A., Bessières, B., et al. (2016). A series of 38 novel germline and somatic mutations of NIPBL in Cornelia de Lange syndrome. *Clin. Genet.* 89, 584–589. doi:10.1111/CGE.12720.
- Noisa, P., and Raivio, T. (2014). Neural crest cells: From developmental biology to clinical interventions. *Birth Defects Res. Part C Embryo Today Rev.* 102, 263–274. doi:10.1002/BDRC.21074.
- O'Donnell, V. B., Thomas, D., Stanton, R., Maillard, J.-Y., Murphy, R. C., Jones, S. A., et al. (2020). Potential Role of Oral Rinses Targeting the Viral Lipid Envelope in SARS-CoV-2 Infection. *Funct. (Oxford, England)* 1. doi:10.1093/FUNCTION/ZQAA002.
- Olley, G., Ansari, M., Bengani, H., Grimes, G. R., Rhodes, J., Von Kriegsheim, A., et al. (2018). BRD4 interacts with NIPBL and BRD4 is mutated in a Cornelia de Lange-like syndrome. *Nat. Genet.* doi:10.1038/s41588-018-0042-y.
- Onn, I., Heidinger-Pauli, J. M., Guacci, V., Ünal, E., and Koshland, D. E. (2008). Sister chromatid cohesion: A simple concept with a complex reality. *Annu. Rev. Cell Dev. Biol.* 24, 105–129. doi:10.1146/annurev.cellbio.24.110707.175350.
- Opitz, J. (1985). The Brachmann-de Lange syndrome. *Am. J. Med. Genet.* 22,

74–76. doi:10.1002/AJMG.1320220110.

Opitz, J. M., Segal, A. T., Lehrke, R., and Nadler, H. (1964). BRACHMANN/DE LANGE SYNDROME. *Lancet* 284, 1019. doi:10.1016/S0140-6736(64)90980-8.

Ottaviano, E., Parodi, C., Borghi, E., Massa, V., Gervasini, C., Centanni, S., et al. (2021). Saliva detection of SARS-CoV-2 for mitigating company outbreaks: a surveillance experience, Milan, Italy, March 2021. *Epidemiol. Infect.* 149, 1–3. doi:10.1017/S0950268821001473.

Pai, R., Tarnawski, A. S., and Tran, T. (2004a). Deoxycholic acid activates beta-catenin signaling pathway and increases colon cell cancer growth and invasiveness. *Mol. Biol. Cell* 15, 2156–2163. doi:10.1091/mbc.E03.

Pai, R., Tarnawski, A. S., and Tran, T. (2004b). Deoxycholic Acid Activates β -Catenin Signaling Pathway and Increases Colon Cell Cancer Growth and Invasiveness. *Mol. Biol. Cell* 15, 2156–2163. doi:10.1091/mbc.E03-12-0894.

Pajkrt, E., Griffin, D. R., and Chitty, L. S. (2010). Brachmann–de Lange syndrome: definition of prenatal sonographic features to facilitate definitive prenatal diagnosis. *Prenat. Diagn.* 30, 865–872. doi:10.1002/PD.2577.

Parenti, I., Gervasini, C., Pozojevic, J., Graul-Neumann, L., Azzollini, J., Braunholz, D., et al. (2016a). Broadening of cohesinopathies: Exome sequencing identifies mutations in ANKRD11 in two patients with Cornelia de Lange-overlapping phenotype. *Clin. Genet.* doi:10.1111/cge.12564.

Parenti, I., Gervasini, C., Pozojevic, J., Wendt, K. S., Watrin, E., Azzollini, J., et al. (2016b). Expanding the clinical spectrum of the “HDAC8-phenotype” - implications for molecular diagnostics, counseling and risk prediction. *Clin.*

Genet. doi:10.1111/cge.12717.

Parenti, I., Teresa-Rodrigo, M. E., Pozojevic, J., Ruiz Gil, S., Bader, I., Braunholz, D., et al. (2017). Mutations in chromatin regulators functionally link Cornelia de Lange syndrome and clinically overlapping phenotypes. *Hum. Genet.* doi:10.1007/s00439-017-1758-y.

Pauli, A., Althoff, F., Oliveira, R. A., Heidmann, S., Schuldiner, O., Lehner, C. F., et al. (2008). Cell-Type-Specific TEV Protease Cleavage Reveals Cohesin Functions in *Drosophila* Neurons. *Dev. Cell* 14, 239. doi:10.1016/J.DEVCEL.2007.12.009.

Pauli, A., Bommel, J. G. van, Oliveira, R. A., Itoh, T., Shirahige, K., Steensel, B. van, et al. (2010). A Direct Role for Cohesin in Gene Regulation and Ecdysone Response in *Drosophila* Salivary Glands. *Curr. Biol.* 20, 1787. doi:10.1016/J.CUB.2010.09.006.

Pearce, P. M., and Pitt, D. B. (1967). Six cases of de Lange's syndrome; parental consanguinity in two. *Med J Aust* 11;1(10):5.

Pinson, K. I., Brennan, J., Monkley, S., Avery, B. J., and Skarnes, W. C. (2000). An LDL-receptor-related protein mediates Wnt signalling in mice. *Nat.* 2000 4076803 407, 535–538. doi:10.1038/35035124.

Pistocchi, A., Fazio, G., Cereda, A., Ferrari, L., Bettini, L. R., Messina, G., et al. (2013a). Cornelia de Lange Syndrome: NIPBL haploinsufficiency downregulates canonical Wnt pathway in zebrafish embryos and patients fibroblasts. *Cell Death Dis.* 4, e866. doi:10.1038/cddis.2013.371.

Pistocchi, A., Fazio, G., Cereda, A., Ferrari, L., Bettini, L. R., Messina, G., et al. (2013b). Cornelia de Lange Syndrome: NIPBL haploinsufficiency downregulates canonical Wnt pathway in zebrafish embryos and patients fibroblasts. *Cell Death Dis.* 4. doi:10.1038/cddis.2013.371.

- Potts, P. R., Porteus, M. H., and Yu, H. (2006). Human SMC5/6 complex promotes sister chromatid homologous recombination by recruiting the SMC1/3 cohesin complex to double-strand breaks. *EMBO J.* 25, 3377. doi:10.1038/SJ.EMBOJ.7601218.
- Real-time RT-PCR Primers and Probes for COVID-19 | CDC Available at: <https://www.cdc.gov/coronavirus/2019-ncov/lab/rt-pcr-panel-primer-probes.html> [Accessed September 20, 2021].
- Revenkova, E., Focarelli, M. L., Susani, L., Paulis, M., Bassi, M. T., Mannini, L., et al. (2009). Cornelia de Lange syndrome mutations in SMC1A or SMC3 affect binding to DNA. *Hum. Mol. Genet.* 18, 418–427. doi:10.1093/hmg/ddn369.
- Rhodes, J., Mazza, D., Nasmyth, K., and Uphoff, S. (2017). Scc2/Nipbl hops between chromosomal cohesin rings after loading. *Elife* 6. doi:10.7554/eLife.30000.
- Rieger, M. E., Zhou, B., Solomon, N., Sunohara, M., Li, C., Nguyen, C., et al. (2016a). P300/ β -Catenin Interactions Regulate Adult Progenitor Cell Differentiation Downstream of WNT5a/Protein Kinase C (PKC). *J. Biol. Chem.* 291, 6569–6582. doi:10.1074/jbc.M115.706416.
- Rohatgi, S., Clark, D., Kline, A. D., Jackson, L. G., Pie, J., Siu, V., et al. (2010). Facial diagnosis of mild and variant CdLS: Insights from a dysmorphologist survey. *Am. J. Med. Genet. Part A* 152, 1641–1653. doi:10.1002/ajmg.a.33441.
- Rollins, R. A., Korom, M., Aulner, N., Martens, A., and Dorsett, D. (2004). Drosophila Nipped-B Protein Supports Sister Chromatid Cohesion and Opposes the Stromalin/Scc3 Cohesion Factor To Facilitate Long-Range Activation of the cut Gene. *Mol. Cell. Biol.* doi:10.1128/mcb.24.8.3100-3111.2004.

- Roshan Lal, T. R., Kliewer, M. A., Lopes, T., Rebsamen, S. L., O'Connor, J., Grados, M. A., et al. (2016). Cornelia de Lange syndrome: Correlation of brain MRI findings with behavioral assessment. *Am. J. Med. Genet. Part C Semin. Med. Genet.* 172, 190–197. doi:10.1002/ajmg.c.31503.
- Rubio, E. D., Reiss, D. J., Welcsh, P. L., Disteche, C. M., Filippova, G. N., Baliga, N. S., et al. (2008). CTCF physically links cohesin to chromatin. *Proc. Natl. Acad. Sci. U. S. A.* 105, 8309. doi:10.1073/PNAS.0801273105.
- Russell, K. L., Ming, J. E., Patel, K., Jukofsky, L., Magnusson, M., and Krantz, I. D. (2001). Dominant Paternal Transmission of Cornelia de Lange Syndrome: A New Case and Review of 25 Previously Reported Familial Recurrences. *Am. J. Med. Genet.* 104, 267. Available at: /pmc/articles/PMC4894663/ [Accessed September 26, 2021].
- S, M., M, E., P, V., O, B., I, F., F, D., et al. (1996). Brachmann-de Lange syndrome: pre- and postnatal findings. *Am. J. Med. Genet.* 62, 268–273. doi:10.1002/(sici)1096-8628(19960329)62:3<268::aid-ajmg12>3.0.co;2-i.
- Sakaue-Sawano, A., Kurokawa, H., Morimura, T., Hanyu, A., Hama, H., Osawa, H., et al. (2008). Visualizing Spatiotemporal Dynamics of Multicellular Cell-Cycle Progression. *Cell* 132, 487–498. doi:10.1016/J.CELL.2007.12.033.
- Saunier, C., Støve, S. I., Popp, B., Gérard, B., Blenski, M., AhMew, N., et al. (2016). Expanding the Phenotype Associated with NAA10-Related N-Terminal Acetylation Deficiency. *Hum. Mutat.* doi:10.1002/humu.23001.
- Schmitz, J., Watrin, E., Lénárt, P., Mechtler, K., and Peters, J. M. (2007). Sororin Is Required for Stable Binding of Cohesin to Chromatin and for Sister Chromatid Cohesion in Interphase. *Curr. Biol.* 17, 630–636. doi:10.1016/J.CUB.2007.02.029.
- Schrier, S. A., Sherer, I., Deardorff, M. A., Clark, D., Audette, L., Gillis, L., et al.

- (2011). Causes of Death and Autopsy Findings in a Large Study Cohort of Individuals with Cornelia de Lange Syndrome and Review of the Literature. *Am. J. Med. Genet. A* 155, 3007. doi:10.1002/AJMG.A.34329.
- Sekimoto, H., Osada, H., Kimura, H., Kamiyama, M., Arai, K., and Sekiya, S. (2000). Prenatal findings in Brachmann-de Lange syndrome. *Arch. Gynecol. Obstet.* 2000 2634 263, 182–184. doi:10.1007/S004040050278.
- Self - Lollisponge™ buccal sponge and swabs | Copan Available at: <https://www.copangroup.com/product-ranges/lollisponge/> [Accessed September 14, 2021].
- Selicorni, A., Mariani, M., Lettieri, A., and Massa, V. (2021). Cornelia de Lange Syndrome: From a Disease to a Broader Spectrum. *Genes* 2021, Vol. 12, Page 1075 12, 1075. doi:10.3390/GENES12071075.
- Sepulveda, W., Wong, A. E., and Casasbuenas, A. (2009). Nuchal translucency and nasal bone in first-trimester ultrasound screening for aneuploidy in multiple pregnancies. *Ultrasound Obstet. Gynecol.* 33, 152–156. doi:10.1002/UOG.6222.
- Serret, S., Thümmeler, S., Dor, E., Vesperini, S., Santos, A., and Askenazy, F. (2015). Lithium as a rescue therapy for regression and catatonia features in two SHANK3 patients with autism spectrum disorder: Case reports. *BMC Psychiatry* 15. doi:10.1186/s12888-015-0490-1.
- Shtutman, M., Zhurinsky, J., Simcha, I., Albanese, C., D’Amico, M., Pestell, R., et al. (1999). The cyclin D1 gene is a target of the β -catenin/LEF-1 pathway. *Proc. Natl. Acad. Sci. U. S. A.* 96, 5522. doi:10.1073/PNAS.96.10.5522.
- Song, L., Li, Y., Wang, K., Wang, Y.-Z., Molotkov, A., Gao, L., et al. (2009). Lrp6-mediated canonical Wnt signaling is required for lip formation and

- fusion. *Development* 136, 3161–3171. doi:10.1242/DEV.037440.
- Stiles, J., and Jernigan, T. L. (2010). The Basics of Brain Development. *Neuropsychol. Rev.* 20, 327. doi:10.1007/S11065-010-9148-4.
- Thrasivoulou, C., Millar, M., and Ahmed, A. (2013). Activation of intracellular calcium by multiple Wnt ligands and translocation of β -catenin into the nucleus: A convergent model of Wnt/Ca²⁺ and Wnt/ β -catenin pathways. *J. Biol. Chem.* 288, 35651–35659. doi:10.1074/jbc.M112.437913.
- Tonkin, E. T., Wang, T. J., Lisgo, S., Bamshad, M. J., and Strachan, T. (2004). NIPBL, encoding a homolog of fungal Scc2-type sister chromatid cohesion proteins and fly Nipped-B, is mutated in Cornelia de Lange syndrome. *Nat. Genet.* 36, 636–641. doi:10.1038/ng1363.
- Tortelote, G. G., Reis, R. R., de Almeida Mendes, F., and Abreu, J. G. (2017). Complexity of the Wnt/ β -catenin pathway: Searching for an activation model. *Cell. Signal.* 40, 30–43. doi:10.1016/j.cellsig.2017.08.008.
- Vaillant, C. Le, Quere, M.-P., David, A., Berlivet, M., and Boog, G. (2004). Prenatal Diagnosis of a 'Minor' Form of Brachmann-de Lange Syndrome by Three-Dimensional Sonography and Three-Dimensional Computed Tomography. *Fetal Diagn. Ther.* 19, 155–159. doi:10.1159/000075141.
- Vogels, C. B. F., Watkins, A. E., Harden, C. A., Brackney, D., Shafer, J., Wang, J., et al. (2020). SalivaDirect: A simplified and flexible platform to enhance SARS-CoV-2 testing capacity. *medRxiv*, 2020.08.03.20167791. doi:10.1101/2020.08.03.20167791.
- Wang, W.-K., Chen, S.-Y., Liu, I.-J., Chen, Y.-C., Chen, H.-L., Yang, C.-F., et al. (2004). Detection of SARS-associated Coronavirus in Throat Wash and Saliva in Early Diagnosis. *Emerg. Infect. Dis.* 10, 1213. doi:10.3201/EID1007.031113.

- Watrin, E., Kaiser, F. J., and Wendt, K. S. (2016). Gene regulation and chromatin organization: Relevance of cohesin mutations to human disease. *Curr. Opin. Genet. Dev.* doi:10.1016/j.gde.2015.12.004.
- Watrin, E., and Peters, J.-M. (2009). The cohesin complex is required for the DNA damage-induced G2/M checkpoint in mammalian cells. *EMBO J.* 28, 2625. doi:10.1038/EMBOJ.2009.202.
- Wendt, K. S., and Peters, J.-M. (2009). How cohesin and CTCF cooperate in regulating gene expression. *Chromosom. Res.* 2009 172 17, 201–214. doi:10.1007/S10577-008-9017-7.
- Westergaard, J. G., Chemnitz, J., Teisner, B., Poulsen, H. K., Ipsen, L., Beck, B., et al. (1983). Pregnancy-associated plasma protein A: A possible marker in the classification and prenatal diagnosis of Cornelia de Lange syndrome. *Prenat. Diagn.* 3, 225–232. doi:10.1002/PD.1970030307.
- Whitehead, M. T., Nagaraj, U. D., and Pearl, P. L. (2015). Neuroimaging features of Cornelia de Lange syndrome. *Pediatr. Radiol.* 45, 1198–1205. doi:10.1007/s00247-015-3300-5.
- Wilmink, F. A., Papatsonis, D. N. M., Grijseels, E. W. M., and Wessels, M. W. (2009). Cornelia de Lange Syndrome: A Recognizable Fetal Phenotype. *Fetal Diagn. Ther.* 26, 50–53. doi:10.1159/000236361.
- Woods, S. A., Robinson, H. B., Kohler, L. J., Agamanolis, D., Sterbenz, G., and Khalifa, M. (2014). Exome sequencing identifies a novel EP300 frame shift mutation in a patient with features that overlap cornelia de lange syndrome. *Am. J. Med. Genet. Part A.* doi:10.1002/ajmg.a.36237.
- Wyllie, A., Fournier, J., Casanovas-Massana, A., Campbell, M., Tokuyama, M., Vijayakumar, P., et al. (2020). Saliva or Nasopharyngeal Swab Specimens for Detection of SARS-CoV-2. *N. Engl. J. Med.* 383, 1283–1286.

doi:10.1056/NEJMC2016359.

- Yuan, B., Pehlivan, D., Karaca, E., Patel, N., Charng, W. L., Gambin, T., et al. (2015). Global transcriptional disturbances underlie Cornelia de Lange syndrome and related phenotypes. *J. Clin. Invest.* doi:10.1172/JCI77435.
- Yuen, K. C., Xu, B., Krantz, I. D., and Gerton, J. L. (2016). NIPBL Controls RNA Biogenesis to Prevent Activation of the Stress Kinase PKR. *Cell Rep.* 14, 93–102. doi:10.1016/j.celrep.2015.12.012.
- Zhang, A., Yeung, P. L., Li, C. W., Tsai, S. C., Dinh, G. K., Wu, X., et al. (2004). Identification of a novel family of ankyrin repeats containing cofactors for p160 nuclear receptor coactivators. *J. Biol. Chem.* 279, 33799–33805. doi:10.1074/jbc.M403997200.
- Zuin, J., Dixon, J. R., van der Reijden, M. I. J. A., Ye, Z., Kolovos, P., Brouwer, R. W. W., et al. (2014). Cohesin and CTCF differentially affect chromatin architecture and gene expression in human cells. *Proc. Natl. Acad. Sci. U. S. A.* 111, 996–1001. doi:10.1073/pnas.1317788111.

Appendix 1

List of Publications

Saliva detection of SARS-CoV-2 for mitigating company outbreaks: a surveillance experience, Milan, Italy, March 2021

From the Field

*These authors contributed equally to this work.

†LollipopStudy Group: Silvia Ancona, Elisa Adele Colombo, Elisabetta Di Fede, Paolo Grazioli, Elena Lesma, Antonella Lettieri. LollipopStudy Group provided advice in the pre-analytical and analytical phase.

Cite this article: Ottaviano E *et al* (2021). Saliva detection of SARS-CoV-2 for mitigating company outbreaks: a surveillance experience, Milan, Italy, March 2021. *Epidemiology and Infection* **149**, e171, 1–3. <https://doi.org/10.1017/S0950268821001473>

Received: 6 April 2021

Revised: 17 June 2021


Accepted: 23 June 2021

Key words:

Control measures; COVID-19; saliva sample; SARS-CoV-2; surveillance

Author for correspondence:

Silvia Bianchi, E-mail: silvia.bianchi@unimi.it

Emerenziana Ottaviano^{1,*}, Chiara Parodi^{1,*}, Elisa Borghi¹, Valentina Massa¹, Cristina Gervasini¹, Stefano Centanni¹, Gianvincenzo Zuccotti², LollipopStudy Group, Silvia Ancona, Elisa Adele Colombo, Elisabetta Di Fede, Paolo Grazioli, Elena Lesma and Antonella Lettieri† and Silvia Bianchi¹ 

¹Department of Health Sciences, Università degli Studi di Milano, Via Rudini, 8, 20142 Milan, Italy and ²Department of Paediatrics, Children Hospital V. Buzzi, Università degli Studi di Milano, Milan, Italy

Abstract

Monitoring the severe acute respiratory syndrome coronavirus 2 (SARS-CoV-2) community-wide transmission with a suitable and effective sampling method would be of great support for public health response to the spreading due to asymptomatic subjects in the community. Here, we describe how using saliva samples for SARS-CoV-2 detection has allowed for a weekly surveillance of a small business company and the early detection of coronavirus disease 2019 cases.

As on 23rd March, two cases were detected and investigated, and control measures were rapidly applied.

At the beginning of November 2020, a small business company implemented a weekly surveillance of all employees based on molecular detection of severe acute respiratory syndrome coronavirus 2 (SARS-CoV-2) infection using saliva as sampling method (planned surveillance). Active surveillance in closed communities based on multiple saliva testing could be a comprehensive approach to identify asymptomatic subjects and to reduce the transmission of SARS-CoV-2 infection [1, 2]. Saliva specimens allow for self-collection and repetitive testing by reducing the discomfort, thus increasing subject compliance [3, 4]. Hence, this strategy was envisaged for an elevated compliance and attendance to the surveillance activity. All 32 employees located in the surrounding area of Milan agreed to participate in such surveillance. The small business company consists of 10 different open space offices (three to six people per office, depending on the office size) located on two different floors, and one office with six employees in a nearby building. In the main building two kitchen areas for coffee breaks (maximum three people at one time) and a lunchroom (maximum six people at one time) were accessible for all the employees.

Employees were asked to provide a self-sampled saliva and a self-evaluation form with information on body temperature and presence of commonly referred coronavirus disease 2019 (COVID-19) symptoms.

COVID-19 cases were defined by a positive SARS-CoV-2 test. SARS-CoV-2 laboratory confirmed cases and their close contacts were tested every three days from the first positive SARS-CoV-2 test for 14 days (tight-mode).

Self-sampled saliva was collected using an *ad hoc* designed disposable prototype (LolliSponge™, Copan, Brescia, Italy) consisting of sponges inserted on a plastic shaft, fixed on a screw cap. A plastic tube allows to protect collected samples during transport to the laboratory. This system was validated by comparing paired nasopharyngeal swab (NPS) and LolliSponge™ samples (Supplementary Fig. S1).

Briefly, the LolliSponge™ was kept for one minute in the mouth allowing for the sponge to soak true saliva. The device is conceived so that the sponge does not come in contact with hands whereas can be safely stored in a collecting tube. Samples, maintained at room temperature (RT) and without transport medium as saliva is self-preservative, were delivered and tested for SARS-CoV-2 by quantitative reverse transcription polymerase chain reaction (qRT-PCR) assay at the microbiology laboratory of the Department of Health Sciences of the University of Milan, as previously described [5] with few adaptations. Saliva was recovered by centrifuging the device for 1 min at 500 × g. Briefly, 5 µl of saliva, upon treatment with proteinase K and heat inactivation, were used for RT-qPCR for the simultaneous detection of N1 (FAM probe), N2 (SUN) and human RNase P (RP, ATTO647) genes using the protocol published by the Centers for Disease Control [6]. Samples were considered positive upon detection of N1 and/or N2 (Ct <40). Invalid samples were assessed by RP (Ct >35).

© The Author(s), 2021. Published by Cambridge University Press. This is an Open Access article, distributed under the terms of the Creative Commons Attribution licence (<http://creativecommons.org/licenses/by/4.0/>), which permits unrestricted re-use, distribution and reproduction, provided the original article is properly cited.

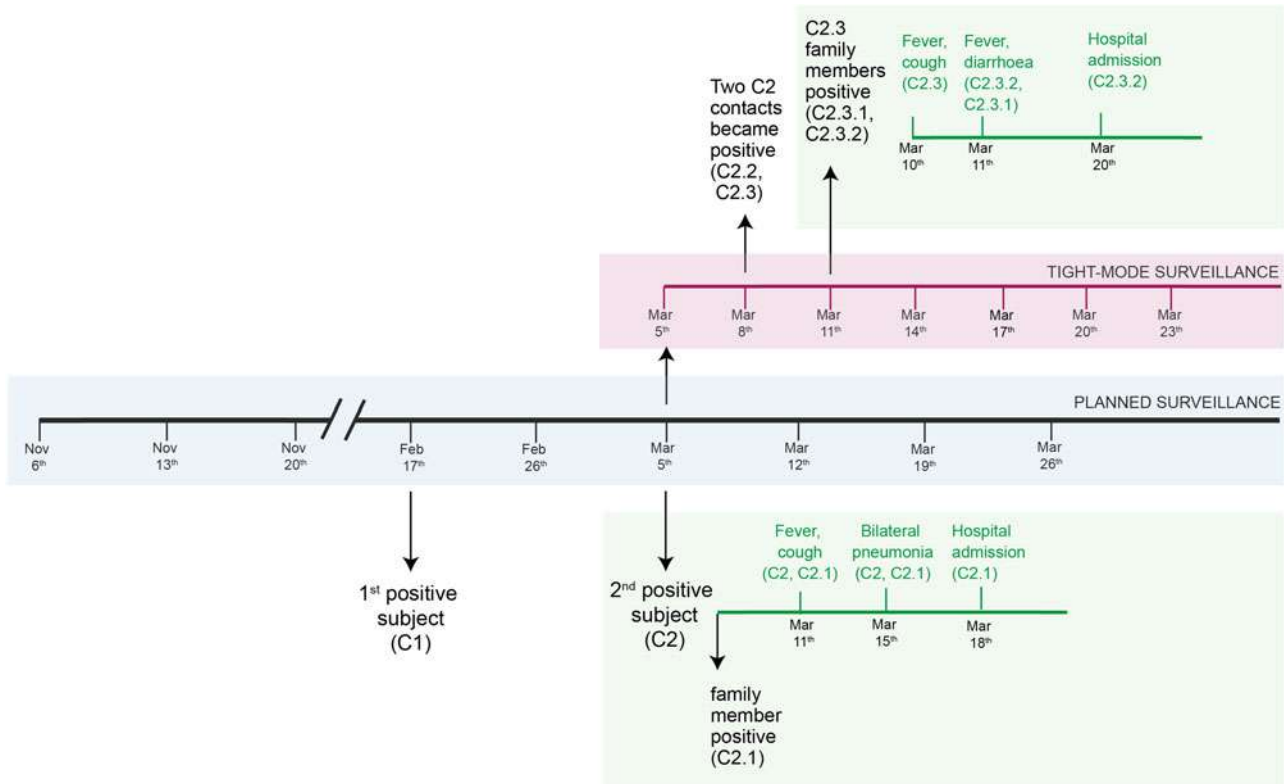


Fig. 1. Timeline of the active surveillance: in grey, planned surveillance; in purple, tight-mode surveillance; in green, self-reported clinical data.

A total of 32 subjects (mean age 39.5 years, range 25–71), 22 females and 10 males, underwent weekly testing. According to National laws [7], 30%–70% of staff was allowed to work in the office, leading to a variation in the planned frequency of sampling.

Starting from the 6th of November, a total of 397 samples were analysed, with a mean of 12.41 samples/persons during the surveillance time and 2.5 samples/month/persons.

On the 17th of February, the first positive case was detected (N1 Ct = 34.8, N2 Ct = Undetected, RP Ct = 27.5). The subject (C1) was a healthy 38-year-old female and was promptly isolated and contact tracing started. Because of the National Law, the subject was attending work fortnightly, and did not report any direct contact with colleagues or family members for the previous seven days. She recounted a meeting with few friends that were later found positive by National Health Service (NHS) NPS testing. The planned tight-mode surveillance did not highlight any other positive results. C1 was always asymptomatic.

On the 5th of March another case (C2), a healthy 71-year-old man, tested positive (N1 Ct = 20.5, N2 Ct = 25.5, RP = Ct 26.6) triggering contact tracing and tight-mode surveillance (work and household contacts of positive cases were offered testing every 3 days). The day after, his family member (C2.1), a previously healthy 71-year-old woman, also tested positive, and developed fever. Both subjects presented with interstitial lung disease (ILD) on the 15th of March, about 10 days after their positivity in saliva.

In the company, five people were considered at risk for sharing open space and three for sharing the lunch break. All these close contacts tested negative for SARS-CoV-2 on the 5th of March. They were all advised to increase protective measures at home. On the 8th of March, two (C2.2 and C2.3) of the eight contacts became positive to SARS-CoV-2 infection, all of whom shared

the open space office with the index case. C2.2, a healthy 42-year-old man, presented mild symptoms and remained positive for 11 days. He was isolated from his family on the 6th of March and none of his four family members showed positive results. C2.3, a healthy 43-year-old woman, did not implement any isolation measures at home and both her family members (C2.3.1 and C2.3.2) tested positive in saliva on day 6. Four days after the detection in saliva, C2.3 and her family members presented COVID-19 symptoms. At the end of the 14 days-tight surveillance none of the 29 other employees was infected (Fig. 1). To note, hospitalised cases in our study resulted from a sustained exposure (at home).

In this report, we present the possible advantage of an active surveillance using saliva samples for the early detection of SARS-CoV-2 [8] and the mitigating effects on COVID-19 outbreak in a small business company in the metropolitan area of Milan, Lombardy, one of the areas most affected by SARS-CoV-2 pandemic in Italy. In our study, positive cases were detected during the two peaks of viral circulation in Lombardy (November 2020 and March 2021) [9]. Given that, in our country, mainly symptomatic subjects are normally tested, the percentage of positive subjects in our asymptomatic cohort is difficult to be compared with officially reported numbers.

Further, it is possible to hypothesise a higher compliance to suggested mitigation measures – i.e., masking, distancing, air changing etc. – in a population actively seeking for surveillance.

Viral replication in saliva starts in the very early phases of SARS-CoV-2 infection, and viral load is independent of symptom severity [10], thus permitting to identify infectious subjects timely, also in asymptomatic individuals [11]. Clearly, saliva droplets represent a too often underestimated but extremely efficient

route of transmission, as described also for other respiratory viruses [12].

This study exemplifies how measures based on case-based surveillance – i.e., of notified cases, mostly symptomatic [13] – fail to control or mitigate viral spread. All the positive subjects identified by the planned surveillance were asymptomatic at the time of testing, with no recognised risk of exposure.

Based on our data, whereby implementing recommended control measures led to interrupting the outbreak [14], we suggest designing active surveillance based on saliva for closed communities, even on a bigger scale such as schools and residential care home. Timing could be fine-tuned according to local epidemiological situation and tightened upon positive cases. Larger studies evaluating costs, logistics and feasibility are currently undergoing in our country.

Supplementary material. The supplementary material for this article can be found at <https://doi.org/10.1017/S0950268821001473>.

Acknowledgements. The authors would like to express their deepest gratitude to all the participants to the study and to Copan Italia Spa for the fruitful collaboration and for donating Lollisponge devices for saliva collection.

Financial support. The authors are grateful to the following funding sources: Nickel & Co S.p.A (to VM); Todini and Co. S.p.A. (to EB); Davide Maternini S.p.A. (to VM); Intramural funding-Dipartimento DISS, Università degli Studi di Milano; Translational Medicine PhD scholarship-Università degli Studi di Milano (to CP).

Conflict of interest. None.

Ethical standards. Ethical approval was not required for this study as no individual data were used. All participants signed an informed consent giving permission for anonymised data use.

Data. The data presented in this study are available on request from the corresponding author.

References

1. **European Centre for Disease Prevention and Control.** COVID-19 testing strategies and objectives. 15 September 2020. ECDC: Stockholm; 2020. Accessed March 2021. Available at: https://www.ecdc.europa.eu/sites/default/files/documents/TestingStrategy_Objective-Sept-2020.pdf.
2. **Centres for Disease Prevention and Control.** Interim Guidance for SARS-CoV-2 Testing in Non-Healthcare Workplaces. Accessed March 2021. Available at: <https://www.cdc.gov/coronavirus/2019-ncov/community/organizations/testing-non-healthcare-workplaces.html>.
3. **Czumbel LM et al.** (2020) Saliva as a candidate for COVID-19 diagnostic testing: a meta-analysis. *Frontiers in Medicine (Lausanne)* 7, 465, eCollection 2020. PMID: 32903849; PMCID: PMC7438940.
4. **U.S. Food and Drug Administration.** Press Announcements. Coronavirus (COVID-19) Update: FDA Issues Emergency Use Authorization to Yale School of Public Health for SalivaDirect, Which Uses a New Method of Saliva Sample Processing. Accessed March 2021. Available at: <https://www.fda.gov/news-events/press-announcements/coronavirus-covid-19-update-fda-issues-emergency-use-authorization-yale-school-public-health>.
5. **Borghesi E et al.; UNIMI SAL Study group** (2021) Saliva sampling for chasing SARS-CoV-2: a game-changing strategy. *Pharmacological Research* 165, 105380. PMID: 33338623; PMCID: PMC7832951.
6. **Centers for Disease Prevention and Control.** Research Use Only 2019-Novel Coronavirus (2019-nCoV) Real-time RT-PCR Primers and Probes. Accessed March 2021. Available at: <https://www.cdc.gov/coronavirus/2019-ncov/lab/rt-pcr-panel-primer-probes.html>.
7. **Italian Ministry of Health.** Covid-19, situation in Italy. Last update 6th April 2021. Accessed April 2021. Available at: <http://www.salute.gov.it/portale/nuovocoronavirus/dettaglioContenutiNuovoCoronavirus.jsp?id=5367&area=nuovoCoronavirus&menu=vuoto>.
8. **Wyllie AL et al.** (2020) Saliva or nasopharyngeal swab specimens for detection of SARS-CoV-2. *New England Journal of Medicine* 383, 1283–1286, PMID: 32857487; PMCID: PMC7484747.
9. **Regione Lombardia.** Dashboard Covid-19. Accessed May 2021. Available at: <https://www.regione.lombardia.it/wps/portal/istituzionale/HP/servizi-e-informazioni/cittadini/salute-e-prevenzione/coronavirus/dashboard-covid19>.
10. **O'Donnell VB et al.** (2020) Potential role of oral rinses targeting the viral lipid envelope in SARS-CoV-2 infection. *Function (Oxford, England)* 1, zqaa002, PMID: 33215159; PMCID: PMC7239187.
11. **Wang WK et al.** (2004) Detection of SARS-associated coronavirus in throat wash and saliva in early diagnosis. *Emerging Infectious Diseases* 10, 1213–1219, PMID: 15324540; PMCID: PMC3323313.
12. **Kutter JS et al.** (2018) Transmission routes of respiratory viruses among humans. *Current Opinion in Virology* 28, 142–151, PMID: 29452994; PMCID: PMC7102683.
13. **European Centre for Disease Prevention and Control.** Strategies for the surveillance of COVID-19. Stockholm: ECDC; 2020. Accessed March 2021. Available at: <https://www.ecdc.europa.eu/sites/default/files/documents/COVID-19-surveillance-strategy-9-Apr-2020.pdf>.
14. **Kucharski AJ et al.** (2020) Effectiveness of isolation, testing, contact tracing, and physical distancing on reducing transmission of SARS-CoV-2 in different settings: a mathematical modelling study. *The Lancet Infectious Diseases* 20, 1151–1160, PMID: 32559451; PMCID: PMC7511527.



Chromatin Imbalance as the Vertex Between Fetal Valproate Syndrome and Chromatinopathies

Chiara Parodi¹, Elisabetta Di Fede¹, Angela Peron^{2,3,4}, Ilaria Viganò¹, Paolo Grazioli¹, Silvia Castiglioni¹, Richard H. Finnell⁵, Cristina Gervasini^{1,6†}, Aglaia Vignoli^{1†} and Valentina Massa^{1,6*†}

¹ Department of Health Sciences, Università degli Studi di Milano, Milan, Italy, ² Human Pathology and Medical Genetics, ASST Santi Paolo e Carlo, San Paolo Hospital, Milan, Italy, ³ Child Neuropsychiatry Unit–Epilepsy Center, Department of Health Sciences, San Paolo Hospital, ASST Santi Paolo e Carlo, Università degli Studi di Milano, Milan, Italy, ⁴ Division of Medical Genetics, Department of Pediatrics, University of Utah School of Medicine, Salt Lake City, UT, United States, ⁵ Departments of Molecular and Cellular Biology, Molecular and Human Genetics and Medicine, Center for Precision Environmental Health, Baylor College of Medicine, Houston, TX, United States, ⁶ “Aldo Ravelli” Center for Neurotechnology and Experimental Brain Therapeutics, Università degli Studi di Milano, Milan, Italy

OPEN ACCESS

Edited by:

Xiajun Li,
ShanghaiTech University, China

Reviewed by:

Taiping Chen,
University of Texas MD Anderson
Cancer Center, United States
Alejandro Vaquero,
Josep Carreras Leukaemia Research
Institute (IJC), Spain

*Correspondence:

Valentina Massa
valentina.massa@unimi.it

†These authors have contributed
equally to this work and share last
authorship

Specialty section:

This article was submitted to
Developmental Epigenetics,
a section of the journal
Frontiers in Cell and Developmental
Biology

Received: 16 January 2021

Accepted: 01 April 2021

Published: 20 April 2021

Citation:

Parodi C, Di Fede E, Peron A,
Viganò I, Grazioli P, Castiglioni S,
Finnell RH, Gervasini C, Vignoli A and
Massa V (2021) Chromatin Imbalance
as the Vertex Between Fetal Valproate
Syndrome and Chromatinopathies.
Front. Cell Dev. Biol. 9:654467.
doi: 10.3389/fcell.2021.654467

Prenatal exposure to valproate (VPA), an antiepileptic drug, has been associated with fetal valproate spectrum disorders (FVSD), a clinical condition including congenital malformations, developmental delay, intellectual disability as well as autism spectrum disorder, together with a distinctive facial appearance. VPA is a known inhibitor of histone deacetylase which regulates the chromatin state. Interestingly, perturbations of this epigenetic balance are associated with chromatinopathies, a heterogeneous group of Mendelian disorders arising from mutations in components of the epigenetic machinery. Patients affected from these disorders display a plethora of clinical signs, mainly neurological deficits and intellectual disability, together with distinctive craniofacial dysmorphisms. Remarkably, critically examining the phenotype of FVSD and chromatinopathies, they shared several overlapping features that can be observed despite the different etiologies of these disorders, suggesting the possible existence of a common perturbed mechanism(s) during embryonic development.

Keywords: fetal valproate syndrome, chromatinopathies, anti-epileptic drugs, neurodevelopment, HDAC inhibitor

INTRODUCTION

Prenatal exposure to antiepileptic drugs (AEDs) are subject to the teratogenic effects associated with all of the frontline AED medications. Most women with epilepsy receiving adequate prenatal care will have uneventful pregnancies, but they are at a well-documented increased risk for having infants with congenital malformations compared to the general population (Viale et al., 2015). *In utero* AED exposure places their offspring at increased risk not only for major congenital malformations, but also for adverse neurological developmental outcomes. However, many of these risks can be mitigated through comprehensive prenatal maternal care by carefully selecting the type and dose of AEDs prior to conception and continuing to follow a proper therapeutic regimen throughout pregnancy (Tomson et al., 2011). Among all AEDs, valproate (2-propylpentanoic acid, VPA) exposure has been associated with the greatest risks of inducing severe teratogenicity (Lammer et al., 1987; Tomson et al., 2015). Several studies demonstrated a correlation between chronic exposure to VPA treatment and higher risk of displaying fetal anomalies—such as neural tube defects (NTDs), distinctive facial dysmorphia, craniofacial, and skeletal defects—in both in

humans and in animal models (Massa et al., 2005, 2006). Among the teratogen-induced congenital malformations, the most commonly observed include spina bifida, atrial septal defects, cleft palate, hypospadias, polydactyly, and craniosynostosis (Macfarlane and Greenhalgh, 2018).

Animal experiments demonstrated morphogenic anomalies throughout the entire axial skeleton and vertebral transformations in rat embryos due to VPA exposure, suggesting a possible compromise of the expression of genes involved in vertebral segments development (Menegola et al., 1998, 1999). In addition, an altered serotonergic differentiation, which correlates with autism-like behavioral abnormalities, was observed both in rodent and zebrafish models in response to prenatal valproate exposure (Dufour-Rainfray et al., 2010; Jacob et al., 2014). The amount of fetal harm appears to be linked to the maternal concentration of the drug (Nau et al., 1981; Nau, 1985), especially when it occurs in the first trimester during fetal organogenesis (Macfarlane and Greenhalgh, 2018). In animal models, such as *Xenopus* and *Hyperolius*, the beginning of gastrulation was delayed up to neurulation upon embryonic exposure to VPA, and eventually they displayed NTDs of different types and degree (Oberemm and Kirschbaum, 1992). To date, the correlation between typical dysmorphic facial features and developmental outcomes is unclear (Kini et al., 2006; Nicolini and Fahnestock, 2018).

Fetal valproate syndrome (FVS, OMIM #609442) is a condition resulting from the therapeutic management of epileptic mothers with VPA during their pregnancy, and it is observed in up to 20–30% of children exposed to high VPA dosage *in utero* (Nau et al., 1991; Ornoy, 2009; Tomson et al., 2011). FVS is characterized by a constellation of congenital malformations and developmental delay, with patients displaying intellectual disability (ID) as well as autism spectrum disorder (ASD), and a distinctive facial appearance strikingly similar to the one described in genetic disorders known as chromatinopathies (DiLiberti et al., 1984). A new term “fetal valproate spectrum disorder” (FVSD) has recently been proposed to describe the range of clinical and developmental effects that are attributed to *in utero* VPA exposure (Clayton-Smith et al., 2019).

Valproate has been commonly used as an anti-seizure medication for over half a century (Meunier et al., 1963). Given its broad antiepileptic effect, it has also been clinically utilized as a mood stabilizer in the treatment of bipolar disorders and in other neurological conditions—i.e., migraine and neuropathic pain, exposing many more women of reproductive age to this medication (Johannessen and Johannessen, 2003). In addition, this antiepileptic drug has shown anticancer properties for several tumors (Shah and Stonier, 2019), and its use in combination regimens with cytotoxic chemotherapy seems to be promising (Brodie and Brandes, 2014). VPA is also known to be a potent histone deacetylase inhibitor (HDACi) and therefore acts on chromatin. It is known to have dose-related teratogenic properties resulting in altered gene expression and potent inhibition of the histone deacetylases (HDAC) enzymes family (Schölz et al., 2015). Among the various hypotheses that have been proposed for the teratogenicity of VPA, its HDACi effects that is believed to be represent the principle underlying

teratogenic mechanism. VPA's anti-seizure activity can also be explained by its ability to modulate gene expression through the inhibition of HDAC enzymes (Göttlicher et al., 2001; Jacob et al., 2013; Brunton et al., 2018).

Valproate perturbs the cell's epigenetic machinery controlling its chromatin state. In this context, a group of heterogeneous genetic disorders known as the chromatinopathies, are believed to be caused by mutations in genes that regulate the conformation and function of chromatin, thus acting in concert with epigenetic mechanisms. Defects in the functional network between the complexes associated with chromatin could lead to alterations in gene expression and protein function. As estimated, there are over 80 Mendelian diseases associated with incorrect functioning of the “epigenetic machinery”, the majority of which presents with neurological defects and ID (Fahrner and Bjornsson, 2019). Kabuki syndrome (OMIM #147920 and #300867) (Niikawa et al., 1981) and CHARGE syndrome (OMIM #214800) (Pagon et al., 1981) are among the most well-known and studied chromatinopathies, for the cascading effect of the causative genes on different cell pathways. These syndromes are associated with ID and distinctive craniofacial dysmorphisms that are pathognomonic.

In this review, we explore shared features between FVSD and selected chromatinopathies, leading us to the hypothesis that these disorders, despite divergent etiologies (i.e., environmental or genetic), could operate through a common perturbed mechanism during embryonic development. As such, VPA-induced FVSD is a phenocopy of select chromatinopathies.

VALPROATE MECHANISM OF ACTION

Valproate has multiple cellular mechanisms of action consistent with its broad clinical efficacy. This compound appears to suppress repetitive high-frequency neuronal focus by blocking voltage-dependent sodium channels, but at sites that are different from other AEDs. VPA also appears to increase GABA concentrations in the brain at clinically relevant doses, without having direct effects on the GABA (A) receptors, potentiated by a presynaptic effect of valproate on GABA (B) receptors. In addition, VPA can increase GABA synthesis by activating the enzyme glutamic acid decarboxylase (GAD).

The molecular mechanisms underlying FVSD have not been fully established, although the consequences of *in utero* VPA exposure have been investigated for several decades. Such effects include apoptotic neurodegeneration observed in the developing rat brain (Bittigau et al., 2002), enhanced synaptic plasticity exhibited in the rat medial prefrontal cortex (Sui and Chen, 2012), and a decrease in folic acid (Wegner and Nau, 1992), suggesting that inadequate embryonic and fetal antioxidant defense mechanisms and consequent oxidative stress could be responsible for brain damage secondary to VPA teratogenicity (Ornoy, 2009).

Despite the fact that VPA has been shown to be neuroprotective in neurons through *Bcl-2* upregulation (Chen et al., 1999), its administration in critical developmental stages causes morphological defects and impaired social behavior in

rats (Kim et al., 2011). *In utero* VPA exposure in mouse pups on gestational day 11 leads to dysfunctional pre-weaning social behavior, together with delayed development, impaired olfactory discrimination and reduced cortical *Bdnf* expression, suggesting that VPA-driven perturbations in neuronal plasticity may underlie the behavioral phenotype (Rouillet et al., 2010). Similar to the results of VPA exposure of pregnant rats, neural progenitor cells (NPCs) of murine embryos exposed on gestational day E12 showed a reduced apoptotic cell death, which is fundamental to the proper regulation of NPCs during a developmentally critical period, suggesting another possible mechanism underlying FVSD defects (Go et al., 2011).

Alterations in embryonic gene expression following VPA exposure appears to be one of the primary mechanisms underlying VPA's teratogenicity. Previous studies showed that VPA alters Wnt signaling by inducing Wnt-dependent gene expression at doses that cause developmental effects (Phiel et al., 2001; Wiltse, 2005). This is due to its role as an HDAC inhibitor, which consists of deregulating class I HDACs, thus counteracting their normal activity of histone acetylation marks removal. This action induces chromatin changes converting segments of heterochromatin into euchromatin. VPA exposure can lead to hyperacetylation of histones and following activation of genes related to cell cycle and apoptosis, possibly explaining its teratogenic action (Göttlicher et al., 2001). For instance, hyperacetylation of all *Hoxb* developmental genes has been observed in mouse embryonic stem cells exposed to VPA, with increased levels of H3K9ac at upstream, promoter and coding regions across the entire *Hoxb* cluster (Boudadi et al., 2013).

Previous studies showed how HDACi is involved in early neuronal processes: exposure of neurulation-stage mouse embryos to VPA can cause NTDs and skeletal malformations (Finnell et al., 2002), supported by *in vivo* studies on chick embryos in which a complete failure of neural tube closure occurred (Murko et al., 2013). Since VPA exposure alters gene expression in the somitic tissues of mouse embryos (Massa et al., 2005) and an increased histone H4 acetylation in the caudal neural tube was observed, modulation of acetylation was hypothesized as mediating the effect of VPA on neurulation (Massa et al., 2005, 2009; Menegola et al., 2005).

VALPROATE IN CLINICAL PRACTICE

Valproate is a wide-spectrum anti-seizure medication that can be used to treat almost all types of seizure disorders (tonic clonic seizures, absence seizures, myoclonic seizures, less frequently in clonic seizures, tonic seizures and atonic seizures) (Perucca, 2002). It is used as first-line antiepileptic drug in generalized seizures; VPA may also be used in focal seizures, although it is no longer the first choice of neurologists (Tomson et al., 2015).

Valproate is also a mood stabilizer that is used in the treatment of bipolar disorders and other psychiatric conditions, including: anxiety disorders, post-traumatic stress disorder, substance abuse, and schizophrenia. VPA also appears to be an effective treatment for tardive dyskinesia thanks to its GABA-potentiating properties (Swann et al., 2002), for migraine prophylaxis, and for

the treatment of neuropathic pain, in particular for trigeminal neuralgia (Johannessen and Johannessen, 2003).

Typically, the initial dose of oral valproate is 10–15 mg/kg per day. If necessary, the dose can be increased with weekly increments of 5–10 mg/kg up to a maximum dose of 60 mg/kg/day. It is recommended to monitor VPA blood level during treatment, as well as blood count, liver enzymes, and coagulation tests, in order to avoid any potential side effects of the drug.

Valproate can alter vitamin D metabolism and affect bone mineral density, therefore 25-hydroxyvitamin D levels should be monitored. It may be useful to obtain serum amylase and lipase levels in cases where symptoms suggestive of pancreatitis, such as abdominal pain, nausea, vomiting and anorexia have occurred. Furthermore, ammonium levels should be monitored in patients receiving VPA who exhibit signs of vomiting or lethargy as the treatment inhibits *N*-acetyl glutamate, leading to systemic disruption and hyperammonemia (Bruni et al., 1979; Batshaw and Brusilow, 1982; Asconapé et al., 1993; Patsalos et al., 2008).

It is strongly recommended that VPA administration should be avoided during pregnancy; however, if necessary, a slow-release formulation that limits peak concentrations of the drug using the lowest efficacious dose possible should be given along with the administration of a high dose of folic acid. While folic acid has not been shown to be effective in reducing the prevalence of NTDs, it has been shown to be protective in limiting adverse cognitive consequences of VPA treatment, especially with respect to language skills (Meador et al., 2020).

CLINICAL FEATURES ASSOCIATED WITH FVSD

Studies conducted by Robert and Guibaud (1982) first drew attention to the increased risk of spina bifida after exposure to VPA in pregnancy. Subsequently, the initial reports of children suffering from FVSD were published (DiLiberti et al., 1984). FVSD is characterized by major and minor malformations, facial dysmorphism and impaired development with particular risks related to NTDs (Lindhout and Schmidt, 1986), congenital heart disease, ophthalmological, (Glover et al., 2002) and genitourinary abnormalities (DiLiberti et al., 1984; Ozkan et al., 2011), cleft palate (Jackson et al., 2016), overlapping fingers, and scalp defects (DiLiberti et al., 1984; Clayton-Smith and Donnai, 1995; Clayton-Smith et al., 2019).

Neurological development is impaired in many affected individuals. An increased risk of attention deficit hyperactivity disorder (ADHD) and ASD is often observed in these patients (Bromley et al., 2013, 2014, 2019; Christensen et al., 2013).

The typical facial features of FVSD include: swelling of the metopic suture, highly-arched eyebrows, hypertelorism, wide nasal bridge, short nose with anteverted nostrils, small mouth with thin upper lip and flat filament of the inverted lower lip (Ardinger et al., 1988; Clayton-Smith and Donnai, 1995; Kozma, 2001; Schorry et al., 2005; Kini et al., 2006; Chandane and Shah, 2014; Mohd Yunus and Green, 2018) (**Figure 1**).

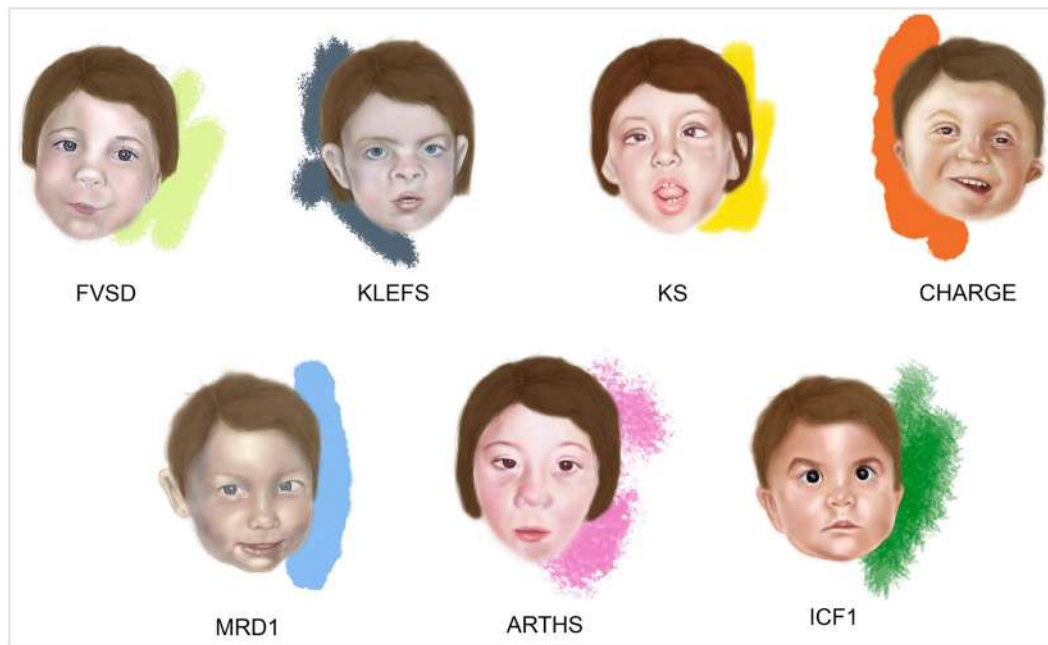


FIGURE 1 | Facies of fetal valproate spectrum disorders (FVSD) and related overlapping chromatinopathies. Distinctive facial phenotypes of patients affected by FVSD (Schorry et al., 2005), KLEFS (Willemsen et al., 2012), KS (Makrythanasis et al., 2013), CHARGE (Hefner and Fassi, 2017), MRD1 (Talkowski et al., 2011), ARTHS (Kennedy et al., 2019), and ICF1 (Gössling et al., 2017).

DIFFERENTIAL DIAGNOSES OF FVSD

Fetal valproate spectrum disorder diagnosis has been challenging in many ways, from gathering correct information about prenatal VPA exposure, to obtaining a comprehensive grasp of the clinically varied diagnostic phenotypic signs. Indeed, clinical presentations of affected patients show variability and the prevalence of neurocognitive dysfunction is higher than the prevalence of structural malformations, complicating the path toward reliable diagnosis (Clayton-Smith et al., 2019). In fact, not all the FVSD individuals even display dysmorphisms, which can be age dependent and rather subtle, thus recognizable only by experienced dysmorphologists. When FVSD signs are ascertained, physicians are often challenged by overlapping phenotypes associated with the following syndromes (Figure 1 and Table 1).

Kleefstra Syndrome

Kleefstra syndrome (KLEFS, OMIM #610253, #617768) is a rare condition characterized by heterozygous genomic deletions at chromosome 9q34.3 removing the *EHMT1* gene or *EHMT1* point mutations (KLEFS1), or pathogenic variants in *KMT2C* on chromosome 7q36.1 (KLEFS2), mostly *de novo*. *EHMT1* and *KMT2C* genes encode two histone methyltransferases. The prevalence is estimated to be 1:120,000 individuals affected by neurodevelopmental disorders. Patients with Kleefstra syndrome exhibit a distinctive phenotype including hypotonia; major anomalies such as congenital heart defects and genitourinary abnormalities; behavioral and developmental manifestations with

ID of variable severity, and in some cases severe speech delay. Typical facial dysmorphisms include: microcephaly, arched or straight with synophrys eyebrows, mildly up-slanted palpebral fissures, hypertelorism, short nose with anteverted nares and bulbous nasal tip, thick mouth, and everted lower lip (Kleefstra and De Leeuw, 1993; Kleefstra et al., 2006, 2012; Koemans et al., 2017) (Figure 1).

Fetal valproate spectrum disorders has been recently defined as a “phenocopy” of Kleefstra syndrome by Arora et al. (2018). Despite a preliminary diagnosis of FVSD—due to maternal intake of VPA during pregnancy and with clear facial characteristics that are typically attributable to FVSD—a more thorough examination of the facial features revealed subtle differences. Specific features of the proband included the presence of a broad forehead and brachycephaly in a child with FVSD, who had cephalic deformation due to the premature fusion of the metopic suture, scattered eyebrows, and pointed chin. Genetic testing revealed a *de novo* deletion on 9q34.3 that is known to cause Kleefstra syndrome. The convergent mechanism present in both conditions is their role in epigenetic modulation that mediates the modification (acetylation, methylation, etc.) of histone proteins and DNA demethylation, which might be responsible for the overlapping phenotype of FVSD and Kleefstra Syndrome (Willemsen et al., 2012; Hadzsiev et al., 2016; Arora et al., 2018) (Table 1).

Kabuki Syndrome

Specific dysmorphisms, postnatal growth delay, skeletal anomalies, and ID are typical features of another

TABLE 1 | Fetal valproate spectrum disorders (FVSD) clinical signs in chromatinopathies.

FVSD clinical signs	KLEFS	KS	CHARGE	MRD1	ARTHS	ICF
Facial dysmorphisms						
Scalp defects	–	–	–	–	–	–
High/prominent forehead	+	–	+	Broad	–	±
Bitemporal narrowing	–	–	±	–	+	–
Arched eyebrows	+	+	–	+	–	±
Hypertelorism	+	±	±	–	–	+
Epicanthal folds	+	–	+	–	±	+
Ears abnormalities	+	+	+	+	±	+
Midface hypoplasia	+	–	+	±	–	–
Short nose	+	–	±	+	–	±
Broad/flat nasal bridge	+	+	–	+	Broad tip	+
Anteverted nostrils	+	–	–	–	–	±
Long smooth philtrum	+	–	–	–	–	–
Small mouth	–	–	–	–	–	–
Thin upper lip	–	–	±	+	+	–
Downturned corners of the mouth	+	–	–	+	±	–
Congenital anomalies						
Cleft palate	+	+	+	±	±	±
Macroglossia	–	–	+	–	–	±
Micro/retrognathia	–	+	+	+	±	±
Microcephaly	+	+	+	+	+	na
Trigonocephaly	–	–	–	–	–	–
Brachycephaly	+	–	–	+	±	–
Other malformations						
Neural tube or CNS defects	+	+	+	–	±	±
Ophthalmological defects	±	+	+	±	+	–
Muscoskeletal anomalies	–	+	+	+	±	–
Congenital heart defects	+	+	+	+	+	±
Genitourinary anomalies	+	+	+	±	±	–
Developmental delay	+	+	+	+	+	±
Intellectual disability	+	+	+	+	+	±
Speech delay	+	+	+	+	+	+
Behavioral problems	+	±	+	+	+	–
References						
DiLiberti et al., 1984; Ardinger et al., 1988; Kozma, 2001; Schorry et al., 2005; Kini et al., 2006; Chandane and Shah, 2014; Mohd Yunos and Green, 2018	Willemsen et al., 2012; Hadzsiev et al., 2016; Arora et al., 2018	Makrythanasis et al., 2013; Adam et al., 2019; Shangguan et al., 2019	Hefner and Fassi, 2017; van Ravenswaaij-Arts and Martin, 2017	Van Bon et al., 2010; Talkowski et al., 2011; Hodge et al., 2014; Mullegama et al., 2016	Arboleda et al., 2015; Tham et al., 2015; Millan et al., 2016; Murray et al., 2017; Kennedy et al., 2019	Hagleitner et al., 2008; Weemaes et al., 2013; van den Boogaard et al., 2017; Kamae et al., 2018

KLEFS, Kleefstra syndrome; KS, Kabuki syndrome; CHARGE, CHARGE syndrome; MRD1, mental retardation autosomal dominant 1; ARTHS, Arboleda-Tham syndrome; ICF1, immunodeficiency, centromeric instability, and facial anomalies syndrome 1; +, present; –, absent; ±, present in few cases; na, not available.

chromatinopathy such as Kabuki syndrome (KS, OMIM #147920 and #300867) (Kuroki et al., 1981; Niikawa et al., 1981; Adam et al., 2019). KS is caused by heterozygous pathogenic variants in *KMT2D* or *KDM6A* genes (Ng et al., 2010; Banka et al., 2012; Lederer et al., 2012; Miyake et al., 2013), on chromosome

12q13.12 and Xp11.3, causing KS1 and KS2, respectively. These genes altered in KS encode for a histone methyltransferase and a histone demethylase exerting their effect on different histone residues that favor the opening of chromatin and leading to the same downstream effects on gene expression, ultimately

resulting in the same condition. Aside from ID, developmental impairment and congenital heart defects, KS shares with FVSD specific craniofacial features such as arched eyebrows, wide nasal bridge, and cleft palate (Makrythanasis et al., 2013; Adam et al., 2019; Shangguan et al., 2019) (**Figure 1** and **Table 1**).

CHARGE Syndrome

CHARGE syndrome (OMIM #214800) is an acronym that summarizes the main clinical manifestations, namely Coloboma of the eye, Heart defect, choanal Atresia, Retardation of psychomotor development and growth, Genital hypoplasia, and Ear abnormalities. This syndrome is caused by heterozygous pathogenic variants in *CHD7* (OMIM # 608892), encoding an epigenetic regulator that is involved in the ATP-dependent remodeling of chromatin (Vissers et al., 2004; van Ravenswaaij-Arts and Martin, 2017). Interestingly, Shah et al. (2014) and Jackson et al. (2014) reported on five children affected by FVSD exhibiting unilateral or bilateral ocular coloboma, one of the main manifestations of CHARGE syndrome. Indeed, VPA acting as a HDAC inhibitor reduces the expression of *PAX2* and *PAX6*, which are implicated in ocular development (Pennati et al., 2001; Balmer et al., 2012). Of note, CHARGE syndrome shares autism-like disturbances, congenital anomalies and malformations together with specific facial features with FVSD (Hefner and Fassi, 2017; van Ravenswaaij-Arts and Martin, 2017) (**Figure 1** and **Table 1**).

Mental Retardation Autosomal Dominant 1

Mental retardation autosomal dominant 1 (*MRD1*, OMIM #156200) or *MBD5* haploinsufficiency is a neurodevelopmental disorder caused by heterozygous variants in *MBD5* or a deletion encompassing all or part of this gene sequence on chromosome 2q23.1 (Vissers et al., 2003; Talkowski et al., 2011). *MBD5* encodes for a methyl-CpG-binding domain protein. *MBD5* is part a class of proteins that bind to DNA with a transcriptional repressor activity. In Camarena et al. (2014) *MBD5* was shown to act as transcriptional activator *in vitro*. Hence, *MBD5* is considered a “reader” of the epigenetic machinery (Camarena et al., 2014). Patients display ID and developmental delay, sleep disturbances, seizures, severe speech impairment, behavioral problems, feeding difficulties, congenital anomalies mainly affecting the skeletal and cardiovascular systems, and dysmorphic signs. Among them, *MRD1* is characterized by broad forehead, highly arched eyebrows, outer ear abnormalities, short nose with broad nasal bridge, thin upper lip, and downturned mouth angles, which are remarkably overlapping with FVSD (Van Bon et al., 2010; Talkowski et al., 2011; Hodge et al., 2014; Mullegama et al., 2016) (**Figure 1** and **Table 1**).

Arboleda-Tham Syndrome

Pathogenic variants in the *KAT6A* gene, located on chromosome 8p11.21 cause Arboleda-Tham syndrome (ARTHS, OMIM #616268) or Mental retardation autosomal dominant 32 (MRD32), a recently described disorder affecting neurodevelopment and associated with ID (Arboleda et al., 2015;

Tham et al., 2015). *KAT6A* is a lysine-acetyltransferase involved in chromatin opening, transcriptional regulation, cellular replication and therefore, in multiple developmental programs (Voss et al., 2009). Kennedy et al. (2019) extensively described phenotypes of novel and previously reported ARTHS patients, who display distinctive clinical signs such as ID, developmental and speech delay, cardiac and ophthalmological defects, gastrointestinal problems, sleep disturbance, autism-like behavior and typical dysmorphisms (Arboleda et al., 2015; Tham et al., 2015; Millan et al., 2016; Murray et al., 2017), many of them overlapping with the FVSD phenotype (**Figure 1** and **Table 1**).

Immunodeficiency, Centromeric Instability and Facial Anomalies Syndrome

Immunodeficiency, centromeric instability and facial anomalies syndrome 1 (ICF1, #OMIM 602900) is a rare autosomal recessive disorder characterized by hypogammaglobulinemia leading to severe recurrent infections, instability of pericentromeric regions of chromosomes 1, 9, and 16 in mitogen-stimulated lymphocytes, and facial dysmorphisms (Maraschio et al., 1988; Ehrlich et al., 2006). When the mapping of a locus associated to ICF syndrome on chromosome 20 was performed in 1998 (Wijmenga et al., 1998), pathogenic variants in *de novo* DNA methyltransferase gene *DNMT3B* were identified, occurring in about half of ICF patients (Hansen et al., 1999; Xu et al., 1999). *DNMT3B* is involved in the establishment of DNA methylation patterns in early life and during cell differentiation. Hypomethylation of pericentromeric satellite 2 and 3 repeats represents the molecular hallmark of ICF syndrome (Jeanpierre et al., 1993), making it the first human disorder linked to a constitutive defect in DNA methylation. In addition to distinctive signs such as immunoglobulin deficiency and consequent recurrent infections (mainly respiratory and gastrointestinal), ICF1 patients also display some features that are common to FVSD: hypertelorism, epicanthus, flat nasal bridge, macroglossia, micrognathia, low-set ears, speech, and developmental delay, and—in a minority of affected individuals—CNS anomalies, congenital heart defects and ID (Hagleitner et al., 2008; Weemaes et al., 2013; van den Boogaard et al., 2017; Kamae et al., 2018) (**Figure 1** and **Table 1**).

Other Genetic Disorders

Qiao et al. (2019) recently described a 19 years-old man with ID and distinctive facial features who had a clinical diagnosis of FVSD and was later found to carry a *de novo* pathogenic variant in the *PURA* gene on chromosome 5q31. *PURA*-related neurodevelopmental disorders include Mental Retardation autosomal Dominant 31 (MRD31, #OMIM 616158) or *PURA* syndrome, caused by heterozygous mutations in the *PURA* gene or a 5q31.3 deletion affecting completely or partially eliminating the *PURA* sequence (Brown et al., 2013; Hunt et al., 2014; Lalani et al., 2014; Tanaka et al., 2015). This causative gene encodes for a DNA- and RNA-binding protein critical for survival and development of mammalian hematopoietic and central nervous systems (Daniel and Johnson, 2018). Shared phenotypic features between *PURA* disorders

and FVSD are ID and developmental delay, heart defects, urinary and ophthalmological abnormalities, and distinctive facial dysmorphism such as high/broad forehead, hypertelorism, wide nasal bridge, and thin upper lip (Reijnders et al., 2018). Furthermore, fetal valproate exposure has been reported to cause other malformation complexes such as Baller-Gerold syndrome (BGS, OMIM #218600), an ultra-rare disorder caused by pathogenic variants in the *RECQL4* gene on chromosome 8p24, and inherited in an autosomal recessive manner (Baller, 1950; Gerold, 1959). BGS patients display a plethora of phenotypic features (Van Maldergem et al., 1992), some of which are overlapping with FVSD. These include: ID, developmental delay, limb and congenital heart defects, genitourinary anomalies and facial dysmorphisms (Iype et al., 2008). Mutations in the *RECQL4* gene that codes for an ATP-dependent DNA helicase

essential for genome integrity and involved in DNA replication, recombination and repair (Bachrati and Hickson, 2008) have also been reported in Rothmund-Thomson (RTS, OMIM #268400) families (Kitao et al., 1999). In particular, children affected with type II RTS share a variety of clinical features with BGS patients (Rothmund, 1868; Thomson, 1936; Megarbane et al., 2000; Van Maldergem et al., 2006; Larizza et al., 2010). Considering the similarities among BGS and RTS patients, there are multiple overlapping features with FVSD that can be observed—e.g., head and nose dysmorphisms, developmental delay, cardiac defects and skeletal anomalies. Although these neurodevelopmental disorders are not considered chromatinopathies, it is worthy of note that *PURA* and *RECQL4* are transcriptional regulators, and helicases are considered a guardian of the genome, such that they are involved in proper chromatin maintenance.

TABLE 2 | Shared pathways between FVSD and chromatinopathies.

Shared pathways	KLFS	KS	CHARGE	MRD1	ARTHS	ICF1
Axon guidance						
Beta1 integrin cell surface interactions						
Cyclins and cell cycle regulation						
ECM-receptor interaction						
Ensemble of genes encoding core extracellular matrix including ECM glycoproteins, collagens and proteoglycans						
Ensemble of genes encoding extracellular matrix and extracellular matrix-associated proteins						
Epithelial cell signaling in Helicobacter pylori infection						
Eukaryotic translation elongation						
Eukaryotic translation termination						
Extracellular matrix organization						
Formation of a pool of free 40S subunits						
GABA receptor activation						
GABAergic synapse						
GTP hydrolysis and joining of the 60S ribosomal subunit						
HIF-1-alpha transcription factor network						
Interactions of neuroligins and neuroligins at synapses						
L13a-mediated translational silencing of ceruloplasmin expression						
L1CAM interactions						
MAPK signaling pathway						
Morphine addiction						
Neuronal system						
Non-sense mediated decay (NMD) enhanced by the exon junction complex (EJC)						
Non-sense mediated decay (NMD) independent of the exon junction complex (EJC)						
Non-sense-mediated decay (NMD)						
p73 transcription factor network						
Peptide chain elongation						
Protein-protein interactions at synapses						
Rac 1 cell motility signaling pathway						
Regulation of Commissural axon pathfinding by Slit and Robo						
Ribosome						
Selenoamino acid metabolism						
Selenocysteine synthesis						
SRP-dependent cotranslational protein targeting to membrane						
Transmission across chemical synapses						
Viral mRNA translation						

KLFS, Kleefstra syndrome; *KS*, Kabuki syndrome; *CHARGE*, CHARGE syndrome; *MRD1*, mental retardation autosomal dominant 1; *ARTHS*, Arboleda-Tham syndrome; *ICF1*, immunodeficiency, centromeric instability, and facial anomalies syndrome 1.

SHARED EPIGENETIC AND GENE EXPRESSION ALTERATIONS

Gene expression deregulation by VPA has been widely investigated over the last few decades (Marchion et al., 2005; Jergil et al., 2009, 2011; Chiu et al., 2013; Shinde et al., 2016; Balasubramanian et al., 2019; Kotajima-Murakami et al., 2019; Lin et al., 2019; Sanaei and Kavousi, 2019). Interestingly, some of the causative genes of the aforementioned syndromes are dysregulated in different experimental models. *Ehmt1* was found to be downregulated in brains of mice exposed to VPA *in utero*, *Kdm6a*, and *Dnmt3b* appeared to be upregulated in the same model (Kotajima-Murakami et al., 2019), while *Chd7* was downregulated in embryonal carcinoma cells upon VPA exposure (Jergil et al., 2009). In addition, *Ehmt1* and its human orthologs were downregulated in neural stem/progenitor cells of a mouse model for KS1 (Carosso et al., 2019) and in lymphoblastoid cell lines derived from 2q23.1 deletion syndrome patients (Mullegama et al., 2016), respectively. Expression of *DNMT3B* was decreased in iPSCs derived from KS1 patient (Carosso et al., 2019). Furthermore, *Kdm6a* and *Chd7* have been reported to be interlinked in terms of gene expression regulation (Mansour et al., 2012; Hsu et al., 2020), and in a mouse model expressing catalytically inactive *Dnmt3b*, they share opposite behavior (Lopusna et al., 2021).

In **Table 2**, shared pathways with genes deregulated by VPA and downregulated in models of causative genes for KLEFS, KS, CHARGE, MRD1, and ARTHS or ICF1 are summarized (Katsumoto et al., 2006; Issaeva et al., 2007; Min et al., 2007; Fan, 2008; Gupta-Agarwal et al., 2012; Mansour et al., 2012; Balemans et al., 2014; Chen et al., 2014; Kim et al., 2014; Schulz et al., 2014; Turner-Ivey et al., 2014; Gigeek et al., 2015; Dhar et al., 2016, 2018; Fang et al., 2016; Mullegama et al., 2016; Sheikh et al., 2016, 2017; Feng et al., 2017a,b; Shpargel et al., 2017; Whittaker et al., 2017; Baell et al., 2018; Marie et al., 2018; Yao et al., 2018, 2020; Carosso et al., 2019; Machado et al., 2019; Nowialis et al., 2019; Cieslar-Pobuda et al., 2020; Frega et al., 2020; Hsu et al., 2020; Kong et al., 2020; Liu et al., 2020; Xu et al., 2020; Ying et al., 2020; Fei et al., 2021; Lopusna et al., 2021). Of note, the most commonly shared pathways involve either morphogenesis signals (for example, beta1 integrin cell surface interactions and extracellular matrix organization), or possible defects of the central nervous system (such as axon guidance and neuronal system). As such, given the recent description of ARTHS, it would be interesting to reassess this matter in the future utilizing state of the art molecular studies.

CONCLUSION

It is well established that the mammalian epigenome can change during embryonic development and be influenced by genetic and/or environmental factors, even though some molecular mechanisms underlying these modifications are yet not clear (Finnell et al., 2002; Xu and Xie, 2018). Chromatinopathies represent a heterogeneous group of Mendelian disorders with defects in the epigenetic apparatus, leading to an imbalance in

the chromatin state and consequent aberrant gene expression. As described above, these disorders share several overlapping clinical signs, though with some specific features allowing dysmorphologists to recognize each individual syndrome. We highlighted similarities between the discussed chromatinopathies and FVSD, pointing out shared features in these genetic- and teratogen-induced disorders. As reported in **Table 1**, overlapping clinical signs are primarily ID and developmental delay, present in 5 out of 5 chromatinopathies described herein (6/6), speech delay (6/6), ASD-like behavior (5/6), microcephaly (5/6), cardiac (6/6) and ophthalmological defects with different degree of severity (5/6), cleft palate (6/6), musculoskeletal anomalies (4/6), and dysmorphic features such as highly arched or thick eyebrows (4/6) and ears abnormalities (6/6).

Intriguingly, despite the different etiology of a FVSD and the chromatinopathies, the action of VPA—i.e., an HDACi acting on chromatin—can suggest a similar pathogenetic mechanism common to the other rare genetic disorders, giving rise to the observed shared phenotypic signs. Furthermore, recent work showed that recognition of FVSD *facies* can identify individuals with high risk of cognitive deficits, independently of VPA exposure and even in the absence of major malformations (Bromley et al., 2019). Taken together, these pieces of evidence support the hypothesis that FVSD may be considered as a phenocopy of chromatinopathy, caused in this case by environmental factors, and that a further investigation of this aspect could help elucidate the correlation between typical congenital anomalies and neurodevelopment.

AUTHOR CONTRIBUTIONS

CG, AV, and VM conceived the manuscript. CP and EDF wrote the manuscript. AP reviewed clinical information. IV wrote sections of the manuscript. PG and SC read and edited the manuscript. RHF reviewed and revised the manuscript. All authors contributed to manuscript revision, they have all read and approved the manuscript.

FUNDING

The authors are grateful to the following funding sources: Fondazione Cariplo (2015-0783 to VM); Intramural funding-Dipartimento DISS, Linea 2, Università degli Studi di Milano (to CG, AV, and VM); Translational Medicine Ph.D. scholarship-Università degli Studi di Milano (to CP and ED); Molecular and Translational Medicine Ph.D. scholarship-Università degli Studi di Milano (to PG); Nickel & Co S.p.A (to VM); and “Aldo Ravelli” Center for Neurotechnology and Experimental Brain Therapeutics-Università degli Studi di Milano (to CG and VM). The authors acknowledge support from the University of Milan through the APC initiative.

ACKNOWLEDGMENTS

The authors would like to thank Susanna Brusa for graphical support.

REFERENCES

- Adam, M. P., Banka, S., Bjornsson, H. T., Bodamer, O., Chudley, A. E., Harris, J., et al. (2019). Kabuki syndrome: international consensus diagnostic criteria. *J. Med. Genet.* 56, 89–95. doi: 10.1136/jmedgenet-2018-105625
- Arboleda, V. A., Lee, H., Dorrani, N., Zadeh, N., Willis, M., Macmurdo, C. F., et al. (2015). De novo nonsense mutations in KAT6A, a lysine acetyl-transferase gene, cause a syndrome including microcephaly and global developmental delay. *Am. J. Hum. Genet.* 96, 498–506. doi: 10.1016/j.ajhg.2015.01.017
- Ardinger, H. H., Atkin, J. F., Blackston, R. D., Elsas, L. J., Clarren, S. K., Livingstone, S., et al. (1988). Verification of the fetal valproate syndrome phenotype. *Am J Med Genet.* 29, 171–185. doi: 10.1002/ajmg.1320290123
- Arora, V., Joshi, A., Lall, M., Agarwal, S., Bijarnia Mahay, S., Dua puri, R., et al. (2018). Fetal valproate syndrome as a phenocopy of Kleeftstra syndrome. *Birth Defects Res.* 110, 1205–1209. doi: 10.1002/bdr2.1379
- Asconapé, J. J., Penry, J. K., Dreifuss, F. E., Riela, A., and Mirza, W. (1993). Valproate-associated pancreatitis. *Epilepsia* 34, 177–183. doi: 10.1111/j.1528-1157.1993.tb02395.x
- Bachrati, C. Z., and Hickson, I. D. (2008). RecQ helicases: guardian angels of the DNA replication fork. *Chromosoma* 117, 219–233. doi: 10.1007/s00412-007-0142-4
- Baell, J. B., Leaver, D. J., Hermans, S. J., Kelly, G. L., Brennan, M. S., Downer, N. L., et al. (2018). Inhibitors of histone acetyltransferases KAT6A/B induce senescence and arrest tumour growth. *Nature* 560, 253–257. doi: 10.1038/s41586-018-0387-5
- Balasubramanian, D., Pearson, J. F., and Kennedy, M. A. (2019). Gene expression effects of lithium and valproic acid in a serotonergic cell line. *Physiol. Genomics* 51, 43–50. doi: 10.1152/physiolgenomics.00069.2018
- Balemans, M. C. M., Ansar, M., Oudakker, A. R., van Caam, A. P. M., Bakker, B., Vitters, E. L., et al. (2014). Reduced Euchromatin histone methyltransferase 1 causes developmental delay, hypotonia, and cranial abnormalities associated with increased bone gene expression in Kleeftstra syndrome mice. *Dev. Biol.* 386, 395–407. doi: 10.1016/j.ydbio.2013.12.016
- Baller, F. (1950). Radiusaplasie und Inzucht. *Z. Mensch. Vererb. Konstitutionsl.* 29, 782–790.
- Balmer, N. V., Weng, M. K., Zimmer, B., Ivanova, V. N., Chambers, S. M., Nikolaeva, E., et al. (2012). Epigenetic changes and disturbed neural development in a human embryonic stem cell-based model relating to the fetal valproate syndrome. *Hum. Mol. Genet.* 21, 4104–4114. doi: 10.1093/hmg/dds239
- Banka, S., Veeramachaneni, R., Reardon, W., Howard, E., Bunstone, S., Ragge, N., et al. (2012). How genetically heterogeneous is Kabuki syndrome: MLL2 testing in 116 patients, review and analyses of mutation and phenotypic spectrum. *Eur. J. Hum. Genet.* 20, 381–388. doi: 10.1038/ejhg.2011.220
- Batshaw, M. L., and Brusilow, S. W. (1982). Valproate-induced hyperammonemia. *Ann. Neurol.* 11, 319–321. doi: 10.1002/ana.410110315
- Bittigau, P., Siffringer, M., Genz, K., Reith, E., Pospischil, D., Govindarajulu, S., et al. (2002). Antiepileptic drugs and apoptotic neurodegeneration in the developing brain. *Proc. Natl. Acad. Sci. U.S.A.* 99, 15089–15094. doi: 10.1073/PNAS.222550499
- Boudadi, E., Stower, H., Halsall, J. A., Rutledge, C. E., Leeb, M., Wutz, A., et al. (2013). The histone deacetylase inhibitor sodium valproate causes limited transcriptional change in mouse embryonic stem cells but selectively overrides Polycomb-mediated Hoxb silencing. *Epigenet. Chromatin* 6:11. doi: 10.1186/1756-8935-6-11
- Brodie, S. A., and Brandes, J. C. (2014). Could valproic acid be an effective anticancer agent? The evidence so far. *Expert Rev. Anticancer Ther.* 14, 1097–1100. doi: 10.1586/14737140.2014.940329
- Bromley, R., Weston, J., Adab, N., Greenhalgh, J., Sanniti, A., McKay, A. J., et al. (2014). Treatment for epilepsy in pregnancy: neurodevelopmental outcomes in the child. *Cochrane Database Syst. Rev.* 2014:CD010236. doi: 10.1002/14651858.CD010236.pub2
- Bromley, R. L., Baker, G. A., Clayton-Smith, J., and Wood, A. G. (2019). Intellectual functioning in clinically confirmed fetal valproate syndrome. *Neurotoxicol. Teratol.* 71, 16–21. doi: 10.1016/j.ntt.2018.11.003
- Bromley, R. L., Mawer, G. E., Briggs, M., Cheyne, C., Clayton-Smith, J., Garcia-Fiñana, M., et al. (2013). The prevalence of neurodevelopmental disorders in children prenatally exposed to antiepileptic drugs. *J. Neurol. Neurosurg. Psychiatry* 84, 637–643. doi: 10.1136/jnnp-2012-304270
- Brown, N., Burgess, T., Forbes, R., McGillivray, G., Kornberg, A., Mandelstam, S., et al. (2013). 5q31.3 microdeletion syndrome: clinical and molecular characterization of two further cases. *Am. J. Med. Genet. Part A* 161, 2604–2608. doi: 10.1002/ajmg.a.36108
- Bruni, J., Wilder, B. J., Willmore, L. J., and Barbour, B. (1979). Valproic acid and plasma levels of phenytoin. *Neurology* 29, 904–905. doi: 10.1212/wnl.29.6.904
- Brunton, L. L., Hilal-Dandan, R., and Knollmann, B. C. (2018). *Goodman & Gilman's The Pharmacological Basis of Therapeutics*. New York, NY: McGraw-Hill.
- Camarena, V., Cao, L., Abad, C., Abrams, A., Toledo, Y., Araki, K., et al. (2014). Disruption of Mbd5 in mice causes neuronal functional deficits and neurobehavioral abnormalities consistent with 2q23.1 microdeletion syndrome. *EMBO Mol. Med.* 6, 1003–1015. doi: 10.15252/emmm.201404044
- Carosso, G. A., Boukas, L., Augustin, J. J., Nguyen, H. N., Winer, B. L., Cannon, G. H., et al. (2019). Precocious neuronal differentiation and disrupted oxygen responses in Kabuki syndrome. *JCI Insight* 4:e129375. doi: 10.1172/jci.insight.129375
- Chandane, P. G., and Shah, I. (2014). Fetal valproate syndrome. *Indian J. Hum. Genet.* 20, 187–188. doi: 10.4103/0971-6866.142898
- Chen, E. S., Gigeck, C. O., Rosenfeld, J. A., Diallo, A. B., Maussion, G., Chen, G. G., et al. (2014). Molecular convergence of neurodevelopmental disorders. *Am. J. Hum. Genet.* 95, 490–508. doi: 10.1016/j.ajhg.2014.09.013
- Chen, G., Zeng, W. Z., Yuan, P. X., Huang, L. D., Jiang, Y. M., Zhao, Z. H., et al. (1999). The mood-stabilizing agents lithium and valproate robustly increase the levels of the neuroprotective protein bcl-2 in the CNS. *J. Neurochem.* 72, 879–882. doi: 10.1046/j.1471-4159.1999.720879.x
- Chiu, C. T., Wang, Z., Hunsberger, J. G., and Chuang, D. M. (2013). Therapeutic potential of mood stabilizers lithium and valproic acid: beyond bipolar disorder. *Pharmacol. Rev.* 65, 105–142. doi: 10.1124/pr.111.005512
- Christensen, J., Grønberg, T. K., Sørensen, M. J., Schendel, D., Parner, E. T., Pedersen, L. H., et al. (2013). Prenatal valproate exposure and risk of autism spectrum disorders and childhood autism. *JAMA* 309, 1696–1703. doi: 10.1001/jama.2013.2270
- Cieslar-Pobuda, A., Ahrens, T. D., Caglayan, S., Behringer, S., Hannibal, L., and Staerk, J. (2020). DNMT3B deficiency alters mitochondrial biogenesis and α -ketoglutarate levels in human embryonic stem cells. *Stem Cells* 38, 1409–1422. doi: 10.1002/stem.3256
- Clayton-Smith, J., Bromley, R., Dean, J., Journal, H., Odent, S., Wood, A., et al. (2019). Diagnosis and management of individuals with fetal valproate spectrum disorder: a consensus statement from the European reference network for congenital malformations and intellectual disability. *Orphanet J. Rare Dis.* 14:180. doi: 10.1186/s13023-019-1064-y
- Clayton-Smith, J., and Donnai, D. (1995). Fetal valproate syndrome. *J. Med. Genet.* 32, 724–727. doi: 10.1136/jmg.32.9.724
- Daniel, D. C., and Johnson, E. M. (2018). PURA, the gene encoding Pur-alpha, member of an ancient nucleic acid-binding protein family with mammalian neurological functions. *Gene* 643, 133–143. doi: 10.1016/j.gene.2017.12.004
- Dhar, S. S., Lee, S. H., Chen, K., Zhu, G., Oh, W. K., Allton, K., et al. (2016). An essential role for UTX in resolution and activation of bivalent promoters. *Nucleic Acids Res.* 44, 3659–3674. doi: 10.1093/nar/gkv1516
- Dhar, S. S., Zhao, D., Lin, T., Gu, B., Pal, K., Wu, S. J., et al. (2018). MLL4 is required to maintain broad h3k4me3 peaks and super-enhancers at tumor suppressor genes. *Mol. Cell* 70, 825.e6–841.e6. doi: 10.1016/j.molcel.2018.04.028
- DiLiberti, J. H., Farndon, P. A., Dennis, N. R., and Curry, C. J. R. R. (1984). The fetal valproate syndrome. *Am. J. Med. Genet.* 19, 473–481. doi: 10.1002/ajmg.1320190308
- Dufour-Rainfray, D., Vourc'h, P., Le Guisquet, A. M., Garreau, L., Ternant, D., Bodard, S., et al. (2010). Behavior and serotonergic disorders in rats exposed prenatally to valproate: a model for autism. *Neurosci. Lett.* 470, 55–59. doi: 10.1016/j.neulet.2009.12.054
- Ehrlich, M., Jackson, K., and Weemaes, C. (2006). Immunodeficiency, centromeric region instability, facial anomalies syndrome (ICF). *Orphanet J. Rare Dis.* 1:2. doi: 10.1186/1750-1172-1-2
- Fahrner, J. A., and Bjornsson, H. T. (2019). Mendelian disorders of the epigenetic machinery: postnatal malleability and therapeutic prospects. *Hum. Mol. Genet.* 28, R254–R264. doi: 10.1093/hmg/ddz174

- Fan, H. (2008). Inhibition of de novo methyltransferase 3B is a potential therapy for hepatocellular carcinoma. *Gastroenterol. Res.* 1, 33–39. doi: 10.4021/gr2008.10.1240
- Fang, X., Poulsen, R. R., Wang-Hu, J., Shi, O., Calvo, N. S., Simmons, C. S., et al. (2016). Knockdown of DNA methyltransferase 3a alters gene expression and inhibits function of embryonic cardiomyocytes. *FASEB J.* 30, 3238–3255. doi: 10.1096/fj.201600346R
- Fei, D., Wang, Y., Zhai, Q., Zhang, X., Zhang, Y., Wang, Y., et al. (2021). KAT6A regulates stemness of aging bone marrow-derived mesenchymal stem cells through Nr2f/ARE signaling pathway. *Stem Cell Res. Ther.* 12:104. doi: 10.1186/s13287-021-02164-5
- Feng, W., Kawachi, D., Körkel-Qu, H., Deng, H., Serger, E., Sieber, L., et al. (2017a). Chd7 is indispensable for mammalian brain development through activation of a neuronal differentiation programme. *Nat. Commun.* 8:14758. doi: 10.1038/ncomms14758
- Feng, W., Shao, C., and Liu, H. K. (2017b). Versatile roles of the chromatin remodeler CHD7 during brain development and disease. *Front. Mol. Neurosci.* 10:309. doi: 10.3389/fnmol.2017.00309
- Finnell, R. H., Gelineau-van Waes, J., Eudy, J. D., and Rosenquist, T. H. (2002). Molecular basis of environmentally induced birth defects. *Annu. Rev. Pharmacol. Toxicol.* 42, 181–208. doi: 10.1146/annurev.pharmtox.42.083001.110955
- Frega, M., Selten, M., Mossink, B., Keller, J. M., Linda, K., Moerschen, R., et al. (2020). Distinct pathogenic genes causing intellectual disability and autism exhibit a common neuronal network hyperactivity phenotype. *Cell Rep.* 30, 173.e6–186.e6. doi: 10.1016/j.celrep.2019.12.002
- Gerold, M. (1959). Frakturheilung bei kongenitaler Anomalie der oberen Gliedmassen. *Zentralbl. Chir.* 84, 831–834.
- Gigek, C. O., Chen, E. S., Ota, V. K., Maussion, G., Peng, H., Vaillancourt, K., et al. (2015). A molecular model for neurodevelopmental disorders. *Transl. Psychiatry* 5:e565. doi: 10.1038/tp.2015.56
- Glover, S. J., Quinn, A. G., Barter, P., Hart, J., Moore, S. J., Dean, J. C. S., et al. (2002). Ophthalmic findings in fetal anticonvulsant syndrome(s). *Ophthalmology* 109, 942–947. doi: 10.1016/s0161-6420(02)00959-4
- Go, H. S., Seo, J. E., Kim, K. C., Han, S. M., Kim, P. K., Kang, Y. S., et al. (2011). Valproic acid inhibits neural progenitor cell death by activation of NF- κ B signaling pathway and up-regulation of Bcl-XL. *J. Biomed. Sci.* 18:48. doi: 10.1186/1423-0127-18-48
- Gössling, K. L., Schipp, C., Fischer, U., Babor, F., Koch, G., Schuster, F. R., et al. (2017). Hematopoietic stem cell transplantation in an infant with immunodeficiency, centromeric instability, and facial anomaly syndrome. *Front. Immunol.* 8:773. doi: 10.3389/fimmu.2017.00773
- Göttlicher, M., Minucci, S., Zhu, P., Krämer, O. H., Schimpf, A., Giavara, S., et al. (2001). Valproic acid defines a novel class of HDAC inhibitors inducing differentiation of transformed cells. *EMBO J.* 20, 6969–6978. doi: 10.1093/emboj/20.24.6969
- Gupta-Agarwal, S., Franklin, A. V., DeRamus, T., Wheelock, M., Davis, R. L., McMahon, L. L., et al. (2012). G9a/GLP histone lysine dimethyltransferase complex activity in the hippocampus and the entorhinal cortex is required for gene activation and silencing during memory consolidation. *J. Neurosci.* 32, 5440–5453. doi: 10.1523/jneurosci.0147-12.2012
- Hadzsvie, K., Komlosi, K., Czako, M., Duga, B., Szalai, R., Szabo, A., et al. (2016). Kleefstra syndrome in Hungarian patients: additional symptoms besides the classic phenotype. *Mol. Cytogenet.* 9:22. doi: 10.1186/s13039-016-0231-2
- Hagleitner, M. M., Lankester, A., Maraschio, P., Hultén, M., Fryns, J. P., Schuetz, C., et al. (2008). Clinical spectrum of immunodeficiency, centromeric instability and facial dysmorphism (ICF syndrome). *J. Med. Genet.* 45, 93–99. doi: 10.1136/jmg.2007.053397
- Hansen, R. S., Wijemanga, C., Luo, P., Stanek, A. M., Canfield, T. K., Weemaes, C. M. R., et al. (1999). The DNMT3B DNA methyltransferase gene is mutated in the ICF immunodeficiency syndrome. *Proc. Natl. Acad. Sci. U.S.A.* 96, 14412–14417. doi: 10.1073/pnas.96.25.14412
- Hefner, M. A., and Fassi, E. (2017). *Genetic Counseling in CHARGE Syndrome: Diagnostic Evaluation Through Follow Up*. Malden, MA: Blackwell Publishing Inc.
- Hodge, J. C., Mitchell, E., Pillalamarri, V., Toler, T. L., Bartel, F., Kearney, H. M., et al. (2014). Disruption of MBD5 contributes to a spectrum of psychopathology and neurodevelopmental abnormalities. *Mol. Psychiatry* 19, 368–379. doi: 10.1038/mp.2013.42
- Hsu, J., Huang, H. T., Lee, C. T., Choudhuri, A., Wilson, N. K., Abraham, B. J., et al. (2020). CHD7 and Runx1 interaction provides a braking mechanism for hematopoietic differentiation. *Proc. Natl. Acad. Sci. U.S.A.* 117, 23626–23635. doi: 10.1073/pnas.2003228117
- Hunt, D., Leventer, R. J., Simons, C., Taft, R., Swoboda, K. J., Gawne-Cain, M., et al. (2014). Whole exome sequencing in family trios reveals de novo mutations in PURA as a cause of severe neurodevelopmental delay and learning disability. *J. Med. Genet.* 51, 806–813. doi: 10.1136/jmedgenet-2014-102798
- Issaeva, I., Zonis, Y., Rozovskaia, T., Orlovsky, K., Croce, C. M., Nakamura, T., et al. (2007). Knockdown of ALR (MLL2) reveals ALR target genes and leads to alterations in cell adhesion and growth. *Mol. Cell. Biol.* 27, 1889–1903. doi: 10.1128/mcb.01506-06
- Iype, M., Henry, P., Aravind, C., and Arun, K. (2008). Baller-Gerold syndrome: further evidence for association with prenatal exposure to valproate. *Ann. Indian Acad. Neurol.* 11, 52–55. doi: 10.4103/0972-2327.40228
- Jackson, A., Bromley, R., Morrow, J., Irwin, B., and Clayton-Smith, J. (2016). In utero exposure to valproate increases the risk of isolated cleft palate. *Arch. Dis. Child. Fetal Neonatal Ed.* 101, F207–F211. doi: 10.1136/archdischild-2015-308278
- Jackson, A., Fryer, A., Clowes, V., and Clayton-Smith, J. (2014). Ocular coloboma and foetal valproate syndrome: four further cases and a hypothesis for aetiology. *Clin. Dysmorphol.* 23, 74–75. doi: 10.1097/MCD.0000000000000028
- Jacob, J., Ribes, V., Moore, S., Constable, S., Wilkinson, D., and Briscoe, J. (2013). *A Chemical-Genetics Approach to Study the Molecular Pathology of Central Serotonin Abnormalities in Fetal Valproate Syndrome*. Available online at: www.thelancet.com (accessed April 1, 2020).
- Jacob, J., Ribes, V., Moore, S., Constable, S. C., Sasai, N., Gerety, S. S., et al. (2014). Valproic acid silencing of ascl1b/Ascl1 results in the failure of serotonergic differentiation in a zebrafish model of fetal valproate syndrome. *DMM Dis. Model. Mech.* 7, 107–117. doi: 10.1242/dmm.013219
- Jeanpierre, M., Turleau, C., Aurias, A., Prieur, M., Ledeist, F., Fischer, A., et al. (1993). An embryonic-like methylation pattern of classical satellite DNA is observed in ICF syndrome. *Hum. Mol. Genet.* 2, 731–735. doi: 10.1093/hmg/2.6.731
- Jergil, M., Forsberg, M., Salter, H., Stockling, K., Gustafson, A. L., Dencker, L., et al. (2011). Short-time gene expression response to valproic acid and valproic acid analogs in mouse embryonic stem cells. *Toxicol. Sci.* 121, 328–342. doi: 10.1093/toxsci/kfr070
- Jergil, M., Kulitima, K., Gustafson, A. L., Dencker, L., and Stigson, M. (2009). Valproic acid-induced deregulation In vitro of genes associated in vivo with neural tube defects. *Toxicol. Sci.* 108, 132–148. doi: 10.1093/toxsci/kfp002
- Johannessen, C. U., and Johannessen, S. I. (2003). Valproate: past, present, and future. *CNS Drug Rev.* 9, 199–216. doi: 10.1111/j.1527-3458.2003.tb00249.x
- Kamae, C., Imai, K., Kato, T., Okano, T., Honma, K., Nakagawa, N., et al. (2018). Clinical and immunological characterization of ICF syndrome in Japan. *J. Clin. Immunol.* 38, 927–937. doi: 10.1007/s10875-018-0559-y
- Katsumoto, T., Aikawa, Y., Iwama, A., Ueda, S., Ichikawa, H., Ochiya, T., et al. (2006). MOZ is essential for maintenance of hematopoietic stem cells. *Genes Dev.* 20, 1321–1330. doi: 10.1101/gad.1393106
- Kennedy, J., Goudie, D., Blair, E., Chandler, K., Joss, S., McKay, V., et al. (2019). KAT6A Syndrome: genotype–phenotype correlation in 76 patients with pathogenic KAT6A variants. *Genet. Med.* 21, 850–860. doi: 10.1038/s41436-018-0259-2
- Kim, J. H., Sharma, A., Dhar, S. S., Lee, S. H., Gu, B., Chan, C. H., et al. (2014). UTX and MLL4 coordinately regulate transcriptional programs for cell proliferation and invasiveness in breast cancer cells. *Cancer Res.* 74, 1705–1717. doi: 10.1158/0008-5472.CAN-13-1896
- Kim, K. C., Kim, P., Go, H. S., Choi, C. S., Yang, S. I. L., Cheong, J. H., et al. (2011). The critical period of valproate exposure to induce autistic symptoms in Sprague-Dawley rats. *Toxicol. Lett.* 201, 137–142. doi: 10.1016/j.toxlet.2010.12.018
- Kini, U., Adab, N., Vinten, J., Fryer, A., and Clayton-Smith, J. (2006). Dysmorphic features: an important clue to the diagnosis and severity of fetal anticonvulsant syndromes. *Arch. Dis. Child. Fetal Neonatal Ed.* 91, 90–95. doi: 10.1136/adc.2004.067421

- Kitao, S., Shimamoto, A., Goto, M., Miller, R. W., Smithson, W. A., Lindor, N. M., et al. (1999). Mutations in RECQL4 cause a subset of cases of Rothmund-Thomson syndrome. *Nat. Genet.* 22, 82–84. doi: 10.1038/8788
- Kleefstra, T., Brunner, H. G., Amiel, J., Oudakker, A. R., Nillesen, W. M., Magee, A., et al. (2006). Loss-of-function mutations in Euchromatin histone methyltransferase 1 (EHMT1) cause the 9q34 subtelomeric deletion syndrome. *Am. J. Hum. Genet.* 79, 370–377. doi: 10.1086/505693
- Kleefstra, T., and De Leeuw, N. (1993). *Kleefstra Syndrome Synonyms: 9q Subtelomeric Deletion Syndrome, 9q34.3 Microdeletion Syndrome, 9qSTDS*. Available online at: <https://www.ncbi.nlm.nih.gov/books/> (accessed January 10, 2021).
- Kleefstra, T., Kramer, J. M., Neveling, K., Willemsen, M. H., Koemans, T. S., Vissers, L. E. L. M., et al. (2012). Disruption of an EHMT1-associated chromatin-modification module causes intellectual disability. *Am. J. Hum. Genet.* 91, 73–82. doi: 10.1016/j.ajhg.2012.05.003
- Koemans, T. S., Kleefstra, T., Chubak, M. C., Stone, M. H., Reijnders, M. R. F., de Munnik, S., et al. (2017). Functional convergence of histone methyltransferases EHMT1 and KMT2C involved in intellectual disability and autism spectrum disorder. *PLoS Genet.* 13:e1006864. doi: 10.1371/journal.pgen.1006864
- Kong, Q., Yu, M., Zhang, M., Wei, C., Gu, H., Yu, S., et al. (2020). Conditional Dnmt3b deletion in hippocampal dCA1 impairs recognition memory. *Mol. Brain* 13:42. doi: 10.1186/s13041-020-00574-9
- Kotajima-Murakami, H., Kobayashi, T., Kashii, H., Sato, A., Hagino, Y., Tanaka, M., et al. (2019). Effects of rapamycin on social interaction deficits and gene expression in mice exposed to valproic acid in utero. *Mol. Brain* 12:3. doi: 10.1186/s13041-018-0423-2
- Kozma, C. (2001). Valproic acid embryopathy: report of two siblings with further expansion of the phenotypic abnormalities and a review of the literature. *Am. J. Med. Genet.* 98, 168–175.
- Kuroki, Y., Suzuki, Y., Chyo, H., Hata, A., and Matsui, I. (1981). A new malformation syndrome of long palpebral fissures, large ears, depressed nasal tip, and skeletal anomalies associated with postnatal dwarfism and mental retardation. *J. Pediatr.* 99, 570–573. doi: 10.1016/S0022-3476(81)80256-9
- Lalani, S. R., Zhang, J., SchAAF, C. P., Brown, C. W., Magoulas, P., Tsai, A. C. H., et al. (2014). Mutations in PURA cause profound neonatal hypotonia, seizures, and encephalopathy in 5q31.3 microdeletion syndrome. *Am. J. Hum. Genet.* 95, 579–583. doi: 10.1016/j.ajhg.2014.09.014
- Lammer, E. J., Sever, L. E., and Oakley, G. P. (1987). Teratogen update: valproic acid. *Teratology* 35, 465–473. doi: 10.1002/tera.1420350319
- Larizza, L., Roversi, G., and Volpi, L. (2010). Rothmund-thomson syndrome. *Orphanet J. Rare Dis.* 5:2. doi: 10.1186/1750-1172-5-2
- Lederer, D., Grisart, B., Digilio, M. C., Benoit, V., Crespin, M., Ghariani, S. C., et al. (2012). Deletion of KDM6A, a histone demethylase interacting with MLL2, in three patients with kabuki syndrome. *Am. J. Hum. Genet.* 90, 119–124. doi: 10.1016/j.ajhg.2011.11.021
- Lin, Y. L., Bialer, M., Cabrera, R. M., Finnell, R. H., and Wlodarczyk, B. J. (2019). Teratogenicity of valproic acid and its constitutional isomer, amide derivative valnoctamide in mice. *Birth Defects Res.* 111, 1013–1023. doi: 10.1002/bdr2.1406
- Lindhout, D., and Schmidt, D. (1986). In-utero exposure to valproate and neural tube defects. *Lancet* 1, 1392–1393. doi: 10.1016/s0140-6736(86)91711-3
- Liu, C., Li, Q., Xiao, Q., Gong, P., and Kang, N. (2020). CHD7 regulates osteogenic differentiation of human dental follicle cells via PTH1R signaling. *Stem Cells Int.* 2020:8882857. doi: 10.1155/2020/8882857
- Lopusna, K., Nowialis, P., Opavska, J., Abraham, A., Riva, A., and Opavsky, R. (2021). Dnmt3b catalytic activity is critical for its tumour suppressor function in lymphomagenesis and is associated with c-Met oncogenic signalling. *EBioMedicine* 63:e103191. doi: 10.1016/j.ebiom.2020.103191
- Macfarlane, A., and Greenhalgh, T. (2018). Sodium valproate in pregnancy: what are the risks and should we use a shared decision-making approach? *BMC Preg. Childbirth* 18:200. doi: 10.1186/s12884-018-1842-x
- Machado, R. A. C., Schneider, H., DeOcesano-Pereira, C., Lichtenstein, F., Andrade, F., Fujita, A., et al. (2019). CHD7 promotes glioblastoma cell motility and invasiveness through transcriptional modulation of an invasion signature. *Sci. Rep.* 9:3952. doi: 10.1038/s41598-019-39564-w
- Makrythanasis, P., van Bon, B. W., Stehouwer, M., Rodríguez-Santiago, B., Simpson, M., Dias, P., et al. (2013). MLL2 mutation detection in 86 patients with Kabuki syndrome: a genotype-phenotype study. *Clin. Genet.* 84, 539–545. doi: 10.1111/cge.12081
- Mansour, A. A., Gafni, O., Weinberger, L., Zviran, A., Ayyash, M., Rais, Y., et al. (2012). The H3K27 demethylase Utx regulates somatic and germ cell epigenetic reprogramming. *Nature* 488, 409–413. doi: 10.1038/nature11272
- Maraschio, P., Zuffardi, O., Dalla Fior, T., and Tiepolo, L. (1988). Immunodeficiency, centromeric heterochromatin instability of chromosomes 1, 9, and 16, and facial anomalies: the ICF syndrome. *J. Med. Genet.* 25, 173–180. doi: 10.1136/jmg.25.3.173
- Marchion, D. C., Bicaku, E., Daud, A. I., Sullivan, D. M., and Munster, P. N. (2005). Valproic acid alters chromatin structure by regulation of chromatin modulation proteins. *Cancer Res.* 65, 3815–3822. doi: 10.1158/0008-5472.CAN-04-2478
- Marie, C., Clavairoly, A., Frah, M., Hmidan, H., Yan, J., Zhao, C., et al. (2018). Oligodendrocyte precursor survival and differentiation requires chromatin remodeling by Chd7 and Chd8. *Proc. Natl. Acad. Sci. U.S.A.* 115, E8246–E8255. doi: 10.1073/pnas.1802620115
- Massa, V., Cabrera, R. M., Menegola, E., Giavini, E., and Finnell, R. H. (2005). Valproic acid-induced skeletal malformations: associated gene expression cascades. *Pharmacogenet. Genomics* 15, 787–800. doi: 10.1097/01.fpc.0000170914.11898.3a
- Massa, V., Greene, N. D. E., and Copp, A. J. (2009). Do cells become homeless during neural tube closure? *Cell Cycle* 8, 2479–2480. doi: 10.4161/cc.8.16.9272
- Massa, V., Wlodarczyk, B., Giavini, E., and Finnell, R. H. (2006). Myo-inositol enhances teratogenicity of valproic acid in the mouse. *Birth Defects Res. Part A Clin. Mol. Teratol.* 76, 200–204. doi: 10.1002/bdra.20228
- Meador, K. J., Pennell, P. B., May, R. C., Brown, C. A., Baker, G., Bromley, R., et al. (2020). Effects of periconceptional folate on cognition in children of women with epilepsy: NEAD study. *Neurology* 94, e729–e740. doi: 10.1212/WNL.00000000000008757
- Megarbane, A., Melki, I., Souraty, N., Gerbaka, J., El Ghouzzi, V., Bonaventure, J., et al. (2000). Overlap between Baller-Gerold and Rothmund-Thomson syndrome. *Clin. Dysmorphol.* 9, 303–305. doi: 10.1097/00019605-200009040-00018
- Menegola, E., Broccia, M., Prati, M., and Giavini, E. (1999). Morphological alterations induced by sodium valproate on somites and spinal nerves in rat embryos. *Teratology* 59, 110–119.
- Menegola, E., Broccia, M. L., Prati, M., and Giavini, E. (1998). Stage-dependent skeletal malformations induced by valproic acid in rat. *Int. J. Dev. Biol.* 42, 99–102. doi: 10.1387/IJDB.9496792
- Menegola, E., Di Renzo, F., Broccia, M. L., Prudenziati, M., Minucci, S., Massa, V., et al. (2005). Inhibition of histone deacetylase activity on specific embryonic tissues as a new mechanism for teratogenicity. *Birth Defects Res. Part B Dev. Reprod. Toxicol.* 74, 392–398. doi: 10.1002/bdrb.20053
- Meunier, H., Carraz, G., Neunier, Y., Eymard, P., and Aimard, M. (1963). Pharmacodynamic properties of N-dipropylacetic acid. *Therapie* 18, 435–438.
- Millan, F., Cho, M. T., Retterer, K., Monaghan, K. G., Bai, R., Vitazka, P., et al. (2016). Whole exome sequencing reveals de novo pathogenic variants in KAT6A as a cause of a neurodevelopmental disorder. *Am. J. Med. Genet. Part A* 170, 1791–1798. doi: 10.1002/ajmg.a.37670
- Min, G. L., Villa, R., Trojer, P., Norman, J., Yan, K. P., Reinberg, D., et al. (2007). Demethylation of H3K27 regulates polycomb recruitment and H2A ubiquitination. *Science* 318, 447–450. doi: 10.1126/science.1149042
- Miyake, N., Mizuno, S., Okamoto, N., Ohashi, H., Shiina, M., Ogata, K., et al. (2013). KDM6A point mutations cause kabuki syndrome. *Hum. Mutat.* 34, 108–110. doi: 10.1002/humu.22229
- Mohd Yunos, H., and Green, A. (2018). Fetal valproate syndrome: the Irish experience. *Ir. J. Med. Sci.* 187, 965–968. doi: 10.1007/s11845-018-1757-6
- Mullegama, S. V., Mendoza-Londono, R., and Elsea, S. H. (2016). *MBD5 Haploinsufficiency*. Available online at: <http://www.ncbi.nlm.nih.gov/pubmed/27786435> (accessed December 2, 2020).
- Murko, C., Lagger, S., Steiner, M., Seiser, C., Schoefer, C., and Pusch, O. (2013). Histone deacetylase inhibitor Trichostatin A induces neural tube defects and promotes neural crest specification in the chicken neural tube. *Differentiation* 85, 55–66. doi: 10.1016/j.diff.2012.12.001
- Murray, C., Abel, S., McClure, M., Foster, J., Walke, M., Jayakar, P., et al. (2017). Novel causative variants in DYRK1A, KARS, and KAT6A associated with

- intellectual disability and additional phenotypic features. *J. Pediatr. Genet.* 06, 077–083. doi: 10.1055/s-0037-1598639
- Nau, H. (1985). Teratogenic valproic acid concentrations: infusion by implanted minipumps vs conventional injection regimen in the mouse. *Toxicol. Appl. Pharmacol.* 80, 243–250. doi: 10.1016/0041-008X(85)90081-X
- Nau, H., Hauck, R. S., and Ehlers, K. (1991). Valproic acid-induced neural tube defects in mouse and human: aspects of chirality, alternative drug development, pharmacokinetics and possible mechanisms. *Pharmacol. Toxicol.* 69, 310–321. doi: 10.1111/j.1600-0773.1991.tb01303.x
- Nau, H., Zierer, R., Spielmann, H., Neubert, D., and Gansau, C. (1981). A new model for embryotoxicity testing: teratogenicity and pharmacokinetics of valproic acid following constant-rate administration in the mouse using human therapeutic drug and metabolite concentrations. *Life Sci.* 29, 2803–2813. doi: 10.1016/0024-3205(81)90541-5
- Ng, S. B., Bigam, A. W., Buckingham, K. J., Hannibal, M. C., McMillin, M. J., Gildersleeve, H. I., et al. (2010). Exome sequencing identifies MLL2 mutations as a cause of Kabuki syndrome. *Nat. Genet.* 42, 790–793. doi: 10.1038/ng.646
- Nicolini, C., and Fahnstock, M. (2018). The valproic acid-induced rodent model of autism. *Exp. Neurol.* 299, 217–227. doi: 10.1016/j.expneurol.2017.04.017
- Niikawa, N., Matsuura, N., Fukushima, Y., Ohsawa, T., and Kajii, T. (1981). Kabuki make-up syndrome: a syndrome of mental retardation, unusual facies, large and protruding ears, and postnatal growth deficiency. *J. Pediatr.* 99, 565–569. doi: 10.1016/S0022-3476(81)80255-7
- Nowialis, P., Lopusna, K., Opavska, J., Haney, S. L., Abraham, A., Sheng, P., et al. (2019). Catalytically inactive Dnmt3b rescues mouse embryonic development by accessory and repressive functions. *Nat. Commun.* 10:4374. doi: 10.1038/s41467-019-12355-7
- Oberemm, A., and Kirschbaum, F. (1992). Valproic acid induced abnormal development of the central nervous system of three species of amphibians: implications for neural tube defects and alternative experimental systems. *Teratog. Carcinog. Mutagen.* 12, 251–262. doi: 10.1002/tcm.1770120603
- Ornoy, A. (2009). Valproic acid in pregnancy: how much are we endangering the embryo and fetus? *Reprod. Toxicol.* 28, 1–10. doi: 10.1016/j.REPROTOX.2009.02.014
- Ozkan, H., Cetinkaya, M., Köksal, N., and Yapici, S. (2011). Severe fetal valproate syndrome: combination of complex cardiac defect, multicystic dysplastic kidney, and trigonocephaly. *J. Matern. Fetal. Neonatal Med.* 24, 521–524. doi: 10.3109/14767058.2010.501120
- Pagon, R. A., Graham, J. M., Zonana, J., and Yong, S. L. (1981). Coloboma, congenital heart disease, and choanal atresia with multiple anomalies: CHARGE association. *J. Pediatr.* 99, 223–227. doi: 10.1016/S0022-3476(81)80454-4
- Patsalos, P. N., Berry, D. J., Bourgeois, B. F. D., Cloyd, J. C., Glauser, T. A., Johannessen, S. I., et al. (2008). Antiepileptic drugs - best practice guidelines for therapeutic drug monitoring: a position paper by the subcommission on therapeutic drug monitoring, ilae commission on therapeutic strategies. *Epilepsia* 49, 1239–1276. doi: 10.1111/j.1528-1167.2008.01561.x
- Pennati, R., Gropelli, S., De Bernardi, F., and Sotgia, C. (2001). Action of valproic acid on *Xenopus laevis* development: teratogenic effects on eyes. *Teratog. Carcinog. Mutagen.* 21, 121–133.
- Perucca, E. (2002). Pharmacological and therapeutic properties of valproate: a summary after 35 years of clinical experience. *CNS Drugs* 16, 695–714. doi: 10.2165/00023210-200216100-00004
- Phiel, C. J., Zhang, F., Huang, E. Y., Guenther, M. G., Lazar, M. A., and Klein, P. S. (2001). Histone deacetylase is a direct target of valproic acid, a potent anticonvulsant, mood stabilizer, and teratogen. *J. Biol. Chem.* 276, 36734–36741. doi: 10.1074/jbc.M101287200
- Qiao, Y., Bagheri, H., Tang, F., Badduke, C., Martell, S., Lewis, S. M. E., et al. (2019). Exome sequencing identified a de novo mutation of PURA gene in a patient with familial Xp22.31 microduplication. *Eur. J. Med. Genet.* 62, 103–108. doi: 10.1016/j.ejmg.2018.06.010
- Reijnders, M. R. F., Janowski, R., Alvi, M., Self, J. E., Van Essen, T. J., Vreeburg, M., et al. (2018). PURA syndrome: clinical delineation and genotype-phenotype study in 32 individuals with review of published literature. *J. Med. Genet.* 55, 104–113. doi: 10.1136/jmedgenet-2017-104946
- Robert, E., and Guibaud, P. (1982). Maternal valproic acid and congenital neural tube defects. *Lancet* 2:937. doi: 10.1016/s0140-6736(82)90908-4
- Rothmund, A. (1868). Ueber Cataracten in Verbindung mit einer eigenthümlichen Hautdegeneration. *Arch. für Ophthalmol.* 14, 159–182. doi: 10.1007/BF02720945
- Roulet, F. I., Wollaston, L., deCatanzaro, D., and Foster, J. A. (2010). Behavioral and molecular changes in the mouse in response to prenatal exposure to the anti-epileptic drug valproic acid. *Neuroscience* 170, 514–522. doi: 10.1016/j.neuroscience.2010.06.069
- Sanaei, M., and Kavousi, F. (2019). Effect of 5-aza-2'-deoxycytidine in comparison to valproic acid and trichostatin a on histone deacetylase 1, dna methyltransferase 1, and cip/kip family (p21, p27, and p57) genes expression, cell growth inhibition, and apoptosis induction in colon cancer sw480 cell line. *Adv. Biomed. Res.* 8:52. doi: 10.4103/abr.abr_91_19
- Schölz, C., Weinert, B. T. B., Wagner, S. A. S., Beli, P., Miyake, Y., Qi, J., et al. (2015). Acetylation site specificities of lysine deacetylase inhibitors in human cells. *Cells* 33, 415–423.
- Schorry, E. K., Oppenheimer, S. G., and Saal, H. M. (2005). Valproate embryopathy: clinical and cognitive profile in 5 siblings. *Am. J. Med. Genet.* 133A, 202–206. doi: 10.1002/ajmg.a.30494
- Schulz, Y., Wehner, P., Opitz, L., Salinas-Riester, G., Bongers, E. M. H. F., van Ravenswaaij-Arts, C. M. A., et al. (2014). CHD7, the gene mutated in CHARGE syndrome, regulates genes involved in neural crest cell guidance. *Hum. Genet.* 133, 997–1009. doi: 10.1007/s00439-014-1444-2
- Shah, K. H., Shailaja, S., and Girisha, K. M. (2014). Is coloboma a feature of fetal valproate syndrome? *Clin. Dysmorphol.* 23, 24–25. doi: 10.1097/MCD.000000000000018
- Shah, R. R., and Stonier, P. D. (2019). Repurposing old drugs in oncology: opportunities with clinical and regulatory challenges ahead. *J. Clin. Pharm. Ther.* 44, 6–22. doi: 10.1111/jcpt.12759
- Shangguan, H., Su, C., Ouyang, Q., Cao, B., Wang, J., Gong, C., et al. (2019). Kabuki syndrome: novel pathogenic variants, new phenotypes and review of literature. *Orphanet J. Rare Dis.* 14:255. doi: 10.1186/s13023-019-1219-x
- Sheikh, B. N., Yang, Y., Schreuder, J., Nilsson, S. K., Bilardi, R., Carotta, S., et al. (2016). MOZ (KAT6A) is essential for the maintenance of classically defined adult hematopoietic stem cells. *Blood* 128, 2307–2318. doi: 10.1182/blood-2015-10-676072
- Sheikh, M. A., Malik, Y. S., and Zhu, X. (2017). RA-induced transcriptional silencing of checkpoint kinase-2 through promoter methylation by Dnmt3b is required for neuronal differentiation of P19 cells. *J. Mol. Biol.* 429, 2463–2473. doi: 10.1016/j.jmb.2017.07.005
- Shinde, V., Perumalivasan, S., Henry, M., Rotshteyn, T., Hescheler, J., Rahnenführer, J., et al. (2016). Comparison of a teratogenic transcriptome-based predictive test based on human embryonic versus inducible pluripotent stem cells. *Stem Cell Res. Ther.* 7:190. doi: 10.1186/s13287-016-0449-2
- Shpargel, K. B., Starmer, J., Wang, C., Ge, K., and Magnuson, T. (2017). UTX-guided neural crest function underlies craniofacial features of Kabuki syndrome. *Proc. Natl. Acad. Sci. U.S.A.* 114, E9046–E9055. doi: 10.1073/pnas.1705011114
- Sui, L., and Chen, M. (2012). Prenatal exposure to valproic acid enhances synaptic plasticity in the medial prefrontal cortex and fear memories. *Brain Res. Bull.* 87, 556–563. doi: 10.1016/J.BRAINRESBULL.2012.01.011
- Swann, A. C., Bowden, C. L., Calabrese, J. R., Diltsaver, S. C., and Morris, D. D. (2002). Pattern of response to divalproex, lithium, or placebo in four naturalistic subtypes of mania. *Neuropsychopharmacology* 26, 530–536. doi: 10.1016/S0893-133X(01)00390-6
- Talkowski, M. E., Mullegama, S. V., Rosenfeld, J. A., Van Bon, B. W. M., Shen, Y., Repnikova, E., et al. (2011). Assessment of 2q23.1 microdeletion syndrome implicates MBD5 as a single causal locus of intellectual disability, epilepsy, and autism spectrum disorder. *Am. J. Hum. Genet.* 89, 551–563. doi: 10.1016/j.ajhg.2011.09.011
- Tanaka, A. J., Bai, R., Cho, M. T., Anyane-Yeboah, K., Ahimaz, P., Wilson, A. L., et al. (2015). De novo mutations in PURA are associated with hypotonia and developmental delay. *Mol. Case Stud.* 1:a000356. doi: 10.1101/mcs.a000356
- Tham, E., Lindstrand, A., Santani, A., Malmgren, H., Nesbitt, A., Dubbs, H. A., et al. (2015). Dominant mutations in KAT6A cause intellectual disability with recognizable syndromic features. *Am. J. Hum. Genet.* 96, 507–513. doi: 10.1016/j.ajhg.2015.01.016
- Thomson, M. S. (1936). POIKILODERMA CONGEXITALE. *Br. J. Dermatol.* 48, 221–234. doi: 10.1111/j.1365-2133.1936.tb10332.x
- Tomson, T., Battino, D., Bonizzoni, E., Craig, J., Lindhout, D., Perucca, E., et al. (2015). Dose-dependent teratogenicity of valproate in mono- and polytherapy. *Neurology* 85, 866–872. doi: 10.1212/WNL.0000000000001772

- Tomson, T., Battino, D., Bonizzoni, E., Craig, J., Lindhout, D., Sabers, A., et al. (2011). Dose-dependent risk of malformations with antiepileptic drugs: an analysis of data from the EURAP epilepsy and pregnancy registry. *Lancet Neurol.* 10, 609–617. doi: 10.1016/S1474-4422(11)70107-7
- Turner-Ivey, B., Guest, S. T., Irish, J. C., Kappler, C. S., Garrett-Mayer, E., Wilson, R. C., et al. (2014). KAT6A, a chromatin modifier from the 8p11-p12 amplicon is a candidate oncogene in luminal breast cancer. *Neoplasia* 16, 644–655. doi: 10.1016/j.neo.2014.07.007
- Van Bon, B. W. M., Koolen, D. A., Brueton, L., McMullan, D., Lichtenbelt, K. D., Adès, L. C., et al. (2010). The 2q23.1 microdeletion syndrome: clinical and behavioural phenotype. *Eur. J. Hum. Genet.* 18, 163–170. doi: 10.1038/ejhg.2009.152
- van den Boogaard, M. L., Thijssen, P. E., Aytekin, C., Licciardi, F., Krykma, A. A., Sposito, L., et al. (2017). Expanding the mutation spectrum in ICF syndrome: evidence for a gender bias in ICF2. *Clin. Genet.* 92, 380–387. doi: 10.1111/cge.12979
- Van Maldergem, L., Siitonen, H. A., Jalkh, N., Chouery, E., De Roy, M., Delague, V., et al. (2006). Revisiting the craniosynostosis-radial ray hypoplasia association: baller-gerold syndrome caused by mutations in the RECQL4 gene. *J. Med. Genet.* 43, 148–152. doi: 10.1136/jmg.2005.031781
- Van Maldergem, L., Verloes, A., Lejeune, L., and Gillerot, Y. (1992). The Baller-Gerold syndrome. *J. Med. Genet.* 29, 266–268. doi: 10.1136/jmg.29.4.266
- van Ravenswaaij-Arts, C., and Martin, D. M. (2017). New insights and advances in CHARGE syndrome: diagnosis, etiologies, treatments, and research discoveries. *Am. J. Med. Genet. Part C Semin. Med. Genet.* 175, 397–406. doi: 10.1002/ajmg.c.31592
- Viale, L., Allotey, J., Cheong-See, F., Arroyo-Manzano, D., McCorry, D., Bagary, M., et al. (2015). Epilepsy in pregnancy and reproductive outcomes: a systematic review and meta-analysis. *Lancet* 386, 1845–1852. doi: 10.1016/S0140-6736(15)00045-8
- Vissers, L. E. L. M., De Vries, B. B. A., Osoegawa, K., Janssen, I. M., Feuth, T., Choy, C. O., et al. (2003). Array-based comparative genomic hybridization for the genomewide detection of submicroscopic chromosomal abnormalities. *Am. J. Hum. Genet.* 73, 1261–1270. doi: 10.1086/379977
- Vissers, L. E. L. M., Van Ravenswaaij, C. M. A., Admiraal, R., Hurst, J. A., De Vries, B. B. A., Janssen, I. M., et al. (2004). Mutations in a new member of the chromodomain gene family cause CHARGE syndrome. *Nat. Genet.* 36, 955–957. doi: 10.1038/ng1407
- Voss, A. K., Collin, C., Dixon, M. P., and Thomas, T. (2009). Moz and retinoic acid coordinately regulate H3K9 acetylation, hox gene expression, and segment identity. *Dev. Cell* 17, 674–686. doi: 10.1016/j.devcel.2009.10.006
- Weemaes, C. M., Van Tol, M. J., Wang, J., Van Ostaijen-Ten Dam, M. M., Van Eggermond, M. C., Thijssen, P. E., et al. (2013). Heterogeneous clinical presentation in icf syndrome: correlation with underlying gene defects. *Eur. J. Hum. Genet.* 21, 1219–1225. doi: 10.1038/ejhg.2013.40
- Wegner, C., and Nau, H. (1992). Alteration of embryonic folate metabolism by valproic acid during organogenesis: implications for mechanism of teratogenesis - PubMed. *Neurology* 42, 17–24.
- Whittaker, D. E., Riegman, K. L. H., Kasah, S., Mohan, C., Yu, T., Sala, B. P., et al. (2017). The chromatin remodeling factor CHD7 controls cerebellar development by regulating reelin expression. *J. Clin. Invest.* 127, 874–887. doi: 10.1172/JCI83408
- Wijmenga, C., Van Den Heuvel, L. P. W. J., Strengman, E., Luyten, J. A. F. M., Van Der Burgt, I. J. A. M., De Groot, R., et al. (1998). Localization of the ICF syndrome to chromosome 20 by homozygosity mapping. *Am. J. Hum. Genet.* 63, 803–809. doi: 10.1086/302021
- Willemsen, M. H., Vulto-Van Silfhout, A. T., Nillesen, W. M., Wissink-Lindhout, W. M., Van Bokhoven, H., Philip, N., et al. (2012). Update on Kleefstra syndrome. *Mol. Syndromol.* 2, 202–212. doi: 10.1159/000335648
- Wiltse, J. (2005). Mode of action: inhibition of histone deacetylase, altering WNT-dependent gene expression, and regulation of beta-catenin—developmental effects of valproic acid. *Crit. Rev. Toxicol.* 35, 727–738. doi: 10.1080/10408440591007403
- Xu, B., Mulvey, B., Salie, M., Yang, X., Matsui, Y., Nityanandam, A., et al. (2020). UTX/KDM6A suppresses AP-1 and a gliogenesis program during neural differentiation of human pluripotent stem cells. *Epigenet. Chromatin* 13:38. doi: 10.1186/s13072-020-00359-3
- Xu, G. L., Bestor, T. H., Bourc'His, D., Hsieh, C. L., Tommerup, N., Bugge, M., et al. (1999). Chromosome instability and immunodeficiency syndrome caused by mutations in a DNA methyltransferase gene. *Nature* 402, 187–191. doi: 10.1038/46052
- Xu, Q., and Xie, W. (2018). Epigenome in early mammalian development: inheritance, reprogramming and establishment. *Trends Cell Biol.* 28, 237–253. doi: 10.1016/j.tcb.2017.10.008
- Yao, H., Hannum, D. F., Zhai, Y., Hill, S. F., Albanus, R. D., Lou, W., et al. (2020). CHD7 promotes neural progenitor differentiation in embryonic stem cells via altered chromatin accessibility and nascent gene expression. *Sci. Rep.* 10:17445. doi: 10.1038/s41598-020-74537-4
- Yao, H., Hill, S. F., Skidmore, J. M., Sperry, E. D., Swiderski, D. L., Sanchez, G. J., et al. (2018). CHD7 represses the retinoic acid synthesis enzyme ALDH1A3 during inner ear development. *JCI Insight* 3:e97440. doi: 10.1172/jci.insight.97440
- Ying, J., Xu, T., Wang, C., Jin, H., Tong, P., Guan, J., et al. (2020). Dnmt3b ablation impairs fracture repair through upregulation of Notch pathway. *JCI Insight* 5:e131816. doi: 10.1172/jci.insight.131816

Conflict of Interest: RF formerly held a leadership position in TeratOmic Consulting LLC. This now dissolved organization provided expert consulting support in birth defects litigation.

The remaining authors declare that the research was conducted in the absence of any commercial or financial relationships that could be construed as a potential conflict of interest.

Copyright © 2021 Parodi, Di Fedè, Peron, Viganò, Grazioli, Castiglioni, Finnell, Gervasini, Vignoli and Massa. This is an open-access article distributed under the terms of the Creative Commons Attribution License (CC BY). The use, distribution or reproduction in other forums is permitted, provided the original author(s) and the copyright owner(s) are credited and that the original publication in this journal is cited, in accordance with accepted academic practice. No use, distribution or reproduction is permitted which does not comply with these terms.



Article

Insights into the Role of the Microbiota and of Short-Chain Fatty Acids in Rubinstein–Taybi Syndrome

Elisabetta Di Fede ^{1,†}, Emerenziana Ottaviano ^{1,†}, Paolo Grazioli ¹, Camilla Ceccarani ^{1,2}, Antonio Galeone ³, Chiara Parodi ¹, Elisa Adele Colombo ¹, Giulia Bassanini ¹, Grazia Fazio ⁴, Marco Severgnini ², Donatella Milani ⁵, Elvira Verduci ^{1,6}, Thomas Vaccari ³, Valentina Massa ^{1,7,‡}, Elisa Borghi ^{1,‡} and Cristina Gervasini ^{1,7,*}

- ¹ Department of Health Sciences, Università degli Studi di Milano, 20142 Milan, Italy; elisabetta.difede@unimi.it (E.D.F.); emerenziana.ottaviano@unimi.it (E.O.); paolo.grazioli@unimi.it (P.G.); camilla.ceccarani@unimi.it (C.C.); chiara.parodi@unimi.it (C.P.); elisaadele.colombo@unimi.it (E.A.C.); giulia.bassanini@unimi.it (G.B.); elvira.verduci@unimi.it (E.V.); valentina.massa@unimi.it (V.M.); elisa.borghi@unimi.it (E.B.)
- ² Institute of Biomedical Technologies, Italian National Research Council, Segrate, 20054 Milan, Italy; marco.severgnini@itb.cnr.it
- ³ Department of Biosciences, Università degli Studi di Milano, 20133 Milano, Italy; antonio.galeone@unimi.it (A.G.); thomas.vaccari@unimi.it (T.V.)
- ⁴ Tettamanti Research Center, Department of Pediatrics, Università degli Studi di Milano-Bicocca, MBBM Foundation/San Gerardo Hospital, 20900 Monza, Italy; grazia.fazio@unimib.it
- ⁵ Fondazione IRCCS Ca' Granda Ospedale Maggiore Policlinico, 20122 Milan, Italy; donatella.milani@policlinico.mi.it
- ⁶ Department of Pediatrics, Vittore Buzzi Children's Hospital, University of Milan, 20154 Milan, Italy
- ⁷ "Aldo Ravelli" Center for Neurotechnology and Experimental Brain Therapeutics, Università degli Studi di Milano, 20142 Milan, Italy
- * Correspondence: cristina.gervasini@unimi.it; Tel.: +39-02-5032-3028
- † These authors contributed equally to this work.
- ‡ These authors contributed equally to this work.



Citation: Di Fede, E.; Ottaviano, E.; Grazioli, P.; Ceccarani, C.; Galeone, A.; Parodi, C.; Colombo, E.A.; Bassanini, G.; Fazio, G.; Severgnini, M.; et al. Insights into the Role of the Microbiota and of Short-Chain Fatty Acids in Rubinstein–Taybi Syndrome. *Int. J. Mol. Sci.* **2021**, *22*, 3621. <https://doi.org/10.3390/ijms22073621>

Academic Editor: Rustam Aminov

Received: 22 February 2021

Accepted: 27 March 2021

Published: 31 March 2021

Publisher's Note: MDPI stays neutral with regard to jurisdictional claims in published maps and institutional affiliations.



Copyright: © 2021 by the authors. Licensee MDPI, Basel, Switzerland. This article is an open access article distributed under the terms and conditions of the Creative Commons Attribution (CC BY) license (<https://creativecommons.org/licenses/by/4.0/>).

Abstract: The short-chain fatty acid butyrate, produced by the gut microbiota, acts as a potent histone deacetylase (HDAC) inhibitor. We assessed possible ameliorative effects of butyrate, relative to other HDAC inhibitors, in in vitro and in vivo models of Rubinstein–Taybi syndrome (RSTS), a severe neurodevelopmental disorder caused by variants in the genes encoding the histone acetyltransferases CBP and p300. In RSTS cell lines, butyrate led to the patient-specific rescue of acetylation defects at subtoxic concentrations. Remarkably, we observed that the commensal gut microbiota composition in a cohort of RSTS patients is significantly depleted in butyrate-producing bacteria compared to healthy siblings. We demonstrate that the effects of butyrate and the differences in microbiota composition are conserved in a *Drosophila melanogaster* mutant for CBP, enabling future dissection of the gut–host interactions in an in vivo RSTS model. This study sheds light on microbiota composition in a chromatinopathy, paving the way for novel therapeutic interventions.

Keywords: Rubinstein–Taybi syndrome; butyrate; microbiota; HDACi; histones

1. Introduction

Gene expression regulation is mediated by tightly balanced epigenetic mechanisms involving histone modifications, such as acetylation and methylation. Correct histone acetylation levels on lysine residues are fundamental for several physiological processes, including embryonic development [1,2]. Two classes of functionally antagonistic enzymes, the acetyltransferases (HAT) and deacetylases (HDAC), are known to modulate histone acetylation levels [3]. Histones hypoacetylation has been associated with alterations in synaptic plasticity, neuronal survival/regeneration, memory formation [4], while defects

in epigenetic components acting on acetylation status cause several neurodevelopmental/malformation syndromes [5]. Among them, Rubinstein–Taybi syndrome (RSTS, OMIM #180849, #613684) is a rare (1:125,000) autosomal-dominant disease characterized by a wide and heterogeneous spectrum of clinical signs [6]. These include intellectual disability of variable entity (ranging from mild to severe), postnatal growth deficiency, distinctive dysmorphisms, skeletal abnormalities (such as typical broad thumbs and large toes), multiple congenital anomalies (e.g., heart defects), and several additional clinical problems such as constipation [7]. Albeit the growth in height is constantly reduced in RSTS patients, growth in weight is reduced neonatally and in the first infancy, but at puberty an excessive weight gain is observed [8].

Most RSTS cases are caused by de novo monoallelic variants of one of two highly conserved genes: *CREBBP*, located at 16p13.3, coding for the CREB (cAMP response element-binding protein) binding protein (CBP) and *EP300*, mapping at 22q13.2, coding for the E1A-associated protein p300. *CREBBP* is found mutated in >50% RSTS patients, while *EP300* gene mutations have been described in a minor fraction of patients [9].

Somatic mutations in *CREBBP* and *EP300* are reported in different benign and malignant tumors, and an association between RSTS patients and tumor development has been investigated. This disorder is related to an increased risk of malignancies up to 5%, in particular involving cutaneous, hematological, and brain tumors such as pilomatrixoma, leukemia, and meningioma, respectively [10,11].

CBP and p300 have ubiquitously expressed paralog proteins belonging to the lysine acetyl transferases (HAT) family [12]. CBP and p300 act as co-factors for transcription and are required in multiple pathways controlling cell growth, DNA repair, cell differentiation, and tumor suppression [13–16]. Their acetylation of target histone tails enables the opening of chromatin, thus promoting gene expression [13,15,17].

In recent years, a novel class of compounds, termed HDAC inhibitors (HDACi), has been used to increase histone acetylation in different pathologies [18,19]. Preliminary studies testing the efficiency of HDACi to revert acetylation defects in RSTS lymphoblastoid cell lines (LCLs) supported the hypothesis that RSTS is caused by an acetylation imbalance [20]. Animal model studies introduced the idea that the chromatin alterations observed in RSTS could be reverted [21].

It has been demonstrated that protein acetylation can be modulated by the commensal microbial community (microbiota from here on) [22]. In fact, short-chain fatty acids (SCFAs), such as acetate, propionate, and butyrate, the most abundant products of anaerobic fermentation of the gut microbiota, can act as HDACi. Among SCFAs, butyrate is exclusively produced by commensal microorganisms and widely reported for its epigenetic activity, making it the most potent HDACi among natural compounds [23,24]. However, the role of butyrate or the composition of the microbiota in RSTS have not been investigated. Altered gut microbiota could itself affect the endogenous levels of SCFAs in patients, it could participate in their typical RSTS growth trend, characterized by a deficit in infancy and excessive weight gain after puberty, and/or it could contribute to the comorbidities often associated with RSTS, such as gastrointestinal discomfort [8].

On these premises, in the present study, we compared butyrate to other HDACi molecules in vitro on lymphoblastoid cell lines (LCLs) derived from RSTS patients. We have found it effective in modulating the acetylation impairment associated with reported CBP/p300 defects [20]. Remarkably, we also find that the microbiota of RSTS patients is poor in SCFA-producing bacteria, perhaps further contributing to acetylation imbalance. Finally, using *Drosophila melanogaster*, we model the effects of butyrate and microbiota alterations for future in vivo studies. Our work points to the importance of the microbiome in the pathogenesis and treatment of ultra-rare diseases.

2. Results

2.1. HDACi Exposure Counteracts Acetylation Imbalance in RSTS Lymphoblastoid Cell Lines (LCLs)

To investigate the effect of SCFAs as HDACi in RSTS, we exposed LCLs derived from eight patients, four with *CREBBP* and four with *EP300* mutations (Table S1) and seven healthy donors (HD) to sodium butyrate (NaB), and we compared the effect to that of three other HDACi: trichostatin A (TSA), suberoylanilide hydroxamic acid (SAHA), and valproic acid (VPA) (Table S2). By AlphaLISA® assay, we analyzed the acetylation levels of lysine 27 of histone H3 (H3K27ac) in LCLs upon three different conditions: HDACi treatments, exposure to the vehicle (DMSO or H₂O), and untreated cells (Figure 1).

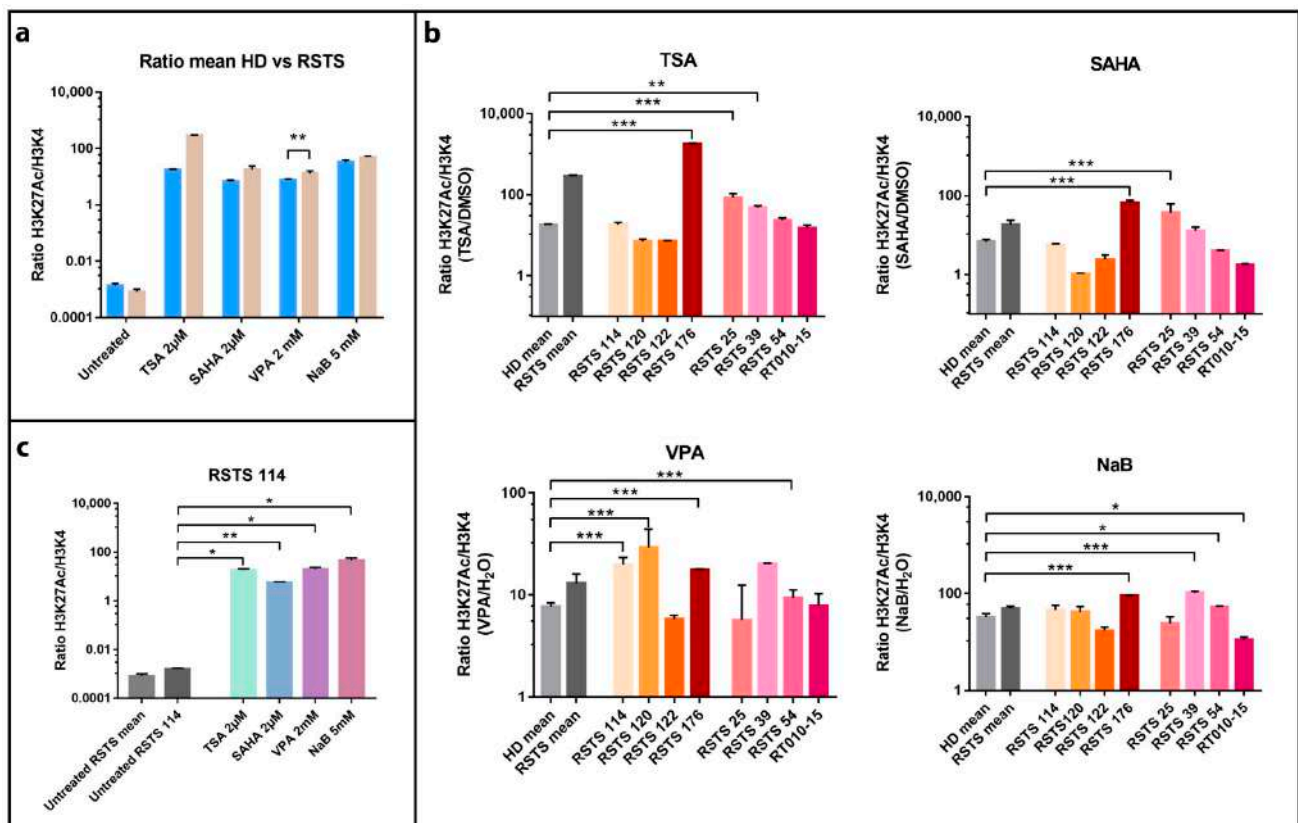


Figure 1. Histone acetylation on Rubinstein–Taybi syndrome (RSTS) lymphoblastoid cell lines (LCLs) upon acetyltransferases (HAT) and deacetylases (HDAC) inhibitors exposure. H3K27 acetylation levels normalized on H3K4 unmodified, assessed by AlphaLISA®; levels of acetylation upon HDAC inhibitors (HDACi) are expressed as a ratio between the treatment and respective vehicle (HDACi/vehicle); on the Log scale, Y-axis H3K27 acetylation levels normalized, on X-axis lists of epigenetic treatments or untreated/treated single LCL or LCLs means. (a) Means of values of H3K27 acetylation in healthy donors (HD, in blue) and patients LCLs (RSTS, in pale brown) untreated and exposed to four different HDACi (trichostatin A (TSA) 2 µM, suberoylanilide hydroxamic acid (SAHA) 2 µM, valproic acid (VPA) 2 mM, and sodium butyrate (NaB) 5 mM). (b) H3K27 acetylation in eight RSTS LCLs (*CREBBP* LCLs in shades of red, *EP300* LCLs in shades of pink) after exposure with the four different HDACi, compared to treated HD and RSTS means. (c) Insight on the single-patient response (RSTS 114) to the four compounds compared to untreated RSTS means and RSTS 114. Groups were compared using Student’s *t*-test as statistical method (* $p < 0.05$; ** $p < 0.01$; *** $p < 0.001$).

All the compounds succeeded in boosting histone acetylation in RSTS LCLs compared to healthy donor (HD) LCLs, with VPA exposure resulting highly significant ($p < 0.01$). This increment was particularly manifest in patient derived LCLs compared to untreated samples (Figure 1a).

We also observed that HDACi compounds induced a variable acetylation response, in a patient-specific manner when compared to treated HD LCLs (Figure 1b). As shown in Figure 1b, treatment with TSA 2 μ M boosted acetylation levels significantly in LCLs RSTS 176 ($p < 0.001$), RSTS 25 ($p < 0.001$) and RSTS 39 ($p < 0.01$), while SAHA 2 μ M showed highly significant effect on RSTS 176 and RSTS 25 ($p < 0.001$). VPA 2mM treatment particularly increased H3K27ac of RSTS 114, RSTS 120, RSTS 176, and RSTS 54 ($p < 0.001$), while exposure to NaB 5 mM significantly affected acetylation of RSTS 176 and RSTS 39 ($p < 0.001$), RSTS 54, and RT010-15 ($p < 0.05$).

Of note, when analyzing specific RSTS patient-derived LCLs response to HDACi compared to the relative untreated conditions, we observed that at least one HDACi significantly boosted acetylation and that RSTS-LCLs response varied among different drug treatments (Figure 1c and Figure S1). These data indicate that SCFAs as NaB show patient-specific acetylation increases, as is the case of other HDACi.

Considering HDACi applications as anticancer drugs for their role in cell cycle arrest, cell death, and immune-mediated mechanisms [25], we studied NaB and other HDACi effects on cell proliferation and apoptosis, performing Ki67 and TUNEL assays upon exposure of LCLs with HDACi (Figures S2 and S3). For both assays, we did not observe a significant correlation with H3K27 acetylation (Figure S4), indicating that the HDACi rescue did not impair cell cycle progression or promote cell death under the experimental conditions used.

2.2. RSTS Patients Are Depleted in the Major Butyrate-Producer *Faecalibacterium* spp.

Because in vitro evaluation indicated that SCFAs can act as HDACi in RSTS, we focused on investigating the production of SCFAs by the commensal microbiota of the patients. To this end, we enrolled 23 RSTS subjects (mean age 10.2 ± 6.4 years; 12 females) and 16 healthy siblings (healthy donors, HD), mean age 12.7 ± 7.2 years; 6 females), as a control group to minimize environmental factors having a well-recognized role on gut microbiota. The dietary survey revealed no differences in intake of macronutrients. However, energy intake was lower in RSTS subjects when compared to HD controls ($p = 0.0054$). Nutritional parameters are detailed in the relative supplementary table (Table S3) [26].

Microbiota profiling was performed through 16S rRNA gene-targeted sequencing. After quality filtering processes, we obtained a mean count of 90,759 reads per sample. The alpha-diversity analysis of the gut microbiota showed no significant differences between RSTS and HD fecal samples in terms of richness (Observed species: $p = 0.255$; Phylogenetic Diversity (PD) whole tree: $p = 0.279$ —see Figure 2a) and of richness and evenness (Chao1: $p = 0.151$; Shannon: $p = 0.287$ —see Figure S5). Beta-diversity analysis, instead, showed that RSTS fecal microbiota differed significantly from that of HD according to both unweighted ($p = 0.013$) and weighted ($p = 0.022$) Unifrac distances (beta-diversity, Figure 2b).

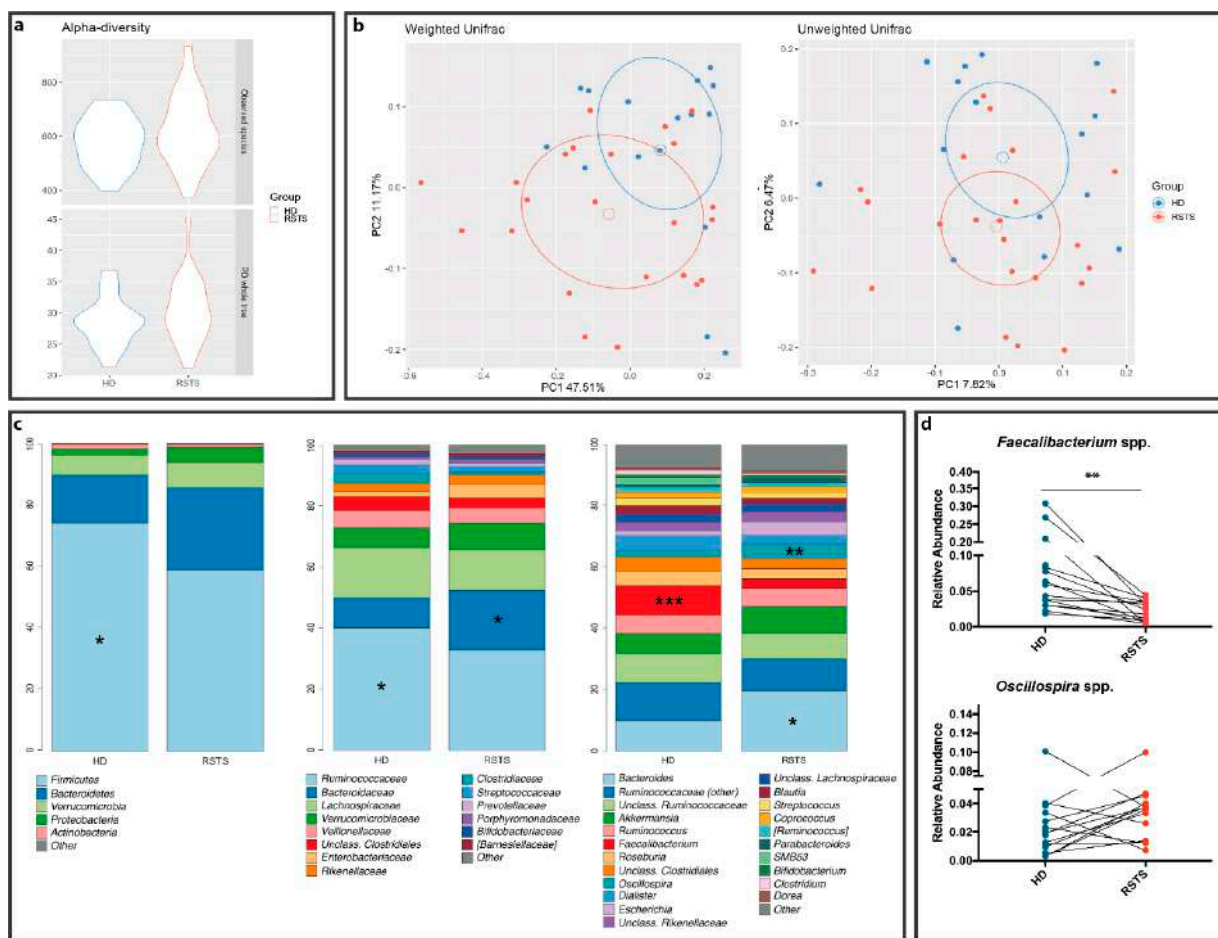


Figure 2. RSTS gut microbiota analysis. (a) alpha diversity. The violin plot shows biodiversity values for observed species and Faith's phylogenetic metrics. No statistically relevant differences were seen. (b) Principal coordinate analysis (PCoA) according to weighted and unweighted Unifrac distances. Microbial communities are statistically different (*Adonis* test: unweighted $p = 0.019$; weighted $p = 0.023$). The first and second principal coordinates are shown in the plot for both distances. (c) Bacterial composition of HD and RSTS groups. Relative taxonomic abundances are shown at phylum, family, and genus phylogenetic levels. All bacterial taxa present at <1% relative abundance were grouped into the "Other" classification. ***: $p < 0.005$; **: $p < 0.01$; *: $p < 0.05$. (d) *Faecalibacterium* spp. and *Oscillospira* spp. relative abundances (both significantly different between RSTS and HD) were compared within matched family members (patient/sibling, $n = 16$). For *Oscillospira* we did not observe a common pattern; *Faecalibacterium* spp. was significantly reduced in RSTS ($p = 0.0021$, Wilcoxon signed-rank test).

The overall composition of the intestinal microbiota (Figure 2c; Table S4) showed a decreased relative abundance of the Firmicutes phylum (58.5% in RSTS vs. 73.4% in HD, $p = 0.019$), of the *Ruminococcaceae* family (32.2% vs. 41.9%, $p = 0.049$) and of the SCFA-producing *Faecalibacterium* spp. (3.3% vs. 9.8% in HD, $p = 0.001$) in RSTS subjects. On the other hand, RSTS samples showed an enrichment in the *Bacteroidaceae* family and in *Bacteroides* spp. (21.1% vs. 10.3%, $p = 0.021$), as well as in *Oscillospira* spp. (5.1% vs. 2.4% in HD, $p = 0.007$). Matched-pair analysis (Wilcoxon signed-rank test), performed on RSTS/sibling pairs showed a significant and environment-independent decrease ($p = 0.0021$) in *Faecalibacterium* spp. (Figure 2d).

Afterward, we directly measured SCFA abundance in patient fecal samples. A decreasing trend in butyrate content was observed (4.13 ± 1.40 vs. 5.14 ± 1.79 mg/g feces, $p = 0.0741$, Mann–Whitney test), whereas acetate, propionate, and branched-chain fatty acids (iso-butyrate and iso-valerate) concentrations were similar ($p = 0.194$, $p = 0.874$, $p = 0.786$, and $p = 0.467$, respectively). These data indicate that RSTS patient microbiota produces low levels of endogenous butyrate.

2.3. HDACi Exposure Leads to Partial Rescue of RSTS Phenotype in *Drosophila* CBP Mutants

To establish an *in vivo* model to study the effect of SCFAs and the microbiome on RSTS pathogenesis, we analyzed *Drosophila melanogaster* mutants in the CBP homolog *nejire* (*nej*). Homozygous *nej* loss of function results in abnormal embryonic development leading to early lethality [27,28]. In particular, mutations in *nej* lead to defects in morphology caused by misregulation of wingless (*wg*) and other signaling pathways at stage 9 of embryonic development [27]. To test whether NaB, or VPA as a control HDACi, upon supplementation in the food could modulate emergence of *nej* mutant defects *in vivo*, we collected embryos deposited by females fed with the drugs and assessed their morphology at stages 8–12 (Figure 3 and Figure S6).

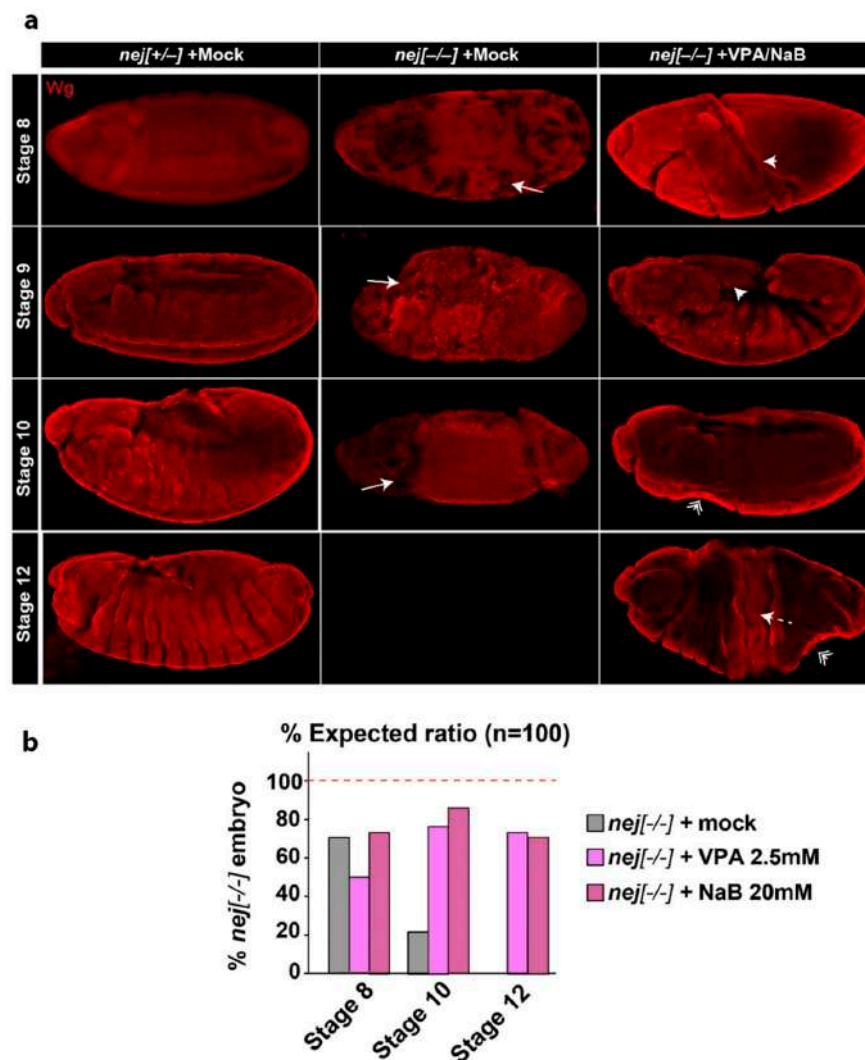


Figure 3. Developmental and morphological defects in *nej* mutant embryos are partially ameliorated by VPA or NaB treatment. (a) wingless (*wg*) staining of *nej* mutant embryos treated as indicated. Representative projections of confocal imaging from stages 8 to 12 are shown. The defects detected in *nej* mutant embryos with or without treatment include loss or uneven *wg* staining (Drilled, arrow), twisting (arrowhead), presence of bottlenecks (double-arrowheads), or cracks (dashed-arrow). (b) Quantification of embryo survival and of the above phenotypes in *nej* mutant embryos at stages 8 to 12. VPA or NaB treatments partially rescue embryo development, allowing *nej* mutant embryos to survive beyond stage 8 although with aberrant phenotypes, with significant embryo survival at stage 10 compared to untreated embryos ($p > 0.01$). Student's t-test was used as statistical method for comparing *nej* groups survival, with $p < 0.05$ considered significant.

Compared to *nej*^{+/-} siblings, we have found that the majority of *nej*^{-/-} embryos die between stages 8 and 10 with the reported twisting of embryo morphology [28] (Figure 3a, quantification in Figure 3b). Upon NaB or VPA treatment, *nej*^{-/-} embryos display a partially rescued embryonic development, statistically significant at stage 10 ($p < 0.01$). Importantly, both treatments extended the survival of *nej*^{-/-} embryos to stage 12, although twisting of the embryos is morphologically visible as bottleneck and cracks (Figure 3 and Figure S6). The reported twisting phenotype in treated *nej*^{-/-} embryos is often less dramatic than in untreated *nej*^{-/-} embryos allowing segmentation. Notably, both VPA and NaB treatment did not show any developmental delay or morphological defects in control embryos (data not shown). Altogether, these results indicate that NaB acts as a HDACi in vivo to ameliorate the developmental defects associated with acute loss of CBP homologs.

2.4. The Fly Gut Microbiota of Heterozygous *Drosophila* CBP Mutants

Because RSTS patients possess a defective microbiota, we analyzed that of heterozygous *nej* (*nej*^{+/-}) flies. In contrast to *nej*^{-/-} embryos, *nej*^{+/-} animals progress to adulthood and display no overt defects. However, they have been shown to reveal genetic interaction with genes involved in developmental processes regulated by CBP [28]. Hence, we reasoned that adult *nej*^{+/-} animals could be used to investigate the fly gut microbiota.

A total of 10 samples were obtained from the two experimental groups (*yw* and *nej*^{+/-}), with five replicates each (three dissected guts in each replicate, with a total of 15 flies per group).

Alpha diversity metrics (Figure 4a) revealed that *nej* gut microbiota were enriched in low abundant species (Chao1 metric, $p = 0.005$), whereas the phylogenetic diversity between groups showed no significant differences (PD whole tree metric, $p = 0.668$).

Similarly, beta-diversity analysis (Figure 4b) highlighted clear discrimination between *yw* and *nej* microbial communities considering both abundant and rare species within the microbiota (unweighted Unifrac distance, $p = 0.007$),

As for the bacterial composition, the Firmicutes phylum was found more abundant in the *nej* flies (64.7% vs. 53.9% in *yw*), with a concurrent reduction of Proteobacteria (31.6 vs. 41.1% in *yw*). The taxonomic analysis revealed a remarkable increase in *Lactobacillaceae* (58.8% in *nej* vs. 7.5% in *yw*; $p = 0.0000254$), and a profound decrease in the *Enterococcaceae* family (0.2% vs. 12.9% in *yw*; $p = 0.00784$) (Figure 4c). These results were confirmed at genus level, with a significant enrichment in *Lactobacillus* (58.4% in *nej* vs. 3.4% in *yw*; $p = 0.00000806$) and a depletion in *Enterococcus* (0% vs. 3% in *yw*; $p = 0.00772$) (data not shown).

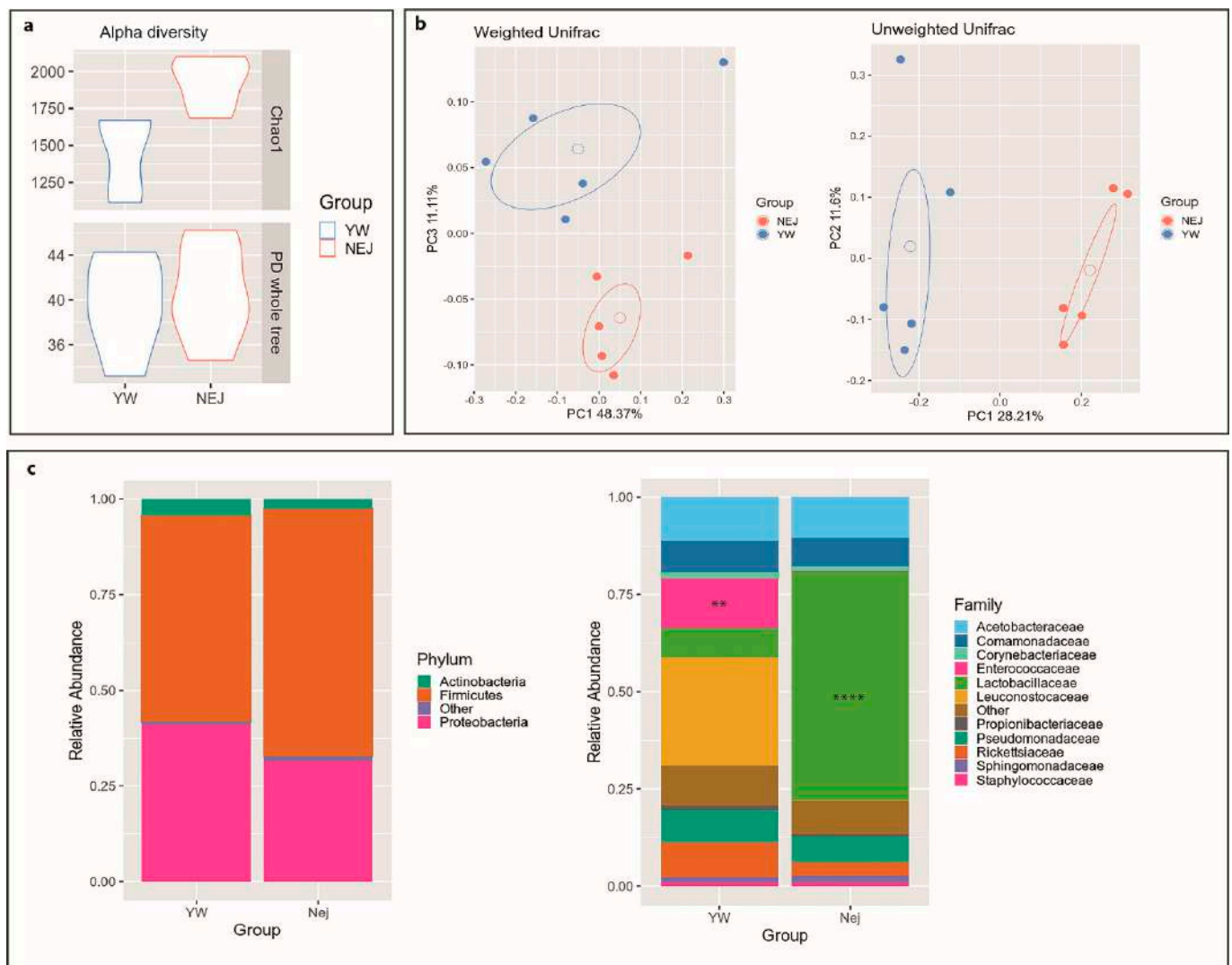


Figure 4. *Drosophila* gut microbiota analysis. Gut microbial communities were characterized by 16S rRNA gene sequencing. (a) Alpha diversity. Violin plots show biodiversity values for Chao1 ($p = 0.005$) and Faith's phylogenetic metrics (PD whole tree; $p = 0.668$). (b) Principal coordinate analysis (PCoA) for both Unifrac distances. (*Adonis* test: weighted $p = 0.216$; unweighted $p = 0.007$). (c) Relative taxonomic abundances of the gut bacterial composition in *yw* and *nej* flies at phylum and family levels. All bacterial taxa present at <1% relative abundance were grouped into the "Other" classification. ****: $p < 0.001$; **: $p < 0.01$.

3. Discussion

Current therapeutic approaches for RSTS patients are not targeted towards modulation of acetylation and are rather directed towards alleviating clinical symptoms and preventing possible known comorbidities. Common interventions include behavioral support and surgical procedures for the correction of orthopedic or cardiac malformations. In this context, exploring the effects of drugs with an established and specific molecular function in acetylation in preclinical studies is a fundamental step to devise effective future therapy. In the case of RSTS, HDACi are available and have already been used to treat neurological disorders [29]. Hence, the presented work explored the effects of HDAC inhibition in RSTS experimental models, focusing on natural SCFAs such as butyrate.

Treatment with a number of HDACi used in cancer therapy [30–33] showed a general boost in histone acetylation levels in RSTS patient-derived cell lines. Such increment was significant in a patient-specific manner. Each line derived from different RSTS patients with discrete pathogenic variants responded differently to tested compounds. These data provide evidence for HDACi's ability to restore acetylation levels in an in vitro model of

RSTS, strongly pointing to the possibility of future therapies tailored to individual patients, a central tenet of personalized medicine.

HDACi are tested in oncology trials for their ability to stop tumor cell proliferation by inducing selected and dose-dependent apoptosis [34]. Thus, our observation that selected HDACi dosing does not modulate cell proliferation or death in RSTS cells indicates that HDACi can boost acetylation at a sub-toxic concentration, at least in vitro.

Due to the HDACi function exerted by SCFAs, they have been tested in clinical trials for recurrent malignant gliomas or myelodysplastic syndrome and they have also been studied in vitro against Burkitt lymphoma, primary acute myeloid leukemia, retinoblastoma, medulloblastoma, prostate cancer, and hepatocellular and colon carcinoma [35,36].

Importantly, NaB, a natural SCFA with potent HDACi activity [37], performed on par with other HDACi in RSTS cells. We propose that it should be evaluated for the treatment of patients, considering that it is present in human diets as a product of the human microbiota or a well-tolerated supplement.

To investigate whether butyrate is normally produced by commensal bacteria of RSTS patients, we sequenced the V3–V4 hypervariable regions of the 16S rRNA genes and measured SCFAs as main microbial metabolites. While we scored no differences in nutritional parameters and in microbiota biodiversity in patients versus healthy siblings, we observed a distinct and highly interesting microbial signature characterized by loss of the butyrate-producer genus *Faecalibacterium* [38] in the microbiota of RSTS patients. Such change could participate in the syndrome comorbidity insurgence, perhaps in the gut, and further study should now aim at elucidation of possible genetic-microbial additive negative effects. Interestingly, a reduction of *Faecalibacterium* relative abundance was also reported in patients affected by Rett syndrome, autism spectrum disorder, and down syndrome, suggesting a shared microbiota signature in neurodevelopmental disorders [39].

A recent study reported that a ketogenic diet, highly impacting microbiota composition and metabolism [40], induces the production of deacetylase inhibitors in a mouse model of Kabuki syndrome (OMIM# 147920, # 300867), a rare disease sharing traits and histone modification defect with Rubinstein–Taybi syndrome [41]. Thus, nutritional interventions could also aim at rebalancing the microbiota of RSTS patients. In line with this approach, brain functions and behavior appear more and more influenced, through a bottom-up modulation, by the gut microbiota [42].

It is worth noting that carbohydrates, and in particular fermentable dietary fibers, the most important substrates for short-chain fatty acid production [43], were very similar in RSTS patients and healthy siblings, inconsistent with the reduction in the relative abundance of *Faecalibacterium* genus, or with the lower butyrate fecal concentration. Nutritional recommendations for RSTS comorbidity management are currently lacking as no studies focused on this. Our findings represent a starting point for the evaluation of specific nutritional regimens, which could also shed light on the basis of observed differences.

Studies with *nej* flies underscored the role of CBP during embryogenesis and as coactivators of critical signaling pathways involved in patterning [28,44]. In support of results from our in vitro RSTS model, we observed that rearing flies with food supplemented with NaB lead to partial rescue of embryogenesis and patterning, suggesting that nutritional intervention may ameliorate RSTS traits in vivo.

However, even if the *Drosophila* model has been used for investigating how different levels of nutrients and drugs influence the development and the metabolic phenotypes of emerging *Drosophila* embryos [45], our data are model behavior of oviparous animals, in which development occurs outside the mother's body. In mammals, maternal HDACi cross the placenta and affect embryogenesis; hence any future intervention should be envisaged after birth when the mammalian central nervous system is still developing.

Lack of an anoxic compartment in the *Drosophila* gut shapes a microaerophilic microbiota constituted, in laboratory strains, by few genera [46]. The most abundant taxa are *Firmicutes*, mainly *Lactobacillus* spp. and *alpha-Proteobacteria*, mainly *Acetobacteraceae*. Despite evolutionary divergence with the human microbiota, recent studies showed that an

altered relative abundance of these genera can result in gut homeostasis disturbance [47], growth delay [48], and behavioral changes [49]. Considering the results obtained from microbiota analysis of RSTS patients, we analyzed the microbial community of heterozygous *nej* insects compared to control animals. Results showed that, accounting for the species-specificity of the microbiota, the differences observed in RSTS patients compared to healthy siblings are recapitulated in RSTS flies compared to control animals, suggesting that patients–microbiota interactions could be modeled in *Drosophila*.

Overall, our results are in line with other studies [12,20,50], making a strong case for HDACi drug repurposing for future RSTS therapy. We envisage that the use of *Drosophila melanogaster* as an information rich in vivo RSTS model will speed up the transition from preclinical studies to clinical practice.

4. Materials and Methods

4.1. Cell Cultures

Lymphoblastoid cell lines (LCLs) from eight different RSTS patients (four carrying *CREBBP* mutations and four carrying *EP300* mutations, listed in Table S1) [20,51–53] and seven healthy donors were obtained in collaboration with the Gaslini Genetic Bank service (Telethon Network of Genetic Biobanks); their use was approved by Ethics Committee of Università degli Studi di Milano (Comitato Etico number 99/20, 17 November 2020). Cells were maintained in RPMI 1640 culture medium supplemented with L-glutamine (Euroclone, Pero, Italy), 20% fetal bovine serum (Euroclone, Pero, Italy), and penicillin/streptomycin (Euroclone, Pero, Italy), and cultured in an incubator with 5% CO₂ at 37 °C.

LCLs were exposed to four different HDAC inhibitors: Trichostatin A (TSA) (sc-3511, Santa Cruz Biotechnology, Dallas, TX, USA), Suberoylanilide hydroxamic acid (SAHA) (MK0683, Selleckchem, Houston, TX, USA), Valproic acid (VPA) (P4543, Sigma Aldrich, St. Louis, MO, USA), and Sodium Butyrate (NaB) (B5887, Sigma-Aldrich, St. Louis, MO, USA). We tested three different concentrations for each HDACi (Table S2) [54–59] and selected the maximum dose and timing of exposure, ensuring acceptable LCLs survival (data not shown). Cells were incubated with vehicles (H₂O or DMSO) at the maximum time (24 h), TSA 2 µM for 2 h, SAHA 2 µM for 24 h, VPA 2 mM for 24 h, or NaB 5 mM for 24 h as suggested from the literature (Table S2). Data were normalized on untreated cells and in vehicles for accounting for proliferation rate differences in basal condition between HD and RSTS lines.

4.2. AlphaLISA[®] Assay

After treatments, lymphoblastoid cellular pellets were obtained by centrifugation and frozen at –80 °C. An amount of 10,000 cells/well resuspended in 60 µL of culture media was used in order to perform AlphaLISA[®] assay (PerkinElmer, Waltham, MA, USA) according to the manufacturer's protocol. Briefly, cells were incubated 15 min with Cell-Histone Lysis buffer and 10 min with Cell-Histone Extraction buffer; 30 µL of lysates were incubated with 10 µL of Acceptor mix 1h at room temperature (RT) and then 10 µL of Donor mix was added overnight at RT. Replicates were tested with both AlphaLISA Acetylated-Histone H3 Lysine 27 (H3K27ac) Cellular Detection Kit (AL720, PerkinElmer, Waltham, MA, USA) and AlphaLISA unmodified Histone H3 Lysine 4 (H3K4) Cellular Detection Kit (AL719, PerkinElmer, Waltham, MA, USA) for normalization. PerkinElmer EnSight[™] plate reader was used for the detection of the chemiluminescent signal.

4.3. Ki67 and TUNEL Assay

After treatments, at least 1.5×10^4 LCLs were seeded in duplicate on SuperFrost Plus slides (ThermoFisher Scientific, Waltham, MA, USA) through 5 min of cytospin at 500 rpm, followed by 10 min of incubation with PFA 4% and washed. Slides were stored at 4 °C until Ki67 or TUNEL assays were performed.

Briefly, for Ki67 assay slides, samples were put in a wet chamber and cells permeabilized with PBT buffer (Phosphate-Buffered Saline (PBS) with 0.2% Triton) for 10 min at room temperature (RT); blocking of non-specific sites was obtained by slide incubation with PBT supplemented with 10% FBS for 30 min at RT. Slides were first incubated overnight at 4 °C with the anti-Ki67 antibody (#9129 Cell Signaling, Danvers, MA, USA, 1:400), washed with PBT, and then incubated with Alexa-488 anti-Rabbit secondary antibody (#6441-30 SouthernBiotech, Birmingham, AL, USA, 1:250) for 2 h. Slides were washed with PBT and water, mounted with EverBrite Mounting Medium with DAPI (23002, Biotium, Landing Parkway Fremont, CA, USA), and fluorescent microscopic images of proliferative cells (Ki67+) were acquired and analyzed with ImageJ software (National Institute of Health, Bethesda, MD, USA).

Terminal deoxynucleotidyl transferase (TdT) dUTP Nick-End Labeling (TUNEL) assay was performed using In Situ Cell Death Detection kit, AP (Roche Diagnostics, Basilea, Switzerland), in order to detect apoptotic cells, according to manufacturer's protocol. Cells, previously seeded on slides were incubated with a permeabilization solution (0.1% Triton 100X and 0.1% sodium citrate) for 2 min at 4 °C, then washed with PBS and incubated with TUNEL mixture (composed by Enzyme Solution added to Label Solution) in a wet chamber for 1h at 37 °C. After 3 PBS washes, slides were incubated with Converter AP for 30 min at 37 °C and then with Substrate Solution (2% NBT/BCIP stock solution in NBT/BCIP Buffer) for 10 min at RT and dark. Finally, following PBS washes, mounted with DABCO mounting medium and brightfield microscopic images of apoptotic cells (TUNEL+) were acquired and analyzed with ImageJ software (National Institute of Health, Bethesda, MD, USA).

Both fluorescent and brightfield slide images were acquired by NanoZoomer S60 Digital Slide Scanner (Hamamatsu Photonics, Hamamatsu City, Japan) at 20× and 80× magnification, and two randomly selected fields for each experimental group at 20× were selected for blinded cells counts by three different operators. Panel images of Ki67+ cells were instead acquired by confocal microscopy A1/A1R (Nikon Corporation, Tokyo, Japan) at 60× and 100× magnification. The number of Ki67+ and TUNEL+ cells was normalized on the total cell number per image.

4.4. Subject Recruitment and Sampling for Gut Microbiota Profiling

For this study, 23 RSTS subjects and 16 healthy siblings were enrolled. All subjects were recruited in collaboration with the Italian family RSTS association "Associazione RTS Una Vita Speciale ONLUS".

For both patients and controls, exclusion criteria were treatments with antibiotic and/or probiotic/prebiotic assumption during the previous 3 months. For RSTS patients, inclusion criteria were confirmed clinical diagnosis with (20/23) or without (3/23) demonstrated *CREBBP/EP300* mutation. RSTS diagnosis of all patients was confirmed by an expert geneticist (DM) and genetic tests were performed in our laboratory (CG).

In conjunction with the stool sample collection, a 3 day dietary survey (preceding the sample collection) was filled by caregivers. Dietary food records were processed using commercially available software (ePhood V2, Openzone, Bresso, Italy).

The study was approved by the Ethics Committee of San Paolo Hospital in Milan (Comitato Etico Milano Area 1, Protocol number 2019/EM/076, 2 May 2019); written informed consent was obtained from enrolled subjects or caregivers.

4.5. Bacterial DNA Extraction and 16S rRNA Gene Sequencing of Human Gut Microbiota

Bacterial genomic DNA in stool samples was extracted as previously described [60] by using the Spin stool DNA kit (Stratec Molecular, Berlin, Germany), according to the manufacturer's instructions. Briefly, after homogenizing fecal samples in the lysis buffer for inactivating DNases, Zirconia Beads II were added for a complete lysis of bacterial cells by using TissueLyser LT. Bacterial lysates were then mixed with InviAdsorb reagent, a step designed to remove PCR inhibitors. Bacterial DNA was eventually eluted in 100 µL of buffer. Then, 25 ng of extracted DNA was used to construct the sequencing library. The V3–V4

hypervariable regions of the bacterial 16S rRNA were amplified with a two-step barcoding approach according to the Illumina 16S Metagenomic Sequencing Library Preparation (Illumina, San Diego, CA, USA). Library quantification was determined using the DNA High Sensitivity Qubit kit (ThermoFisher Scientific, Waltham, MA, USA) and Agilent 2100 Bioanalyzer System (Agilent, Santa Clara, CA, USA); libraries were pooled and sequenced on a MiSeq platform (Illumina, San Diego, CA, USA) in a 2×250 bp paired-end run. Obtained 16S rRNA gene sequences were analyzed using PANDAseq [61], and low-quality reads were filtered and discarded. Reads were then processed using the Quantitative Insights Into Microbial Ecology (QIIME) pipeline (release 1.8.0) [62] and clustered into Operational Taxonomic Unit (OTUs) at 97% identity level and discarding singletons (i.e., OTUs supported by only 1 read across all samples) as likely chimeras. Taxonomic assignment was performed via the Ribosomal Database Project (RDP) classifier [63] against the Greengenes database (version 13_8; ftp://greengenes.microbio.me/greengenes_release/gg_13_8_otus, accessed on 22 February 2021), with a 0.5 identity threshold. Alpha-diversity was computed using the Chao1, the number of OTUs, Shannon diversity, and Faith's Phylogenetic Diversity whole tree (PD whole tree) metrics throughout the QIIME pipeline. Beta-diversity was assessed by weighted and unweighted UniFrac distances [64] and principal coordinates analysis (PCoA).

4.6. Fecal Short-Chain Fatty Acid Quantification

Concentrations of acetate, propionate, iso-butyrate, butyrate, and iso-valerate were assessed according to Bassanini et al. [65]. The measurement of SCFAs was performed by gas chromatography, using a Varian model 3400 CX Gas chromatograph fitted with FID detector, split/splitless injector, and a SPB-1 capillary column (30 m \times 0.32 mm ID, 0.25 μ m film thickness; Supelco, Bellefonte, PA, USA). Calibration curves of SCFAs in concentration between 0.25 and 10 mM were constructed to obtain SCFAs quantification, and 10 mM 2-ethylbutyric acid was used as an internal standard. Results are expressed as mg/g of dry weight of feces.

4.7. *Drosophila Melanogaster* Stocks and HDACi Feeding

The following fly strains were used in this study: *Drosophila yw* strain used as control and $w[*] P\{w[+mC]=lacW\}nej[P]/FM7c$ known as *nejire* (*nejP/+*) mutant strain (#3728; Bloomington *Drosophila* Stock Center, Bloomington, IN, USA). *nejP* contains a P-element 347bp upstream of the second exon of *nej* gene and behaves as a loss of function mutant [27]. Flies were maintained and raised into vials containing a standard food medium composed of yeast, cornmeal, molasses, agar, propionic acid, tegosept, and water. All the strains were kept at 25 °C. To prepare food with HDACi, stock solutions of VPA (1 and 2.5 mM) and NaB (10 and 20 mM) solutions were diluted 1:10 in the food before solidification but under 65 °C to prevent heat damage of the compounds.

4.8. Fly Treatment and Embryo Immunostaining

To identify homozygous animals in sibling crosses, *nej* mutants were balanced over *FM7*, *kr-GAL4 UAS-GFP* chromosome. Adult *nej* mutant flies were life cycle-synchronized and treated with mock, VPA (2.5 mM) or NaB (20 mM) for four days. The drugs were mixed with standard food as described above at room temperature. For egg collection, adult flies were placed in cages for 4 h and then removed. Fertilized eggs were collected after 8h and stained as previously described [66]. Briefly, embryos were collected, dechorionated and fixed with a mixture of 4% paraformaldehyde and heptane. Following washes, embryos were permeabilized and blocked with PBT (PBS containing 0.1% Triton X-100 and 1% BSA) for 3 h. Staining was performed overnight with primary mouse anti-wg 1:50 (4D4, Developmental Studies Hybridoma Bank, Iowa City, IA, USA). Secondary goat anti-mouse-Cy3 (1:500) was used for 2 h. Images were taken with a Nikon AR1 confocal microscope using a 10X objective (Nikon Corporation, Tokyo, Japan).

4.9. Bacterial DNA Extraction and 16S rRNA Gene Sequencing of *Drosophila Melanogaster* Gut Microbiota

For microbiota sequencing, adult fly guts were dissected to avoid environmental contamination. Briefly, flies were anesthetized in ice for 5 min in a Petri dish and transferred, one by one, to the dissection dish and immersed in 50 μ L-drop of cold PBS. First, wings and legs were removed. Surgical forceps were used to gently separate the insect head from the body and exposing the foregut. The abdominal cuticle was then cut and dissected out, and the hindgut pulled outside the abdominal cavity. To completely free the entire gastrointestinal tract, the insect head and Malpighian tubes were removed. Only undamaged organs were further processed. Dissected guts, three per experimental condition, were immediately transferred into vials containing 100 μ L of cold PBS and kept at -80°C until use. A total of 15 *nej* and 15 *yw* flies were processed.

Bacterial DNA was extracted by means of QIAamp DNA Microbiome Kit (Qiagen, Hilden, Germany), designed to achieve enrichment of bacterial DNA from low biomass samples. Briefly, the depletion of host cells was performed by adding lysis buffer and benzonase to samples. Bacterial cell lysis was carried out by bead beating in the TissueLyser LT instrument (Qiagen, Hilden, Germany). Lysates were transferred to QIAamp UCP Mini Columns and processed according to the manufacturer's instructions. DNA was eluted in 30 μ L of the provided buffer. Library preparation and sequencing were performed as described above for human samples on the Illumina platform.

4.10. Statistical Analysis

Biological cell data were analyzed using Prism software (GraphPad Software, Sand Diego, CA, USA) and expressed as mean \pm Standard Deviation (SD). Student's t-tests were used to compare means between groups in AlphaLISA, Ki67, and TUNEL assays (LCLs acetylation, proliferation, and death rate), and in phenotypic evaluation (*Drosophila* embryo survival), with $p < 0.05$ considered significant (* $p < 0.05$; ** $p < 0.01$; *** $p < 0.001$ for graphics relative to in vitro model); the correlation between HDACi-induced acetylation and proliferative or apoptotic cells was calculated using Pearson correlation coefficient ($-1 < r < 1$) and Pearson correlation p -value, significant for $p < 0.05$.

For microbiota analysis, statistical evaluation among alpha-diversity indices was performed by a non-parametric Monte Carlo-based test, using 9999 random permutations. The PERMANOVA test (adonis function) in the R package vegan (version 2.0-10) was used to compare the microbial community structure of RSTS and HD subjects within the beta-diversity analysis. For evaluating differences in taxonomic relative abundances, the pairwise t-test from the package "rstatix" (version 0.6.0) in the RStudio software (version 1.2.1335; R version 3.6.3) was used. p -values < 0.05 were considered significant for each analysis.

Supplementary Materials: The following are available online at <https://www.mdpi.com/article/10.3390/ijms22073621/s1>, Figure S1: Insight on single-RSTS LCLs histone acetylation, Figure S2: HDAC inhibitors cytotoxicity analysis on RSTS LCLs, Figure S3: Insights on cell proliferation and cell death rate of RSTS LCLs upon HDAC inhibitors exposure, Figure S4: Correlation between HDACi-induced acetylation versus cell proliferation and apoptosis in RSTS LCLs, Figure S5: Gut microbiota composition in HD and RSTS subjects, Figure S6: Normal and altered phenotypes of *nej* mutant embryos from stage 8 to 12 treated or not with HDACi, Table S1: RSTS LCLs used for in vitro treatments, Table S2: Conditions of in vitro treatments used on LCLs, Table S3: Nutritional values of the enrolled patients, Table S4: Gut microbiota composition in HD and RSTS subjects.

Author Contributions: V.M., E.B. and C.G. conceived the project; E.D.F., E.O., P.G., A.G., C.P. and G.F. performed the experiments; C.C. and M.S. performed bioinformatics analyses; E.A.C. and G.B. contributed to molecular analyses; D.M. contributed to patient recruitment and clinical assessment; T.V. provided flies, reagents, animals, and design of in vivo experiments; E.D.F., E.O., V.M., E.B. and C.G. performed data analysis and interpretation; E.D.F., E.O., V.M., E.B. and C.G. wrote the manuscript; E.V., D.M. and T.V. provided guidance in the manuscript revision. All authors have read and agreed to the published version of the manuscript.

Funding: This work was supported by Fondazione Cariplo (2015-0783 to V.M.), by intramural funding (Università degli Studi di Milano linea 2 to C.G.), by Associazione “RTS Una Vita Speciale ONLUS” (#DigiRare to C.G.), by grant “Aldo Ravelli Center” (to V.M. and C.G.); by Translational Medicine PhD-Università degli Studi di Milano scholarship (to E.D.F. and C.P.); by Molecular and Translational Medicine PhD-Università degli Studi di Milano scholarship (to E.O., C.C. and P.G.), by H2020 Marie Skłodowska-Curie Actions (H2020-MSCA individual fellowship #844147) (to A.G.).

Institutional Review Board Statement: The study was conducted according to the guidelines of the Declaration of Helsinki and its later amendments. The use of lymphoblastoid cell lines was approved by Ethics Committee of Università degli Studi di Milano (Comitato Etico number 99/20). The study on gut microbiota profiling of the enrolled subjects was approved by Ethics Committee of San Paolo Hospital in Milan (Comitato Etico Milano Area 1, Protocol number 2019/EM/076).

Informed Consent Statement: Informed consent was obtained from all subjects involved in the study or their caregivers.

Data Availability Statement: Sequencing data of 16S rRNA amplicons have been deposited in NCBI Short-Read Archive (SRA) under accession number PRJNA616211 (<http://www.ncbi.nlm.nih.gov/bioproject/PRJNA616211>, accessed on 22 February 2021).

Acknowledgments: We thank the patients’ families for participating in this study. C.G. thanks the Italian Association of Rubinstein–Taybi patients “RTS Una Vita Speciale ONLUS” for its support. This work belongs to the ERN ITHACA network (DM). Microscopy observations were carried out at The Advanced Microscopy Facility Platform-UNitech NOLIMITS-University of Milan. All authors acknowledged support from the University of Milan through the APC initiative.

Conflicts of Interest: The authors declare no conflict of interest.

References

1. Atlasi, Y.; Stunnenberg, H.G. The interplay of epigenetic marks during stem cell differentiation and development. *Nat. Rev. Genet.* **2017**, *18*, 643–658. [[CrossRef](#)] [[PubMed](#)]
2. Xu, Q.; Xie, W. Epigenome in Early Mammalian Development: Inheritance, Reprogramming and Establishment. *Trends Cell Biol.* **2018**, *28*, 237–253. [[CrossRef](#)] [[PubMed](#)]
3. Grunstein, M. Histone acetylation in chromatin structure and transcription. *Nature* **1997**, *389*, 349–352. [[CrossRef](#)]
4. Uchida, S.; Shumyatsky, G.P. Epigenetic regulation of Fgf1 transcription by CRTCL1 and memory enhancement. *Brain Res. Bull.* **2018**, *141*, 3–12. [[CrossRef](#)]
5. Bjornsson, H.T. The Mendelian disorders of the epigenetic machinery. *Genome Res.* **2015**, *25*, 1473–1481. [[CrossRef](#)] [[PubMed](#)]
6. Rubinstein, J.H.; Taybi, H. Broad thumbs and toes and facial abnormalities. A possible mental retardation syndrome. *Am. J. Dis. Child.* **1963**, *105*, 588–608. [[CrossRef](#)] [[PubMed](#)]
7. Hennekam, R.C.M. Rubinstein–Taybi syndrome. *Eur. J. Hum. Genet.* **2006**, *14*, 981–985. [[CrossRef](#)]
8. Milani, D.; Manzoni, F.; Pezzani, L.; Ajmone, P.; Gervasini, C.; Menni, F.; Esposito, S. Rubinstein-Taybi syndrome: Clinical features, genetic basis, diagnosis, and management. *Ital. J. Pediatr.* **2015**, *41*, 4. [[CrossRef](#)]
9. Fergelot, P.; Van Belzen, M.; Van Gils, J.; Afenjar, A.; Armour, C.M.; Arveiler, B.; Beets, L.; Burglen, L.; Busa, T.; Collet, M.; et al. Phenotype and genotype in 52 patients with Rubinstein–Taybi syndrome caused by EP300 mutations. *Am. J. Med. Genet. Part A* **2016**, *170*, 3069–3082. [[CrossRef](#)]
10. Miller, R.W.; Rubinstein, J.H. Tumors in Rubinstein-Taybi syndrome. *Am. J. Med. Genet.* **1995**, *56*, 112–115. [[CrossRef](#)]
11. Boot, M.V.; van Belzen, M.J.; Overbeek, L.I.; Hijmering, N.; Mendeville, M.; Waisfisz, Q.; Wesseling, P.; Hennekam, R.C.; de Jong, D. Benign and malignant tumors in Rubinstein-Taybi syndrome. *Am. J. Med. Genet. Part A* **2018**, *176*, 597–608. [[CrossRef](#)]
12. Valor, L.M.; Viosca, J.; Lopez-Atalaya, J.P.; Barco, A. Lysine acetyltransferases CBP and p300 as therapeutic targets in cognitive and neurodegenerative disorders. *Curr. Pharm. Des.* **2013**, *19*, 5051–5064. [[CrossRef](#)] [[PubMed](#)]
13. Yao, T.P.; Oh, S.P.; Fuchs, M.; Zhou, N.D.; Ch’ng, L.E.; Newsome, D.; Bronson, R.T.; Li, E.; Livingston, D.M.; Eckner, R. Gene dosage-dependent embryonic development and proliferation defects in mice lacking the transcriptional integrator p300. *Cell* **1998**, *93*, 361–372. [[CrossRef](#)]
14. Oike, Y.; Hata, A.; Mamiya, T.; Kaname, T.; Noda, Y.; Suzuki, M.; Yasue, H.; Nabeshima, T.; Araki, K.; Yamamura, K. Truncated CBP protein leads to classical Rubinstein-Taybi syndrome phenotypes in mice: Implications for a dominant-negative mechanism. *Hum. Mol. Genet.* **1999**, *8*, 387–396. [[CrossRef](#)] [[PubMed](#)]
15. Chan, H.M.; La Thangue, N.B. p300/CBP proteins: HATs for transcriptional bridges and scaffolds. *J. Cell Sci.* **2001**, *114*, 2363–2373.
16. Dutto, I.; Scalera, C.; Prosperi, E. CREBBP and p300 lysine acetyl transferases in the DNA damage response. *Cell. Mol. Life Sci.* **2018**, *75*, 1325–1338. [[CrossRef](#)] [[PubMed](#)]

17. Weinert, B.T.; Narita, T.; Satpathy, S.; Srinivasan, B.; Hansen, B.K.; Schölz, C.; Hamilton, W.B.; Zucconi, B.E.; Wang, W.W.; Liu, W.R.; et al. Time-Resolved Analysis Reveals Rapid Dynamics and Broad Scope of the CBP/p300 Acetylome. *Cell* **2018**, *174*, 231–244.e12. [CrossRef]
18. Kazantsev, A.G.; Thompson, L.M. Therapeutic application of histone deacetylase inhibitors for central nervous system disorders. *Nat. Rev. Drug Discov.* **2008**, *7*, 854–868. [CrossRef] [PubMed]
19. Heerboth, S.; Lapinska, K.; Snyder, N.; Leary, M.; Rollinson, S.; Sarkar, S. Use of epigenetic drugs in disease: An overview. *Genet. Epigenet.* **2014**, *6*, 9–19. [CrossRef] [PubMed]
20. Lopez-Atalaya, J.P.; Gervasini, C.; Mottadelli, F.; Spena, S.; Piccione, M.; Scarano, G.; Selicorni, A.; Barco, A.; Larizza, L. Histone acetylation deficits in lymphoblastoid cell lines from patients with Rubinstein-Taybi syndrome. *J. Med. Genet.* **2012**, *49*, 66–74. [CrossRef]
21. Alarcón, J.M.; Malleret, G.; Touzani, K.; Vronskaya, S.; Ishii, S.; Kandel, E.R.; Barco, A. Chromatin Acetylation, Memory, and LTP Are Impaired in CBP+/- Mice. *Neuron* **2004**, *42*, 947–959. [CrossRef]
22. Simon, G.M.; Cheng, J.; Gordon, J.I. Quantitative assessment of the impact of the gut microbiota on lysine epsilon-acetylation of host proteins using gnotobiotic mice. *Proc. Natl. Acad. Sci. USA* **2012**, *109*, 11133–11138. [CrossRef]
23. Stilling, R.M.; van de Wouw, M.; Clarke, G.; Stanton, C.; Dinan, T.G.; Cryan, J.F. The neuropharmacology of butyrate: The bread and butter of the microbiota-gut-brain axis? *Neurochem. Int.* **2016**, *99*, 110–132. [CrossRef] [PubMed]
24. Astbury, S.M.; Corfe, B.M. Uptake and metabolism of the short-chain fatty acid butyrate, a critical review of the literature. *Curr. Drug Metab.* **2012**, *13*, 815–821. [CrossRef] [PubMed]
25. Eckschlager, T.; Plch, J.; Stiborova, M.; Hrabeta, J. Histone deacetylase inhibitors as anticancer drugs. *Int. J. Mol. Sci.* **2017**, *18*, 1414. [CrossRef] [PubMed]
26. Italian Society of Human Nutrition Nutrients and Energy Reference Intake Levels for Italian Population. Available online: <https://sinu.it/tabelle-larn-2014/> (accessed on 18 February 2021).
27. Akimaru, H.; Chen, Y.; Dai, P.; Hou, D.-X.; Nonaka, M.; Smolik, S.M.; Armstrong, S.; Goodman, R.H.; Ishii, S. Drosophila CBP is a co-activator of cubitus interruptus in hedgehog signalling. *Nature* **1997**, *386*, 735–738. [CrossRef] [PubMed]
28. Akimaru, H.; Hou, D.-X.; Ishii, S. Drosophila CBP is required for dorsal-dependent twist gene expression. *Nat. Genet.* **1997**, *17*, 211–214. [CrossRef] [PubMed]
29. Cobos, S.N.; Bennett, S.A.; Torrente, M.P. The impact of histone post-translational modifications in neurodegenerative diseases. *Biochim. Biophys. Acta Mol. Basis Dis.* **2019**, *1865*, 1982–1991. [CrossRef] [PubMed]
30. José-Enériz, E.S.; Gimenez-Camino, N.; Agirre, X.; Prosper, F. HDAC inhibitors in acute myeloid leukemia. *Cancers* **2019**, *11*, 1794. [CrossRef]
31. Spartalis, E.; Athanasiadis, D.I.; Chrysikos, D.; Spartalis, M.; Boutzios, G.; Schizas, D.; Garmpis, N.; Damaskos, C.; Paschou, S.A.; Ioannidis, A.; et al. Histone deacetylase inhibitors and anaplastic thyroid carcinoma. *Anticancer Res.* **2019**, *39*, 1119–1127. [CrossRef]
32. Tarnowski, M.; Tkacz, M.; Kopytko, P.; Bujak, J.; Piotrowska, K.; Pawlik, A. Trichostatin A Inhibits Rhabdomyosarcoma Proliferation and Induces Differentiation through MyomiR Reactivation. *Folia Biol.* **2019**, *65*, 43–52.
33. Lipska, K.; Gumieniczek, A.; Filip, A.A. Anticonvulsant valproic acid and other short-chain fatty acids as novel anticancer therapeutics: Possibilities and challenges. *Acta Pharm.* **2020**, *70*, 291–301. [CrossRef] [PubMed]
34. Yuan, X.G.; Huang, Y.R.; Yu, T.; Jiang, H.W.; Xu, Y.; Zhao, X.Y. Chidamide, a histone deacetylase inhibitor, induces growth arrest and apoptosis in multiple myeloma cells in a caspase-dependent manner. *Oncol. Lett.* **2019**, *18*, 411–419. [CrossRef] [PubMed]
35. Iannitti, T.; Palmieri, B. Clinical and experimental applications of sodium phenylbutyrate. *Drugs R D* **2011**, *11*, 227–249. [CrossRef]
36. Cappellacci, L.; Perinelli, D.R.; Maggi, F.; Grifantini, M.; Petrelli, R. Recent Progress in Histone Deacetylase Inhibitors as Anticancer Agents. *Curr. Med. Chem.* **2018**, *27*, 2449–2493. [CrossRef] [PubMed]
37. Davie, J.R. Inhibition of Histone Deacetylase Activity by Butyrate. *J. Nutr.* **2003**, *133*, 2485S–2493S. [CrossRef]
38. Louis, P.; Flint, H.J. Diversity, metabolism and microbial ecology of butyrate-producing bacteria from the human large intestine. *FEMS Microbiol. Lett.* **2009**, *294*, 1–8. [CrossRef]
39. Borghi, E.; Vignoli, A. Rett syndrome and other neurodevelopmental disorders share common changes in gut microbial community: A descriptive review. *Int. J. Mol. Sci.* **2019**, *20*, 4160. [CrossRef] [PubMed]
40. Lindefeldt, M.; Eng, A.; Darban, H.; Bjerkner, A.; Zetterström, C.K.; Allander, T.; Andersson, B.; Borenstein, E.; Dahlin, M.; Prast-Nielsen, S. The ketogenic diet influences taxonomic and functional composition of the gut microbiota in children with severe epilepsy. *Npj Biofilms Microbiomes* **2019**, *5*, 5. [CrossRef] [PubMed]
41. Benjamin, J.S.; Pilarowski, G.O.; Carosso, G.A.; Zhang, L.; Huso, D.L.; Goff, L.A.; Vernon, H.J.; Hansen, K.D.; Bjornsson, H.T. A ketogenic diet rescues hippocampal memory defects in a mouse model of Kabuki syndrome. *Proc. Natl. Acad. Sci. USA* **2017**, *114*, 125–130. [CrossRef] [PubMed]
42. Heijtz, R.D.; Wang, S.; Anuar, F.; Qian, Y.; Björkholm, B.; Samuelsson, A.; Hibberd, M.L.; Forsberg, H.; Pettersson, S. Normal gut microbiota modulates brain development and behavior. *Proc. Natl. Acad. Sci. USA* **2011**, *108*, 3047–3052. [CrossRef] [PubMed]
43. Bach Knudsen, K.E.; Lærke, H.N.; Hedemann, M.S.; Nielsen, T.S.; Ingerslev, A.K.; Gundelund Nielsen, D.S.; Theil, P.K.; Purup, S.; Hald, S.; Schioldan, A.G.; et al. Impact of Diet-Modulated Butyrate Production on Intestinal Barrier Function and Inflammation. *Nutrients* **2018**, *10*, 1499. [CrossRef]

44. Tanaka, Y.; Naruse, I.; Maekawa, T.; Masuya, H.; Shiroishi, T.; Ishii, S. Abnormal skeletal patterning in embryos lacking a single Cbp allele: A partial similarity with Rubinstein-Taybi syndrome. *Proc. Natl. Acad. Sci. USA* **1997**, *94*, 10215–10220. [[CrossRef](#)] [[PubMed](#)]
45. Matzkin, L.M.; Johnson, S.; Paight, C.; Markow, T.A. Preadult Parental Diet Affects Offspring Development and Metabolism in *Drosophila melanogaster*. *PLoS ONE* **2013**, *8*, e59530. [[CrossRef](#)]
46. Capo, F.; Wilson, A.; Di Cara, F. The intestine of *Drosophila melanogaster*: An emerging versatile model system to study intestinal epithelial homeostasis and host-microbial interactions in humans. *Microorganisms* **2019**, *7*, 336. [[CrossRef](#)] [[PubMed](#)]
47. Fast, D.; Duggal, A.; Foley, E. Monoassociation with *Lactobacillus plantarum* Disrupts Intestinal Homeostasis in Adult *Drosophila melanogaster*. *mBio* **2018**, *9*, e01114–e01118. [[CrossRef](#)]
48. Shin, S.C.; Kim, S.-H.; You, H.; Kim, B.; Kim, A.C.; Lee, K.-A.; Yoon, J.-H.; Ryu, J.-H.; Lee, W.-J. *Drosophila* microbiome modulates host developmental and metabolic homeostasis via insulin signaling. *Science* **2011**, *334*, 670–674. [[CrossRef](#)]
49. Sharon, G.; Segal, D.; Ringo, J.M.; Hefetz, A.; Zilber-Rosenberg, I.; Rosenberg, E. Commensal bacteria play a role in mating preference of *Drosophila melanogaster*. *Proc. Natl. Acad. Sci. USA* **2010**, *107*, 20051–20056. [[CrossRef](#)] [[PubMed](#)]
50. Babu, A.; Kamaraj, M.; Basu, M.; Mukherjee, D.; Kapoor, S.; Ranjan, S.; Swamy, M.M.; Kaypee, S.; Scaria, V.; Kundu, T.K.; et al. Chemical and genetic rescue of an ep300 knockdown model for Rubinstein Taybi Syndrome in zebrafish. *Biochim. Biophys. Acta Mol. Basis Dis.* **2018**, *1864*, 1203–1215. [[CrossRef](#)]
51. Spena, S.; Milani, D.; Rusconi, D.; Negri, G.; Colapietro, P.; Elcioglu, N.; Bedeschi, F.; Pilotta, A.; Spaccini, L.; Ficcidenti, A.; et al. Insights into genotype-phenotype correlations from CREBBP point mutation screening in a cohort of 46 Rubinstein-Taybi syndrome patients. *Clin. Genet.* **2015**, *88*, 431–440. [[CrossRef](#)]
52. Negri, G.; Milani, D.; Colapietro, P.; Forzano, F.; Della Monica, M.; Rusconi, D.; Consonni, L.; Caffi, L.G.; Finelli, P.; Scarano, G.; et al. Clinical and molecular characterization of Rubinstein-Taybi syndrome patients carrying distinct novel mutations of the EP300 gene. *Clin. Genet.* **2015**, *87*, 148–154. [[CrossRef](#)] [[PubMed](#)]
53. Negri, G.; Magini, P.; Milani, D.; Colapietro, P.; Rusconi, D.; Scarano, E.; Bonati, M.T.; Priolo, M.; Crippa, M.; Mazzanti, L.; et al. From Whole Gene Deletion to Point Mutations of EP300-Positive Rubinstein-Taybi Patients: New Insights into the Mutational Spectrum and Peculiar Clinical Hallmarks. *Hum. Mutat.* **2016**, *37*, 175–183. [[CrossRef](#)] [[PubMed](#)]
54. Schölz, C.; Weinert, B.T.; Wagner, S.A.; Beli, P.; Miyake, Y.; Qi, J.; Jensen, L.J.; Streicher, W.; McCarthy, A.R.; Westwood, N.J.; et al. Acetylation site specificities of lysine deacetylase inhibitors in human cells. *Nat. Biotechnol.* **2015**, *33*, 415–423. [[CrossRef](#)]
55. Chang, M.C.; Chen, Y.J.; Lian, Y.C.; Chang, B.E.; Huang, C.C.; Huang, W.L.; Pan, Y.H.; Jeng, J.H. Butyrate stimulates histone H3 acetylation, 8-isoprostane production, RANKL expression, and regulated osteoprotegerin expression/secretion in MG-63 osteoblastic cells. *Int. J. Mol. Sci.* **2018**, *19*, 4071. [[CrossRef](#)] [[PubMed](#)]
56. Freese, K.; Seitz, T.; Dietrich, P.; Lee, S.M.L.; Thasler, W.E.; Bosserhoff, A.; Hellerbrand, C. Histone deacetylase expressions in hepatocellular carcinoma and functional effects of histone deacetylase inhibitors on liver cancer cells in vitro. *Cancers* **2019**, *11*, 1587. [[CrossRef](#)]
57. Tarasenko, N.; Chekroun-Setti, H.; Nudelman, A.; Rephaeli, A. Comparison of the anticancer properties of a novel valproic acid prodrug to leading histone deacetylase inhibitors. *J. Cell. Biochem.* **2018**, *119*, 3417–3428. [[CrossRef](#)]
58. Gottlicher, M.; Minucci, S.; Zhu, P.; Krämer, O.H.; Schimpf, A.; Giavara, S.; Sleeman, J.P.; Lo Coco, F.; Nervi, C.; Pelicci, P.G.; et al. Valproic acid defines a novel class of HDAC inhibitors inducing differentiation of transformed cells. *PubMed NCBI EMBO J.* **2001**, *20*, 6969–6978. [[CrossRef](#)]
59. Chriett, S.; Dąbek, A.; Wojtala, M.; Vidal, H.; Balcerczyk, A.; Pirola, L. Prominent action of butyrate over β -hydroxybutyrate as histone deacetylase inhibitor, transcriptional modulator and anti-inflammatory molecule. *Sci. Rep.* **2019**, *9*, 742. [[CrossRef](#)] [[PubMed](#)]
60. Verduci, E.; Moretti, F.; Bassanini, G.; Banderali, G.; Rovelli, V.; Casiraghi, M.C.; Morace, G.; Borgo, F.; Borghi, E. Phenylketonuric diet negatively impacts on butyrate production. *Nutr. Metab. Cardiovasc. Dis.* **2018**, *28*, 385–392. [[CrossRef](#)] [[PubMed](#)]
61. Masella, A.P.; Bartram, A.K.; Truskowski, J.M.; Brown, D.G.; Neufeld, J.D. PANDAsseq: Paired-end assembler for illumina sequences. *BMC Bioinf.* **2012**, *13*, 31. [[CrossRef](#)] [[PubMed](#)]
62. Caporaso, J.G.; Kuczynski, J.; Stombaugh, J.; Bittinger, K.; Bushman, F.D.; Costello, E.K.; Fierer, N.; Pêa, A.G.; Goodrich, J.K.; Gordon, J.I.; et al. QIIME allows analysis of high-throughput community sequencing data. *Nat. Methods* **2010**, *7*, 335–336. [[CrossRef](#)] [[PubMed](#)]
63. Wang, Q.; Garrity, G.M.; Tiedje, J.M.; Cole, J.R. Naïve Bayesian classifier for rapid assignment of rRNA sequences into the new bacterial taxonomy. *Appl. Environ. Microbiol.* **2007**, *73*, 5261–5267. [[CrossRef](#)]
64. Lozupone, C.; Lladser, M.E.; Knights, D.; Stombaugh, J.; Knight, R. UniFrac: An effective distance metric for microbial community comparison. *ISME J.* **2011**, *5*, 169–172. [[CrossRef](#)] [[PubMed](#)]
65. Bassanini, G.; Ceccarani, C.; Borgo, F.; Severgnini, M.; Rovelli, V.; Morace, G.; Verduci, E.; Borghi, E. Phenylketonuria Diet Promotes Shifts in Firmicutes Populations. *Front. Cell. Infect. Microbiol.* **2019**, *9*, 101. [[CrossRef](#)] [[PubMed](#)]
66. Ashburner, M. *Drosophila: A Laboratory Handbook*; Cold Spring Harbor Laboratory Press: New York, NY, USA, 1989.

Chapter 2

Neural tube defects: embryonic origin, cell survival equilibrium impact, and clinical features

Chiara Parodi^{1,a}, Paolo Grazioli^{1,a}, Laura Avagliano¹, Timothy M. George², Gaetano P. Bulfamante¹, Richard H. Finnell³ and Valentina Massa¹

¹Department of Health Sciences, University of Milan, Milano, Italy; ²Department of Neurosurgery, The University of Texas Dell Medical School, Austin, TX, United States; ³Center for Precision Environmental Health, Department of Molecular and Cellular Biology and Medicine, Baylor College of Medicine, Houston, TX, United States

List of abbreviations

CM-II Chiari II malformation

CNS Central nervous system

NTDs Neural tube defects

Mini-dictionary of terms

Anencephaly: the absence of a major portion of the brain, skull, and scalp.

Anoikis: form of programmed cell death that happens following loss of cell contact (with neighboring cells or extracellular matrix).

Craniorachischisis: most severe NTD by which the entire spinal cord and brain are exposed to the amniotic environment.

Encephalocele: protrusion of the cranial contents beyond the normal confines of the skull through a defect in the calvarium.

Exencephaly: exposure of the brain outside of the skull.

Iniencephaly: NTD characterized by extreme retroflexion of the head associated with severe spinal distortion.

Meningocele: developmental defect allows the meninges to herniate between the vertebrae while the nervous system remains intact.

Myelomeningocele: birth defect due to impaired closure of the posterior region of the neural tube with a protruding cystic mass through vertebral arches.

Neural tube defect: congenital malformation due to a failure of neurulation.

Primary neurulation: formation of neural tube during the third and fourth gestational week, in humans.

Secondary neurulation: process necessary for the sacral and caudal formation of the spinal cord by cavitation.

Spina bifida occulta: common birth defect characterized by protrusion of the meninges forming a sack covered by skin in which cerebrospinal fluid is present.

Introduction

This chapter aims at describing the most common neural tube defects (NTDs) and their embryonic origins. Such birth defects may result from abnormalities occurring during primary or secondary neurulation in early phases of development. Depending on the type and site of lesion, the defect might lead to devastating neurological consequences, including death.

^a These authors contributed equally to this work.

Main text

Neural tube defects: embryonic origin

Neurulation in mammals

In humans, the development of the central nervous system (CNS) is a long and complicated process that starts very early during pregnancy (Fig. 2.1). Twenty-one days postfertilization the embryo, referred to as neurula, is ready to initiate shaping the CNS. This early process is divided in two consecutive and coordinated steps: *primary* and *secondary* neurulation. Primary neurulation shapes the neural tube of the future brain and majority of the spinal cord, while secondary neurulation determines the formation of the most posterior spinal cord. Primary and secondary neurulation processes are conserved in mammals, although there are some differences in the precise sequence of neural tube closure events (Copp, Greene, & Murdoch, 2003).

Primary and secondary neurulation

The formation of the brain and the spinal cord begins with the development of the neural tube, through the process of embryonic neurulation. The neural plate originates from thickening of the dorsal surface ectoderm that folds and merges into the midline to create the neural tube. In mammals, closure of the neural tube starts sequentially at different levels of the body axis (multisite closure).

Primary neurulation can be divided into four main steps: (a) formation, (b) shaping and (c) bending of the neural plate, (d) closure of the neural tube.

- (a) The formation of the neural tube starts from the ectoderm, one of the three embryonic layers, that upon inductive molecular cues thickens to become the typical pseudostratified epithelium.
- (b) Cells of the neural plate change their shape from cuboidal to columnar.
- (c) Formation of the neural groove; elevation of the lateral walls; formation of dorsolateral hinge points.
- (d) These steps are followed by a remodeling process leading to a closed neural tube covered by the surface ectoderm.

The closure of the primary neural tube is a discontinuous process that starts at different points along the rostrum–caudal axis. The fusion spreads bidirectionally in the brain and back along the spinal region. The fusion progression (“zipping”) proceeds along the spine, culminating in the final closure of the posterior neuropore, at the level of the second sacral segment. This completes the process of primary neurulation (by neural folding) (Copp & Greene, 2010) (Fig. 2.2A–G).

In the posterior part of the growing embryos, the neural tube formation occurs via a different process that is not fully elucidated (Catala, 2002). The most accepted mechanism is through cavitation. Undifferentiated mesenchymal cells change their shape to form a neural epithelium by mesenchymal-to-epithelial transition (Shimokita & Takahashi, 2011) (Fig. 2.2H–N).

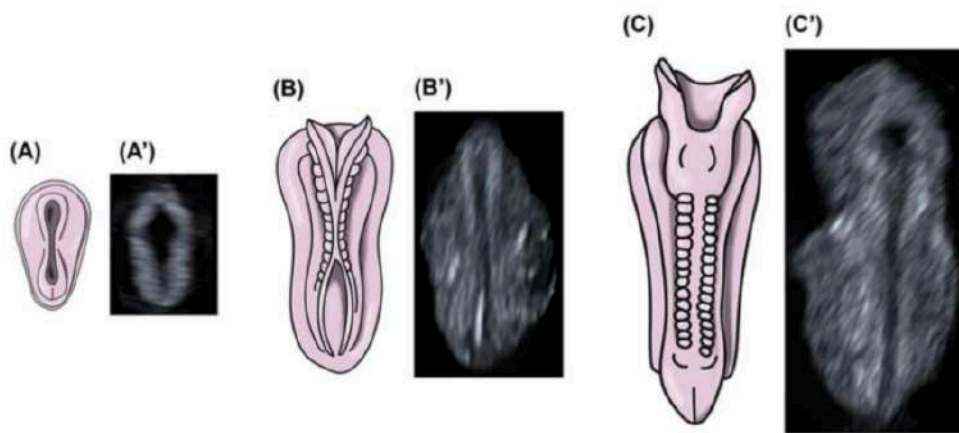


FIGURE 2.1 Development of the human neural tube. Schematic drawings (A–C) and ultrasounds scans (A'–C') of the neural tube formation and closure, from early (third to fourth gestational week) to late (fifth to sixth gestational week) embryonic stages, are shown.

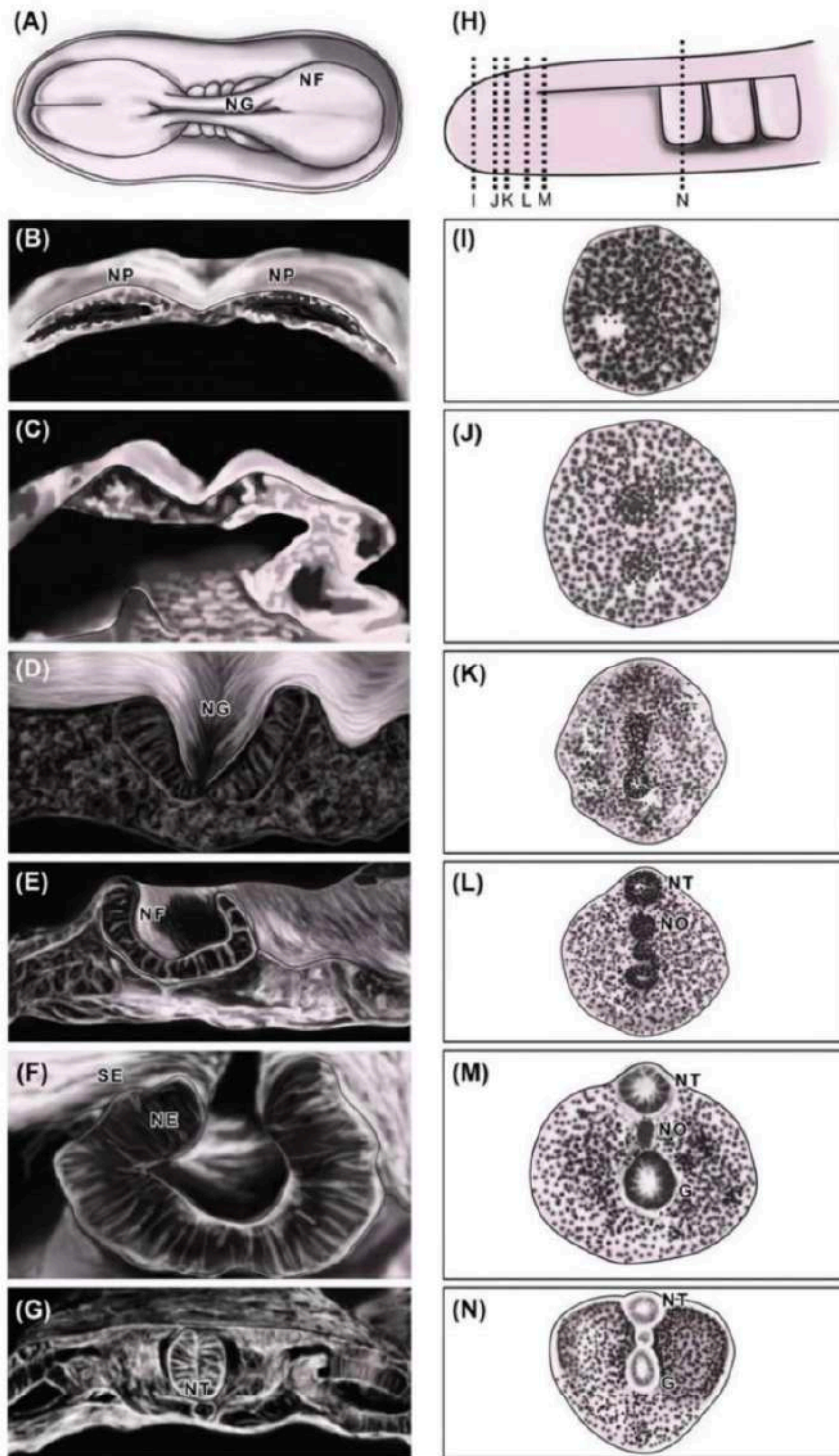


FIGURE 2.2 Schematic representation of primary and secondary neurulation. Schematic drawings of the primary neurulation (A: caudal to the left; B–G: ventral to the bottom) and secondary neurulation (H: caudal to the left; I–N: ventral to the bottom). At the end of the third gestational week, the neural folds form at the lateral extremes of the neural plate (A), elevate (B–D) and converge toward the dorsal midline forming the neural groove (D–F), and fuse at their dorsal tips to form the closed neural tube (G). Secondary neurulation happens by cavitation of a solid mass of cells, the tail bud. A rod-like condensation of mesenchymal cells forms beneath the dorsal ectoderm of the tail bud (I–L), these mesenchymal cells then transform into an epithelium and a lumen develops to form the neural tube (M–N). (*G*, gut; *NE*, neuroepithelium; *NF*, neural fold; *NG*, neural groove; *NO*, notochord; *NP*, neural plate; *NT*, neural tube; *SE*, surface ectoderm).

The secondary neurulation, or *canalization*, in which a multipotential cellular population in the caudal eminence differentiates into future neuronal cells, permits the formation of the spinal cord at the lower sacral and caudal level. Therefore, the formation of a sacred caudal lumen occurs, which will eventually join with the newly established primary lumen.

Neural tube defects: cell survival equilibrium impact

During the primary neurulation process, the embryo grows rapidly, and cells proliferate and differentiate in a highly dynamic way. One of the processes that has been observed during neurulation process and neural tube closure in several experimental models involves programmed cell death (Nikolopoulou, Galea, Rolo, Greene, & Copp, 2017) (Fig. 2.3A–C). This morphogenetic process is known to occur during several embryonic milestones (i.e., cell removal in the developing interdigital region in mammals) (Suzanne & Steller, 2013), and it is known to be of fundamental importance during nervous system development during the later stages of embryonic development (Yamaguchi & Miura, 2015).

Such cell death is thought to be a peculiar type: “anoikis” (Greek for homelessness). For both surviving and proliferating, cells require a continuous cross talk with the extracellular matrix (ECM) or neighboring cells. During the highly dynamic process of neurulation, some cells become “homeless,” associated with marked changes in shape and loss of contact and association with ECM components. During the elevation and folding of the neuroepithelium, some cells at the fold tips will alter their contacts with the adjacent cells and/or with ECM (Gilmore, 2005) (Fig. 2.3D–E).

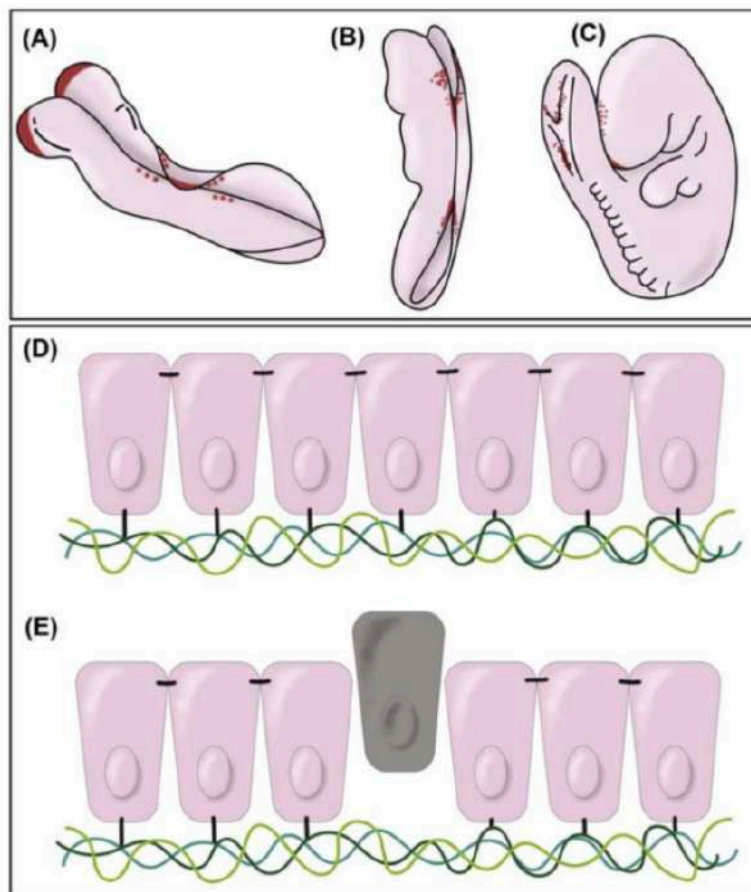


FIGURE 2.3 Cell death during neurulation. Schematic drawings of the cells undergoing death in mouse embryo (A: E8.5; B: E9.0 C: E9.5). In red are shown the main sites of apoptosis during neural tube formation. Schematic drawings of the anoikis process in the neuroepithelium (D–E). The neuroepithelium is composed of a pseudostratified layer of epithelial cells with basal nuclei, in which cells are in contact with surrounding cells laterally and with the extracellular matrix on basal surfaces through junctional complexes (D). When a cell loses contact with the extracellular matrix and/or the neighbor cells, *anoikis* happens. This event happens during the dynamic process of neurulation, and it is due to the cellular reorganization that helps the fusion process during the closure of neural tube. (E, embryonic day).

In this context, an important cross talk occurs between integrins and their receptors. Integrins regulate signaling pathways that control apoptosis in growth-factor-mediated survival, DNA damage responses, and death-receptor-mediated apoptosis (Boudreau, Sympton, Werb, & Bissell, 1995; Hynes, 2002; Pullan et al., 1996). The role of integrin receptor signaling in cell survival has been demonstrated through a number of experimental evidences (Salmela et al., 2017), as well as the ECM–cytoskeleton intimate relationship in this frame (Chen, Mrksich, Huang, Whitesides, & Ingber, 1997).

Moreover, it is undoubted that embryonic tissue fusion events, including proper neural tube closure, are associated with abundant apoptosis. However, it has been shown that this is not an essential step for the completion of the process, but more likely a secondary step due to the cellular reorganization that helps the fusion process during the closure of neural tube (Massa, Savery, et al., 2009) and/or as a consequence of excessive cells, the removal of which is a necessary embryonic event, for guaranteeing the success of a fundamental embryonic step as the formation of CNS primordium (Massa, Greene, & Copp, 2009).

Neural tube defects: clinical features

Failure of primary neurulation leads to NTDs, which are common congenital anomalies in humans. Despite the growing understanding of many molecular and cellular events through the use of different experimental models (Butler & Wallingford, 2017; Colas & Schoenwolf, 2001; Greene & Copp, 2014; Wallingford, Niswander, Shaw, & Finnell, 2013), the elucidation of the etiopathogenesis of NTDs is yet to be defined.

A strict classification of human NTDs is still lacking consensus, especially with regard to clinical effects and embryonic origin. However, NTDs can be divided in two main subgroups: open, whereby neural tissue is directly exposed to the environment, and closed, in which neural tissue is covered.

Epidemiology

NTDs are the second most common congenital malformation (Committee on Practice Bulletins-Obstetrics, 2017). While their prevalence is believed to be underestimated because of terminations of pregnancy and spontaneous abortions, the incidence of new cases has greatly decreased following antenatal folic acid maternal supplementation (Kondo et al., 2017).

The prevalence of NTDs varies considerably among different geographic areas: in the United States and in many European countries, it is estimated between 0.5 and 0.8/1000 births (Castilla, Botto, & Bakker, 2011), while in China it is estimated 20 times higher (Li et al., 2006). Further, areas with higher prevalence of NTDs show higher frequencies of rarer subtypes such as craniorachischisis and iniencephaly (Copp et al., 2015; Moore et al., 1997). Globally, it is estimated that approximately 300,000 babies are born each year with NTDs worldwide (Zaganjor et al., 2016).

There is also evidence that in twins, the concordance for NTDs is higher between same-sex twin pairs than with twins of the opposite sex (Copp & Greene, 2013). In addition, in humans, anencephaly affects females more often than males, suggesting either a genetic relationship or a sex-related epigenetic impact. Conversely, less than 10% of NTDs cases are syndromic (Juriloff & Harris, 2012; Rampersaud et al., 2005; Wen et al., 2010).

Worldwide differences in prevalence may be related to the complexity of the pathogenesis of NTDs. In fact, NTDs are an archetype of complex birth defects caused by gene–environment interactions (Wallingford et al., 2013). In support of this causative interaction, several distinct lines of evidence have been reported in the literature. For example, the prevalence varies among different countries. Such variation persists when considering different ethnic groups independently of countries of origin supporting a greater impact of genetics compared to the environment (Leck, 1974; Shaw, Velie, & Wasserman, 1997). Despite numerous genetic studies, a single causative gene that can explain the population burden for NTDs has not been found. Several studies have reported an increased risk of NTD outcome in association with select gene variants (Ross, Mason, & Finnell, 2017). Among them, an association has been identified between the presence of mutations in *VANGL1* (MIM # 610132) and the appearance of NTDs. These mutations affect highly conserved residues in the Vangl family (Kibar et al., 2007; Lei et al., 2010). However, mutations in *VANGL1* have only been found in a small proportion of patients with NTDs. This could be due to several factors, for example, *VANGL1* mutations in NTDs could be present in noncoding regulatory regions or DNA methylation changes in *VANGL1* could be associated with NTDs. This methylation hypothesis is particularly interesting and suggests how folic acid protects against NTDs by stimulating cell methylation reactions (Blom, Shaw, den Heijer, & Finnell, 2006).

Accordingly, most of the sporadic cases seem to be related to a deficiency of folate (Blom et al., 2006). Folate deficiency may be secondary to a reduced intestinal intake or malabsorption or consumption of drugs that interfere with its metabolism, known as folic acid antagonists (Hernández-Díaz, Werler, Walker, & Mitchell, 2000; Robert & Guibaud, 1982). Some studies have shown that the maintenance of homeostasis of folate plays a role for many cellular reactions,

including the biosynthesis of purines (for the synthesis of DNA and RNA) and the production of methyl donor S-adenosyl-methionine, which is essential in methylation processes. Folate could therefore play a role in the methylation of important cytoskeletal proteins and ciliogenesis necessary for proper neural tube closure (Toriyama, Toriyama, Wallingford, & Finnell, 2017). A robust maternal folate status is not sufficient to prevent all NTD cases. Recently another related compound, inositol (Vitamin B8), has been suggested as a possible player in the supplementation studies (Greene et al., 2016; Greene, Leung, & Copp, 2017). It is interesting to note that both folic acid and inositol, despite molecularly acting at different levels (i.e., one-carbon metabolism and intracellular kinases cascade), are known to be pivotal in cell cycle regulation promoting and supporting cell proliferation (Kibar et al., 2007; Noventa et al., 2016; Wong et al., 2008), hence participating in the finely tuned cell survival equilibrium during development.

NTDs are commonly subdivided into open and closed defects. Craniorachischisis, exencephaly–anencephaly, and myelomeningoceles are considered to be open and are characterized by exposure of neural tissue. Closed defects are encephalocele, meningocele, and spina bifida occulta, which present an epithelium covering the neural tissue. Open NTDs are clinically more severe than closed ones (Copp & Greene, 2013; McComb, 2015). NTDs incidence/prevalence, clinical outcome and management are summarized in Table 2.1.

Open NTDs

Exencephaly/anencephaly

When the main defect implies a failure of the cranial neural tube closure, the defect is named exencephaly (compare Fig. 2.4B–A and D–C). Upon degeneration of the brain-neural tissues, due to destructive exposure of the brain to the intraamniotic environment, the exencephaly becomes an anencephaly.

The bones of the face appear structurally normal, although the eyes often seem to protrude due to the superficiality of the orbits and the forehead is absent or shortened.

Some cerebral remnants are present, called cerebrovasculosa area appearing as a dark brown undifferentiated mass (Anand, Javia, & Lakhani, 2015). Residual brain tissue appears as an irregular mass containing vascular tissue, islands of nervous tissue including interspersed glial cells, nerve cells, and cavities surrounded by the epithelium. Despite a severe abnormality of the rostral neural tube, the spinal cord in anencephalic fetuses appears to be structurally normal (Golden & Harding, 2004).

Anencephaly is a lethal condition (Fig. 2.4E). Detection of anencephaly during early gestation is generally followed by legal termination of the pregnancy. In those cases of pregnancies that come to term, most anencephalic newborns die in the first day or two postpartum (The Medical Task Force of Anencephaly, 1990).

It is estimated that approximately three out of 10,000 pregnancies in the United States will present with anencephaly every year. This means that approximately 1206 pregnancies are affected by these conditions every year in the United States (Williams et al., 2015).

Prenatal diagnosis is mainly based on the absence of a normal cranial format and the brain above the orbital line. The cerebrovascular area can be detected as fluctuating echogenic tissue. The differential diagnosis between anencephaly and other causes of an absence of the cranial vault is very important for family counseling, as the presence of anencephaly increases the risk of the onset of other NTDs in any subsequent pregnancy (Goldstein & Filly, 1988; Keeling & Kjaer, 1994). Nowadays, the approaches used for NTD screening are: biochemical tests of maternal blood for alpha-fetoprotein or the use of traditional 2D ultrasounds. Some screening programs combine the two techniques. The development of more sophisticated imaging techniques (for example, 3D ultrasound) could improve the understanding of the injury allowing a better definition of structural anomalies. This information is vital when informing prospective parents about the likely prognosis for their child (Cameron & Moran, 2009).

Open spina bifida: myelomeningocele/myelocele

The failure to close the posterior regions of the neural tube, or the rupture of the posterior neuropore, leads to the formation of spina bifida. Spina bifida has a greater or lesser severity depending on the site of lesion, with more rostral lesions being more clinically severe.

The developmental defect involves the inability to close the posterior spinal portion of the neural tube, shape and size of the lesion can vary significantly, the lumbar portion is the most frequently observed; a cystic mass that protrudes although a bony defect in the vertebral arches is detectable; this condition is called myelomeningocele. In myelomeningocele, the fetus presents with a cystic meningeal sac that contains cerebrospinal fluid and nervous tissue, including nerve roots and spinal cord (Figs. 2.5A and 2.6B). The histological sections show the protrusion of the marrow through the bone defect of

TABLE 2.1 Features of neural tube defects.

	Type	Incidence/prevalence	Clinical outcome	Clinical management
Open NTDs	Exencephaly/anencephaly	Three every 10,000 pregnancies in the United States (Williams et al., 2015)	Lethal (The Medical Task Force of Anencephaly, 1990)	There are no neurosurgical management options and almost all live children die shortly after birth. Considering this poor prognosis, most pregnancies are interrupted shortly after diagnosis. (Weprin & Oakes, 2000)
	Myelomeningocele/myelocele/open spina bifida (or rachischisis)	1.8 per 10,000 live births in the United States (Zaganjor et al., 2016)	Motor and sensorial deficit below the level of the spinal lesion. Often bladder and rectal incontinence. Hydrocephaly. Intellectual disability is relatively infrequent (20%–25% of cases) and related to hydrocephalus. Deformity of the lower extremities.	<i>In utero</i> surgical repair might be considered for open spina bifida, and this procedure has shown significant benefits for the newborns, leading to a significant improvement in spinal neurological function. (Adzick et al., 2011). In order to prevent infections, swelling, and damage to the spinal cord, an early surgery is often suggested.
	Craniorachischisis	Different geographic distribution prevalence. In northern China, 0.01 per 1000 newborns (Moore et al., 1997) and in a Texas–Mexico border population, the prevalence was 0.51 per 10,000 live births (Johnson et al., 2004).	Lethal	Such defect is not compatible with life. No neurosurgical management options.
Closed NTDs	Encephalocele	One in 12,200 live births in the United States each year (Parker et al., 2010)	Clinical characteristics depend on the site and extent of the lesion. Often cognitive, neurodevelopmental delay and sometimes hydrocephalus.	Encephaloceles always require surgery correction under general anesthetic. The timing of surgery will vary depending on whether the sac is covered with skin or a thin membrane.
	Meningocele	Generally unknown. In one study the incidence of meningocele was 2.9 per 1000 in a Nigerian population (Uba et al., 2004)	Generally normal neurologic examination without deformity of the lower extremities or sphincter abnormality.	In order to prevent infections, swelling, and damage to the spinal cord, an early surgery is often suggested.
	Spina bifida occulta	Common defect, estimated in one out of 10 people (Eubanks & Cheruvu, 2009)	Asymptomatic in 10% of cases. Possible: Motor and sensorial deficit below the level of the spinal lesion. Bowel and/or bladder dysfunction, scoliosis, foot or leg length discrepancies, deformity of the lower extremities.	Neurosurgical intervention is the therapy chosen in cases of symptomatic patients with neurological deterioration.
	Iniencephaly	The incidence ranges from 0.1 to 10/10,000 and most of the patients are females (Aytar et al., 2007)	Most iniencephalic children who are born alive die shortly after birth (Khatami et al., 2015).	No neurosurgical management options.

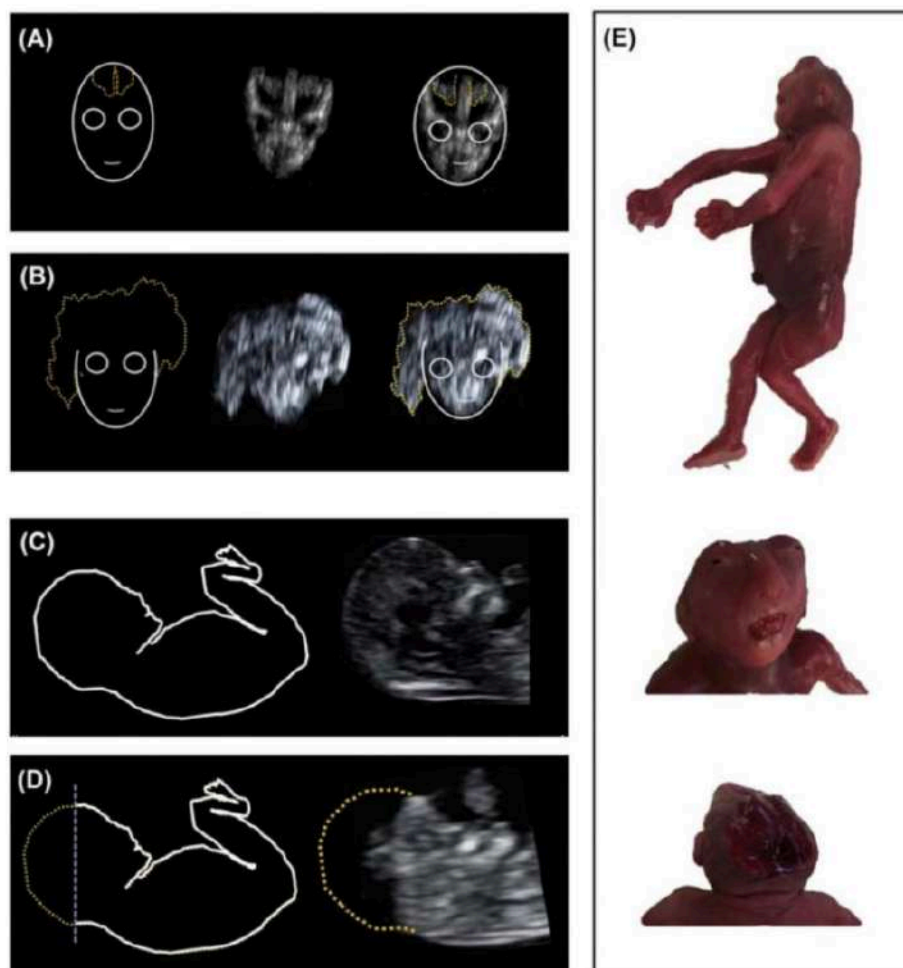


FIGURE 2.4 Exencephaly/anencephaly. Comparison between normal (A) and abnormal (B) frontal view of human embryo affected by exencephaly. The developmental defect of cranial portion was observed at 11 weeks of gestation. The defect involves the cranial portion of the neural tube. The calvarium is absent and brain tissues are externally exposed and float in the amniotic fluid (B: orange dotted line), whereas the face is normally structured. Comparison between normal (C) and abnormal (D) sagittal view of human embryo affected by anencephaly. The absence of the upper portion of the cranial vault was detected at 13 weeks of gestation, without external appearance of brain remnants (D: orange dotted line). Macroscopic aspect of anencephalic fetus is shown (E; from top to bottom: sagittal, front, and posterior view). Legal interruption of pregnancy was performed at 18 weeks of gestation. The face of the fetus is normal, although the eyes are protruded because of the shallow of the orbits, the forehead and the calvarium are absent. Posteriorly, the macroscopic aspect of the brain remnant appears as a dark brown undifferentiated mass (area cerebrovasculosa).

the vertebral arches. Even the meninges are herniated forming the cystic mass. Both the spinal cord and the meninges are damaged. The spinal cord is generally hypervascularized and in some cases the spinal cord could be closed with a dilated central channel, while in other cases the spinal cord appears open as a flat mass (Golden & Harding, 2004).

According to the Center for Disease Control and Prevention, myelomeningocele incidence is estimated to occur with a prevalence of 1.8 per 10,000 live births in United States (Zaganjor et al., 2016).

In some cases, the open defect is present but without protrusion of the meningeal sac. These cases are referred to as myelocele. In infants with a myelocele, it is possible to detect the neural tissue through the vertebral cleft (Emery & Lendon, 1973; Naik & Emery, 2008).

In myelomeningocele and myelocele, the cerebral trunk is stretched as a consequence of the lower open spinal cord, and this leads to their association with Chiari Type II malformation (CM-II), also known as Arnold–Chiari malformation. CM-II is characterized by a downward shift of the cerebellar vermis, tonsils and presents a mesencephalon malformation. The stretching of the structures into the medullary canal alters the normal cerebrospinal flow through the ventricles, leading to

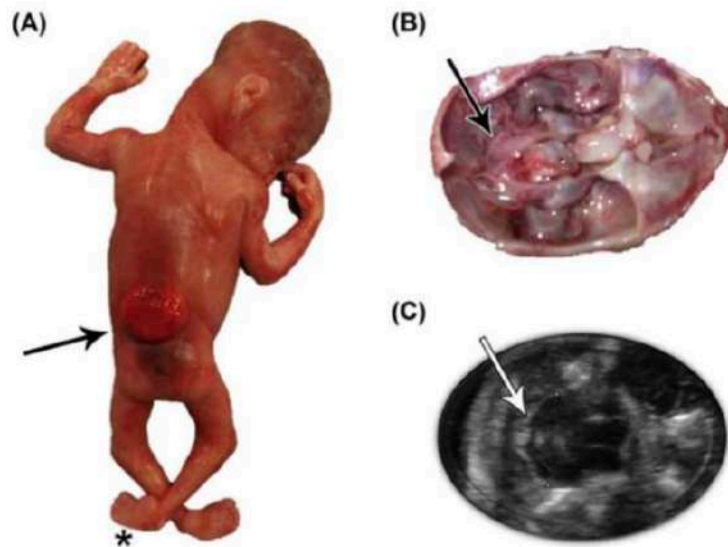


FIGURE 2.5 Myelomeningocele. Posterior sac-like protrusion from the spine is shown (A: *arrow*) in an embryo affected by myelomeningocele. The cystic lesion herniates from a cleft in vertebral arch and contains meninges, cerebrospinal fluid, nerve roots, and spinal cord. The abnormal foot position in which the foot is internally rotated (*asterisk*) is called “clubfoot.” Generally, it is due to the damage of the nerve roots and virtually always involves both feet. The abnormal shape of the cerebellum (called “banana sign”) is shown (B, C), at both macroscopic and ultrasound evaluation of the posterior cranial fossa (*arrows*). The banana sign is due to downward traction on the cerebellum related to tethering of the spine through the spinal opening.

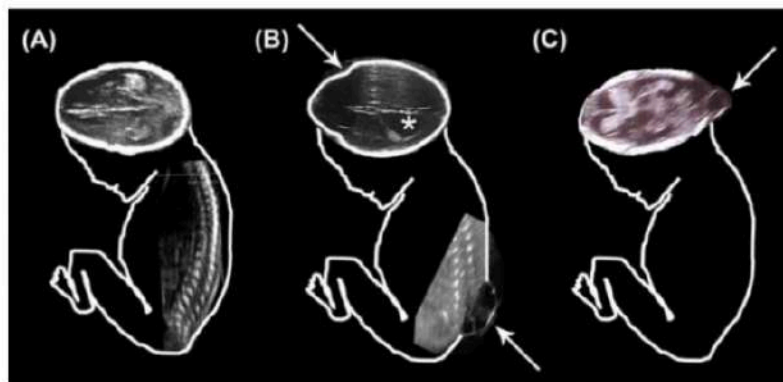


FIGURE 2.6 Myelomeningocele/encephaloceles. Normal ultrasonographic aspects of transverse cephalic scan and sagittal spinal scan are shown (A). Fetus affected by myelomeningocele (B) displays vertebral dysraphism with an associated cystic mass protruding from the lumbar portion of the spine (*lower arrow*) and containing tissues and internal septations. Cranial signs are also associated: abnormal shape of the skull in transverse section is present, displaying the so called “lemon sign” related to scalloping of the frontal bones (*upper arrow*); the cerebrospinal fluid through the ventricles is increased, resulting in secondary hydrocephalus (*asterisk*). Fetus affected by cephalocele (C) displays skull defect with a paracranial anechogenic sac. The posterior shape of choroid plexus is abnormal and brain tissues are herniated in the sac that protrudes through the opening of the skull (*arrow*).

progressive hydrocephalus (Sarnat, 2008) (Figs. 2.5B–C and 2.6B). CM-II is usually detected prenatally or at birth. Manifestations during childhood can include dysphagia, weakness in the arms, and episodes of apnea and aspiration.

In the absence of other serious congenital malformations, newborns with myelomeningocele or myelocele survive albeit presenting clinical features of motor and sensory deficits below the spinal cord injury and, in some cases, exhibit varying degrees of intellectual disability (related to the presence of hydrocephalus) (Copp et al., 2015; Thompson, 2009). *In utero* surgical repair might be considered for open spina bifida, and this procedure has shown significant benefits for the newborns, leading to a significant improvement in spinal neurological function despite the obvious risks associated to the surgical intervention (Adzick et al., 2011).

Craniorachischisis

The craniorachischisis represents the most severe NTD resulting in open brain and spine. In this condition, both anencephaly and open spina bifida are present. Such a malformation is not compatible with life. Typically, the posterior telencephalon and spinal cord tissue are exposed externally. The fetuses lack a cranial vault, with the defect extending with various degrees to the vertebrae. In craniorachischisis, both the brain and the spinal cord are exposed to the intraamniotic environment, leading to the destruction of nervous tissue due to the toxic effect of amniotic fluid. Craniorachischisis is a lethal condition for which there is no cure or possible surgery. The prevalence differs geographically. For example, in Northern China, the prevalence is 0.01 per 1000 newborns (Moore et al., 1997) and in a Texas–Mexico border population, the prevalence was 0.51 per 10,000 live births (Johnson, Suarez, Felkner, & Hendricks, 2004).

Closed NTDs

Closed NTDs form a less defined group of defects. Embryologically, there is scant experimental evidence to clearly establish the origin of the closed spinal lesions. Caudal closed defects result from alterations in secondary neurulation and are less severe birth defects. In fact, these defects typically occur at the sacrococcygeal level (i.e., at the level of secondary neurulation) and do not open to the external environment. The spinal cord remains bound to adjacent tissues, as expected for a defective separation of tissues during secondary neurulation (Copp & Greene, 2013). As a whole, closed defects typically have less severe loss of neurological function. Rostral closed defects result from alterations confined to the calvarium and may have more severe consequences.

Rostral closed defects: encephalocele

Encephalocele is the protrusion of the cranial contents beyond the normal confines of the skull through a defect in the calvarium (Raja, Qureshi, Memon, Ali, & Dev, 2008) (compare Fig. 2.6C–A).

It is classified according to the site: anterior, parietal, occipital, basal. Depending on the type of tissue involved in the herniation, cephaloceles are classified as meningocele (herniation of meninges), encephalomeningocele (herniation of meninges and brain), and encephalomeningocystocele (herniation of meninges, brain, and ventricle) (Pilu, Buyukkurt, Youssef, & Tonni, 2014). Moreover, cystic variants also exist, containing only cerebrospinal fluid (Gao, Massimi, Rogerio, Raybaud, & Di Rocco, 2014). According to the localization, the herniated mass can contain various types of tissues including the cerebral and cerebellar part, the ventricles with choroid plexus, gray matter heterotopia. Brain tissues involved in the hernia are generally nonfunctional. Meningeal inflammation was also detected (Ivashchuk, Loukas, Blount, Tubbs, & Oakes, 2015). Encephaloceles are one of the most common NTDs, and each year in the United States 1 out of 12,200 babies is born with this condition. Encephaloceles always require surgery correction under general anesthetic. The timing of surgery will vary depending on whether the sac is covered with skin or a thin membrane. If it is only covered with a thin membrane, surgery soon after birth will be required to prevent infection and damage/drying of the exposed tissue. If there is a covering of skin, surgery can be delayed for a month or two to allow the baby to grow and develop.

Caudal closed defects: Meningocele

Meningocele is a congenital malformation characterized by failed closure of the spine in its posterior part, generally at last lumbar vertebrae level (Copp & Greene, 2013). The skin is often dysplastic but present to some degree. Nervous disorders in the lower limbs are sometimes associated with this malformation. Posterior meningocele is the less common form of spina bifida. In this subtype, the nervous system remains intact, but a single developmental defect allows the meninges to herniate between the vertebrae. Therefore, meningocele is characterized by a protrusion of the meninges.

The incidence of this condition is unknown. As for the earlier described NTDs, in order to prevent infections, swelling, and damage to the spinal cord, an early surgery is often suggested.

Caudal closed defects: Closed spina bifida

Closed spina bifida represents a range of anomalies of the caudal spinal cord and has many variants. Spina bifida occulta is one form and likely the most common defect. Most of the cases are undiagnosed and without clinical manifestations or consequences. The prevalence is estimated in 1 out of 10 people (Eubanks & Cheruvu, 2009; Fidas et al., 1987). Closed spina bifida also includes lipomyelomeningocele, low conus, and thickened or fibrolipoma of the filum terminal. Midline cutaneous stigmata are often associated to closed spina bifida. These skin markers include nevi, nodules, depigmented region, subcutaneous lipomas, capillary hemangiomas, tufts of hair (localized hypertrichosis), and dermal sinus tract (Hertzler, DePowell, Stevenson, & Mangano, 2010; Sewell, Chiu, & Drolet, 2015). Neurosurgical intervention is the therapy chosen in cases of symptomatic patients with neurological deterioration.

Mixed defect: iniencephaly

Iniencephaly is an uncommon and fatal NTD characterized by an occipital bone defect, open spina bifida of the cervical vertebra, and an increase in cervical lordosis. The retroflexion of the head and the severe distortion of the spine are related to the localization of the defects that involve occiput, inion, and cervical and thoracic spine. Fetuses with iniencephaly are rarely live born, but at least one live birth has been reported (Khatami, Hasanzadeh, Norouzi, Esfandiari, & Mehrafarin, 2015). The prevalence of iniencephaly ranges from 0.1 to 10/10,000, and most of the patients are females (Aytar et al., 2007).

Conclusions

NTDs are the second most common congenital malformations in humans, and despite their potentially devastating consequences on patients and families, they represent an example of possible successful preventable birth defect. Numerous studies using an array of experimental models have been reported in the literature, leading to a better understanding of molecular and cellular events (Butler & Wallingford, 2017; Greene & Copp, 2014; Wallingford et al., 2013); however, NTD pathogenesis is not yet fully elucidated. It is possible to hypothesize that genetic predisposition and/or environmental factors impact on cell survival equilibrium, which must be finely tuned in this pivotal embryonic process.

Application to other areas of development

Cellular and molecular mechanisms regulating neurulation process are shared among several other pivotal developmental events. Indeed, anoikis has been suggested to intervene also in palatal shelves fusion and trachea—esophagus separation. In this context, it is possible to hypothesize that key embryonic steps are facilitated by abundant cells that obviously must be removed in subsequent developmental phases.

Key facts

Key facts on neurulation:

- Neurulation is a multistep process leading to the development of the central nervous system.
- It starts at 21-day postfertilization in humans.
- Neurulation is a process divided into primary neurulation and secondary neurulation.
- Primary neurulation is a discontinuous process that starts at different points along the rostrum—caudal axis necessary for the neural tube closure.
- The secondary neurulation permits the formation of the spinal cord at the lower sacral and caudal level.

Key facts on cell survival:

- Programmed cell death has been observed during neurulation and neural tube closure in several models.
- Cell death/survival occurs during the morphogenetic process of embryo development, and it is known to be of fundamental importance during nervous system formation.
- During neurulation, some cells become “homeless” because of the loss of contact and association with neighboring cells and/or ECM components (anoikis).
- Anoikis is not necessary, but more likely a secondary step due to the cellular reorganization that facilitates the fusion processes.
- It is possible that several core molecular cascades converge in controlling such cellular events.

Key facts on neural tube defects:

- Neural tube defects can be grouped as closed or open.
- Open NTDs result from failure of primary neurulation.
- Closed NTDs result from impairment of secondary neurulation.
- NTDs might result in mild clinical manifestation or in extremely severe, including death.
- NTDs represent an archetype of complex birth defect (i.e., of both genetic and environmental origin).

Summary points

- This chapter focuses on neural tube defects (NTDs), which are common congenital anomalies arising from a failure neural tube formation (early neurulation).
- Primary neurulation is the process that shapes the neural plate in the anterior part and secondary neurulation happens in the caudal region.
- During neural tube formation, cells undergo apoptosis, probably as anoikis.
- NTDs are complex birth defects: both genetic and environmental factors participate in the pathogenesis.
- Despite the pathogenesis of NTDs being not fully elucidated, maternal folic acid supplementation significantly reduces the incidence.
- NTDs are classified as *open* (characterized by exposure of neural tissue) and *closed* (presenting an epithelium covering the neural tissue).
- Open NTDs are clinically more severe than closed ones.

Acknowledgments

The authors would like to express their deep gratitude to Ms. Susanna Brusa for graphic support.

References

- Adzick, N. S., Thom, E. A., Spong, C. Y., Brock, J. W., Burrows, P. K., Johnson, M. P., ... Farmer, D. L. (2011). A randomized trial of prenatal versus postnatal repair of myelomeningocele. *New England Journal of Medicine*, *364*(11), 993–1004. <https://doi.org/10.1056/NEJMoa1014379>
- Anand, M. K., Javia, M. D., & Lakhani, C. J. (2015). Development of brain and spinal cord in anencephalic human fetuses. *Anatomy*, *9*(2), 60–65. <https://doi.org/10.2399/ana.15.009>
- Aytar, M. H., Doğulu, F., Cemil, B., Ergün, E., Kurt, G., & Baykaner, K. (2007). Iniencephaly and long-term survival: A rare case report. *Child's Nervous System: ChNS: Official Journal of the International Society for Pediatric Neurosurgery*, *23*(6), 719–721. <https://doi.org/10.1007/s00381-007-0309-6>
- Blom, H. J., Shaw, G. M., den Heijer, M., & Finnell, R. H. (2006). Neural tube defects and folate: Case far from closed. *Nature Reviews Neuroscience*, *7*(9), 724–731. <https://doi.org/10.1038/nrn1986>
- Boudreau, N., Sympson, C., Werb, Z., & Bissell, M. (1995). Suppression of ICE and apoptosis in mammary epithelial cells by extracellular matrix. *Science*, *267*(5199), 891–893. <https://doi.org/10.1126/science.7531366>
- Butler, M. T., & Wallingford, J. B. (2017). Planar cell polarity in development and disease. *Nature Reviews Molecular Cell Biology*, *18*(6), 375. <https://doi.org/10.1038/NRM.2017.11>
- Cameron, M., & Moran, P. (2009). Prenatal screening and diagnosis of neural tube defects. *Prenatal Diagnosis*, *29*(4), 402–411. <https://doi.org/10.1002/pd.2250>
- Castilla, E. E., Botto, L. D., & Bakker, M. K. (2011). Annual report 2011, with data for 2009. *International clearinghouse for birth defects surveillance and research*. Roma, Italia: The International Centre on Birth Defects – ICBDsr Centre. Retrieved from: www.icbdsr.org.
- Catala, M. (2002). Genetic control of caudal development. *Clinical Genetics*, *61*(2), 89–96. <https://doi.org/10.1034/j.1399-0004.2002.610202.x>
- Chen, C. S., Mrksich, M., Huang, S., Whitesides, G. M., & Ingber, D. E. (1997). Geometric control of cell life and death. *Science*, *276*(5317), 1425–1428. <https://doi.org/10.1126/science.276.5317.1425>
- Colas, J.-F., & Schoenwolf, G. C. (2001). Towards a cellular and molecular understanding of neurulation. *Developmental Dynamics*, *221*(2), 117–145. <https://doi.org/10.1002/dvdy.1144>
- Committee on Practice Bulletins-Obstetrics. (2017). Practice bulletin No. 187. *Obstetrics and Gynecology*, *130*(6), e279–e290. <https://doi.org/10.1097/AOG.0000000000002412>
- Copp, A. J., Adzick, N. S., Chitty, L. S., Fletcher, J. M., Holmbeck, G. N., & Shaw, G. M. (2015). Spina bifida. *Nature Reviews Disease Primers*, *1*(1), 15007. <https://doi.org/10.1038/nrdp.2015.7>
- Copp, A. J., & Greene, N. D. E. (2010). Genetics and development of neural tube defects. *The Journal of Pathology*, *220*(2), 217–230. <https://doi.org/10.1002/path.2643>
- Copp, A. J., & Greene, N. D. E. (2013). Neural tube defects-disorders of neurulation and related embryonic processes. *Wiley Interdisciplinary Reviews: Developmental Biology*, *2*(2), 213–227. <https://doi.org/10.1002/wdev.71>
- Copp, A. J., Greene, N. D. E., & Murdoch, J. N. (2003). The genetic basis of mammalian neurulation. *Nature Reviews Genetics*, *4*(10), 784–793. <https://doi.org/10.1038/nrg1181>
- Emery, J. L., & Lendon, R. G. (1973). The local cord lesion in neurospinal dysraphism (meningomyelocele). *The Journal of Pathology*, *110*(1), 83–96. <https://doi.org/10.1002/path.1711100110>
- Eubanks, J. D., & Cheruvu, V. K. (2009). Prevalence of sacral spina bifida occulta and its relationship to age, sex, race, and the sacral table angle: An anatomic, osteologic study of three thousand one hundred specimens. *Spine*, *34*(15), 1539–1543. <https://doi.org/10.1097/BRS.0b013e3181a98560>
- Fidas, A., MacDonald, H. L., Elton, R. A., Wild, S. R., Chisholm, G. D., & Scott, R. (1987). Prevalence and patterns of spina bifida occulta in 2707 normal adults. *Clinical Radiology*, *38*(5), 537–542. [https://doi.org/10.1016/s0009-9260\(87\)80150-2](https://doi.org/10.1016/s0009-9260(87)80150-2)

- Gao, Z., Massimi, L., Rogerio, S., Raybaud, C., & Di Rocco, C. (2014). Vertex cephaloceles: A review. *Child's Nervous System*, 30(1), 65–72. <https://doi.org/10.1007/s00381-013-2249-7>
- Gilmore, A. P. (2005). Anokis. *Cell Death and Differentiation*, 12(S2), 1473–1477. <https://doi.org/10.1038/sj.cdd.4401723>
- Golden, J. A., & Harding, B. N. (2004). *Pathology and genetics: Developmental neuropathology*. Los Angeles: ISN Neuropathology Press.
- Goldstein, R., & Filly, R. (1988). Prenatal diagnosis of anencephaly: Spectrum of sonographic appearances and distinction from the amniotic band syndrome. *American Journal of Roentgenology*, 151(3), 547–550. <https://doi.org/10.2214/ajr.151.3.547>
- Greene, N. D. E., & Copp, A. J. (2014). Neural tube defects. *Annual Review of Neuroscience*, 37, 221–242. <https://doi.org/10.1146/annurev-neuro-062012-170354>
- Greene, N. D. E., Leung, K., & Copp, A. J. (2017). Inositol, neural tube closure and the prevention of neural tube defects. *Birth Defects Research*, 109(2), 68. <https://doi.org/10.1002/BDR.A.23533>
- Greene, N. D. E., Leung, K.-Y., Gay, V., Burren, K., Mills, K., Chitty, L. S., & Copp, A. J. (2016). Inositol for the prevention of neural tube defects: A pilot randomised controlled trial. *British Journal of Nutrition*, 115(6), 974. <https://doi.org/10.1017/S0007114515005322>
- Hernández-Díaz, S., Werler, M. M., Walker, A. M., & Mitchell, A. A. (2000). Folic acid antagonists during pregnancy and the risk of birth defects. *New England Journal of Medicine*, 343(22), 1608–1614. <https://doi.org/10.1056/NEJM200011303432204>
- Hertzler, D. A., DePowell, J. J., Stevenson, C. B., & Mangano, F. T. (2010). Tethered cord syndrome: A review of the literature from embryology to adult presentation. *Neurosurgical Focus*, 29(1), E1. <https://doi.org/10.3171/2010.3.FOCUS1079>
- Hynes, R. O. (2002). Integrins: Bidirectional, allosteric signaling machines. *Cell*, 110(6), 673–687. [https://doi.org/10.1016/s0092-8674\(02\)00971-6](https://doi.org/10.1016/s0092-8674(02)00971-6)
- Ivashchuk, G., Loukas, M., Blount, J. P., Tubbs, R. S., & Oakes, W. J. (2015). Chiari III malformation: A comprehensive review of this enigmatic anomaly. *Child's Nervous System: Official Journal of the International Society for Pediatric Neurosurgery*, 31(11), 2035–2040. <https://doi.org/10.1007/s00381-015-2853-9>
- Johnson, K. M. K., Suarez, L., Felkner, M. M., & Hendricks, K. (2004). Prevalence of craniorachischisis in a Texas-Mexico border population. *Birth Defects Research Part A: Clinical and Molecular Teratology*, 70(2), 92–94. <https://doi.org/10.1002/bdra.10143>
- Juriloff, D. M., & Harris, M. J. (2012). A consideration of the evidence that genetic defects in planar cell polarity contribute to the etiology of human neural tube defects. *Birth Defects Research Part A: Clinical and Molecular Teratology*, 94(10), 824–840. <https://doi.org/10.1002/bdra.23079>
- Keeling, J. W., & Kjaer, I. (1994). Diagnostic distinction between anencephaly and amnion rupture sequence based on skeletal analysis. *Journal of Medical Genetics*, 31(11), 823–829. <https://doi.org/10.1136/jmg.31.11.823>
- Khatami, A., Hasanzadeh, M., Norouzi, H., Esfandiari, E., & Mehrafarin, M. (2015). Iniencephaly clausus: A new case with clinical and imaging findings. *Iranian Journal of Radiology: A Quarterly Journal Published by the Iranian Radiological Society*, 12(3), e4790. <https://doi.org/10.5812/iranradiol.4790v2>
- Kibar, Z., Torban, E., McDermid, J. R., Reynolds, A., Berghout, J., Mathieu, M., ... Gros, P. (2007). Mutations in *VANGL1* associated with neural-tube defects. *New England Journal of Medicine*, 356(14), 1432–1437. <https://doi.org/10.1056/NEJMoa060651>
- Kondo, A., Matsuo, T., Morota, N., Kondo, A. S., Okai, I., & Fukuda, H. (2017). Neural tube defects: Risk factors and preventive measures. *Congenital Anomalies*, 57(5), 150–156. <https://doi.org/10.1111/cga.12227>
- Leck, I. (1974). Letter: Neural-tube defects and twinning. *Lancet*, 1(7849), 178. [https://doi.org/10.1016/s0140-6736\(74\)92487-8](https://doi.org/10.1016/s0140-6736(74)92487-8)
- Lei, Y.-P., Zhang, T., Li, H., Wu, B.-L., Jin, L., & Wang, H.-Y. (2010). *VANGL2* mutations in human cranial neural-tube defects. *New England Journal of Medicine*, 362(23), 2232–2235. <https://doi.org/10.1056/NEJMc0910820>
- Li, Z., Ren, A., Zhang, L., Ye, R., Li, S., Zheng, J., ... Li, Z. (2006). Extremely high prevalence of neural tube defects in a 4-county area in Shanxi Province, China. *Birth Defects Research Part A: Clinical and Molecular Teratology*, 76(4), 237–240. <https://doi.org/10.1002/bdra.20248>
- Massa, V., Greene, N. D. E., & Copp, A. J. (2009). Do cells become homeless during neural tube closure? *Cell Cycle*. <https://doi.org/10.4161/cc.8.16.9272>
- Massa, V., Savery, D., Ybot-Gonzalez, P., Ferraro, E., Rongvaux, A., Cecconi, F., ... Copp, A. J. (2009). Apoptosis is not required for mammalian neural tube closure. *Proceedings of the National Academy of Sciences*, 106(20), 8233–8238. <https://doi.org/10.1073/pnas.0900333106>
- McComb, J. G. (2015). A practical clinical classification of spinal neural tube defects. *Child's Nervous System*, 31(10), 1641–1657. <https://doi.org/10.1007/s00381-015-2845-9>
- Moore, C. A., Li, S., Li, Z., Hong, S. X., Gu, H. Q., Berry, R. J., ... Erickson, J. D. (1997). Elevated rates of severe neural tube defects in a high-prevalence area in northern China. *American Journal of Medical Genetics*, 73(2), 113–118. Retrieved from: <http://www.ncbi.nlm.nih.gov/pubmed/9409858>.
- Naik, D. R., & Emery, J. L. (2008). The position of the spinal cord segments related to the vertebral bodies in children with meningocele and hydrocephalus. *Developmental Medicine and Child Neurology*, 10, 62–68. <https://doi.org/10.1111/j.1469-8749.1968.tb04848.x>
- Nikolopoulou, E., Galea, G. L., Rolo, A., Greene, N. D. E., & Copp, A. J. (2017). Neural tube closure: Cellular, molecular and biomechanical mechanisms. *Development*, 144(4), 552–566. <https://doi.org/10.1242/dev.145904>
- Noventa, M., Vitagliano, A., Quaranta, M., Borgato, S., Abdulrahim, B., & Gizzo, S. (2016). Preventive and therapeutic role of dietary inositol supplementation in periconceptional period and during pregnancy. *Reproductive Sciences*, 23(3), 278–288. <https://doi.org/10.1177/1933719115594018>
- Parker, S. E., Mai, C. T., Canfield, M. A., Rickard, R., Wang, Y., Meyer, R. E., ... Streuli, C. H. (2010). Updated national birth prevalence estimates for selected birth defects in the United States, 2004–2006. *Birth Defects Research Part A - Clinical and Molecular Teratology*, 88(12), 1008–1016. <https://doi.org/10.1002/bdra.20735>
- Pilu, G., Buyukkurt, S., Youssef, A., & Tonni, G. (2014). *Visual encyclopedia of ultrasound in obstetrics and gynecology*. VISUOG.

- Pullan, S., Wilson, J., Metcalfe, A., Edwards, G. M., Goberdhan, N., Tilly, J., ... Streuli, C. H. (1996). Requirement of basement membrane for the suppression of programmed cell death in mammary epithelium. *Journal of Cell Science*, 109(Pt 3), 631–642. Retrieved from: <http://www.ncbi.nlm.nih.gov/pubmed/8907708>.
- Raja, R. A., Qureshi, A. A., Memon, A. R., Ali, H., & Dev, V. (2008). Pattern of encephaloceles: A case series. *Journal of Ayub Medical College, Abbottabad: JAMC*, 20(1), 125–128. Retrieved from: <http://www.ncbi.nlm.nih.gov/pubmed/19024205>.
- Rampersaud, E., Bassuk, A. G., Enterline, D. S., George, T. M., Siegel, D. G., Melvin, E. C., ... Speer, M. C. (2005). Whole genomewide linkage screen for neural tube defects reveals regions of interest on chromosomes 7 and 10. *Journal of Medical Genetics*, 42(12), 940–946. <https://doi.org/10.1136/jmg.2005.031658>
- Robert, E., & Guibaud, P. (1982). Maternal valproic acid and congenital neural tube defects. *Lancet*, 2(8304), 937. [https://doi.org/10.1016/s0140-6736\(82\)90908-4](https://doi.org/10.1016/s0140-6736(82)90908-4)
- Ross, M. E., Mason, C. E., & Finnell, R. H. (2017). Genomic approaches to the assessment of human spina bifida risk. *Birth Defects Research*, 109(2), 120–128. <https://doi.org/10.1002/bdra.23592>
- Salmela, M., Jokinen, J., Tiitta, S., Rappu, P., Cheng, R. H., & Heino, J. (2017). Integrin $\alpha 2\beta 1$ in nonactivated conformation can induce focal adhesion kinase signaling. *Scientific Reports*, 7(1), 3414. <https://doi.org/10.1038/s41598-017-03640-w>
- Sarnat, H. B. (2008). Disorders of segmentation of the neural tube: Chiari malformations. In *Handbook of clinical neurology* (Vol. 87, pp. 89–103). [https://doi.org/10.1016/S0072-9752\(07\)87006-0](https://doi.org/10.1016/S0072-9752(07)87006-0)
- Sewell, M. J., Chiu, Y. E., & Drolet, B. A. (2015). Neural tube dysraphism: Review of cutaneous markers and imaging. *Pediatric Dermatology*, 32(2), 161–170. <https://doi.org/10.1111/pde.12485>
- Shaw, G. M., Velie, E. M., & Wasserman, C. R. (1997). Risk for neural tube defect-affected pregnancies among women of Mexican descent and white women in California. *American Journal of Public Health*, 87(9), 1467–1471. <https://doi.org/10.2105/ajph.87.9.1467>
- Shimokita, E., & Takahashi, Y. (2011). Secondary neurulation: Fate-mapping and gene manipulation of the neural tube in tail bud. *Development Growth and Differentiation*, 53(3), 401–410. <https://doi.org/10.1111/j.1440-169X.2011.01260.x>
- Suzanne, M., & Steller, H. (2013). Shaping organisms with apoptosis. *Cell Death and Differentiation*, 20(5), 669–675. <https://doi.org/10.1038/cdd.2013.11>
- The Medical Task Force of Anencephaly. (1990). The infant with anencephaly. *New England Journal of Medicine*, 322(10), 669–674. <https://doi.org/10.1056/NEJM199003083221006>
- Thompson, D. N. P. (2009). Postnatal management and outcome for neural tube defects including spina bifida and encephaloceles. *Prenatal Diagnosis*, 29(4), 412–419. <https://doi.org/10.1002/pd.2199>
- Toriyama, M., Toriyama, M., Wallingford, J. B., & Finnell, R. H. (2017). Folate-dependent methylation of septins governs ciliogenesis during neural tube closure. *The FASEB Journal: Official Publication of the Federation of American Societies for Experimental Biology*, 31(8), 3622–3635. <https://doi.org/10.1096/fj.201700092R>
- Uba, A., Isamade, E., Chirdan, L., Edino, S., Ogbe, M. E., & Igun, G. (2004). Epidemiology of neural tube defects in North Central Nigeria title: Neural tube defects in Nigeria. *Child Health International African Journal of Paediatric Surgery*, 1. Retrieved from: <http://www.afrijaedsurg.org>.
- Wallingford, J. B., Niswander, L. A., Shaw, G. M., & Finnell, R. H. (2013). The continuing challenge of understanding, preventing, and treating neural tube defects. *Science*, 339(6123). <https://doi.org/10.1126/science.1222002>, 1222002–1222002.
- Wen, S., Zhu, H., Lu, W., Mitchell, L. E., Shaw, G. M., Lammer, E. J., & Finnell, R. H. (2010). Planar cell polarity pathway genes and risk for spina bifida. *American Journal of Medical Genetics, Part A*, 152A(2), 299–304. <https://doi.org/10.1002/ajmg.a.33230>
- Weprin, B., & Oakes, W. (2000). Occult spinal dysraphism: The clinical presentation and diagnosis. *Operative Techniques in Plastic and Reconstructive Surgery*, 7, 39.
- Williams, J., Mai, C. T., Mulinare, J., Isenburg, J., Flood, T. J., Ethen, M., & Centers for Disease Control and Prevention. (2015). Updated estimates of neural tube defects prevented by mandatory folic acid fortification - United States, 1995–2011. *MMWR. Morbidity and Mortality Weekly Report*, 64(1), 1–5. Retrieved from: <http://www.ncbi.nlm.nih.gov/pubmed/25590678>.
- Wong, R. L. Y., Wlodarczyk, B. J., Min, K. S., Scott, M. L., Kartiko, S., Yu, W., ... Finnell, R. H. (2008). Mouse Fkbp8 activity is required to inhibit cell death and establish dorso-ventral patterning in the posterior neural tube. *Human Molecular Genetics*, 17(4), 587–601. <https://doi.org/10.1093/hmg/ddm333>
- Yamaguchi, Y., & Miura, M. (2015). *Developmental cell review programmed cell death in neurodevelopment*. <https://doi.org/10.1016/j.devcel.2015.01.019>
- Zaganjor, I., Sekkarie, A., Tsang, B. L., Williams, J., Razzaghi, H., Mulinare, J., ... Rosenthal, J. (2016). Describing the prevalence of neural tube defects worldwide: A systematic literature review. *PLoS One*, 11(4), e0151586. <https://doi.org/10.1371/journal.pone.0151586>



Since January 2020 Elsevier has created a COVID-19 resource centre with free information in English and Mandarin on the novel coronavirus COVID-19. The COVID-19 resource centre is hosted on Elsevier Connect, the company's public news and information website.

Elsevier hereby grants permission to make all its COVID-19-related research that is available on the COVID-19 resource centre - including this research content - immediately available in PubMed Central and other publicly funded repositories, such as the WHO COVID database with rights for unrestricted research re-use and analyses in any form or by any means with acknowledgement of the original source. These permissions are granted for free by Elsevier for as long as the COVID-19 resource centre remains active.



Contents lists available at ScienceDirect

Pharmacological Research

journal homepage: www.elsevier.com/locate/yphrs

Letter to the Editor



Saliva sampling for chasing SARS-CoV-2: A Game-changing strategy

Sir,

despite tremendous efforts of containing SARS-CoV-2 spreading in Europe through a test-and-trace system, at the beginning of November most European Countries experienced a second wave of pandemic, posing serious challenges to the civil society and health systems.

Recent research indicates that symptoms screening alone will not enable to contain COVID-19 outbreaks, because an estimated 40 % of COVID-19 cases are asymptomatic and 50 % of transmissions results from asymptomatic subjects [1].

An important breakthrough would be identifying a testing system allowing for multiple screening and early detection, thus changing the timing and effectiveness of tracing asymptomatic spreaders. Moreover, autumn-winter season is characterized by other common respiratory infections with overlapping COVID-19 symptoms with an obvious economical and logistic burden for the National Health System. This aspect is of relevance among the pediatric population as young children, especially pre-school toddlers, have recurrent viral infections, and mitigation measures (distancing, masks) are difficult to implement, all resulting in more frequent testing. Moreover, SARS-CoV-2 transmission dynamics in children is not fully elucidated.

Recently, Wyllie et al. reported that saliva and nasopharyngeal swab samples have similar sensitivity in detecting SARS-CoV-2 in symptomatic patients, and that SARS-CoV-2 can be detected in saliva, before nasopharyngeal swab (NPS), of asymptomatic individuals [2].

To address this issue, starting from the FDA emergency approved SalivaDirect™ protocol of Yale University [3], we optimized a saliva collection method able to guarantee a correct self-sampling or caregiver-guided sampling. Briefly, a sterile dental cotton roll was kept for two minutes in the vestibular space next to the lower premolar-molar area, then under the tongue close to the Wharton duct opening for additional two minutes. Once duly soaked with saliva, the dental roll was preserved in a sterile 50 mL tube, at room temperature until use (up to 7 days). Saliva was then recovered under sterile conditions using a 10 mL syringe to squeeze the cotton roll. Collected saliva was processed as recommended by Vogels et al. [3], with a modification of the thermal cyclers profile: 5' at 95 °C followed by 5' at 4 °C. Five microliters of the processed saliva was used directly for qPCR using N1 (FAM, BHQ-1 labeled probe) and RP (Cy5, BHQ-1) primers/probes published by the Centers for Disease Control (<https://www.cdc.gov/coronavirus/2019-nCoV/lab/rt-pcr-panel-primer-probes.html>) and Applied Biosystem 7500 Fast instrument. Samples were considered positive upon detection of N1 (Ct<40). Invalid samples were assessed by RP (Ct>35).

Here we report the results of the comparison between paired samples of self-collected saliva and NPS. This analysis is part of a prospective study at Vittore Buzzi Children Hospital and San Paolo Hospital in Milan. This study was carried out in accordance with the recommendations of the Comitato Etico Interaziendale Milano Area A, protocol

approval numbers N. 31554 (adults) and N. 0050308 (children). All subjects/caregivers gave written informed consent in accordance with the Declaration of Helsinki.

For assessing this method reliability, first we tested paired nasopharyngeal swabs and saliva samples in 192 adults (age 18–85, 52.2 % females). Concordance between tests was assessed using the Kappa statistic (Cohen's unweighted Kappa, k) as: poor ($k = 0$), slight ($0.01 < k < 0.20$), fair ($0.21 < k < 0.40$), moderate ($0.41 < k < 0.60$), substantial ($0.61 < k < 0.80$), almost perfect ($0.81 < k < 1.00$), or perfect ($k = 1$). Overall, concordance was 0.85 and k coefficient was 0.69, indicating a substantial concordance (Fig. 1A). When analyzing asymptomatic subjects, concordance rose to 0.96 with k equal to 0.83, indicating an almost perfect concordance (Fig. 1B).

Having confirmed the reliability of the test in the adult population, especially in asymptomatic individuals, we then coupled the saliva test to NPS in a pediatric population (N. 109; age: 0–17, 46.4 % females). Concordance was analyzed using the Kappa statistics and overall concordance was 0.94 and k was 0.81, considered almost perfect (Fig. 1C).

Ct values for N1 SARS-CoV-2 gene of 55 matched saliva (blue dots) and NPS (red dots) samples (Fig. 1D) were used to calculate Pearson correlation coefficient (Fig. 1E) that resulted 0.47, indicating a statistically significant moderate positive correlation ($p = 0.0003$).

Among the differing results in the adult cohort having a positive NPS and negative saliva, two subjects already developed IgG antibodies against SARS-CoV-2, three individuals underwent the second NPS test 14 days following the COVID-19 diagnosis (according to the Italian protocol), ten subjects reported symptoms onset 8–15 days earlier.

Among the differing results in the pediatric cohort, in one case the saliva test was negative and NPS positive, while in six cases the saliva test detected SARS-CoV-2 RNA in asymptomatic individuals who resulted negative with the NPS. In two instances, saliva tested positive two days before NPS, suggesting oropharynx as the first site for viral replication.

Our data are in accordance with Yokota and colleagues [4] arguing that saliva molecular testing could be a more sensitive tool for contact-tracing.

The saliva sampling as an alternative for NPS has been proposed since the first SARS-CoV-2 wave [5] albeit two limiting factors: i) the infection dynamic within different body fluids is still debated [6]; ii) saliva results are highly dependent on the tested cohort and on the presence/absence of sputum, which in our hands is strongly confounding. In light of our data, we believe further experiments should be directed towards settling whether long positive NPS subjects with no virus in saliva are to be considered infectious.

In conclusion, we feel that this tool represents an opportunity for testing SARS-CoV-2 infection in between pandemic/epidemic wave

<https://doi.org/10.1016/j.yphrs.2020.105380>

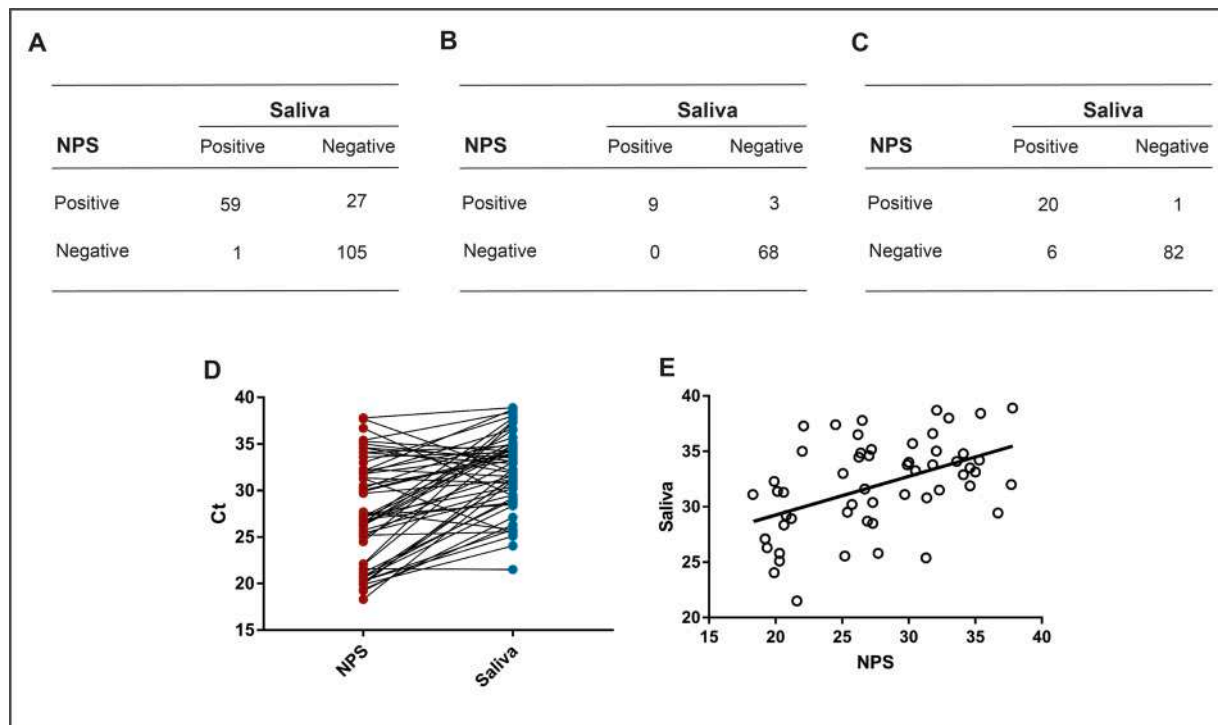


Fig. 1. SARS-CoV-2 RNA detection concordance tables for adult cohort (A), asymptomatic subjects (B), and children (C). Cycle Threshold (Ct) Values for 55 matched NPS and saliva positive samples (D), and linear regression for Pearson's r (E).

peaks. In addition, an active surveillance in close communities based on multiple saliva testing could be envisaged. Further, using broadly available and inexpensive cotton dental rolls would allow for boosting sampling capacity for low-compliant subjects and in low-income countries.

UNIMI SAL Study group: Stefano Centanni, Silvia Bianchi, Anna Caretti, Elena Canciani, Elisa Adele Colombo, Elisabetta Di Fede, Cristina Gervasini, Paolo Grazioli, Dolaji Henin, Elena Lesma, Antonella Lettieri, Giulia Marchetti, Gaia Pellegrini, Mariachiara Perrotta, Carlotta Pipolo.

Declaration of Competing Interest

All the authors declare no conflict of interest.

References

- [1] A.D. Paltiel, A. Zheng, R.P. Walensky, Assessment of SARS-CoV-2 screening strategies to permit the safe reopening of college campuses in the United States, *JAMA Netw. Open.* 3 (2020), <https://doi.org/10.1001/jamanetworkopen.2020.16818> e2016818.
- [2] A.L. Wyllie, J. Fournier, A. Casanovas-Massana, M. Campbell, M. Tokuyama, P. Vijayakumar, J.L. Warren, B. Geng, M.C. Muenker, A.J. Moore, C.B.F. Vogels, M. E. Petrone, I.M. Ott, P. Lu, A. Venkataraman, A. Lu-Culligan, J. Klein, R. Earnest, M. Simonov, R. Datta, R. Handoko, N. Naushad, L.R. Sewanan, J. Valdez, E.B. White, S. Lapidus, C.C. Kalinich, X. Jiang, D.J. Kim, E. Kudo, M. Linehan, T. Mao, M. Moriyama, J.E. Oh, A. Park, J. Silva, E. Song, T. Takahashi, M. Taura, O.-E. Weizman, P. Wong, Y. Yang, S. Bermejo, C.D. Odio, S.B. Omer, C.S. Dela Cruz, S. Farhadian, R.A. Martinello, A. Iwasaki, N.D. Grubaugh, A.I. Ko, Saliva or

- nasopharyngeal swab specimens for detection of SARS-CoV-2, *N. Engl. J. Med.* 383 (2020) 1283–1286, <https://doi.org/10.1056/NEJMc2016359>.
- [3] C.B.F. Vogels, A.E. Watkins, C.A. Harden, D. Brackney, J. Shafer, J. Wang, C. Caraballo, C.C. Kalinich, I. Ott, J.R. Fauver, E. Kudo, P. Lu, A. Venkataraman, M. Tokuyama, A.J. Moore, M.C. Muenker, A. Casanovas-Massana, J. Fournier, S. Bermejo, M. Campbell, R. Datta, A. Nelson, Y.I.R. Team, C. Dela Cruz, A. Ko, A. Iwasaki, H.M. Krumholz, J. Matheus, P. Hui, C. Liu, S. Farhadian, R. Sikka, A. L. Wyllie, N. Grubaugh, SalivaDirect: A simplified and flexible platform to enhance SARS-CoV-2 testing capacity, *MedRxiv* (2020), <https://doi.org/10.1101/2020.08.03.20167791>, 2020.08.03.20167791.
- [4] I. Yokota, P.Y. Shane, K. Okada, Y. Unoki, Y. Yang, T. Inao, K. Sakamaki, S. Iwasaki, K. Hayasaka, J. Sugita, M. Nishida, S. Fujisawa, T. Teshima, Mass screening of asymptomatic persons for SARS-CoV-2 using saliva, *Clin. Infect. Dis.* (2020), <https://doi.org/10.1093/cid/ciaa1388>.
- [5] S. Iwasaki, S. Fujisawa, S. Nakakubo, K. Kamada, Y. Yamashita, T. Fukumoto, K. Sato, S. Oguri, K. Taki, H. Senjo, J. Sugita, K. Hayasaka, S. Konno, M. Nishida, T. Teshima, Comparison of SARS-CoV-2 detection in nasopharyngeal swab and saliva, *J. Infect.* 81 (2020), <https://doi.org/10.1016/j.jinf.2020.05.071> e145–e147.
- [6] M. Riccò, S. Ranzieri, S. Peruzzi, M. Valente, F. Marchesi, F. Balzarini, N.L. Bragazzi, C. Signorelli, RT-qPCR assays based on saliva rather than on nasopharyngeal swabs are possible but should be interpreted with caution: results from a systematic review and metaanalysis, *Acta Biomed.* 91 (2020) 1–15, <https://doi.org/10.23750/abm.v91i3.10020>.

Elisa Borghi¹, Valentina Massa¹, Daniela Carmagnola¹,
Claudia Dellavia¹, Chiara Parodi, Emerenziana Ottaviano,
Arianna Sangiorgio, Lucia Barcellini, Greta Gambacorta,
Federica Forlanini, Gian Vincenzo Zuccotti*, UNIMI SAL Study group
Università degli Studi di Milano, Milan, Italy

* Corresponding author.

E-mail address: gianvincenzo.zuccotti@unimi.it (G.V. Zuccotti).

¹ These authors contributed equally to this work.

ARTICLE

Open Access

Lithium as a possible therapeutic strategy for Cornelia de Lange syndrome

Paolo Grazioli¹, Chiara Parodi¹, Milena Mariani², Daniele Bottai^{1,3}, Elisabetta Di Fede¹, Aida Zulueta¹, Laura Avagliano¹, Anna Cereda⁴, Romano Tenconi⁵, Jolanta Wierzbza⁶, Raffaella Adami¹, Maria Iacone⁴, Paola Francesca Ajmone⁷, Thomas Vaccari⁸, Cristina Gervasini^{1,3}, Angelo Selicorni² and Valentina Massa^{1,3}

Abstract

Cornelia de Lange Syndrome (CdLS) is a rare developmental disorder affecting a multitude of organs including the central nervous system, inducing a variable neurodevelopmental delay. CdLS malformations derive from the deregulation of developmental pathways, inclusive of the canonical WNT pathway. We have evaluated MRI anomalies and behavioral and neurological clinical manifestations in CdLS patients. Importantly, we observed in our cohort a significant association between behavioral disturbance and structural abnormalities in brain structures of hindbrain embryonic origin. Considering the cumulative evidence on the cohesin-WNT-hindbrain shaping cascade, we have explored possible ameliorative effects of chemical activation of the canonical WNT pathway with lithium chloride in different models: (I) *Drosophila melanogaster* CdLS model showing a significant rescue of mushroom bodies morphology in the adult flies; (II) mouse neural stem cells restoring physiological levels in proliferation rate and differentiation capabilities toward the neuronal lineage; (III) lymphoblastoid cell lines from CdLS patients and healthy donors restoring cellular proliferation rate and inducing the expression of *CyclinD1*. This work supports a role for WNT-pathway regulation of CdLS brain and behavioral abnormalities and a consistent phenotype rescue by lithium in experimental models.

Introduction

Cornelia de Lange Syndrome (CdLS, OMIM #122470, #300590, #610759, #614701, #300882, #611192, #608749) is a rare genetic disorder affecting a variety of organs, including the Central Nervous System (CNS). This syndrome is mainly caused by dominant autosomal or X-linked de novo mutations and it is a genetically and clinically heterogeneous disorder.

The recent International Consensus Statement¹ has defined the phenotypes classified as CdLS as a spectrum including the classic CdLS phenotype with or without a pathogenic variant in a gene involved in cohesin functioning,

as well as individuals with a non-classic CdLS phenotype with a pathogenic variant in a cohesin function-relevant gene. The spectrum does not include those patients with a variant in a cohesin gene without the CdLS phenotype.

The prevalence of CdLS is estimated to be 1:10.000–30.000 newborns but, most likely this represents an underestimation, as milder cases may not be recognized².

The features of this disorder vary widely among affected individuals and range from relatively mild to severe. CdLS is characterized by slow growth, abnormalities of the bones in the arms, hands, and fingers, and disorders in the gastro-intestinal tract. Patients present distinctive facial features, including arched eyebrows, long eyelashes, low-set ears, small and widely spaced teeth, and a small and upturned nose. CdLS patients are characterized by intellectual disabilities and behavior of the autism-spectrum indicating neural development alterations^{3,4}.

Correspondence: Valentina Massa (valentina.massa@unimi.it)

¹Department of Health Sciences, Università degli Studi di Milano, Milan, Italy

²UOC Pediatria, ASST Lariana, Como, Italy

Full list of author information is available at the end of the article

These authors contributed equally: Paolo Grazioli, Chiara Parodi, Milena Mariani

Edited by Ivano Amelio

© The Author(s) 2021



Open Access This article is licensed under a Creative Commons Attribution 4.0 International License, which permits use, sharing, adaptation, distribution and reproduction in any medium or format, as long as you give appropriate credit to the original author(s) and the source, provide a link to the Creative Commons license, and indicate if changes were made. The images or other third party material in this article are included in the article's Creative Commons license, unless indicated otherwise in a credit line to the material. If material is not included in the article's Creative Commons license and your intended use is not permitted by statutory regulation or exceeds the permitted use, you will need to obtain permission directly from the copyright holder. To view a copy of this license, visit <http://creativecommons.org/licenses/by/4.0/>.

CdLS is primarily caused by mutations in one of 7 genes: *NIPBL*, *SMC1A*, *SMC3*, *RAD21*, *HDAC8*, *ANKRD11*, and *BRD4*^{1,4}. These genes encode for proteins of the cohesin complex that is a multimeric system, highly conserved in the course of cellular evolution from the most primitive life forms to human cells^{5–7}. Cohesins are essential Structural Maintenance of Chromosomes (SMC) protein-containing complexes that interact with chromatin and modulate chromatin organization. Cohesins mediate sister chromatid cohesion and cellular long-distance chromatin interactions affecting genome maintenance and gene expression^{8–10}.

The current hypothesis regarding CdLS pathogenesis is that malformations arise from a deregulation of developmental pathways¹ and in this context, ours and other previous studies^{4,11–13} have shown that the canonical WNT pathway is perturbed.

The WNT pathway regulates cell-cell signaling by means of two branches. A canonical pathway acts through frizzled family receptors, which relay the signals to the intracellular transducer protein Dishevelled and regulates the expression of key developmental target genes¹⁴. In vertebrates, a non-canonical WNT pathway (also called β -catenin-independent pathway) is known to regulate both cell polarity and dorsal mesodermal cell movements during convergent extension, and later during neural tube closure^{15,16}.

WNT signaling is involved in numerous events in animal development and in the maintenance of adult tissue homeostasis by regulating cell proliferation, differentiation (including the proliferation of stem cells and the specification of the neural crest), migration, genetic stability, and apoptosis, as well as by maintaining adult stem cells in a pluripotent state¹⁷.

The WNT pathway plays a fundamental role in all steps of development of the CNS. In fact, WNT signaling alterations have been associated with a plethora of CNS abnormalities⁴. We have previously shown that the canonical WNT pathway is perturbed in CdLS models and underlies the observed cellular and developmental alterations. It is well known that lithium, a clinically effective therapeutic agent for bipolar disorders¹⁸, also recently used for amyotrophic lateral sclerosis¹⁹, is a specific inhibitor of the conserved WNT transducer GSK-3 β ^{20,21}. Indeed, our group recently reported that lithium activates the WNT pathway and is able to rescue phenotypes of *nipbl* and *smc1a* knock-down zebrafish mutants. Moreover, we observed that lithium-dependent activation of WNT pathway was able to rescue phenotypes of *nipbl* and *smc1a* knockdown zebrafish mutants^{11,12}. Other research groups also took advantage of zebrafish CdLS models to demonstrate a phenotype rescue using L-leucine or anti-oxidant treatments^{22,23}.

Based on these data, our working model for CdLS is that the canonical WNT pathway is downregulated as a consequence of a haploinsufficiency of cohesin genes. Such downregulation leads to lower expression of *CylinD1* which, in turn, leads to an increase in cell death at specific times and in specific tissues of the developing embryo^{8,11,12}.

Our experimental data was placed in context with CdLS patient clinical findings: in particular, with radiological anomalies and behavioral and neurological phenotypes. Thus, herein we decided to investigate the possible ameliorative effects of treatment with lithium, exploiting in vivo and in vitro CdLS models.

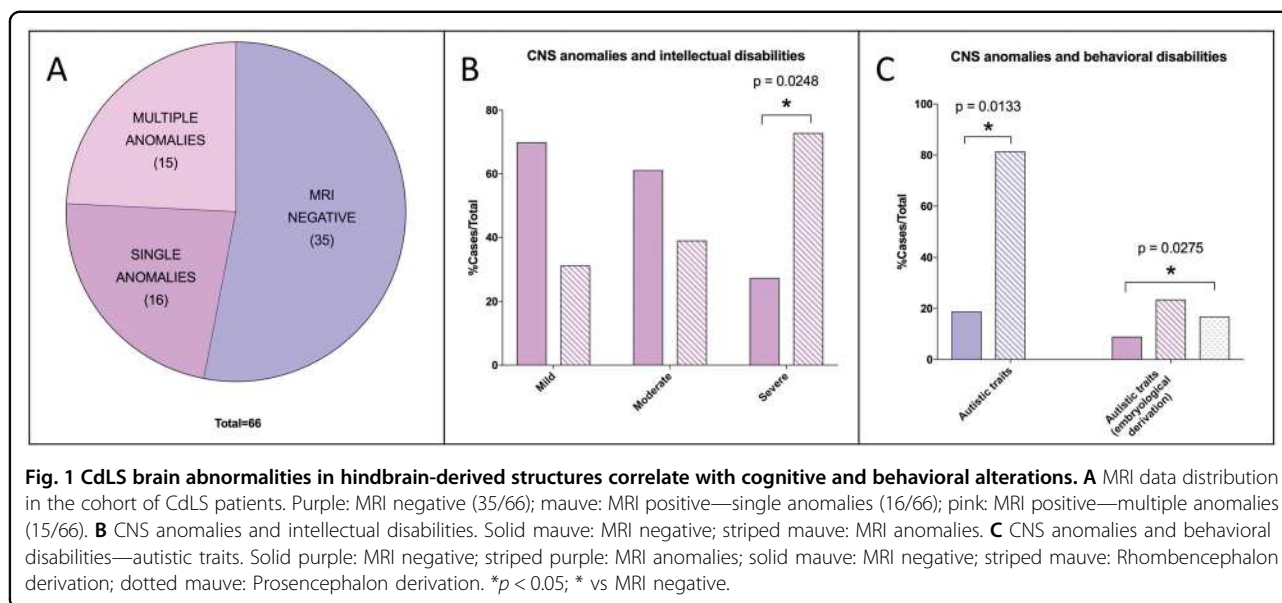
Results

Cognitive and behavioral deficits in CdLS patients are associated with abnormalities of hindbrain-derived structures

The relationship between WNT pathway and cohesin complex genes haploinsufficiency has been previously demonstrated especially in the case of hindbrain embryonic development⁴. For this reason, we sought to ascertain if alterations in cognitive, neurological, and behavioral aspects of CdLS patients could be associated with morphological abnormalities in hindbrain-derived structures²⁴. To this end, we evaluated magnetic resonance imaging (MRI) images of a CdLS cohort (Supplementary Fig. 1B). Among the 66 brain MRI, 31 showed brain abnormalities, half of which exhibited more than one anomaly (Fig. 1A; Supplementary Fig. 2A). The cerebellum and cisterna magna were the most frequently affected structures among recorded abnormalities (both affecting 25% of patients) and the most frequently coexisting anomalies. Subdividing MRI data according to individual behavioral assessment, we observed a significant correlation between CNS abnormalities and autism-spectrum disorder (ASD) (Fig. 1B, C). Subdividing MRI data according to cognitive level, we observed a significant correlation between CNS malformations and severe cognitive impairment (Supplementary Fig. 2B-C). MRI findings were not associated with the presence/absence of seizure (observed in 13/66 individuals). Importantly, behaviors associated with ASD significantly correlated to abnormalities of structures derived from the hindbrain (Fig. 1C).

WNT activation restores correct mushroom body development in CdLS flies

To study the effects of lithium on organ development, we next moved on to an in vivo CdLS model. To this end, we decided to evaluate the morphology of mushroom bodies of *Drosophila melanogaster*, a well-studied specialized CNS structure involved in olfactory learning and memory in adults (Fig. 2A). Indeed, flies heterozygous for an



inactivating mutation in the fly *NIPBL* ortholog gene *Nipped-B* (*Nipped-B*⁴⁰⁷ haploinsufficient animals from here on), often display mushroom bodies anomalies such as aberrant or missing lobes (Fig. 2C), when compared to control animals (Fig. 2B and ref. ²⁵). Importantly, upon rearing *Nipped-B*⁴⁰⁷ haploinsufficient animals on food supplemented with lithium (100 mM), a statistically significant ($p = 0.0036$) ratio of adults did not show signs of altered mushroom body development (Fig. 2D). In particular, the percentage of *Nipped-B*⁴⁰⁷ haploinsufficient animals with abnormal mushroom body morphology decreased from 88% in the untreated sample to 30% in the treated animals (Fig. 2E). To assess whether such significant anatomic rescue was WNT-dependent, we analyzed gene expression in our experimental groups. We observed a significant increase in expression of *engrailed* (*en* Fig. 2H, I)—a known fly WNT signaling target²⁶, in the *Nipped-B*⁴⁰⁷ haploinsufficient flies treated with lithium, when compared to flies reared on unsupplemented food. As expected²⁷, we did not observe gene expression changes in *armadillo* (*arm*, the fly ortholog of vertebrate β -catenin. Fig. 2F, G) both in *yw*, control strain, and in *Nipped-B*⁴⁰⁷ haploinsufficient animals.

WNT activation restores physiological proliferation and increases neuronal differentiation in CdLS mouse neural stem cells

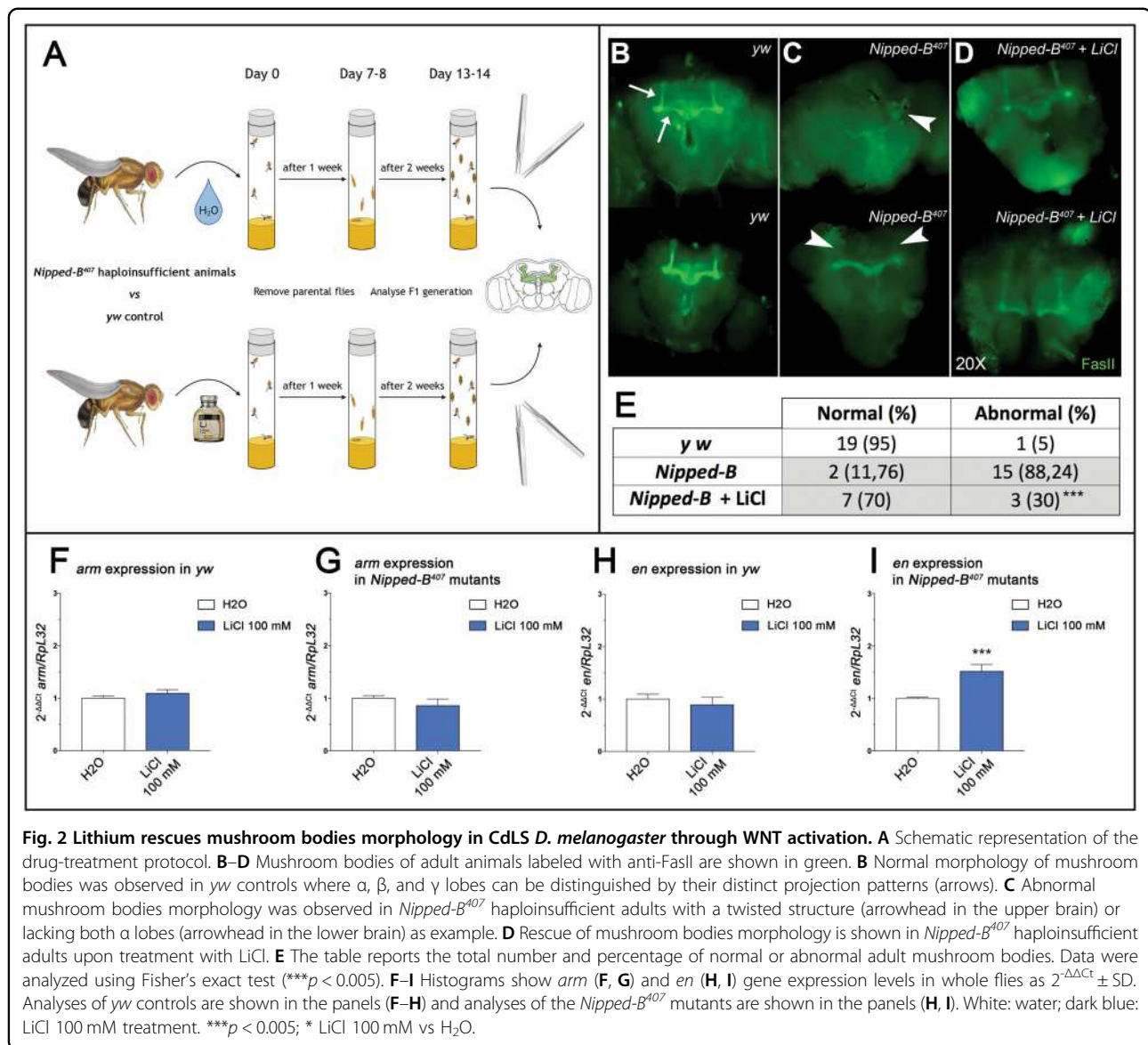
To study the possible beneficial effects of lithium treatments in CdLS models, we exploited mouse neural stem cells (NSCs) treated with a selective inhibitor of HDAC8 enzymatic activity (PCI34051), to mimic the molecular defects observed in patients^{1,7,28}. We have previously shown that PCI34051 was able to alter the rate of mouse NSCs proliferation and differentiation¹³. Thus, we tested the effects of lithium to prevent the detrimental

effects of HDAC8 inhibition (Fig. 3A, C). We confirmed that PCI34051 exposure induces a drastic reduction of NSCs proliferation. However, simultaneous exposure to 3 mM lithium reduced the adverse effects of HDAC8 inhibition, inducing a significant increase in NSC proliferation (Fig. 3A, C). The protective effect of lithium was also tested using *Nipbl* knockdown by siRNA. Such knockdown caused a significant reduction of NSCs proliferation as expected. However, lithium exposure was able to completely correct the effect of *Nipbl* knockdown, leading to a significantly increased proliferation when compared to siRNA treatment, ultimately restoring proliferation levels to those observed in control NSCs (All-Star/control siRNA or AllStar/control siRNA + lithium) (Fig. 3B, D). In order to confirm that the ameliorative effects of lithium were mediated by WNT activation, we analyzed the expression of the Wnt target *Ccnd1* and observed a significant increase (Fig. 3E).

Selective chemical HDAC8 inhibition also impairs NSCs differentiation toward the neuronal lineage¹³. Hence, we sought to mitigate the adverse effects of chemical WNT activation in this context. Lithium exposure induced a significant increase in differentiated Tuj1-positive cells (neuronal lineage) in CdLS NSCs, which is comparable to the differentiation rate observed in controls (Fig. 3F–H), in essence counteracting the inhibitory effect of PCI34051.

Lithium restores proliferation rate in CdLS lymphoblastoid cell lines

To evaluate possible ameliorative effects of lithium treatment in patients in vitro, we studied lymphoblastoid cell lines from CdLS patients and healthy donors. As expected²⁹, proliferation appeared to be reduced in



patient-derived cells, when compared to control lines. Interestingly, upon lithium exposure proliferation of CdLS cells was significantly increased (Fig. 4A and Supplementary Fig. 3A, B). In fact, CdLS lines exposed to a range of lithium chloride (LiCl) concentrations (1 mM, 2.5 mM, and 5 mM) showed increased proliferation, when compared to untreated CdLS cells, or to treated healthy donors (HD) cells (Fig. 4A and Supplementary Fig. 3A, B). Importantly, these effects on proliferation were associated with changes in cell death. In fact, assay analyses showed a decrease in death cells derived from patients treated with lithium (Fig. 4B-C). Interestingly, lithium exposure showed an increase in proliferation in vital count mirrored by a trend in decrease of cell death in patient-derived cells, both compared to untreated cells or to HD control lines. To confirm that such ameliorative effects

were mediated by WNT activation, we evaluated *Cyclin D1* expression, a known target of WNT canonical pathway. In CdLS cells, *Cyclin D1* showed a trend of increased expression following lithium exposure in CdLS cell lines (Fig. 4D-E). Finally, the same positive effects were observed exposing the cell lines to other chemical compounds (i.e. BIO, IQ-1, deoxycholic acid, CHIR99021) with known WNT-activation effects (Supplementary Fig. 3C-F).

Discussion

Basic research on cohesins, whose haploinsufficient inactivation causes cohesinopathies such as CdLS, has had a growing impetus in recent years since the role of cohesins on gene expression regulation was identified³⁰. This function adds to those which have long been

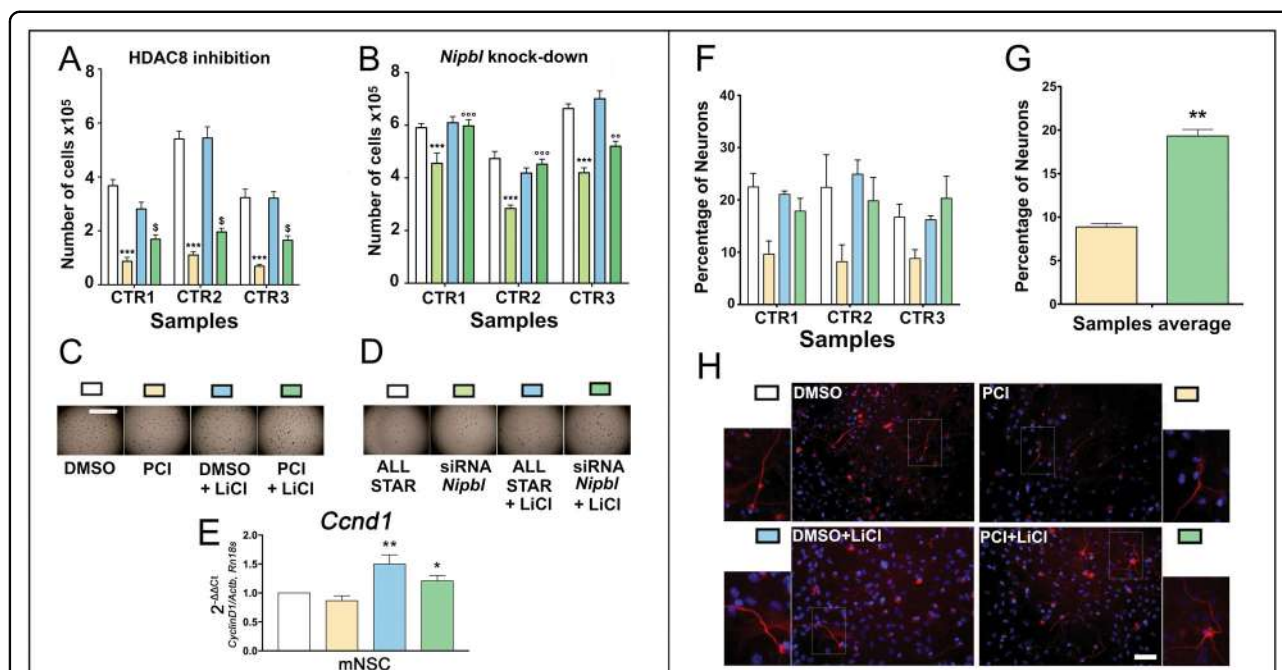


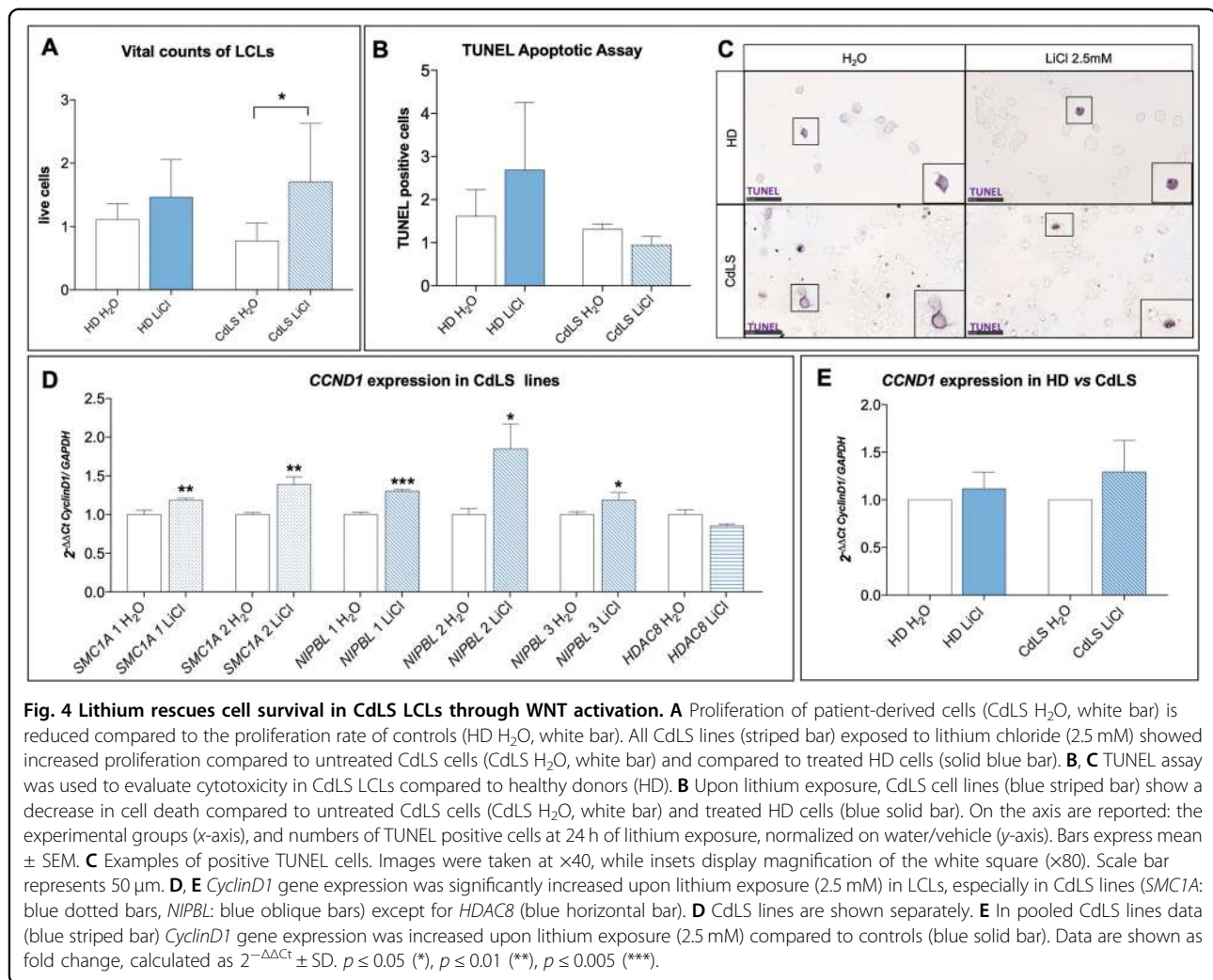
Fig. 3 Lithium rescues proliferation and differentiation capabilities in CdLS mouse NSCs through WNT activation. **A** Analysis of the effects of PCI34051 and lithium exposure on the proliferation capabilities of the NSCs. White: NSCs treated with DMSO; yellow: NSCs treated with PCI34051; light blue: NSCs treated with DMSO + LiCl; dark green: NSCs treated with PCI34051 and LiCl. *** $p < 0.001$; $\$ p < 0.05$; * DMSO vs PCI34051; $\$$ PCI34051 vs PCI34051 + LiCl. **B** Analysis of the effects of *Nipbl* knockdown and lithium exposure on the proliferation capabilities of the NSCs. White: NSCs treated with AllStar; light green: NSCs treated with siRNA against *Nipbl*; light blue: NSCs treated with AllStar and LiCl; dark green: NSCs treated with siRNA against *Nipbl* and LiCl. *** and $^{\circ\circ\circ} p < 0.001$; * AllStar vs siRNA against *Nipbl*; $^{\circ}$ siRNA against *Nipbl* vs siRNA against *Nipbl* + LiCl. **C** Representative pictures of the neurospheres growing in the well during various treatments as in panel (A). Scale bar: 2 mm. **D** Representative pictures of the neurospheres growing in the well during various treatments as in panel (B). **E** Analysis of the effects of PCI34051 and lithium exposure on the gene expression of *Ccnd1* in the NSCs. White: NSCs treated with DMSO; yellow: NSCs treated with PCI34051; light blue: NSCs treated with DMSO + LiCl; dark green: NSCs treated with PCI34051 and LiCl. ** $p < 0.01$; * $p < 0.05$; ** DMSO + LiCl vs PCI34051; * PCI34051 + LiCl vs PCI34051. **F** Analysis of the effects of PCI34051 and lithium on the differentiation capabilities of the NSCs. Cells were immunostained for neuron and nuclei detection. White: NSCs treated with DMSO; yellow: NSCs treated with PCI34051; light blue: NSCs treated with LiCl; dark green: NSCs treated with PCI34051 and LiCl. **G** Comparison of the effects of PCI34051 and PCI34051 + LiCl of NSCs differentiation. ** $p < 0.01$; * PCI34051 vs PCI34051 + LiCl. **H** Representative staining of the differentiated NSCs. Differentiated neurons were labeled with β -tubulin III antibody (red) and nuclei were labeled with DAPI (blue). Scale bar: 50 μ m.

extensively studied in the control of DNA damage and in the regulation of chromatid separation during the cell cycle, which have been defined as the “canonical role”⁷. Several studies have attempted to clarify which cohesin function is most commonly implicated in CdLS pathogenesis: thanks to in vitro and in vivo experimental studies, it is now currently believed that the “non-canonical” functions are mainly altered by pathogenic mutations^{7,31}.

Control and regulation of different gene pathways could account for the heterogeneity of the clinical involvement of patients with CdLS:³² in fact, these patients have multi-organ malformations, as well as mental retardation and medical complications depending on the degree of disability.

In a previous work of our group⁸, aimed at defining the cohesins expression in the different mammalian tissues, a significant expression of cohesins was demonstrated in the developing hindbrain and in the adult cerebellum. The

share of replicating cells in the adult cerebellum is limited, so it is possible to assume that the role of cohesins in maintaining the correct adhesion of sister chromatids is marginal in this context, and that there may be involvement of the “non-canonical” role of these proteins. Our previous studies on a *D. rerio* embryonic model of CdLS found a high expression of *nipblb* in the hindbrain, the structure from which the cerebellum originates¹². Morphological alterations have been identified precisely at the development of the rhombencephalon and a disruption of the WNT pathway was shown¹¹. It would be extremely significant to pinpoint the molecular cascade regulated by cohesins in differentiating CNS cells, and cohesin contribution to proper hindbrain and hindbrain-derived structures patterning. The difficulty in performing an accurate and objective neurological examination in a CdLS patient, stemming from the seriousness of the cognitive delay, explains the apparent absence of symptoms referable



to anomalies affecting the cerebellum. The CNS anomalies reported in the scientific literature often concern single case reports or cases with a small number of patients. In the context of rare conditions, it is in fact difficult to have large cohorts of patients and, in particular, for problems and complications that do not involve all affected individuals. Previous studies are represented on small cohorts, i.e. 8 and 15 patients^{33,34}. The cohort presented in this study, therefore, represents the largest ever described, with 66 patients undergoing a brain MRI examination. The number of neuroradiological tests is limited considering the original cohort (155 patients), but this is in line with what has also been highlighted by recent international guidelines that recommend performing brain MRI only in the case of manifest neurological symptoms¹. The evaluation of the MRI reports showed that in a considerable percentage of patients, morphological alterations of the cerebellum are present. Cerebellar anomalies are, in fact, visible in 24.5% of the patients whose MRI data are available. These primarily include hypoplasia of the cerebellar

vermis. The finding of cerebellar hypoplasia in patients with genetic syndromes is relatively frequent and, to date, there is much debate regarding the clinical neurological consequences that this malformation may entail³⁵. Over the years, pathological findings of the cerebellum have been frequently linked and held responsible for the development of behavioral problems attributable to the autistic spectrum: many autopsies of patients with ASD have demonstrated a decrease in the number of Purkinje cells and hypoplasia of the cerebellar vermis or cerebellar lobes³⁶. The analysis of our cohort shows a statistically significant correlation between CNS anomalies, in particular the structures of the posterior cranial fossa of rhombencephalic derivation, and the presence of autistic features. Analyzing the case history of 15 patients, the Kline group³⁴ had not reported a correlation between behavioral problems and CNS anomalies, perhaps precisely because of the small number of patients evaluated. Our finding represents additional support of the potential relationship between cerebellar anomalies and autism.

We then used *Drosophila* to model CdLS brain abnormalities in vivo. We have shown how the activation of WNT through the administration of lithium helps recover the morphology and structure of brain mushroom bodies also in adults. Our data show how molecular recovery can lead to macroscopic structural improvement. It would be interesting to assess possible feedback in circadian behavior, as it has also been associated with WNT and mushroom bodies patterning in flies³⁷ and it is known to be disturbed in CdLS patients³⁸. It is known that WNT has a fundamental role in the development of the CNS, specifically the development of the rhombencephalon⁴. Hence, we assessed lithium effects in CdLS mouse NSCs¹³. Upon *Nipbl* knockdown by siRNA or Hdac8 inhibition by PCI34051 administration, we observed decreased proliferation and increased apoptosis. By administering lithium, proliferation/death rate was restored to control levels. Furthermore, lithium exposure restores neuronal differentiation capabilities. We also confirmed that this effect was mediated by WNT activation, through the observed increase of *Ccnd1* expression. Finally, we studied LCLs derived from CdLS patients (with pathogenic variants in several causative genes) which were compared to healthy controls. In this experimental model, we confirmed results on CdLS-WNT pathway relationship.

The correlation between rhombencephalic anomalies and autistic features suggests that the use of lithium may represent a therapeutic strategy aimed at improving the behavioral disability of CdLS patients. As previously described, the WNT pathway modulated by lithium, has an essential role in the development of the CNS and a reactivation of the signaling of this pathway determines effects in terms of proliferation and differentiation that could potentially improve cellular deficits caused by an altered timing and differentiation success. We believe that it would be fundamental to study at the cellular level in the CNS possible defects and their correlation with neurological signs. A clinical trial has proposed lithium therapy for the treatment of fragile X syndrome showing promising results³⁹ compared to the effects on behavioral problems. Another work showed the efficacy of lithium as a mood stabilizer in two patients with *SHANK3* mutation who had been diagnosed with an ASD⁴⁰. Furthermore, hypoplasia of the cerebellum has been linked to psychomotor retardation of varying degrees even in patients without autistic symptoms⁴¹. In our case history, we find a statistically significant correlation between CNS abnormalities and severe mental retardation but not a relationship with specific abnormalities. Our group⁴² has recently developed a prognostic score capable of predicting the severity of intellectual impairment of patients on the basis of clinical features detectable in the first 6 months of life.

Should the data emerging from this work be confirmed, the presence of CNS anomalies could represent one of those markers, indicative of a more unfavorable prognosis in terms of intellectual impairment.

In conclusion, in the present study, we have further analyzed the significant role of the canonical WNT pathway in the development of the CdLS adverse phenotype. We have demonstrated with in vivo and in vitro models how lithium, a known WNT-activator, ameliorates phenotypes associated with CdLS by modulating WNT pathway. The comparison with the clinical data revealed a greater prevalence of anomalies of the central nervous system of rhombencephalic derivation, in full consistency with the data of the experimental models. Our findings should be confirmed, possibly through an ad hoc prospective study, designed with predefined neuro-behavioral parameters functionally assessed and a homogeneous analysis of the MRI images. This could allow for assessing the use of prognostic brain MRI data with respect to prevalence of behavioral disorders and severity of intellectual impairment.

Materials and methods

CdLS imaging

MRI brain analyses

The cohort of patients was composed of 155 patients (10 Polish and 145 Italian) with a diagnosis of CdLS according to diagnostic criteria⁴³. 51.6% were males, and age spanned between 1 month and 53 years (mean 19.83 years old). Exclusion criteria were genetic rearrangement not involving known causative genes (Supplementary Fig. 1B). Behavioral and cognitive parameters were assessed by specialized clinicians. Among them 66 patients had performed brain MRI (Fig. 1A).

Drosophila melanogaster

Husbandry

Flies were reared on cornmeal, yeast and molasses media in agar at 25 °C. For all experiments, heterozygous *Nipped-B*⁴⁰⁷ haploinsufficient mutants (*yw*; *Nipped-B*⁴⁰⁷, *pw*⁺/*CyO*, *Kr-GPF*)²⁵ and *yw* controls were grown at the same time with the same batch of food preparation. The loss of function allele *Nipped-B*⁴⁰⁷ was obtained by γ -ray mutagenesis and previously described⁴⁴.

Animal treatments

LiCl was added during the cooling step (temperature below 60 °C), of the food cooking process, to reach a final concentration of 100 mM; this concentration was determined according to the literature^{37,45–47}. Treatments' outcomes have been assessed after 15–20 days of culturing on the offspring of the fly population exposed to control or supplemented food.

Mushroom bodies immunostaining

The protocol for dissection and staining has been optimized from the literature⁴⁸. *Drosophila* brains were dissected in 1% Triton-X 100 in phosphate buffered saline (PBT), then fixed in paraformaldehyde (PFA) 4% for 1 h and stained with mouse anti-FasII 1:20 (clone 1D4; Developmental Studies Hybridoma Bank) for 2 nights, followed by incubation with Alexa-488 anti-mouse secondary antibody (1:1000 - ThermoFisher Scientific, #A21202) for 1 h. Between each step, samples were washed with PBT on mild agitation. Brain samples were then whole mounted in glycerol based mounting media and slides were sealed. Mushroom bodies were visualized using a fluorescence microscope (Leica DMRB) and acquired using a digital camera (Leica DFC480).

qPCR analysis (*Drosophila melanogaster*)

Total RNA was extracted from 15 flies per genotype using the RNeasy Mini Kit (#74106, Qiagen) following the manufacturer's protocol. RNA was quantified using a NanoDrop™ One (#ND-ONE-W, ThermoFisher Scientific) and 2 µg per sample were used for cDNA synthesis by performing a retro-transcription reaction with the SuperScript™ VILO™ cDNA Synthesis Kit (#11754050, Invitrogen) following manufacturer's protocol. SsoFast™ EvaGreen® Supermix (#1725201, Biorad) with 500 nmol primers were used for qPCR analyses on a CFX96 Touch Real-Time PCR Detection System (#1855196, Biorad). Primers used were home-made designed and tested (Supplementary Table S2). The experiments were performed with three independent biological samples ($n = 3$) and carried out with technical triplicates. Data are shown as fold change, calculated as $2^{-\Delta\Delta C_t}$ using *RpL32* as the calibrator gene.

Mouse neural stem cells

Neural stem cells preparation

Primary cultures and cultivation of the NSCs from adult mice, their differentiation and their immunostaining were carried out as previously described^{49,50} (Supplementary materials and methods). Cells were maintained in the proliferation state using an optimized medium (proliferation medium PM) described in a previous work⁵¹ as neurospheres that were mechanically dissociated every 4–6 days and replated. Every dissociation represents a passage; in the present study, we used cells cultivated for less than 15 passages.

Proliferation assays on NSCs exposed to PCI34051 and lithium

Cells maintained in the proliferative state were treated with PCI34051 25 µM for inhibiting HDAC8. For WNT pathway activation LiCl was used⁵². For each experiment, 4 groups were studied: (1) DMSO 1:1000 (as control), (2)

PCI34051 25 µM, (3) DMSO 1:1000 + LiCl 3 mM and (4) PCI34051 25 µM + LiCl 3 mM. Three different NSCs cultures were used for each experiment and the experiments were run in triplicate. Cells were counted by dissociating the neurospheres in the well and counting the single cells in suspension to determine the total number of cells in the well.

Differentiation assays on NSCs exposed to PCI34051 and lithium

The differentiation of NSC was accomplished by plating the dissociated neurospheres. 40,000 cells were seeded into a 48-multiwell plate containing one 10 mm coated (Cultrex, Tema Ricerca, Italy) round glass coverslip without epidermal growth factor (EGF) for 2 days, then a medium containing 1% of fetal calf serum was used.

During this step, the treatment with dimethyl sulfoxide (DMSO) (1:1000 as control), PCI34051 (25 µM) or LiCl (3 mM) and PCI 34051 (25 µM) + LiCl (3 mM) was also performed. Differentiation was reached after 7 days at 37 °C, 5% CO₂^{13,53}. Cells were then washed once with PBS and fixed with 4% paraformaldehyde (PFA) for 10 min at RT, then kept in PBS until the staining. Two-way ANOVA analysis of the effect of different combinations of PCI34051, and LiCl on NSCs differentiation was carried out.

Immunostaining of differentiated NSC

To assess the differentiation of treated NSCs, we used an approach previously described¹³ based on antibodies against β -Tubulin III (Tuj1 1:250, Immunological Sciences AB-10288) and Glial Fibrillary Acidic Protein (GFAP 1:250, Immunological Sciences AB-10635). The cells immunolabeled with β -Tubulin III were counted and the percentage of these cells was calculated by dividing for the overall number of cells (counting the nuclei stained with DAPI).

Silencing of proliferating NSCs

Silencing of *Nipbl* was performed using the same protocol described for HDAC8¹³. We used Qiagen siRNA (Flexitube siRNA 5 nmol cat. no. SI00853111 and cat. nr. SI00853118) and AllStars Negative Control siRNA (cat. no. 1027280). For allowing siRNA to penetrate into the cells, we used a specifically designed Qiagen Transfection Reagent, HiPerFect.

LiCl treatment was used to assess possible ameliorative effects. To this end, four experimental groups were established: (1) control with scramble miRNA (Allstar); (2) *Nipbl*-siRNA obtained using a mix of two different siRNAs at the total concentration of 20 nM;¹³ (3) control with LiCl treatment (AllStar + LiCl); and (4) *Nipbl* knockdown with LiCl. Three different NSCs cultures were used and the experiments were performed in triplicates.

Cells were counted dissociating the neurospheres in the well, counting the single cell suspension and calculating the total number of cells in the well.

qPCR (NSCs)

Cells were resuspended in Trizol reagent (Sigma-Aldrich); subsequently, RNA extraction was performed and contaminating DNA was removed with DNase I (#E1010, Zymo Research) following manufacturer's protocol. First strand cDNAs were synthesized using SensiFAST™ cDNA Synthesis Kit (#BIO-65054, Bioline) following the manufacturer's protocol. qPCRs were carried out using *TB Green* Premix Ex Taq (Tli RNase H Plus) (#RR420A, Takara Bio Inc., Kusatsu, Japan) and the *Applied Biosystems StepOnePlus™ Real-Time* PCR System (Thermo Fisher Scientific, Waltham, MA, United States). Each sample was assayed in technical triplicates and *Ccnd1* levels are expressed as $2^{-\Delta\Delta Ct} \pm SEM$ and normalized on values derived from the geometric mean of two tested housekeeping genes (*Actb* and *Rn18s*). Both biological and technical triplicates were used and paired groups. The primers used are reported in (Supplementary Table S1). Experiments were performed using RNA from two NSCs colonies cultured in biological triplicates.

Lymphoblastoid immortalized cell lines

Cell culturing

Lymphoblastoid lines (LCL) from patients with different mutations were used: 6 lines from CdLS patients carrying mutations in *NIPBL* (3), *HDAC8* (1), or *SMCIA* (2)⁵⁴ (Supplementary Table S3) and 4 lines from healthy donors (HD) serving as controls (Gaslini Genetic Bank service - Telethon Network of Genetic Biobanks, Genova). Cells were cultured in suspension in RPMI-1640 medium supplemented with 20% fetal bovine serum (FBS), 1% penicillin/streptomycin and were maintained at 37 °C in a humidified incubator with 5% CO₂.

Lithium exposure and additional compounds

Cells were exposed to three different concentrations of LiCl: 1 mM, 2.5 mM, and 5 mM or water (vehicle) as control^{55,56}. In addition, we used 4 other WNT activators compounds: BIO (6-bromoindirubin-3'-oxime) (0.1 μM, 0.5 μM, and 1 μM); IQ-1 (5 μM, 10 μM, and 20 μM); Deoxycholic acid (5 μM, 100 μM, and 250 μM); and CHIR99021 (1 μM, 5 μM, and 10 μM)^{57–59} (Supplementary Fig. 3C–F). Proliferation/death rates were measured counting cells upon trypan blue staining to evaluate the compounds' effects on viability and cytotoxicity.

TUNEL assay

Apoptosis rate in LCLs was evaluated using terminal deoxynucleotidyl transferase (TdT) dUTP Nick-End Labeling (TUNEL) assay, designed to detect apoptotic

cells during the late stages of apoptosis, as previously described¹³. Briefly, cells were cytospinned on glass slides and then fixed in 4% PFA for 10 min at room temperature (RT) and washed three times in phosphate buffer saline (PBS) for 5 min. Staining for apoptotic cells was performed using the AP-In situ Cell Death Detection Kit (Roche Diagnostics, Penzberg, Germany) following the manufacturer's protocol. Slides were mounted for microscopic imaging with home-made glycerol-based mounting media with anti-fading (1,4-diazabicyclo[2.2.2]octane, DABCO). Apoptotic cells were detected with NanoZoomer-XR Digital slide scanner (Hamamatsu, Japan) for counting.

Immunofluorescence assay

For assessing cell proliferation rate, Ki67 immunoassay⁶⁰ was used. Slides were stained with primary antibody anti-Ki-67 (1:250, #9129 (D3B5) Cell Signaling) overnight, followed by incubation with Alexa-488 anti-rabbit secondary antibody (1:1000, #6441-30 SouthernBiotech) for 2 h. Slides were mounted for microscopic imaging with EverBrite Hardset Mounting Medium with DAPI (#23004, Biotium) and positive cells were detected and acquired with NanoZoomer-XR Digital slide scanner (Hamamatsu, Japan) for counting.

qPCR (Lymphoblastoid cell lines)

RNA was extracted with Trizol (Sigma Aldrich, Italy) following the manufacturer's protocol. First strand cDNA was synthesized using SensiFAST™ cDNA Synthesis Kit (#BIO-65054, Bioline, Italy) following the manufacturer's protocol. qPCR was carried out using *TB Green* Premix Ex Taq (Tli RNase H Plus) (#RR420A, Takara Bio Inc., Kusatsu, Japan) and the *Applied Biosystems StepOnePlus™ Real-Time* PCR System (Thermo Fisher Scientific, Waltham, MA, United States). Primers used are reported in (Supplementary Table S4). Each sample was assayed in technical triplicates and *CCND1* levels were quantified relative to the expression of the *GAPDH* gene. Data are shown as fold change, calculated as $2^{-\Delta\Delta Ct}$.

Data analysis and statistics

Morphological analysis of *Drosophila* mushroom bodies was performed by two operators blinded to experimental groups, and results were analyzed with Fisher's exact test. The sample size was determined considering two independent study groups, with primary end point dichotomous (normal/abnormal), with α error: 0.05, β error 0.2 and power: 0.8. qPCR data for *Drosophila* and LCL were analyzed with Student's unpaired *t* test. NSCs proliferation statistical analysis was performed using student's *t*-test and two-way analysis of variance followed by Bonferroni's Multiple Comparison Test. NSCs immunostaining statistical analysis was performed using the One-

way analysis of variance followed by Bonferroni's Multiple Comparison Test. The sample size was determined considering two independent study groups, with primary end point continuous (mean), with α error: 0.05, β error 0.2 and power: 0.8. qPCR data for NSCs were analyzed multiple comparison in one-way ANOVA. LCL counting was made picking three randomly selected fields per experimental group ($\times 20$ magnification), and positive cells were calculated by counting within the three fields, by two operators blinded to experimental groups. Vital count (Fig. 4A), TUNEL apoptotic assay (Fig. 4B) and qPCR analyses (Fig. 4E) data were pooled based on cell derivation (HD vs. CdLS) and treatment (H₂O vs. LiCl). The sample size was determined considering two independent study groups, with primary end point continuous (mean), with α error: 0.05, β error 0.2, and power: 0.8. MRI data from CdLS patients were analyzed using the Fisher test. For all the analyses, $p \leq 0.05$ (*) was set as statistically significant, $p \leq 0.01$ (**), $p \leq 0.005$ (***). Graphs were made using Graphpad Prism 7 and figures were assembled using either GIMP-2.1 or Adobe Photoshop CC.

Acknowledgements

Microscopy observations were carried out at The Advanced Microscopy Facility Platform - UniTECH NoLimits - University of Milan. The authors are grateful to Prof. Richard H. Finnell, Dr Jon Wilson and Ms Dawn Savery for helpful comments. The authors would also like to express their deepest gratitude to CdLS patients and families for constant support and inspiration. The authors thank Susanna Brusa for graphical support. The authors acknowledge support from the University of Milan through the APC initiative. Fondazione Cariplo (2015-0783 to V.M.); Università degli Studi di Milano Intramural Fundings (to V.M. and G.C.); Molecular and Translational Medicine PhD-Università degli Studi di Milano scholarship (to P.G.); Translational Medicine PhD-Università degli Studi di Milano scholarship (to C.P. and E.D.F.); AIRC (Associazione Italiana Ricerca contro il Cancro) Investigator grant 20661 and WCR (Worldwide Cancer Research) grant 18-0399 (to T.V.); Nickel & Co S.p.A and CRC Aldo Ravelli (to VM).

Author details

¹Department of Health Sciences, Università degli Studi di Milano, Milan, Italy. ²UOC Pediatria, ASST Lariana, Como, Italy. ³"Aldo Ravelli" Center for Neurotechnology and Experimental Brain Therapeutics, Università degli Studi di Milano, Milan, Italy. ⁴Department of Pediatrics-ASST Papa Giovanni XXIII, Bergamo, Italy. ⁵Department of Pediatrics, University of Padova, Padova, Italy. ⁶Department of Pediatrics and Internal Medicine Nursing, Department of Rare Disorders, Medical University of Gdansk, Gdańsk, Poland. ⁷Child and Adolescent Neuropsychiatric Unit, Fondazione IRCCS Cà Granda Ospedale Maggiore Policlinico, Milan, Italy. ⁸Department of Biosciences, Università degli Studi di Milano, Milano, Italy

Author contributions

V.M. conceived the project and analyzed data; P.G., C.P., D.B., E.D.F. and A.Z. performed the experiments; M.M., J.W., M.I., P.F.A., L.A. and A.S. analyzed patients data; R.A. assisted in confocal microscope imaging; T.V. provided flies reagents and animals; P.G., C.P., M.M., D.B. and V.M. wrote the manuscript; A.C., R.T., T.V. and C.G. provided guidance in the manuscript revision and data interpretation. All authors: approved the manuscript.

Conflict of interest

The study is in accordance with the 1964 Helsinki declaration and its later amendments or comparable ethical standards. Written informed consent of patients or caregivers were collected for biological samples studies.

Publisher's note

Springer Nature remains neutral with regard to jurisdictional claims in published maps and institutional affiliations.

Supplementary information The online version contains supplementary material available at <https://doi.org/10.1038/s41420-021-00414-2>.

Received: 1 December 2020 Revised: 28 December 2020 Accepted: 17 January 2021

Published online: 17 February 2021





References

- Kline, A. D. et al. Diagnosis and management of Cornelia de Lange syndrome: first international consensus statement. *Nat. Rev. Genet.* <https://doi.org/10.1038/s41576-018-0031-0> (2018).
- Barisic, I. et al. Descriptive epidemiology of Cornelia de Lange syndrome in Europe. *Am. J. Med. Genet. Part A* **146**, 51–59 (2008).
- Sinkey, R. G., Odibo, A. O. & Bradshaw, R. J. *Cornelia de Lange syndrome. Obstetric Imaging: Fetal Diagnosis and Care*, 2nd edn (University of Washington, Seattle, 2017). <https://doi.org/10.1016/B978-0-323-44548-1.00127-3>
- Avagliano, L. et al. Integrating molecular and structural findings: Wnt as a possible actor in shaping cognitive impairment in Cornelia de Lange syndrome. *Orphanet J. Rare Dis.* **12**, 174 (2017).
- Banerji, R., Skibbens, R. V. & Iovine, M. K. How many roads lead to cohesinopathies? *Dev. Dyn.* **246**, 881–888 (2017).
- Nasmyth, K. Cohesin: A catenase with separate entry and exit gates? *Nat. Cell Biol.* **13**, 1170–1177 (2011).
- Deardorff, M. A. et al. HDAC8 mutations in Cornelia de Lange syndrome affect the cohesin acetylation cycle. *Nature* <https://doi.org/10.1038/nature11316> (2012)
- Bettini, L. R. et al. Rings and bricks: expression of cohesin components is dynamic during development and adult life. *Int. J. Mol. Sci.* **19**, 438 (2018).
- Kagey, M. H. et al. Mediator and cohesin connect gene expression and chromatin architecture. *Nature* **467**, 430–435 (2010).
- Zuin, J. et al. Cohesin and CTCF differentially affect chromatin architecture and gene expression in human cells. *Proc. Natl Acad. Sci.* **111**, 996–1001 (2014).
- Pistocchi, A. et al. Cornelia de Lange Syndrome: NIPBL haploinsufficiency downregulates canonical Wnt pathway in zebrafish embryos and patients fibroblasts. *Cell Death Dis.* **4**, e866 (2013).
- Fazio, G. et al. CyclinD1 down-regulation and increased apoptosis are common features of cohesinopathies. *J. Cell Physiol.* **231**, 613–622 (2016).
- Bottai, D. et al. Modeling Cornelia de Lange syndrome in vitro and in vivo reveals a role for cohesin complex in neuronal survival and differentiation. *Hum. Mol. Genet.* **28**, 64–73 (2019).
- Miyabayashi, T. et al. Wnt/beta-catenin/CBP signaling maintains long-term murine embryonic stem cell pluripotency. *Proc. Natl Acad. Sci.* **104**, 5668–5673 (2007).
- De, A. Wnt/Ca²⁺ signaling pathway: a brief overview. *Acta Biochim. Biophys. Sin. (Shanghai)*. **43**, 745–756 (2011).
- Komiya, Y. & Habas, R. Wnt signal transduction pathways. *Organogenesis* **4**, 68–75 (2008).
- Kahn, M. Can we safely target the WNT pathway? *Nat. Rev. Drug Discov.* **13**, 513–532 (2014).
- Volkman, C., Bschor, T. & Köhler, S. Lithium treatment over the lifespan in bipolar disorders. *Front. Psychiatry* **11**, 377 (2020).
- Limanaqi, F., Biagioni, F., Ryskalin, L., Busceti, C. L. & Fornai, F. Molecular mechanisms linking ALS/FTD and psychiatric disorders, the potential effects of lithium. *Front. Cell. Neurosci.* **13**, 450 (2019).
- Klein, P. S. & Melton, D. A. A molecular mechanism for the effect of lithium on development. *Proc. Natl Acad. Sci. USA* **93**, 8455–8459 (1996).
- O'Brien, W. T. et al. Glycogen synthase kinase-3 β haploinsufficiency mimics the behavioral and molecular effects of lithium. *J. Neurosci.* **24**, 6791–6798 (2004).
- Xu, B., Sowa, N., Cardenas, M. E. & Gerton, J. L. L-leucine partially rescues translational and developmental defects associated with zebrafish models of Cornelia de Lange syndrome. *Hum. Mol. Genet.* **24**, 1540–1555 (2015).
- Cukrov, D. et al. Antioxidant treatment ameliorates phenotypic features of SMC1A-mutated Cornelia de Lange syndrome in vitro and in vivo. *Hum. Mol. Genet.* **27**, 3002–3011 (2018).

24. Parisi, L., Di Filippo, T. & Roccella, M. Behavioral phenotype and autism spectrum disorders in Cornelia de Lange syndrome. *Ment. Illn.* **7**, 32–35 (2015).
25. Wu, Y. et al. Drosophila nipped-B mutants model Cornelia de Lange syndrome in growth and behavior. *PLoS Genet.* **11**, e1005655 (2015).
26. Danielian, P. S. & McMahon, A. P. Engrailed-1 as a target of the Wnt-1 signalling pathway in vertebrate midbrain development. *Nature* **383**, 332–334 (1996).
27. Bejsovec, A. Wingless/Wnt signaling in Drosophila: the pattern and the pathway. *Mol. Reprod. Dev.* **80**, 882–894 (2013).
28. Gao, X. et al. A functional mutation in HDAC8 gene as novel diagnostic marker for Cornelia de Lange Syndrome. *Cell. Physiol. Biochem.* **47**, 2388–2395 (2018).
29. Yuen, K. C., Xu, B., Krantz, I. D. & Gerton, J. L. NIPBL controls RNA biogenesis to prevent activation of the stress kinase PKR. *Cell Rep.* **14**, 93–102 (2016).
30. Kaiser, F. J. et al. Loss-of-function HDAC8 mutations cause a phenotypic spectrum of Cornelia de Lange syndrome-like features, ocular hypertelorism, large fontanelle and X-linked inheritance. *Hum. Mol. Genet.* **23**, 2888–2900 (2014).
31. Dorsett, D. Roles of the sister chromatid cohesion apparatus in gene expression, development, and human syndromes. *Chromosoma* **116**, 1–13 (2007).
32. Moss, J. et al. Genotype–phenotype correlations in Cornelia de Lange syndrome: behavioral characteristics and changes with age. *Am. J. Med. Genet. A* **173**, 1566–1574 (2017).
33. Whitehead, M. T., Nagaraj, U. D. & Pearl, P. L. Neuroimaging features of Cornelia de Lange syndrome. *Pediatr. Radio.* **45**, 1198–1205 (2015).
34. Roshan Lal, T. R. et al. Cornelia de Lange syndrome: correlation of brain MRI findings with behavioral assessment. *Am. J. Med. Genet. Part C. Semin. Med. Genet.* **172**, 190–197 (2016).
35. Steinlin, M. Cerebellar disorders in childhood: cognitive problems. *Cerebellum* **7**, 607–610 (2008).
36. Noelanders, R. & Vlemminckx, K. How Wnt signaling builds the brain: bridging development and disease. *Neuroscientist* **23**, 314–329 (2017).
37. Dokucu, M. E., Yu, L. & Taghert, P. H. Lithium- and valproate-induced alterations in circadian locomotor behavior in Drosophila. *Neuropsychopharmacology* <https://doi.org/10.1038/sj.npp.1300764> (2005)
38. Rajan, R. et al. Insomnia in Cornelia de Lange Syndrome. *Int. J. Pediatr. Otorhinolaryngol.* **76**, 972–975 (2012).
39. Liu, Z. & Smith, C. B. Lithium: a promising treatment for fragile X syndrome. *ACS Chem. Neurosci.* **5**, 477–483 (2014).
40. Serret, S. et al. Lithium as a rescue therapy for regression and catatonia features in two SHANK3 patients with autism spectrum disorder: Case reports. *BMC Psychiatry* **15**, (2015).
41. Fatemi, S. H. & Folsom, T. D. The role of fragile X mental retardation protein in major mental disorders. *Neuropharmacology* **60**, 1221–1226 (2011).
42. Cereda, A. et al. A new prognostic index of severity of intellectual disabilities in Cornelia de Lange syndrome. *Am. J. Med. Genet. C. Semin. Med. Genet.* **172**, 179–189 (2016).
43. Kline, A. D. et al. Natural history of aging in Cornelia de Lange syndrome. *Am. J. Med. Genet. C. Semin. Med. Genet.* **145**, 248–260 (2007).
44. Rollins, R. A., Morcillo, P. & Dorsett, D. Nipped-B, a Drosophila homologue of chromosomal adherins, participates in activation by remote enhancers in the cut and Ultrabithorax genes. *Genetics* **152**, 577–593 (1999).
45. Castillo-Quan, J. I. et al. Lithium promotes longevity through GSK3/NRF2-dependent hormesis. *Cell Rep.* (2016). <https://doi.org/10.1016/j.celrep.2016.03.041> (2016).
46. Sofola-Adesakin, O. et al. Lithium suppresses A β pathology by inhibiting translation in an adult Drosophila model of Alzheimer's disease. *Front. Aging Neurosci.* <https://doi.org/10.3389/fnagi.2014.00190> (2014).
47. Stambolic, V., Ruel, L. & Woodgett, J. R. Lithium inhibits glycogen synthase kinase-3 activity and mimics Wingless signalling in intact cells. *Curr. Biol.* [https://doi.org/10.1016/S0960-9822\(02\)70790-2](https://doi.org/10.1016/S0960-9822(02)70790-2) (1996)
48. Kelly, S. M., Elchert, A. & Kahl, M. Dissection and immunofluorescent staining of mushroom body and photoreceptor neurons in adult Drosophila melanogaster brains. *J. Vis. Exp.* **129**, 56174 (2017).
49. Givogri, M. I. et al. Multipotential neural precursors transplanted into the metachromatic leukodystrophy brain fail to generate oligodendrocytes but contribute to limit brain dysfunction. *Dev. Neurosci.* **30**, 340–357 (2008).
50. Adami, R. et al. Reduction of movement in neurological diseases: effects on neural stem cells characteristics. *Front. Neurosci.* **12**, 336 (2018).
51. Daniela, F., Vescovi, A. L. & Bottai, D. The stem cells as a potential treatment for neurodegeneration. *Methods Mol. Biol.* **399**, 199–213 (2007).
52. Hedgepeth, C. M. et al. Activation of the Wnt signaling pathway: a molecular mechanism for lithium action. *Dev. Biol.* **185**, 82–91 (1997).
53. Bottai, D., Madaschi, L., Di Giulio, A. M. & Gorio, A. Viability-dependent promoting action of adult neural precursors in spinal cord injury. *Mol. Med.* **14**, 634–644 (2008).
54. Gervasini, C. et al. Cornelia de Lange individuals with new and recurrent SMC1A mutations enhance delineation of mutation repertoire and phenotypic spectrum. *Am. J. Med. Genet. A* **161A**, 2909–2919 (2013).
55. Goodenough, S., Schäfer, M. & Behl, C. Estrogen-induced cell signalling in a cellular model of Alzheimer's disease. *J. Steroid Biochem. Mol. Biol.* **84**, 301–305 (2003).
56. Abu-Baker, A. et al. Lithium chloride attenuates cell death in oculopharyngeal muscular dystrophy by perturbing Wnt/ β -catenin pathway. *Cell Death Dis.* **4**, e821 (2013).
57. Naujok, O., Lentjes, J., Diekmann, U., Davenport, C. & Lenzen, S. Cytotoxicity and activation of the Wnt/ β -catenin pathway in mouse embryonic stem cells treated with four GSK3 inhibitors. *BMC Res. Notes* **7**, 273 (2014).
58. Rieger, M. E. et al. P300/ β -catenin interactions regulate adult progenitor cell differentiation downstream of WNT5a/protein kinase C (PKC). *J. Biol. Chem.* **291**, 6569–6582 (2016).
59. Pai, R., Tarnawski, A. S. & Tran, T. Deoxycholic acid activates β -catenin signaling pathway and increases colon cell cancer growth and invasiveness. *Mol. Biol. Cell* **15**, 2156–2163 (2004).
60. Gerdes, J. et al. Cell cycle analysis of a cell proliferation-associated human nuclear antigen defined by the monoclonal antibody Ki-67. *J. Immunol.* **133**, 1710–1715 (1984).

BRIEF REPORT

Dynamic acetylation profile during mammalian neurulation

Valentina Massa¹  | Laura Avagliano¹ | Paolo Grazioli¹  |
 Sandra C. P. De Castro² | Chiara Parodi¹ | Dawn Savery² | Patrizia Vergani³ |
 Serena Cuttin⁴ | Patrizia Doi¹ | Gaetano Bulfamante¹ | Andrew J. Copp²  |
 Nicholas D. E. Greene² 

¹Department of Health Sciences, University of Milan, Milan, Italy

²UCL Great Ormond Street Institute of Child Health, University College London, London, UK

³Department of Obstetrics and Gynaecology, Foundation MBBM, University of Milano-Bicocca, Monza, Italy

⁴Department of Pathology, San Gerardo Hospital, University of Milano-Bicocca, Monza, Italy

Correspondence

Valentina Massa, Dipartimento di Scienze della Salute, Università degli Studi di Milano, Via A. di Rudinì, 8, 20142 Milano, Italy.
 Email: valentina.massa@unimi.it

Funding information

Great Ormond Street Children's Charity; Medical Research Council, Grant/Award Number: G0802163; National Institute for Health Research Biomedical Research Centre; Università degli Studi di Milano intramural funds; Università degli Studi di Milano scholarship; Wellcome Trust, Grant/Award Number: 087525

Abstract

Background: Neural tube defects (NTDs) result from failure of neural tube closure during embryogenesis. These severe birth defects of the central nervous system include anencephaly and spina bifida, and affect 0.5–2 per 1,000 pregnancies worldwide in humans. It has been demonstrated that acetylation plays a pivotal role during neural tube closure, as animal models for defective histone acetyltransferase proteins display NTDs. Acetylation represents an important component of the complex network of posttranslational regulatory interactions, suggesting a possible fundamental role during primary neurulation events. This study aimed to assess protein acetylation contribution to early patterning of the central nervous system both in human and murine specimens.

Methods: We used both human and mouse (*Cited2*^{-/-}) samples to analyze the dynamic acetylation of proteins during embryo development through immunohistochemistry, western blot analysis and quantitative polymerase chain reaction.

Results: We report the dynamic profile of histone and protein acetylation status during neural tube closure. We also report a rescue effect in an animal model by chemical p53 inhibition.

Conclusions: Our data suggest that the p53-acetylation equilibrium may play a role in primary neurulation in mammals.

KEYWORDS

acetylation profile, *Cited2*, neural tube defects, neurodevelopment, p53

1 | INTRODUCTION

The neural tube is the embryonic precursor of the brain and spinal cord, and formation of this structure is a critical process in embryonic development. In humans, neural tube closure occurs during the third and fourth weeks

after conception. Neural tube defects (NTDs) arise if closure is not completed, and the neuroepithelium remains vulnerable to damage as it is not covered or protected. The most common open NTDs include anencephaly and spina bifida (Avagliano et al., 2018). Neurulation requires the coordinated function of many gene products, as

This is an open access article under the terms of the Creative Commons Attribution License, which permits use, distribution and reproduction in any medium, provided the original work is properly cited.

© 2019 The Authors. *Birth Defects Research* published by Wiley Periodicals, Inc.

revealed by the large number (more than 290) of genetic mouse mutant strains in which closure fails, resulting in NTDs (Copp, Greene, & Murdoch, 2003; Harris & Juriloff, 2007). Defects in mice closely parallel the corresponding severe birth defects in humans which affect 0.5–2 per 1,000 pregnancies (Greene & Copp, 2014; Wallingford, Niswander, Shaw, & Finnell, 2013). Although mouse mutants implicate a large number of genes in neural tube closure, the molecular basis of NTDs is not well understood in the majority of human cases.

Acetylation is a post-translational modification occurring on histones and non-histone proteins that is capable of regulating protein functions, localization, and stability (Narita, Weinert, & Choudhary, 2018). A potential requirement for acetylation in neural tube closure has been suggested by the observation of cranial NTDs in mouse embryos that carry even one null allele of *p300*, a transcriptional co-activator that has potent histone acetyltransferase (HAT) activity (Harris & Juriloff, 2007). Interestingly, NTDs also occur at high frequency in null embryos for *Cited2* (Barbera et al., 2002), a CBP/P300-interacting transactivator protein containing a Glu/Asp-rich C-terminal domain. Null embryos for the acetyltransferase gene *Gcn5*, die early in gestation with developmental delay and extensive apoptosis in mesodermal lineages (Bu, Evrard, Lozano, & Dent, 2007; Xu et al., 2000). Double mutants of *Gcn5* and *p53* survive longer and have reduced levels of apoptosis but they still do not develop to the stage of neural tube closure (Bu et al., 2007). A knock-in allele: *Gcn5^{hat}*, was generated which incorporates point mutations in the catalytic domain that result in specific ablation of HAT activity. Homozygous *Gcn5^{hat/hat}* embryos exhibit cranial NTDs, without growth retardation or excessive apoptosis (Lin et al., 2008). Thus, both decreased acetylation (HAT mutants) and increased acetylation (*Cited2*) might be associated with the development of NTDs. A possible role for disturbed acetylation in NTDs also arises from consideration of possible mechanisms underlying teratogenic effects of antiepileptic drugs such as valproic acid (VPA), whose use during pregnancy is a major risk factor for spinal NTDs in humans (Wlodarczyk, Palacios, George, & Finnell, 2012) and in animal models (Finnell, 1991; Hughes, Greene, Copp, & Galea, 2018). VPA has efficient histone deacetylase (HDAC) inhibitor activity, especially in embryonic tissue susceptible to its toxicity (Menegola et al., 2005).

In summary, acetylation represents an important component of the complex network of post-translational regulatory interactions. Evidence from mouse models indicates a possible fundamental role during primary neurulation events. It is assumed that acetylation also occurs during human development (Goodman & Smolik,

2000), but is not known whether this alters with stage or is affected in NTDs. In mice, the overall acetylation status during neurulation stages has not been evaluated. Hence, the aim of this study was to assess protein acetylation in the context of early development of the mouse and human central nervous system.

2 | MATERIALS AND METHODS

2.1 | Human samples

2.1.1 | Human cohort

Controls: formalin fixed, paraffin-embedded samples were obtained from four healthy Caucasian women undergoing legal termination of singleton pregnancy from 9 to 26 weeks of gestation (WG). Samples were obtained from archival tissues from the Unit of Human Pathology of the San Paolo Hospital Medical School, Milano, Italy. In this group, fetuses did not exhibit any malformations. The NTD case was from legal termination at 21 WG of a singleton pregnancy affected by spina bifida in a Caucasian woman with epilepsy who was treated with VPA. Termination of pregnancy occurred at Department of Obstetrics and Gynecology, Foundation MBBM, Monza, Italy.

2.1.2 | Immunohistochemistry

Immunohistochemistry was performed as previously described (Avagliano et al., 2016) on 5 μ m sections of paraffin-embedded tissue using a Ventana system (Ventana Medical Systems, Tucson, AZ) according to the manufacturer's instructions. The primary antibody was specific for acetyl-histone H4 (Acetyl-Histone H4 (Lys5) (D12B3) Rabbit mAb #8647, Cell Signaling). Staining was achieved using Ultraview Universal DAB detection kit (Ventana Medical Systems) and counterstained with hematoxylin. One fetus per stage was selected for this study. Slides were immunostained in the same batch to prevent technical variability and ensure identical conditions for comparison.

2.1.3 | Counting

Images were digitalized and captured using a NanoZoomer-XR Digital slide scanner (Hamamatsu, Japan). After scanning the entire section, five randomly selected fields of view per case and controls were photographed at $\times 20$ magnification and analyzed using ImageJ 1.47v software (Bethesda, MD). Images were calibrated

with a stage micrometer. H4 positive cells were calculated by counting within the five fields, by three operators blinded to experimental groups.

2.2 | Animal studies

2.2.1 | Animals

Animal studies were carried out under regulations of the Animals (Scientific Procedures) Act 1986 of the UK Government, and according to guidance issued by the Medical Research Council, United Kingdom, in Responsibility in the Use of Animals for Medical Research (July 1993). Random-bred CD1 mice were purchased from Charles River Laboratories, United Kingdom. *Cited2* mutant, heterozygous and corresponding wild-type embryos were obtained from four litters in each experimental group and genotyped as previously reported (Barbera et al., 2002). Animals were paired overnight and females checked for vaginal plugs the following morning, designated embryonic day (E) 0.5. Embryos were dissected from the uterus at desired developmental stages, morphologically assessed, somites counted for staging, and frozen at -80°C for further analyses. Pifithrin- α (Komarov et al., 1999) (2 mg/kg) or vehicle (PBS and saline) was administered by intraperitoneal (i.p.) injection at E7.5, E8.5, and E9.5.

2.2.2 | Western blot

Total proteins were extracted from embryos by standard procedures ($n = 3$ embryos per pool per genotype). Following protein quantification, equal amounts of quantified extracts were used for western blot analyses as previously described (de Castro et al., 2012) using antibodies against acetylated lysines (Acetylated-Lysine Antibody #9441, Cell Signaling) or acetylated-p53 (Acetyl-p53 [Lys379-specific for mouse] Antibody #2570, Cell Signaling). Positive bands were quantified, and analyses were performed using GraphPad.

2.2.3 | Quantitative polymerase chain reaction

RNA was extracted with TRIzol (Invitrogen, United Kingdom) as previously described (Fazio et al., 2017). First strand cDNA was synthesized using a Superscript first-strand Synthesis system (Invitrogen) following manufacturer's protocol. GreenER qPCR Supermix (Invitrogen) with Biotaq DNA polymerase (Bioline, United Kingdom)

was used for quantitative polymerase chain reaction (qPCR) analyses on a Fast System 7500 with SDS system software (Applied Biosystems). Primers used were:

p53_Left: GCTTCTCCGAAGACTGGATG

p53_Right: CTTCACTTGGGCCTTCAAAA

GAPDH_Left: ATGACATCAAGAAGGTGGTG

GAPDH_Right: CATACCAGGAAATGAGCTTG

2.2.4 | Data analysis

For human data, acetyl-histone H4 positive cells were counted as described and Mann-Whitney test was used to compare cases and controls. For animal studies, t test on qPCR data was applied. In both cases $p \leq 0.05$ was set as significant. GraphPad 6 software (San Diego, CA) and Photoshop (Adobe Photoshop CC) software were utilized for data analysis and figure preparation.

3 | RESULTS

To assess the overall histone acetylation profile during early human spinal cord development, immunohistochemical analysis was used to enable counting of acetylated-histone H4 positive cells. At 9 WG, many positive cells could be detected in the developing spinal cord (Figure 1a,b). The density of acetylated-histone H4 expressing cells decreased at 12 WG, and then remained constant until at least 26 WG (Figure 1a,b). An NTD-affected fetus (open spina bifida following VPA exposure, 21 WG) displayed a similar density of positive cells as controls of comparable developmental stages.

Neural tube closure events occur at earlier stages of development, 3–4 weeks, than in this group of human fetuses. Therefore, for an assessment of the acetylation profile during neurulation we turned to the mouse, in which the neurulation process is similar to humans. In wild-type embryos, global protein acetylation levels were compared, using an antibody to acetylated lysine, shortly after initiation of neural tube closure (E8.5), during cranial and upper spinal closure (E9.5), and during the final stages of closure when the low spine is formed (E10.5). This analysis showed a dynamic pattern (Figure 1c), with an overall increase of protein acetylation at E9.5. Intriguingly some protein bands (e.g., 50 K protein in Figure 1c) showed a distinct up-regulation of acetylation status at E9.5, showing a temporal correlation with neurulation events.

We asked whether the observed changes in acetyl-lysine staining are likely to reflect differential regulation of acetylation. For this analysis, we used *Cited2* mutants as a positive control. *Cited2* interacts with the known

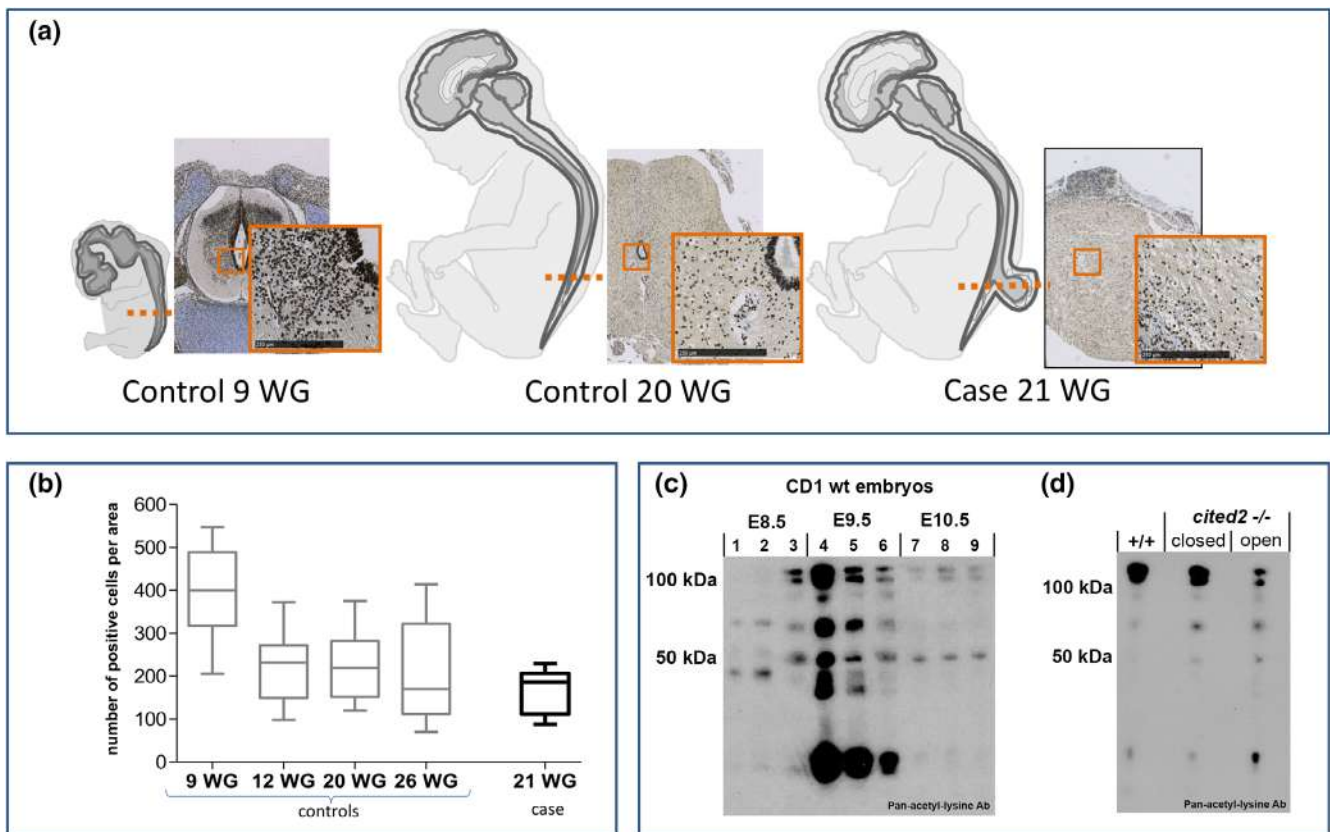


FIGURE 1 Acetylation status is dynamic during human and mouse neural tube development. (a) Cells staining for acetylated-histone H4 antibody are present in the normal developing human neural tube (Control), both at 9 and 20 WG. Note positive-staining cells also in the spinal cord of a 21 WG individual with spina bifida (Case). Bar represents 250 μm. The orange line represent the level of histological section (lumbar for all analyzed fetuses). (b) Quantification of acetylated-histone H4 staining: the median value is shown as a horizontal line inside the boxes; upper and lower limits of the boxes represent upper and lower quartiles, respectively; whiskers represent the maximum and minimum values. Among normal fetuses (controls), an early stage of gestation (9 WG) has a higher number of acetylated-histone H4 positive cells per unit area than stages from 12 WG onward. The fetus with spina bifida (case) shows a similar density of positive cells as unaffected individuals of a comparable stage. (c) Western blot demonstrates the dynamic acetylation profile of wild-type mouse embryos at different developmental stages. Note the band at 50 kDa which has a peak of expression intensity at E9.5. (d) The acetylation profile of wild-type and *Cited2*^{-/-} embryos without (closed) and with (open) exencephaly. A 50 kDa band is upregulated in *Cited2*^{-/-} embryos compared with wild-type, with particularly strong acetylation in mutants with open neural tube

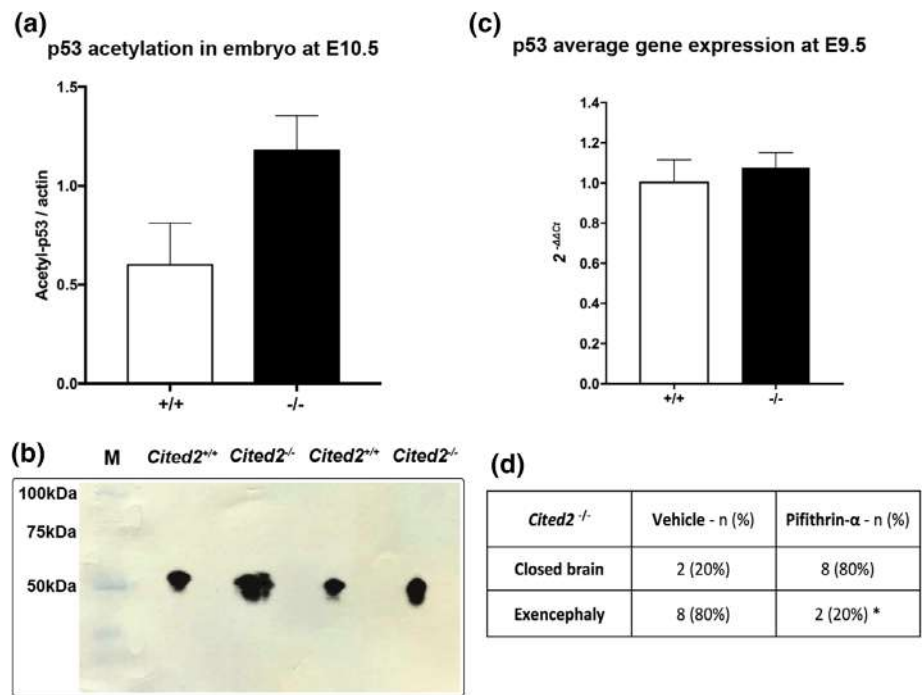
HAT, p300, hence we studied the acetylation profile of mouse embryos from litters carrying a loss-of-function mutation in *Cited2* (Bhattacharya et al., 1999). Embryo protein samples from E10.5 wild-type embryos were compared with those from littermate *Cited2* null embryos that were either unaffected (closed brain) or with an NTD (open brain; exencephaly). Intriguingly, a consistent difference in acetylation profile was observed in the three pools of embryos. In particular, a band at around 50 kDa, was absent from wild-type extracts, became visible in unaffected *Cited2*^{-/-} embryos, and appeared strongly acetylated in *Cited2*^{-/-} embryos in which neural tube closure had recently failed (Figure 1d).

Considering the importance of p53 in cell death and differentiation during embryonic development (Van Nostrand, Bowen, Vogel, Barna, & Attardi, 2017), and the

requirement for acetylation to prevent p53 degradation (Reed & Quelle, 2014), we explored the possibility that p53 is itself acetylated to a greater extent in affected *Cited2*^{-/-} mutants compared with wild-type embryos. Protein extracts from wild-type and affected *Cited2*^{-/-} embryos were used for western blot analysis of acetylated-p53 and, a 30% increase in normalized band intensity was found in mutant samples (Figure 2a). Analysis of *Trp53* mRNA abundance found no significant difference between wild-type, *Cited2*^{+/-} and *Cited2*^{-/-} embryos at E9.5 (Figure 2b), showing that p53 abundance was not misregulated at the transcriptional level. Hence, acetylated-p53 shows a specific increase in abundance in affected *Cited2* mutant embryos.

We explored the possible functional relevance of p53 activity in the causation of NTDs in this mouse model.

FIGURE 2 p53 acetylation contribution to the *Cited2*^{-/-} NTD phenotype. (a) Quantification of acetylated p53, normalized to actin expression, shows an increase in affected *Cited2*^{-/-} embryos (three embryos per pool per genotype were used. Three replicates were performed). Bars show standard deviation. (b) Relative western blot analysis of acetylated p53. (c) In contrast, total p53 gene expression (qPCR) does not differ between *Cited2* genotypes at E9.5. (d) Chemical inhibition of p53 activity using pifithrin- α results in a significant decrease in the frequency of NTDs in *Cited2*^{-/-} embryos (Fisher's exact test: * $p = 0.023$)



Pregnant *Cited2*^{+/-} females were treated by i.p. injection either with vehicle (PBS and saline) or with a chemical compound known to selectively inhibit p53 activity (pifithrin- α) at three time-points (E7.5, E8.5, and E9.5). On morphological evaluation of litters at E10.5, pifithrin- α treatment was found to result in a significant reduction in the frequency of NTDs in *Cited2*^{-/-} embryos. Hence, while 80% of control mutant embryos had exencephaly, only 20% of pifithrin- α treated mutants had such defects ($p < 0.05$). This experiment suggests a direct role of increased p53 function in the development of NTDs in *Cited2* mutants which we hypothesize to be mediated through altered acetylation.

4 | DISCUSSION

In contrast to N-terminal acetylation, which occurs co-translationally on most proteins, selected proteins are also subject to post-translational acetylation of specific lysine residues. The lysine acetylation status of specific proteins depends on a finely tuned equilibrium between histone acetylases (HATs), which catalyze acetylation, and HDACs, which remove acetyl groups (Glozak, Sengupta, Zhang, & Seto, 2005).

Exposure of neurulation-stage mouse embryos to pharmacological inhibitors of HDACs, such as VPA and trichostatin A (TSA), can cause NTDs as well as skeletal defects (Finnell, Waes, Eudy, & Rosenquist, 2002). Pivotal work in chick embryos in vivo demonstrated that TSA treatment induces NTDs with a complete failure of

neural tube closure, accompanied by morphological modifications in neuroepithelial cells and induction of apoptosis (Murko et al., 2013). In previous studies, microarray approaches were used to analyze gene expression alterations in somitic tissues of mouse embryos following VPA exposure (Massa, Cabrera, Menegola, Giavini, & Finnell, 2005). Cluster analysis showed major misregulation of expression in the HDAC ontology group, suggesting a possible role in the subsequent skeletal defects. Modulation of acetylation was hypothesized to mediate the effect of VPA on neurulation, and accordingly increased acetylation of histone H4 in the caudal neural tube was found (Menegola et al., 2005).

Considering the potential clinical relevance of altered acetylation in NTDs and skeletal development, we sought to ascertain the relevance of protein acetylation during spinal cord development in human and mouse embryos. Using different experimental approaches, our study shows a dynamic profile of protein acetylation during the stages of nervous system development in both humans and mice. We also found p53-acetylation levels to be abnormal in a mouse NTD model, the *Cited2* gene knock-out, in which occurrence of NTDs is associated with increased acetylation. p53 was the first nonhistone protein to be shown to be subjected to acetylation modification by HATs and HDACs, with important effects on its stability and consequently on its transcriptional activity (Brooks & Gu, 2011). Importantly, our data are in line with a report of shRNA-mediated knock-down of CITED2, resulting in increased acetylated-p53 in human cancer cells (Wu, Sun, & Chao, 2011). Notably, rescue of

the adverse effects of Cited2 loss of function was observed following pifithrin- α -mediated inhibition of p53 activity, suggesting a direct role for p53 in causing the exencephaly observed in this model. In conclusion, this study reports a dynamic profile of histone and protein acetylation during CNS development and suggests p53-acetylation equilibrium as fundamental for primary neurulation in mammals.

ACKNOWLEDGMENTS

The project was funded by the Medical Research Council (G0802163 to NG, AC) and Wellcome Trust (087525 to AC, NG). NG and AC are supported by Great Ormond Street Children's Charity. Research was supported by the National Institute for Health Research Biomedical Research Centre at Great Ormond Street Hospital for Children NHS Foundation Trust and University College London. This work was also supported by intramural funds from Università degli Studi di Milano (V.M), Molecular and Translational Medicine PhD-Università degli Studi di Milano scholarship (to P.G.); Translational Medicine PhD-Università degli Studi di Milano scholarship (to C.P.)

CONFLICT OF INTEREST

The authors declare no conflict of interest.

DATA AVAILABILITY STATEMENT

Data sharing is not applicable to this article as no new data were created or analyzed.

ORCID

Valentina Massa  <https://orcid.org/0000-0003-2246-9515>

Paolo Grazioli  <https://orcid.org/0000-0001-9120-4217>

Andrew J. Copp  <https://orcid.org/0000-0002-2544-9117>

Nicholas D. E. Greene  <https://orcid.org/0000-0002-4170-5248>

REFERENCES

- Avagliano, L., Doi, P., Tosi, D., Scagliotti, V., Gualtieri, A., Gaston-Massuet, C., ... Massa, V. (2016). Cell death and cell proliferation in human spina bifida. *Birth Defects Research Part A: Clinical and Molecular Teratology*, 106, 104–113. <https://doi.org/10.1002/bdra.23466>
- Avagliano, L., Massa, V., George, T. M., Qureshy, S., Bulfamante, G. P., & Finnell, R. H. (2018). Overview on neural tube defects: From development to physical characteristics. *Birth Defects Research*, 1–13. <https://doi.org/10.1002/bdr2.1380>
- Barbera, J. P. M., Rodriguez, T. A., Greene, N. D. E., Weninger, W. J., Simeone, A., Copp, A. J., ... Dunwoodie, S. (2002). Folic acid prevents exencephaly in Cited2 deficient mice. *Human Molecular Genetics*, 11, 283–293. <https://doi.org/10.1093/hmg/11.3.283>
- Bhattacharya, S., Michels, C. L., Leung, M. K., Arany, Z. P., Kung, A. L., & Livingston, D. M. (1999). Functional role of p35srj, a novel p300/CBP binding protein, during transactivation by HIF-1. *Genes & Development*, 13, 64–75. <https://doi.org/10.1101/gad.13.1.64>
- Brooks, C. L., & Gu, W. (2011). The impact of acetylation and deacetylation on the p53 pathway. *Protein & Cell*, 2, 456–462. <https://doi.org/10.1007/s13238-011-1063-9>
- Bu, P., Evrard, Y. A., Lozano, G., & Dent, S. Y. R. (2007). Loss of Gcn5 Acetyltransferase activity leads to neural tube closure defects and Exencephaly in mouse embryos. *Molecular and Cellular Biology*, 27, 3405–3416. <https://doi.org/10.1128/MCB.00066-07>
- Copp, A. J., Greene, N. D. E., & Murdoch, J. N. (2003). The genetic basis of mammalian neurulation. *Nature Reviews. Genetics*, 4, 784–793. <https://doi.org/10.1038/nrg1181>
- de Castro, S. C. P., Malhas, A., Leung, K. Y., Gustavsson, P., Vaux, D. J., Copp, A. J., & Greene, N. D. E. (2012). Lamin b1 polymorphism influences morphology of the nuclear envelope, cell cycle progression, and risk of neural tube defects in mice. *PLoS Genetics*, 8, e1003059. <https://doi.org/10.1371/journal.pgen.1003059>
- Fazio, G., Bettini, L. R., Rigamonti, S., Meta, D., Biondi, A., Cazzaniga, G., ... Massa, V. (2017). Impairment of retinoic acid Signaling in Cornelia de Lange syndrome fibroblasts. *Birth Defects Research*, 109, 1–9. <https://doi.org/10.1002/bdr2.1070>
- Finnell, R. H. (1991). Genetic differences in susceptibility to anti-convulsant drug-induced developmental defects. *Pharmacology & Toxicology*, 69, 223–227. <https://doi.org/10.1111/bcpt.1991.69.4.223>
- Finnell, R. H., Waes, J. G., Eudy, J. D., & Rosenquist, T. H. (2002). Molecular basis of environmentally induced birth defects. *Annual Review of Pharmacology and Toxicology*, 42, 181–208. <https://doi.org/10.1146/annurev.pharmtox.42.083001.110955>
- Glozak, M. A., Sengupta, N., Zhang, X., & Seto, E. (2005). Acetylation and deacetylation of non-histone proteins. *Gene*, 363, 15–23. <https://doi.org/10.1016/j.gene.2005.09.010>
- Goodman, R. H., & Smolik, S. (2000). CBP/p300 in cell growth, transformation, and development. *Genes & Development*, 14, 1553–1577.
- Greene, N. D. E., & Copp, A. J. (2014). Neural tube defects. *Annual Review of Neuroscience*, 37, 221–242. <https://doi.org/10.1016/B978-0-12-385157-4.01049-6>
- Harris, M. J., & Juriloff, D. M. (2007). Mouse mutants with neural tube closure defects and their role in understanding human neural tube defects. *Birth Defects Research Part A: Clinical and Molecular Teratology*, 79, 187–210. <https://doi.org/10.1002/bdra.20333>
- Hughes, A., Greene, N. D. E., Copp, A. J., & Galea, G. L. (2018). Valproic acid disrupts the biomechanics of late spinal neural tube closure in mouse embryos. *Mechanisms of Development*, 149, 20–26. <https://doi.org/10.1016/j.mod.2017.12.001>
- Komarov, P. G., Komarova, E. A., Kondratov, R. V., Christov-Tselkov, K., Coon, J. S., Chernov, M. V., & Gudkov, A. V. (1999). A chemical inhibitor of p53 that protects mice from the side effects of cancer therapy. *Science (80-)*, 285, 1733–1737. <https://doi.org/10.1126/science.285.5434.1733>
- Lin, W., Zhang, Z., Srajer, G., Yi, C. C., Huang, M., Phan, H. M., & Dent, S. Y. R. (2008). Proper expression of the Gcn5 histone

- acetyltransferase is required for neural tube closure in mouse embryos. *Developmental Dynamics*, 237, 928–940. <https://doi.org/10.1002/dvdy.21479>
- Massa, V., Cabrera, R. M., Menegola, E., Giavini, E., & Finnell, R. H. (2005). Valproic acid-induced skeletal malformations: Associated gene expression cascades. *Pharmacogenetics and Genomics*, 15, 787–800. <https://doi.org/10.1097/01.fpc.0000170914.11898.3a>
- Menegola, E., Di Renzo, F., Broccia, M. L., Prudenziati, M., Minucci, S., Massa, V., & Giavini, E. (2005). Inhibition of histone deacetylase activity on specific embryonic tissues as a new mechanism for teratogenicity. *Birth Defects Research Part A: Clinical and Molecular Teratology*, 74, 392–398. <https://doi.org/10.1002/bdrb.20053>
- Murko, C., Lagger, S., Steiner, M., Seiser, C., Schofer, C., & Pusch, O. (2013). Histone deacetylase inhibitor Trichostatin A induces neural tube defects and promotes neural crest specification in the chicken neural tube. *Differentiation*, 85, 55–66. <https://doi.org/10.1016/j.diff.2012.12.001>
- Narita, T., Weinert, B. T., & Choudhary, C. (2018). Functions and mechanisms of non-histone protein acetylation. *Nature Reviews. Molecular Cell Biology*, 20, 156–174. <https://doi.org/10.1038/s41580-018-0081-3>
- Reed, S. M., & Quelle, D. E. (2014). P53 acetylation: Regulation and consequences. *Cancers (Basel)*, 7, 30–69. <https://doi.org/10.3390/cancers7010030>
- Van Nostrand, J. L., Bowen, M. E., Vogel, H., Barna, M., & Attardi, L. D. (2017). The p53 family members have distinct roles during mammalian embryonic development. *Cell Death and Differentiation*, 24, 575–579. <https://doi.org/10.1038/cdd.2016.128>
- Wallingford, J. B., Niswander, L. A., Shaw, G. M., & Finnell, R. H. (2013). The continuing challenge of understanding, preventing, and treating neural tube defects. *Science (80-)*, 339, 1222002–1–1222002–7. <https://doi.org/10.1126/science.1222002>
- Wlodarczyk, B. J., Palacios, A. M., George, T. M., & Finnell, R. H. (2012). Antiepileptic drugs and pregnancy outcomes. *American Journal of Medical Genetics - Part A*, 158A, 2071–2090. <https://doi.org/10.1002/ajmg.a.35438>
- Wu, Z. Z., Sun, N. K., & Chao, C. C. K. (2011). Knockdown of CITED2 using short-hairpin RNA sensitizes cancer cells to cisplatin through stabilization of p53 and enhancement of p53-dependent apoptosis. *Journal of Cellular Physiology*, 226, 2415–2428. <https://doi.org/10.1002/jcp.22589>
- Xu, W., Edmondson, D. G., Evrard, Y. a., Wakamiya, M., Behringer, R. R., & Roth, S. Y. (2000). Loss of Gcn5l2 leads to increased apoptosis and mesodermal defects during mouse development. *Nat. Genet*, 26, 229–232. <https://doi.org/10.1038/79973>


SUPPORTING INFORMATION

Additional supporting information may be found online in the Supporting Information section at the end of this article.

How to cite this article: Massa V, Avagliano L, Grazioli P, et al. Dynamic acetylation profile during mammalian neurulation. *Birth Defects Research*. 2019;1–7. <https://doi.org/10.1002/bdr2.1618>

REVIEW

Chromatinopathies: A focus on Cornelia de Lange syndrome

Laura Avagliano¹ | Ilaria Parenti^{2,3} | Paolo Grazioli¹  | Elisabetta Di Fede¹ |
 Chiara Parodi¹ | Milena Mariani⁴ | Frank J. Kaiser^{2,5,6} | Angelo Selicorni⁴ |
 Cristina Gervasini^{1†} | Valentina Massa^{1†}

¹Department of Health Sciences, Università degli Studi di Milano, Milano, Italy

²Section for Functional Genetics, Institute of Human Genetics, University of Lübeck, Lübeck, Germany

³Institute of Science and Technology (IST) Austria, Klosterneuburg, Austria

⁴UOC Pediatria, ASST Lariana, Como, Italy

⁵DZHK e.V. (German Center for Cardiovascular Research), Partner Site Hamburg/Kiel/Lübeck, Lübeck, Germany

⁶Institut für Humangenetik, Universitätsklinikum Essen, Universität Duisburg-Essen, Essen, Germany

Correspondence

Laura Avagliano, Department of Health Sciences, Università degli Studi di Milano, Via Antonio di Rudini, 8, Milano 20142, Italy.
 Email: laura.avagliano@unimi.it

Funding information

Dipartimento DiSS, Università degli Studi di Milano, Grant/Award Number: Linea 2; Fondazione Cariplo, Grant/Award Number: 2015-0783; German Federal Ministry of Education and Research (BMBF), Grant/Award Number: CHROMATIN-Net; Medical Faculty of the University of Lübeck, Grant/Award Number: J09-2017; Nickel & Co S.p.A.; Università degli Studi di Milano, Grant/Award Numbers: Molecular & Translational Medicine PhD Scholarship, Translational Medicine PhD Scholarship

Peer Review

The peer review history for this article is available at <https://publons.com/publon/10.1111/cge.13674>.

Abstract

In recent years, many genes have been associated with chromatinopathies classified as “Cornelia de Lange Syndrome-like.” It is known that the phenotype of these patients becomes less recognizable, overlapping to features characteristic of other syndromes caused by genetic variants affecting different regulators of chromatin structure and function. Therefore, Cornelia de Lange syndrome diagnosis might be arduous due to the seldom discordance between unexpected molecular diagnosis and clinical evaluation. Here, we review the molecular features of Cornelia de Lange syndrome, supporting the hypothesis that “CdLS-like syndromes” are part of a larger “rare disease family” sharing multiple clinical features and common disrupted molecular pathways.

KEYWORDS

chromatin disorders, cohesinopathies, Cornelia de Lange syndrome, genotype-phenotype relationship

1 | INTRODUCTION

Cornelia de Lange syndrome (CdLS, OMIM #122470, #300590, #610759, #614701, #300882) is a rare and clinically variable

syndrome manifesting with developmental disability, growth impairment, multi-organ abnormalities (including limb anomalies, congenital heart defects, gastrointestinal dysfunction and neurodevelopmental alterations) and typical facial dysmorphisms (such as hirsute forehead, arched eyebrows with synophrys, short nose with depressed nasal bridge, anteverted nares, long and smooth philtrum, thin lips,

[†]Cristina Gervasini and Valentina Massa contributed equally to this study.

TABLE 1 Relationship between CdLS genes and function for the cohesin complex

Gene	Affected patients (%)	Locus	Genetic variants	Relationship with cohesin complex	Phenotype
<i>NIPBL</i>	85	5p13.2	Out-of-frame deletions or insertions, missense, nonsense, and splicing mutations The higher severity of clinical feature is more frequently associated with loss-of-function gene variants than missense variants Microdeletions or intragenic exon deletions have been identified in a minority of cases (approximately in 3%) Cases of mosaic <i>NIPBL</i> variants have been also reported	Cohesin loader	Usually classical phenotype
<i>SMC1A</i>	5	Xp11	Missense mutations or in-frame deletions Mosaic <i>SMC1A</i> variants have been reported A mosaic <i>SMC1A</i> variant was also reported in individual without symptoms or signs of CdLS (parent of affected baby)	Member of the structural maintenance of chromosome (SMC) family that acts to form a ring-like structure that is responsible for holding sister chromatids together Together with <i>SMC3</i> constitute the heterodimer that represents the core of the cohesin complex	Mainly non-classical CdLS phenotype: fuller eyebrows, nasal bridge with less striking shortening and a rounder face than cases with <i>NIPBL</i> variants
<i>SMC3</i>	<1	10q25.2	Missense variants, in-frame deletions	Member of the SMC family that acts to form a ring-like structure that is responsible for holding sister chromatids together Together with <i>SMC1A</i> constitute the heterodimer that represents the core of the cohesin complex	<i>SMC3</i> variants are rare and have been associated to patients with intellectual disability, short stature and congenital anomalies, with a high frequency of heart defects Frequently patients do not fulfill CdLS diagnostic criteria
<i>RAD21</i>	<1	8q24.11	Truncating, missense variants and intragenic deletions	Determines the closure of the cohesin ring by bridging the head domains of the SMC proteins	Rare patients Generally non-classical CdLS phenotype, with significantly milder cognitive impairment and skeletal anomalies
<i>HDAC8</i>	5	Xq13.1	Missense, nonsense, deletions and splice-site variants	Permits correct dissolution of pro-cohesive elements and allows recycling of "refreshed" cohesin for the following cell cycle	Mainly non-classical (frequently showing large anterior fontanel, and hypertelorism, widely spaced teeth) Female carriers can be either affected or completely healthy, depending on X inactivation

Abbreviation: CdLS, Cornelia de Lange syndrome.

downwards turning corners of the mouth).^{1,2} According to the recently published international *consensus* statement, “CdLS-spectrum” includes the classical and non-classical phenotype caused by pathogenic variants in genes encoding the cohesin complex and its interactors.³

Genetically, CdLS is a cohesinopathy disorder caused by autosomal heterozygous or X-linked mutations in the cohesin core subunits *SMC1A*, *SMC3*, *RAD21*, or in the cohesin-associated factors *NIPBL* and *HDAC8*.⁴⁻⁸

Cohesin is a chromatin-associated multi-subunit protein complex, highly conserved during evolution and involved in several aspects of chromosome biology⁹: cohesin is involved in chromatids cohesion, fundamental for a correct mitosis.¹⁰ Sister chromatid cohesion is also pivotal both for DNA recombinational repair^{11,12} and for correct distribution of chromosomes upon cell division.^{13,14}

In addition to its canonical role, this complex acts as one of the many players involved in transcriptional regulation. In fact, the cohesin complex is important in controlling gene expression together with tissue specific transcription factors and/or in combination with the CCCTC-binding factor (CTCF) insulator protein,¹⁵ although mostly indirectly through chromatin organization and architecture control.^{16,17}

In particular, *SMC1*, *SMC3*, *RAD21* and *STAG1/STAG2* (or *STAG3* in germ cells) assemble to form a structure, defined as ring-shaped, for

holding sister chromatids together.¹⁸ *NIPBL* is implicated in loading the cohesin complex onto chromatin during S-phase, G1 and G2.¹⁹ *HDAC8* regulates the deacetylation of *SMC3* following its removal from chromatin in both prophase and anaphase pathways to permit correct dissolution of pro-cohesive elements and allowing for recycling of “refreshed” cohesin for the following cell cycle⁸ (see Table 1).

Interestingly, cells from CdLS patients do not display sister chromatid cohesion defects²⁰ suggesting that the pathogenesis of CdLS may not be directly linked to the disruption of sister chromatid cohesion but to inability of the complex to regulate other cellular functions such as gene-expression regulation.²¹

The aim of this review is to summarize the relationship between CdLS and these alterations, focusing on chromatin dysregulation pathways.

2 | CHROMATIN REGULATION AND CdLS: CLINICAL AND GENETIC FEATURES

Almost 20 years ago, before precise molecular confirmation, it has been hypothesized that CdLS was a developmental disorder resulting

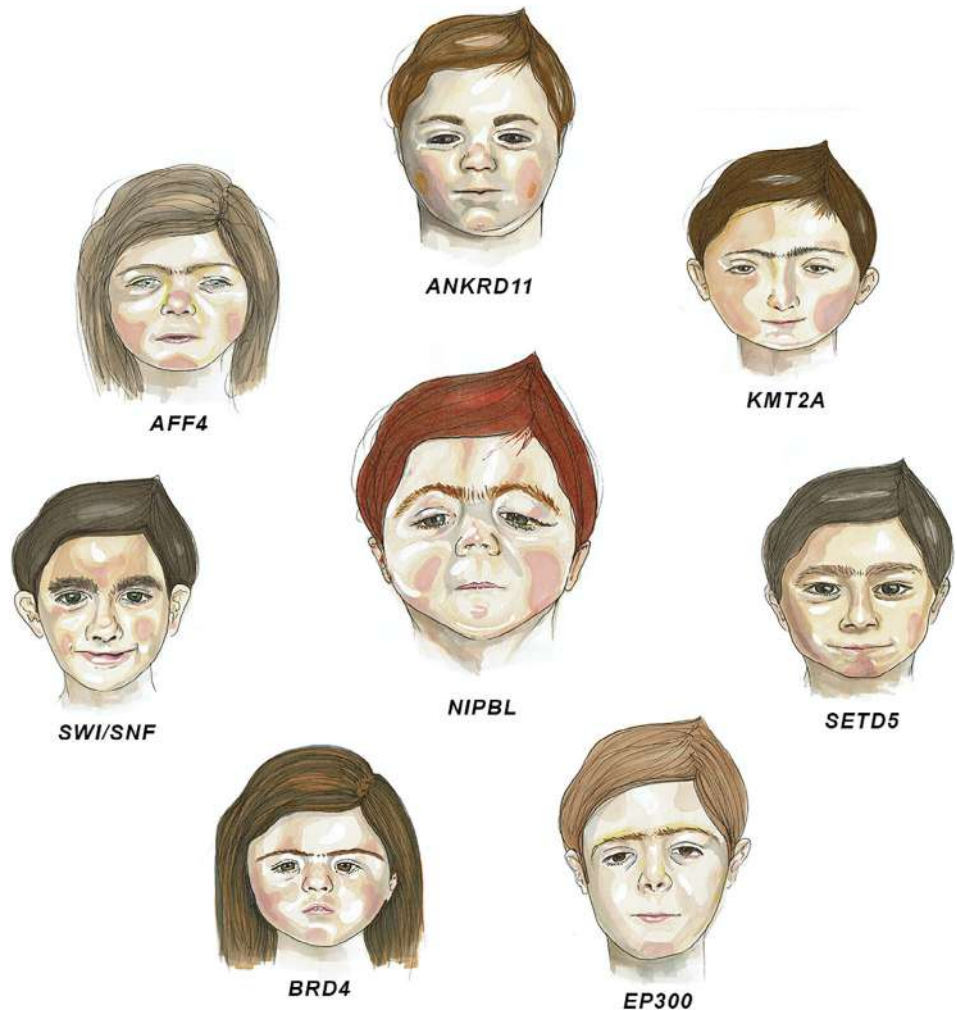


FIGURE 1 Classical facial dysmorphisms of CdLS and related overlapping syndromes. Patient's representation in the middle of the figure displays typical CdLS phenotype with mutations in *NIPBL* (representative of classic CdLS dysmorphisms); all the other patients' representations surrounding *NIPBL* display all the related phenotypic variants that overlap with the classic CdLS: *AFF4*,³² *ANKRD11*,³³ *KMT2A*,³⁰ *SETD5*,³⁰ *EP300*,³¹ *BRD4*,³⁶ *SWI/SNF*.³⁰ CdLS, Cornelia de Lange syndrome [Colour figure can be viewed at wileyonlinelibrary.com]

TABLE 2 CdLS-like phenotype associated with “non-canonical” CdLS genes mutations (each reported case may show all or just some of the reported phenotypic features)

Gene	Anthropometric measures	Head circumference and intellectual development	Facial dysmorphism	Limb abnormalities	Other clinical issues	References
AFF4	Short stature Obesity	Sometimes microcephaly, intellectual disabilities	Coarse face: thick eyebrows, synophrys, long eyelashes, short nose, anteverted nostril, long philtrum	Brachydactyly	Pulmonary involvement	Izumi et al ³²
ANKRD11	Short stature and low weight	Microcephaly, intellectual disabilities, autistic spectrum disorder, self-injurious behavior	Severe atypical facial gestalt (not better specified) broad and arched eyebrows, synophrys, down-slanting palpebral fissures, anteverted nares, prominent nasal bridge, long philtrum, thin lips with downturned corners of the mouth, micrognathia, macrodontia	Unreported; mild brachydactyly, proximally set thumbs, clinodactyly of the fifth finger	Vertebral anomalies	Parenti et al ³³ and Ansari et al ³⁴
BRD4	Short stature	Microcephaly, intellectual disability, self-injurious behavior	Arched, thick eyebrows, synophrys, long eyelashes, depressed nasal bridge, anteverted nostrils, long, smooth philtrum, thin upper vermillion, downturned corners of the mouth, micrognathia	Small hands, proximally placed thumbs, clinodactyly or short fifth finger	Cardiovascular anomalies, no hirsutism	Olley et al ³⁶
EP300	Sometimes short stature	Microcephaly, intellectual disabilities	Down-slanted palpebral fissures, thick arched eyebrows, long eyelashes, convex nasal ridge, short upper lip, pointing lower lip, retrognathia	Broad thumbs and halluces		Woods et al ³¹
KMT2A	Short stature and low weight	Microcephaly, CNS abnormalities, intellectual disabilities	Arched eyebrows, thick eyebrows, synophrys, long eyelashes, depressed nasal bridge, broad nasal tip, long and smooth philtrum, thin upper vermilum	Clinodactyly fifth finger, syndactyly of toes, small hands and feet	Hypertrichosis cubiti, back hypertrichosis	Yuan et al ²⁹ and Parenti et al ³⁰
SETD5	Short stature and low weight	Intellectual disabilities	Arched eyebrows (not always), thick eyebrows, synophrys (not always), long eyelashes (not always), depressed nasal bridge (not always), broad nasal tip (not always), long and smooth philtrum, thin upper vermilum (not always)	Unreported		Parenti et al ³⁰
SWI/SNF complex genes	Short stature and low weight	Microcephaly, CNS abnormalities, intellectual disabilities	Arched eyebrows, thick eyebrows, synophrys, long eyelashes, depressed nasal bridge, anteverted nostril, broad nasal tip, smooth philtrum, thin upper vermilum, thick lower vermilum	Clinodactyly fifth finger (not always), syndactyly of toes, small hands and feet (not always)		Parenti et al ³⁰

Abbreviation: CdLS, Cornelia de Lange syndrome.

from defective expression of a multi-functional protein involved in chromosome function, gene regulation and double-strand DNA repair.²²

More recently, in the post human genome era, CdLS has been categorized as a “cohesinopathy.” According to the concept that the cohesin complex functions in sister chromatid cohesion, and also plays a role in the regulation of gene expression, it has been suggested that the five aforementioned genes associated with CdLS are involved in transcriptional regulation^{8,23-28} and structural maintenance of chromatin.

Moreover, multiple next-generation sequencing (NGS) technologies identified mutations in key chromatin-associated factors, genetically different from cohesin, in patients presenting features of CdLS or CdLS-like phenotype. These mutations affect genes coding for methyltransferases such as *KMT2A*,²⁹ for subunits of the chromatin-remodeler SWI/SNF complex³⁰ and for transcriptional regulators such as *EP300*, *AFF4*, *ANKRD11*, *SETD5*²⁹⁻³⁵ or the Bromodomain-containing protein 4 *BRD4* gene, encoding a chromatin-associated protein.^{3,36} In Figure 1 the facial dysmorphisms associated with the genes mentioned above are shown and clinical features associated with mutations in these genes are summarized in Table 2.

Applying NGS techniques, new genetic variants have also been associated to CdLS phenotypes: a homozygous *TAF6* variant was found in patients with clinical features overlapping with those of CdLS,²⁹ whereas a variant in *NAA10* was reported in a patient with periorbital region features comparable to individuals with CdLS.³⁷

In this review, genes recently described associated to CdLS phenotype are described.

2.1 | *AFF4*

AFF4 is a scaffold protein comprising the core component of the super elongation complex. Gain-of-function missense mutations in *AFF4* create a resistance to ubiquitination-dependent proteasomal degradation, resulting in the accumulation of excessive amounts of mutant *AFF4* protein³² leading to increased transcriptional activation,³² as observed in patients with CHOPS syndrome (cognitive impairment and coarse facies, heart defects, obesity, pulmonary involvement short stature and skeletal dysplasia, OMIM #616368).³² Patients with CHOPS or CdLS display a similar disruption in RNAP2 (RNA polymerase II) distribution,³² suggesting a common molecular pathogenesis for both conditions. Such impairment leads to disturbance of transcriptional elongation and consequent gene-expression alterations.

2.2 | *ANKRD11*

ANKRD11 mutations have been originally reported as cause of KBG syndrome (OMIM #148050). *ANKRD11* codes for the ankyrin repeat-containing protein 11, also known as ankyrin repeat-containing co-factor 1 (ANCO-1).^{38,39} This protein recruits the histone deacetylases HDAC3, HDAC4 and HDAC5, leading to transcriptional silencing of

nuclear receptors targets.^{38,39} Heterozygous loss-of-function mutations in *ANKRD11* have been identified by exome-sequencing approaches in CdLS-like patients.^{33,34} Similar to the cohesin complex, also *ANKRD11* is involved in transcriptional regulation, mediating both its activation and repression. It is therefore licit to hypothesize that dysregulation of functionally interconnected genes regulated by the cohesin complex or *ANKRD11* leads to overlapping phenotypical features.³³

2.3 | *BRD4*

Recently, *BRD4* variants have been reported in patients with clinical features of CdLS.³⁶ Recently, a study reported overlap of gene-expression regulation between *NIPBL* and *BRD4*, consequence of promoters co-occupancy.⁴⁰ Both *BRD4* and cohesin are known to bind super-enhancer regions, controlling cell fate decision, hence a role of super-enhancers function has been postulated in the pathogenesis of CdLS. Overlapping features between the facial phenotype of CdLS patients with canonical mutations and patients with mutation associated with “chromatin dysregulation disorders” are shown in Figure 1.

2.4 | *EP300*

EP300 mutations are generally associated with Rubinstein-Taybi syndrome (RSTS, OMIM #180849, #613684). *EP300* coded protein (p300) has a histone acetyltransferase domain involved in chromatin remodeling and acts as transcription co-factor by bridging transcription factors and intergenic RNA polymerase II.⁴¹ Therefore p300 is involved in the regulation of genes important for embryonic development, cell growth and cellular differentiation.³¹ A possible association between *EP300* and known genes causative of CdLS has been suggested: both p300 and HDAC8 control p53 transcriptional activity.^{42,43} Moreover, p300 and other chromatin-associated proteins, including *NIPBL*, *SMC1A*, and *SMC3*, have been found at enhancer regions in different cell types although further studies needed to clarify their interaction.⁴⁴ It is therefore possible to hypothesize that *EP300* and canonical CdLS-related genes are part of a common gene network/pathway and, accordingly, alterations in the expression of specific genes will result in superimposable phenotypic features.³⁴

2.5 | *KMT2A*

KMT2A is one of the most frequently mutated gene in patients with non-syndromic intellectual disability. In addition, genetic variants in *KMT2A* can also cause Wiedemann-Steiner syndrome (WDSTS, OMIM #605130).⁴⁵ With the establishment and application of exome sequencing and other NGS in molecular diagnostics the number of identified pathogenic variants in *KMT2A* is rapidly increasing.⁴⁶⁻⁴⁸ *KMT2A* is a histone methyltransferase that preferentially targets histone H3 lysine 4, known to play fundamental role in controlling transcription with direct effects on embryogenesis and cell-cycle progression.²⁹ The clinical findings of CdLS observed in patients with

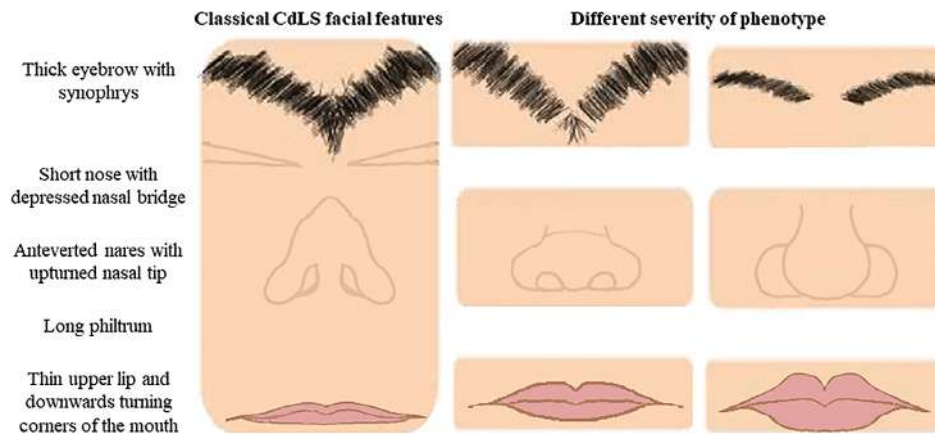


FIGURE 2 Five major CdLS facial features and their different severity. Classical facial features characteristic of Cornelia de Lange syndrome are shown on the left and include thick eyebrows that meet in the midline (called synophrys), depressed nasal ridge with a short nose and upturned nasal tip, a long and smooth philtrum, a thin upper lip vermilion and downturned corners of the mouth. Variants of this classical phenotype are shown on the right, from mild to little features. Indeed, clinical diagnosis of Cornelia de Lange syndrome based on facial features may be challenging due to different degree of manifestation. CdLS, Cornelia de Lange syndrome [Colour figure can be viewed at wileyonlinelibrary.com]

KMT2A mutations suggest that *KMT2A* may potentially contribute to the phenotypic expansion of CdLS.²⁹

2.6 | *SETD5*

SETD5 loss-of-function mutations have been shown to cause both syndromic and non-syndromic intellectual disability and haploinsufficiency of *SETD5* is thought to be the main cause of the clinical manifestation in 3p25 microdeletion syndrome (MRD23, OMIM #615761).^{49–54} *SETD5* is a chromatin-regulatory protein involved in transcriptional regulation. In the pioneer work by Parenti and colleagues, the two described patients showed some CdLS classical features combined with typical *SETD5* phenotypical presentation (ie, intellectual disability, short stature, microcephaly, hypotonia and heart defects⁵⁴), opening the possibility of a wider clinical presentation of CdLS patients with variants in *SETD5*.³⁰

2.7 | *SWI/SNF* complex

The chromatin-remodeler SWI/SNF complex, a conserved nucleosome remodeler, is generally involved in Coffin-Siris syndrome (CSS, OMIM #135900) and Nicolaides-Baraitser syndrome (NCBRS, OMIM #601358). SWI/SNF complex presents functions overlapping to those of cohesins^{55,56} such as transcriptional regulation, chromatin remodeling and epigenetic modifications.⁵⁷ Moreover, in yeast, a direct functional interaction between the cohesin loader NIPBL and the SWI/SNF complex has been observed,⁵⁷ where the SWI/SNF complex recruits NIPBL for maintaining chromatin in an open and active state. These observations suggest a combined role of cohesin and SWI/SNF complex in regulating the expression of common target genes and/or genomic regulatory elements leading to CdLS or CdLS-like phenotype. Four patients have been described with mutations in *SMARCB1* and *ARID1B* encoding subunits of the SWI/SNF complex²⁸ presenting

several CdLS-like features, such as typical facial dysmorphisms, growth delay, intellectual disability and three out of four showing limb abnormalities.

2.8 | CdLS as an endo-phenotype of chromatinopathies

According to the international consensus statement published in 2018,³ classical CdLS phenotype includes characteristic facial features that are easy to identify, such as thick eyebrows that meet in the midline, short nose with depressed nasal ridge, anteverted nares with upturned nasal tip, long and smooth philtrum, a thin upper lip and downturned corners of the mouth (Figure 2).

Conversely, a wide spectrum of CdLS phenotype exists from classical to mild, with little or no similarity. In this huge clinical variability, patients with mutations in “canonical CdLS genes” (ie, *NIPBL*, *SMC1A*, *SMC3*, *RAD21*, *HDAC8*) can display a wide range of phenotypes, even in the presence of variants affecting the same causative gene.

The phenotype of CdLS-like patients can overlap with features characteristic for other syndromes, typically chromatin disorders.⁵⁸ Reciprocally, patients with diagnosis of chromatin disorders (eg, WDSTS, RSTS, CSS) can present with clinical signs characteristic for CdLS.^{29–31} Clinical diagnosis of these cases is often challenging or rather impossible without genetic evidence. CdLS and other chromatin disorders are genetically heterogeneous and causative genes are not always identified, leaving a consistent fraction of patients without a molecular cause.

The clinical overlap among CdLS and other chromatin disorders can be explained molecularly by the functional network between cohesin and other chromatin-associated complexes that might lead to alterations in the expression of overlapping genes and proteins networks. Indeed, it is conceivable that mutations in cohesin or chromatin remodelers impair a common protein network and are therefore

TABLE 3 Patients clinical features accordingly to the first international consensus statement on CdLS

	Clinical features	AFF4	ANKRD11	BRD4	EP300	KMT2A	SETD5	SWI/SNF complex gene
Cardinal features	Synophrys and/or thick eyebrows	+	+	+	+	+	+	+
	Short nose concave nasal ridge and/or upturned nasal tip	+	–	+	–	+	+/–	+
	Long and/or smooth philtrum	+	+	+		+	+	+
	Thin upper lip vermilion and/or downturned corners of mouth		+	+	–	+	+/–	+
	Hand oligodactyly and/or adactyly	–	–	–	–	–	–	–
	Congenital diaphragmatic hernia							
Suggestive features	Global developmental delay and/or intellectual disability	+	+	+	+	+	+	+
	Prenatal growth retardation		+		+	+		+
	Postnatal growth retardation	+	+	+	+	+	+	+
	Microcephaly	+	+	+	+	+	–	+
	Small hands			+		+		+
	Short fifth finger	–	–	+	–	–	–	–
	Hirsutism		+	–	+	+	+	

Note: Empty cells indicate unreported clinical sign.

Abbreviation: +, present; –, absent; +/-, seldom; CdLS, Cornelia de Lange syndrome; SWI/SNF, SWItch/sucrose non-fermentable.

responsible for a similar, albeit wide, clinical presentation^{30–33} called “CdLS-spectrum.”

In CdLS-like patients, mutations in different but functionally related genes leading to a phenotype characterized by variable clinical signs can be identified. Clearly, the consistency with CdLS signs, present variability in these patients, both in type and severity (Table 3). Hence, are CdLS, cohesinopathies and chromatin disorders different but overlapping syndromes? Recent publications describing overlapping phenotypes among different syndromes and molecular etiopathogenesis converging to transcription dysregulation suggest that each syndrome (ie, CdLS, WDSTS, RSTS, etc) could be considered to be part or an endo-phenotype of a larger “disease family” sharing different clinical features. We believe that this consideration should be taken into account when evaluating each patient with her/his proper clinical presentation in the context of a same multifaceted group of syndromes. An open debate would help caregivers, including experienced clinicians practiced in recognizing distinctive dysmorphisms, that might not match the molecular alterations.

In conclusion, the increasing number of identified genetic variants associated to clinically defined syndromes and the better understanding of their molecular interactions might generate confusion for patients and caretakers for the definitive diagnosis. However, the understanding of common molecular mechanisms and overlapping clinical features caused by different type of mutations in different genes or syndromes will allow the development of common support programs and treatment strategies. Furthermore, the exchange of personal daily life experience of individual families and patient support groups might help to identify similarities and differences between different patient groups and syndromes. We believe that this will be an

opportunity for clinicians that, maintaining the specificity of single patient needs, might manage the entire group in a more efficient and wiser manner. This is a transition era with consequent inevitable challenges for all subjects involved but continuous improvement in technologies and the fundamental cooperation between clinicians and scientists will significantly improve patient care and open up new strategies in treatment and the development of future therapies.

ACKNOWLEDGEMENTS

The authors are grateful to the following fundings: Fondazione Cariplo (2015-0783 to V.M.); Dipartimento DISS, Linea 2, Università degli Studi di Milano (to C.G. and V.M.); Molecular and Translational Medicine PhD—Università degli Studi di Milano scholarship (to P.G.); Translational Medicine PhD—Università degli Studi di Milano scholarship (to C.P.); Nickel & Co S.p.A; Medical Faculty of the University of Lübeck (J09-2017 to I.P.); German Federal Ministry of Education and Research (BMBF) (CHROMATIN-Net to F.J.K.). The authors would also like to thank the Italian National Association of Volunteers Cornelia de Lange for support and inspiration and Susanna Brusa for graphical support.

CONFLICT OF INTEREST

The authors declare no conflict of interest.

DATA AVAILABILITY STATEMENT

Data sharing is not applicable to this article as no new data were created in this study.

ORCID

Paolo Grazioli  <https://orcid.org/0000-0001-9120-4217>

REFERENCES

- Avagliano L, Bulfamante GP, Massa V. Cornelia de Lange syndrome: to diagnose or not to diagnose in utero? *Birth Defects Res.* 2017;109(10):771-777. <https://doi.org/10.1002/bdr2.1045>.
- Avagliano L, Grazioli P, Mariani M, Bulfamante GP, Selicorni A, Massa V. Integrating molecular and structural findings: Wnt as a possible actor in shaping cognitive impairment in Cornelia de Lange syndrome. *Orphanet J Rare Dis.* 2017;12(1):174. <https://doi.org/10.1186/s13023-017-0723-0>.
- Kline AD, Moss JF, Selicorni A, et al. Diagnosis and management of Cornelia de Lange syndrome: first international consensus statement. *Nat Rev Genet.* 2018;19:649-666. <https://doi.org/10.1038/s41576-018-0031-0>.
- Krantz ID, McCallum J, DeScipio C, et al. Cornelia de Lange syndrome is caused by mutations in NIPBL, the human homolog of *Drosophila melanogaster* Nipped-B. *Nat Genet.* 2004;36:631-635. <https://doi.org/10.1038/ng1364>.
- Tonkin ET, Wang TJ, Lisgo S, Bamshad MJ, Strachan T. NIPBL, encoding a homolog of fungal Scc2-type sister chromatid cohesion proteins and fly Nipped-B, is mutated in Cornelia de Lange syndrome. *Nat Genet.* 2004;36:636-641. <https://doi.org/10.1038/ng1363>.
- Musio A, Selicorni A, Focarelli ML, et al. X-linked Cornelia de Lange syndrome owing to SMC1L1 mutations. *Nat Genet.* 2006;38:528-530. <https://doi.org/10.1038/ng1779>.
- Deardorff MA, Kaur M, Yaeger D, et al. Mutations in cohesin complex members SMC3 and SMC1A cause a mild variant of cornelia de Lange syndrome with predominant mental retardation. *Am J Hum Genet.* 2007;80(3):485-494. <https://doi.org/10.1086/511888>.
- Deardorff MA, Bando M, Nakato R, et al. HDAC8 mutations in Cornelia de Lange syndrome affect the cohesin acetylation cycle. *Nature.* 2012;489:313-317. <https://doi.org/10.1038/nature11316>.
- Watrin E, Kaiser FJ, Wendt KS. Gene regulation and chromatin organization: relevance of cohesin mutations to human disease. *Curr Opin Genet Dev.* 2016;37:59-66. <https://doi.org/10.1016/j.gde.2015.12.004>.
- Peters JM, Tedeschi A, Schmitz J. The cohesin complex and its roles in chromosome biology. *Genes Dev.* 2008;22:3089-3114. <https://doi.org/10.1101/gad.1724308>.
- Losada A. Cohesin in cancer: chromosome segregation and beyond. *Nat Rev Cancer.* 2014;14:389-393. <https://doi.org/10.1038/nrc3743>.
- Watrin E, Peters JM. The cohesin complex is required for the DNA damage-induced G2/M checkpoint in mammalian cells. *EMBO J.* 2009;28:2625-2635. <https://doi.org/10.1038/emboj.2009.202>.
- Jeppsson K, Kanno T, Shirahige K, Sjögren C. The maintenance of chromosome structure: positioning and functioning of SMC complexes. *Nat Rev Mol Cell Biol.* 2014;15:601-614. <https://doi.org/10.1038/nrm3857>.
- Mehta GD, Kumar R, Srivastava S, Ghosh SK. Cohesin: functions beyond sister chromatid cohesion. *FEBS Lett.* 2013;587:2299-2312. <https://doi.org/10.1016/j.febslet.2013.06.035>.
- Kagey MH, Newman JJ, Bilodeau S, et al. Mediator and cohesin connect gene expression and chromatin architecture. *Nature.* 2010;467(7314):430-435. <https://doi.org/10.1038/nature09380>.
- Rao SSP, Huang S-C, Glenn St Hilaire B, et al. Cohesin loss eliminates all loop domains. *Cell.* 2017;171(2):305-320.e24. <https://doi.org/10.1016/j.cell.2017.09.026>.
- Schwarzer W, Abdennur N, Goloborodko A, et al. Two independent modes of chromatin organization revealed by cohesin removal. *Nature.* 2017;551(7678):51-56. <https://doi.org/10.1038/nature24281>.
- Nasmyth K, Haering CH. Cohesin: its roles and mechanisms. *Annu Rev Genet.* 2009;43:525-558. <https://doi.org/10.1146/annurev-genet-102108-134233>.
- Ciosk R, Shirayama M, Shevchenko A, et al. Cohesin's binding to chromosomes depends on a separate complex consisting of Scc2 and Scc4 proteins. *Mol Cell.* 2000;5:243-254. [https://doi.org/10.1016/S1097-2765\(00\)80420-7](https://doi.org/10.1016/S1097-2765(00)80420-7).
- Castronovo P, Gervasini C, Cereda A, et al. Premature chromatid separation is not a useful diagnostic marker for Cornelia de Lange syndrome. *Chromosome Res.* 2009;17:763-771. <https://doi.org/10.1007/s10577-009-9066-6>.
- Liu J, Krantz ID. Cornelia de Lange syndrome, cohesin, and beyond. *Clin Genet.* 2009;76(4):303-314. <https://doi.org/10.1111/j.1399-0004.2009.01271.x>.
- Strachan T. Cornelia de Lange syndrome and the link between chromosomal function, DNA repair and developmental gene regulation. *Curr Opin Genet Dev.* 2005;15:258-264. <https://doi.org/10.1016/j.gde.2005.04.005>.
- Deardorff MA, Wilde JJ, Albrecht M, et al. RAD21 mutations cause a human cohesinopathy. *Am J Hum Genet.* 2012;90:1014-1027. <https://doi.org/10.1016/j.ajhg.2012.04.019>.
- Nolen LD, Boyle S, Ansari M, Pritchard E, Bickmore WA. Regional chromatin decompaction in cornelia de lange syndrome associated with NIPBL disruption can be uncoupled from cohesin and CTCF. *Hum Mol Genet.* 2013;22:4180-4193. <https://doi.org/10.1093/hmg/ddt265>.
- Dorsett D. Cohesin: genomic insights into controlling gene transcription and development. *Curr Opin Genet Dev.* 2011;21:199-206. <https://doi.org/10.1016/j.gde.2011.01.018>.
- Zuin J, Franke V, van IJcken WFJ, et al. A cohesin-independent role for NIPBL at promoters provides insights in CdLS. *PLoS Genet.* 2014;10:e1004153. <https://doi.org/10.1371/journal.pgen.1004153>.
- Dowen JM, Bilodeau S, Orlando DA, et al. Multiple structural maintenance of chromosome complexes at transcriptional regulatory elements. *Stem Cell Reports.* 2013;1:371-378. <https://doi.org/10.1016/j.stemcr.2013.09.002>.
- Schaaf CA, Kwak H, Koenig A, et al. Genome-wide control of RNA polymerase II activity by cohesin. *PLoS Genet.* 2013;9:e1003382. <https://doi.org/10.1371/journal.pgen.1003382>.
- Yuan B, Pehlivan D, Karaca E, et al. Global transcriptional disturbances underlie Cornelia de Lange syndrome and related phenotypes. *J Clin Invest.* 2015;125:636-651. <https://doi.org/10.1172/JCI77435>.
- Parenti I, Teresa-Rodrigo ME, Pozojevic J, et al. Mutations in chromatin regulators functionally link Cornelia de Lange syndrome and clinically overlapping phenotypes. *Hum Genet.* 2017;136:307-320. <https://doi.org/10.1007/s00439-017-1758-y>.
- Woods SA, Robinson HB, Kohler LJ, Agamanolis D, Sterbenz G, Khalifa M. Exome sequencing identifies a novel EP300 frame shift mutation in a patient with features that overlap Cornelia de Lange syndrome. *Am J Med Genet Part A.* 2014;164:251-258. <https://doi.org/10.1002/ajmg.a.36237>.
- Izumi K, Nakato R, Zhang Z, et al. Germline gain-of-function mutations in AFF4 cause a developmental syndrome functionally linking the super elongation complex and cohesin. *Nat Genet.* 2015;47:338-344. <https://doi.org/10.1038/ng.3229>.
- Parenti I, Gervasini C, Pozojevic J, et al. Broadening of cohesinopathies: exome sequencing identifies mutations in ANKRD11 in two patients with Cornelia de Lange-overlapping phenotype. *Clin Genet.* 2016;89:74-81. <https://doi.org/10.1111/cge.12564>.
- Ansari M, Poke G, Ferry Q, et al. Genetic heterogeneity in Cornelia de Lange syndrome (CdLS) and CdLS-like phenotypes with observed and

- predicted levels of mosaicism. *J Med Genet.* 2014;51:659-668. <https://doi.org/10.1136/jmedgenet-2014-102573>.
35. Aoi S, Ohashi T, Bamba R, et al. Neuromusculoskeletal model that walks and runs across a speed range with a few motor control parameter changes based on the muscle synergy hypothesis. *Sci Rep.* 2019; 9(1):369. <https://doi.org/10.1038/s41598-018-37460-3>.
 36. Olley G, Ansari M, Bengani H, et al. BRD4 interacts with NIPBL and BRD4 is mutated in a Cornelia de Lange-like syndrome. *Nat Genet.* 2018;50:329-332. <https://doi.org/10.1038/s41588-018-0042-y>.
 37. Saunier C, Støve SI, Popp B, et al. Expanding the phenotype associated with NAA10-related N-terminal acetylation deficiency. *Hum Mutat.* 2016;37:755-764. <https://doi.org/10.1002/humu.23001>.
 38. Zhang A, Yeung PL, Li CW, et al. Identification of a novel family of ankyrin repeats containing cofactors for p160 nuclear receptor coactivators. *J Biol Chem.* 2004;279:33799-33805. <https://doi.org/10.1074/jbc.M403997200>.
 39. Sirmaci A, Spiliopoulos M, Brancati F, et al. Mutations in ANKRD11 cause KBG syndrome, characterized by intellectual disability, skeletal malformations, and macrodontia. *Am J Hum Genet.* 2011;89:289-294. <https://doi.org/10.1016/j.ajhg.2011.06.007>.
 40. Luna-Peláez N, March-Díaz R, Ceballos-Chávez M, et al. The Cornelia de Lange syndrome-associated factor NIPBL interacts with BRD4 ET domain for transcription control of a common set of genes. *Cell Death Dis.* 2019;10(8):548. <https://doi.org/10.1038/s41419-019-1792-x>.
 41. Chen X, Xu H, Yuan P, et al. Integration of external signaling pathways with the core transcriptional network in embryonic stem cells. *Cell.* 2008;133:1106-1117. <https://doi.org/10.1016/j.cell.2008.04.043>.
 42. Scolnick DM, Chehab NH, Stavridi ES, et al. CREB-binding protein and p300/CBP-associated factor are transcriptional coactivators of the p53 tumor suppressor protein. *Cancer Res.* 1997;57(17):3693-3696.
 43. Yan W, Liu S, Xu E, et al. Histone deacetylase inhibitors suppress mutant p53 transcription via histone deacetylase 8. *Oncogene.* 2013; 32:599-609. <https://doi.org/10.1038/onc.2012.81>.
 44. Chen CY, Morris Q, Mitchell JA. Enhancer identification in mouse embryonic stem cells using integrative modeling of chromatin and genomic features. *BMC Genomics.* 2012;13:152. <https://doi.org/10.1186/1471-2164-13-152>.
 45. Wiedemann HR, Kunze J, Grosse H, Dibbern FR. A syndrome of abnormal facies, short stature, and psychomotor retardation. *Atlas of Clinical Syndromes: A Visual Aid to Diagnosis for Clinicians and Practicing Physicians*; 1989:198-199. St. Louis: Mosby Year Book.
 46. Jones WD, Dafou D, McEntagart M, et al. De novo mutations in MLL cause Wiedemann-Steiner syndrome. *Am J Hum Genet.* 2012;91:358-364. <https://doi.org/10.1016/j.ajhg.2012.06.008>.
 47. Baer S, Afenjar A, Smol T, et al. Wiedemann-Steiner syndrome as a major cause of syndromic intellectual disability: a study of 33 French cases. *Clin Genet.* 2018;94:141-152. <https://doi.org/10.1111/cge.13254>.
 48. Li N, Wang Y, Yang Y, et al. Description of the molecular and phenotypic spectrum of Wiedemann-Steiner syndrome in Chinese patients. *Orphanet J Rare Dis.* 2018;13(1):178. <https://doi.org/10.1186/s13023-018-0909-0>.
 49. Fernandes IR, Cruz ACP, Ferrasa A, Phan D, Herai RH, Muotri AR. Genetic variations on SETD5 underlying autistic conditions. *Dev Neurobiol.* 2018;78:500-518. <https://doi.org/10.1002/dneu.22584>.
 50. Green C, Willoughby J, Balasubramanian M. De novo SETD5 loss-of-function variant as a cause for intellectual disability in a 10-year old boy with an aberrant blind ending bronchus. *Am J Med Genet Part A.* 2017;173:3165-3171. <https://doi.org/10.1002/ajmg.a.38461>.
 51. Stur E, Soares LA, Louro ID. SETD5 gene variant associated with mild intellectual disability—a case report. *Genet Mol Res.* 2017;16:1-6. <https://doi.org/10.4238/gmr16029615>.
 52. Szczaluba K, Brzezinska M, Kot J, et al. SETD5 loss-of-function mutation as a likely cause of a familial syndromic intellectual disability with variable phenotypic expression. *Am J Med Genet Part A.* 2016;170: 2322-2327. <https://doi.org/10.1002/ajmg.a.37832>.
 53. Grozeva D, Carss K, Spasic-Boskovic O, et al. Targeted next-generation sequencing analysis of 1,000 individuals with intellectual disability. *Hum Mutat.* 2015;36:1197-1204. <https://doi.org/10.1002/humu.22901>.
 54. Kuechler A, Zink AM, Wieland T, et al. Loss-of-function variants of SETD5 cause intellectual disability and the core phenotype of microdeletion 3p25.3 syndrome. *Eur J Hum Genet.* 2015;23:753-760. <https://doi.org/10.1038/ejhg.2014.165>.
 55. Santen GWE, Aten E, Sun Y, et al. Mutations in SWI/SNF chromatin remodeling complex gene ARID1B cause Coffin-Siris syndrome. *Nat Genet.* 2012;44:379-380. <https://doi.org/10.1038/ng.2217>.
 56. Tsurusaki Y, Okamoto N, Ohashi H, et al. Mutations affecting components of the SWI/SNF complex cause Coffin-Siris syndrome. *Nat Genet.* 2012;44:376-378. <https://doi.org/10.1038/ng.2219>.
 57. Lopez-Serra L, Kelly G, Patel H, Stewart A, Uhlmann F. The Scc2-Scc4 complex acts in sister chromatid cohesion and transcriptional regulation by maintaining nucleosome-free regions. *Nat Genet.* 2014;46: 1147-1151. <https://doi.org/10.1038/ng.3080>.
 58. Izumi K. Disorders of transcriptional regulation: an emerging category of multiple malformation syndromes. *Mol Syndromol.* 2016;7:262-273. <https://doi.org/10.1159/000448747>.

How to cite this article: Avagliano L, Parenti I, Grazioli P, et al. Chromatinopathies: A focus on Cornelia de Lange syndrome. *Clin Genet.* 2019;1-9. <https://doi.org/10.1111/cge.13674>

GENERAL ARTICLE

Modeling Cornelia de Lange syndrome *in vitro* and *in vivo* reveals a role for cohesin complex in neuronal survival and differentiation

Daniele Bottai^{1,‡}, Marco Spreafico^{2,‡}, Anna Pistocchi², Grazia Fazio³, Raffaella Adami¹, Paolo Grazioli¹, Adriana Canu², Cinzia Bragato^{4,5}, Silvia Rigamonti^{1,3}, Chiara Parodi¹, Gianni Cazzaniga³, Andrea Biondi⁶, Franco Cotelli⁷, Angelo Selicorni⁸ and Valentina Massa^{1,*},†

¹Dipartimento di Scienze della Salute, Università degli Studi di Milano, Milan 20142, Italy, ²Dipartimento di Biotecnologie Mediche e Medicina Traslazionale, Università degli Studi di Milano, Milan 20090, Italy, ³Centro Ricerca Tettamanti, Clinica Pediatrica, Università degli Studi di Milano-Bicocca, Fondazione MBBM/Ospedale S. Gerardo, Monza 20900, Italy, ⁴Fondazione IRCCS Istituto Neurologico C. Besta, Milano 20131, Italy, ⁵PhD program in Neuroscience, University of Milano-Bicocca, Monza, Italy, ⁶Clinica Pediatrica, Università degli Studi di Milano-Bicocca, Fondazione MBBM/Ospedale S. Gerardo, Monza 20900, Italy, ⁷Dipartimento di Bioscienze, Università degli Studi di Milano, Milan 20131, Italy and ⁸UOC Pediatria, ASST Lariana, Como 22042, Italy

*To whom correspondence should be addressed at: Dipartimento di Scienze della Salute, Università degli Studi di Milano, via A. Di Rudini, 8, Milano 20142, Italy. Tel/Fax: +39 0250323207; Email: Valentina.Massa@unimi.it

Abstract

Cornelia de Lange syndrome (CdLS), which is reported to affect ~1 in 10 000 to 30 000 newborns, is a multisystem organ developmental disorder with relatively mild to severe effects. Among others, intellectual disability represents an important feature of this condition. CdLS can result from mutations in at least five genes: nipped-B-like protein, structural maintenance of chromosomes 1A, structural maintenance of chromosomes 3, RAD21 cohesin complex component and histone deacetylase 8 (*HDAC8*). It is believed that mutations in these genes cause CdLS by impairing the function of the cohesin complex (to which all the aforementioned genes contribute to the structure or function), disrupting gene regulation during critical stages of early development. Since intellectual disorder might result from alterations in neural development, in this work, we studied the role of *Hdac8* gene in mouse neural stem cells (NSCs) and in vertebrate (*Danio rerio*) brain development by knockdown and chemical inhibition experiments. Underlying features of *Hdac8* deficiency is an increased cell death in the developing neural tissues, either in mouse NSCs or in zebrafish embryos.

†Valentina Massa, <http://orcid.org/0000-0003-2246-9515>

‡These authors should be regarded as joint first authors.

Received: July 31, 2018. Revised: September 11, 2018. Accepted: September 12, 2018

© The Author(s) 2018. Published by Oxford University Press. All rights reserved.

For Permissions, please email: journals.permissions@oup.com

Introduction

During embryonic development and, in mouse, up to 4 weeks after birth, the brain is shaped by immature neurons generated in excessive number that die before maturation is completed. This process is fundamental for achieving optimal brain connectivity, and a number of brain disorders have been associated with altered neuronal cell death (1,2). It has also been shown that disturbing this finely tuned developmental process exerts detrimental effects on cell composition and global brain activity impacting on cognition (3). Signals involved in this balance are numerous and vary both during developmental stages and within involved brain areas. Some signals are considered 'core', thereby inhibiting cell death allowing for proliferation and differentiation, others are 'neuron-type specific' reflecting differences in receptors expressed on the cell membrane (4,5). Neurogenesis during embryonic development, hence, envisages excessive differentiated neurons that will be removed if not fully integrated, starting from a pool of progenitor cells named neural stem cells (NSCs). In lower mammals such as mice primitive NSCs are present from embryonic day 5.5 (E5.5). At E7.5, neural induction begins and the forming neural tube gives rise to the brain and the spinal cord. The cell population composing the neural tube consists of a relatively homogenous population of neuroepithelial cells that proliferate and expand through symmetric division. In the developing embryo, radial glial cells comprise NSCs that divide symmetrically to increase pool size and originate progenitors that migrate away from the periventricular germinal zone (6). In adults, the subventricular zone (SVZ), which extends along the length of the lateral wall of the lateral ventricles, and the dentate gyrus of the hippocampus represent the two most important reservoirs of NSCs (7). NSCs' self-renewal, expansion, division and differentiation are controlled by a number of factors, both extrinsic (such as morphogens) and intrinsic (such as epigenetic modifications). Among these, hierarchically prominent role has been shown for chromatin remodeling, including accessibility and histone modifications (8). Interestingly, Cornelia de Lange syndrome (CdLS) is a genetic disorder caused by mutations in genes codifying for proteins regulating both chromatin features (CdLS1 MIM Mendelian Inheritance in Man 122470, CdLS2 MIM 300590, CdLS3 MIM 610759, CdLS4 MIM614701, CdLS5 MIM 300882). Indeed, 80% of CdLS patients present mutations in one of five genes: NIPBL Nipped-B-like protein, structural maintenance of chromo-

somes 1A (SMC1A), structural maintenance of chromosomes 3 (SMC3), RAD21 cohesin complex component (RAD21) and histone deacetylase 8 (HDAC8) (9). The first four genes are part of the cohesin complex, a multimeric structure controlling chromosomal cohesion in all eukaryotic cells (10). The fifth gene, HDAC8, encodes for a class I histone deacetylase, hence considered an 'eraser' in the epigenetic machinery components (11) with a known target (SMC3) in the cohesin complex (12). The present study sought to ascertain HDAC8 role in mammalian NSCs' capabilities and during vertebrate embryonic brain development, with a particular emphasis on cell death as previous studies have shown the fundamental role of cohesin complex to maintain viable cells during embryonic development in neural tissues and given the importance of HDAC8 in regulating a master regulator of cell death (i.e. p53) (13–18).

Results

HDAC8 inhibition reduces murine NSCs' proliferation rate, inducing apoptosis and differentiating capabilities

During the proliferative phase, cells continuously treated with a specific inhibitor of HDAC8 activity N-hydroxy-1-[(4-methoxyphenyl)methyl]-1H-indole-6-carboxamide showed a lower proliferative capability. The proliferation of PCI34051-treated NSCs was significantly lower compared to controls, as shown in Figure 1A, in which the average of three experiments for each culture is shown. The slopes of the growth curves are significantly different ($P < 0.044$) and the overall number of cells treated with PCI34051 decreased during culture whereas the number of the cells treated with dimethyl sulfoxide (DMSO) (CTR) Control exponentially increased during the experiment. Analysis of cell death revealed a significant increase in apoptosis following treatment with the inhibitor (Fig. 1B).

Treatment with HDAC8 inhibitor caused a change in differentiation capabilities significantly reducing the levels of expression of β -tubulin III $P < 0.01$ (Fig. 2) of ~50% at both time points (Fig. 2B and C).

Hdac8 silencing reduces murine NSCs' proliferation rate and differentiating capabilities

The knockdown of *Hdac8* transcript in NSCs using specific small interfering ribonucleic acids (siRNAs) induced a significant reduction of the proliferative capability. siRNAs effects were synergist, although of less impact compared to inhibitor

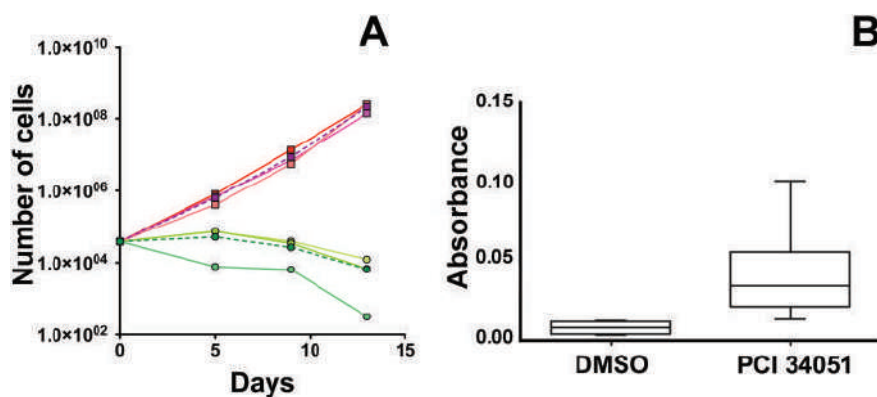


Figure 1. Growth curve and apoptosis of the PCI34051 treated cells. Reddish colors represent the controls, greenish colors represent PCI34051 treated cells. (A) In red #A DMSO, in purple #B DMSO, in pink #C DMSO; in light green #A PCI34051, in green #B PCI34051, in bright green #C PCI34051; in purple with dashed line represents the mean of the three samples treated with DMSO, in green with dashed line represents the mean of the samples treated with PCI34051. (B) Apoptosis levels induced by PCI34051 treatment expressed as absorbance (Y axis) per samples (x axis).

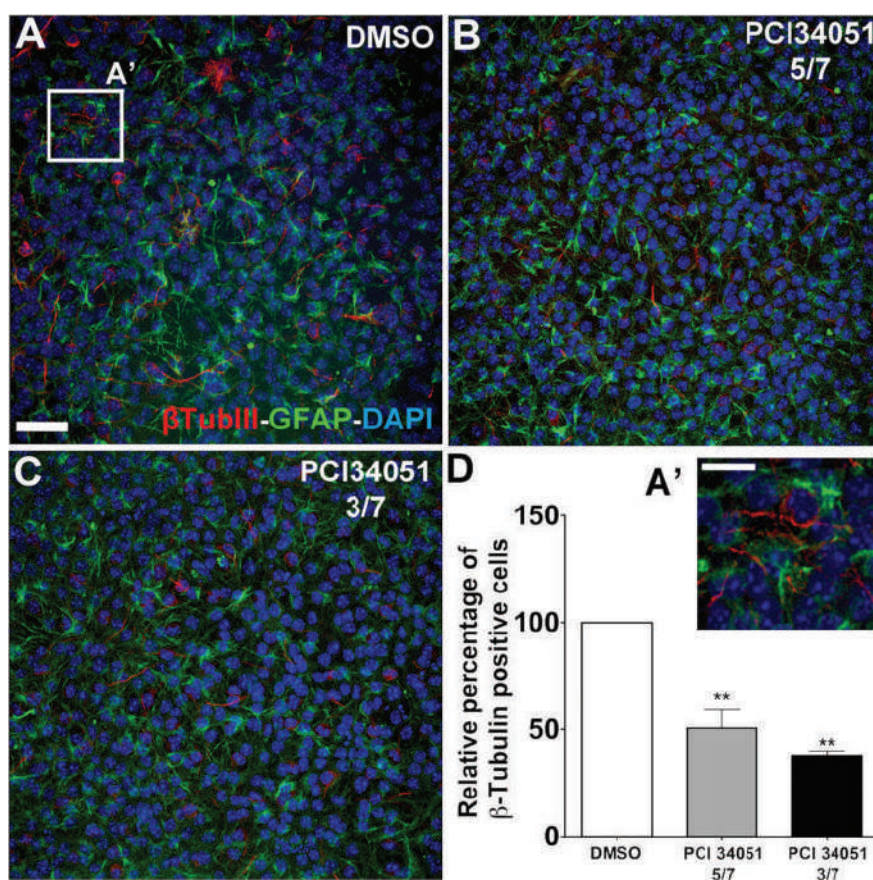


Figure 2. Immunofluorescence analysis of NSCs differentiation. (A) DMSO-treated sample (controls). (B) PCI34051-treated sample for 3 days. (C) PCI34051-treated sample for 5 days. (A') Magnification of white box in A showing β -tubulin III and GFAP positive cells. (D) White column CTR (DMSO-treated), gray column PCI34051-treated cell between days 5 and 7 of the differentiation, black column PCI34051-treated cell between days 3 and 7 of the differentiation. ** = $P < 0.0017$. Scale bar indicates in A = 25 μ m, in A' = 10 μ m, Blue DAPI, green GFAP, red β -tubulin III.

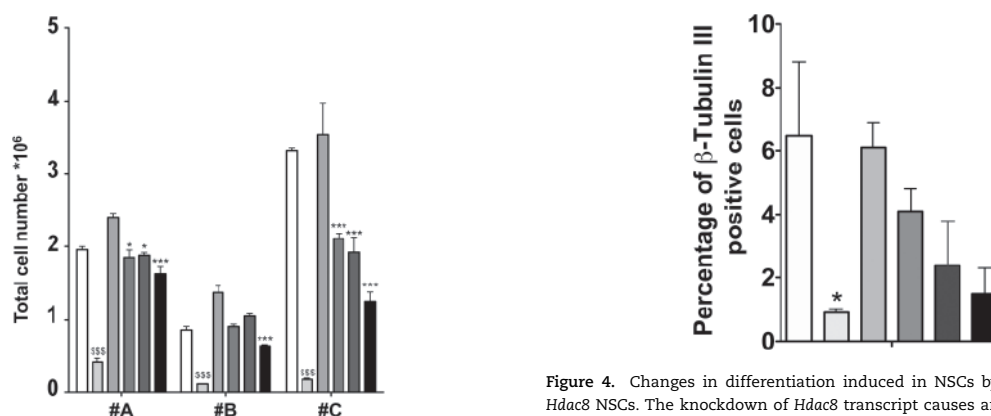


Figure 3. Proliferative changes induced in NSCs by the knockdown of *Hdac8* NSCs. The knockdown of *Hdac8* transcript causes a significant reduction of NSCs proliferation in all three analyzed cultures. The analysis was performed comparing also PCI34051 effects. Bars represent from left to right, for each dataset, CTR, PCI34051, CTR siRNA, HDAC8.1, HDAC8.2 and HDAC8.1+ HDAC8.2.

treatment (Fig. 3). The knockdown of *Hdac8* transcript in NSCs induced a significant reduction of proliferation in all analyzed samples, with a stronger effect upon using a combination of HDAC8.1 and HDAC8.2 siRNA (10 nM each). Nevertheless, even

Figure 4. Changes in differentiation induced in NSCs by the knockdown of *Hdac8* NSCs. The knockdown of *Hdac8* transcript causes an alteration of NSCs' differentiation. The analysis was performed comparing also PCI34051 effects. Bars represent from left to right CTR (3/7), PCI34051 (3/7), CTR siRNA (3/7), HDAC8.1 + HDAC8.2 (3/7), CTR siRNA (5/7) and HDAC8.1 + HDAC8.2 (5/7).

the single treatments were able to induce a significant ($P < 0.05$; sample A) or highly significant ($P < 0.001$; sample C) reduction of NSCs' proliferation. The knockdown of *Hdac8* transcript in differentiating NSCs reduces, $\sim 30\%$, in a not significant fashion the expression of β -tubulin III (Fig. 4), supporting the outcome observed following chemical inhibition.

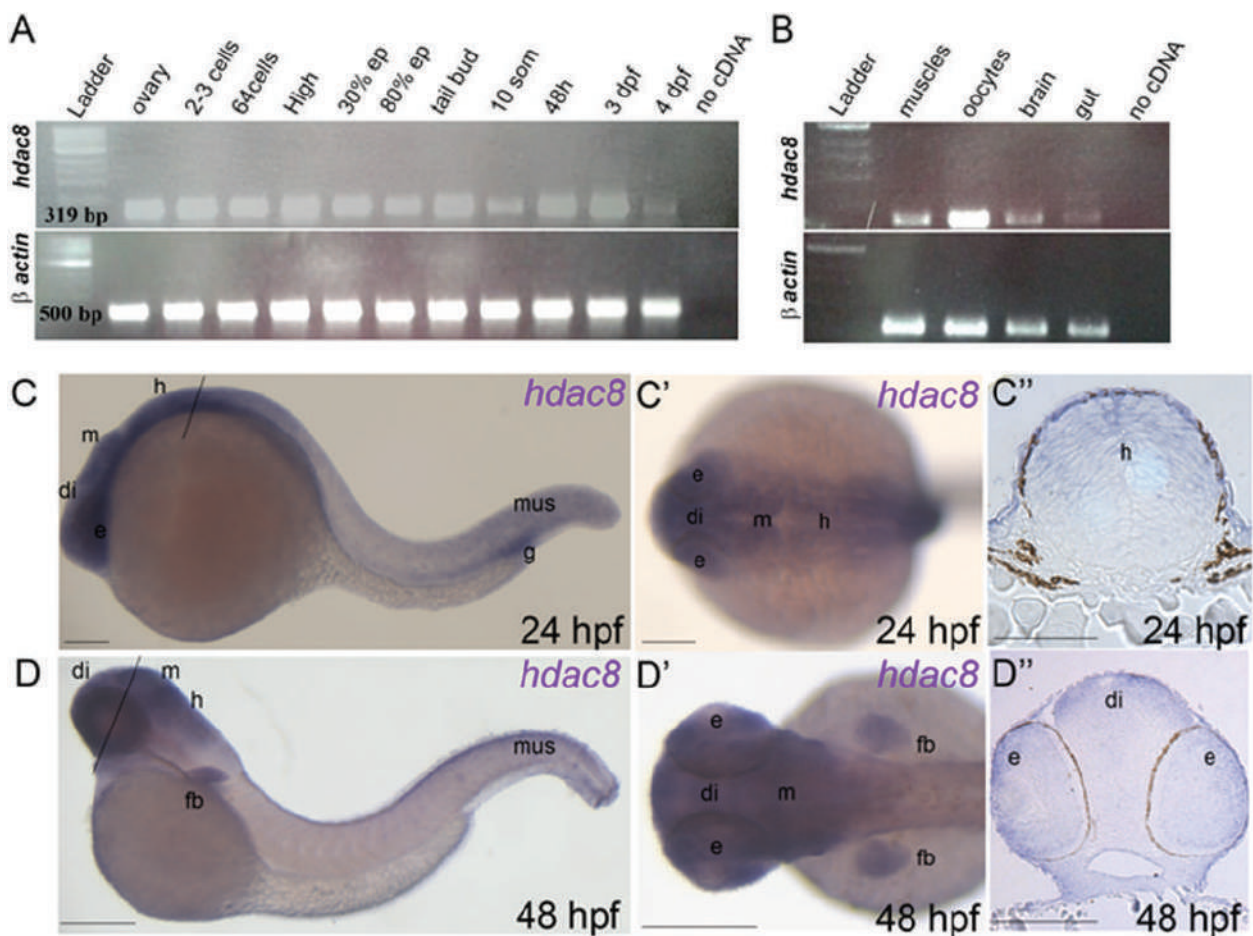


Figure 5. Expression analysis of *hdac8* in zebrafish. (A and B) RT-PCR performed on different embryonic stages: *hdac8* and β -actin expression are shown. (C–D'') *hdac8* WISH analyses on zebrafish embryos at 24 and 48 hpf developmental stages. (C) 24 hpf embryo showing *hdac8* expression in different regions of the CNS (eyes, diencephalon, mesencephalon, hindbrain), in muscles and in the gut. (C') Dorsal view (anterior to the left) of the different regions of *hdac8* expression in the CNS. (C'') Transverse histological sections (section level is indicated in C with black line) of a previously hybridized embryo at 24 hpf. *hdac8* was expressed in the hindbrain. (D–D'') *hdac8* WISH at 48 hpf. The transcript persisted in the eyes, diencephalon, mesencephalon, hindbrain and muscles. *hdac8* expression was present also in the fin buds at 48 hpf. (D'') Transverse sections of the head at 48 hpf (section level is indicated in D with black line). ep, epiboly; e, eye; di, diencephalon; m, midbrain; h, hindbrain; fb, fin bud; mus, muscles; g, gut. Scale bars indicate 100 μ m.

Zebrafish *hdac8* identification and expression analyses

The human HDAC8 amino acid sequence was used as a query for identifying *in silico* the zebrafish *hdac8* gene. NCBI (<http://www.ncbi.nlm.nih.gov/BLAST/>), ClustalW (<http://www.ebi.ac.uk/Tools/clustalw/>) and SMART (<http://smart.embl-heidelberg.de/>) tools were used for basic handling and analyses of the nucleotide and protein sequences. Zebrafish *hdac8* is present in a single copy on chromosome 7 (nucleotide position: 51 710 354–51 749 895).

Characterization of zebrafish *hdac8* expression, using reverse transcription-Polymerase Chain Reaction assays (RT-PCR) techniques, revealed that the transcript was present from the first stages of development up to 4 days post-fertilization (dpf), thus including maternal and zygotic transcription (Fig. 5A). Moreover, zebrafish *hdac8* was found to be expressed through development and in adult organs such as muscles, oocytes, brain and gut (Fig. 5B).

Whole-mount *in situ* hybridization (WISH) expression analyses in embryos at 24 h post-fertilization (hpf) with a specific probe for zebrafish *hdac8* showed the presence of the transcript

in the central nervous system (CNS), specifically in the dorsal part and eyes (Fig. 5C–C''). Moreover, in line with the expression in adult organs, *hdac8* was expressed in muscles and gut (Fig. 5C). At 48 hpf, *hdac8* was expressed in the CNS, eyes, muscles and fin buds (Fig. 5D–D'').

hdac8 loss-of-function results in increased cell death in the CNS

Loss-of-function studies were carried out by injecting a morpholino (*hdac8*-MO; Gene Tools LLC, Philomath, OR, USA), a modified antisense oligonucleotide which binds specifically to *hdac8* messenger RNA (mRNA) blocking the production of protein. Embryos were initially injected with different concentrations of ATG- or splice-*hdac8*-MO (0.5, 1 and 1.5 pmol per embryo) in order to assess the dose-dependent effect. One picomole per embryo was identified as the dose capable of generating the greatest number of embryos with typical phenotypic defects without causing global or drastic alterations in the body plane development. Embryos injected with 1 pmole per embryo of ATG- or splice-*hdac8*-MOs were developmentally abnormal with defects in the cephalic structures

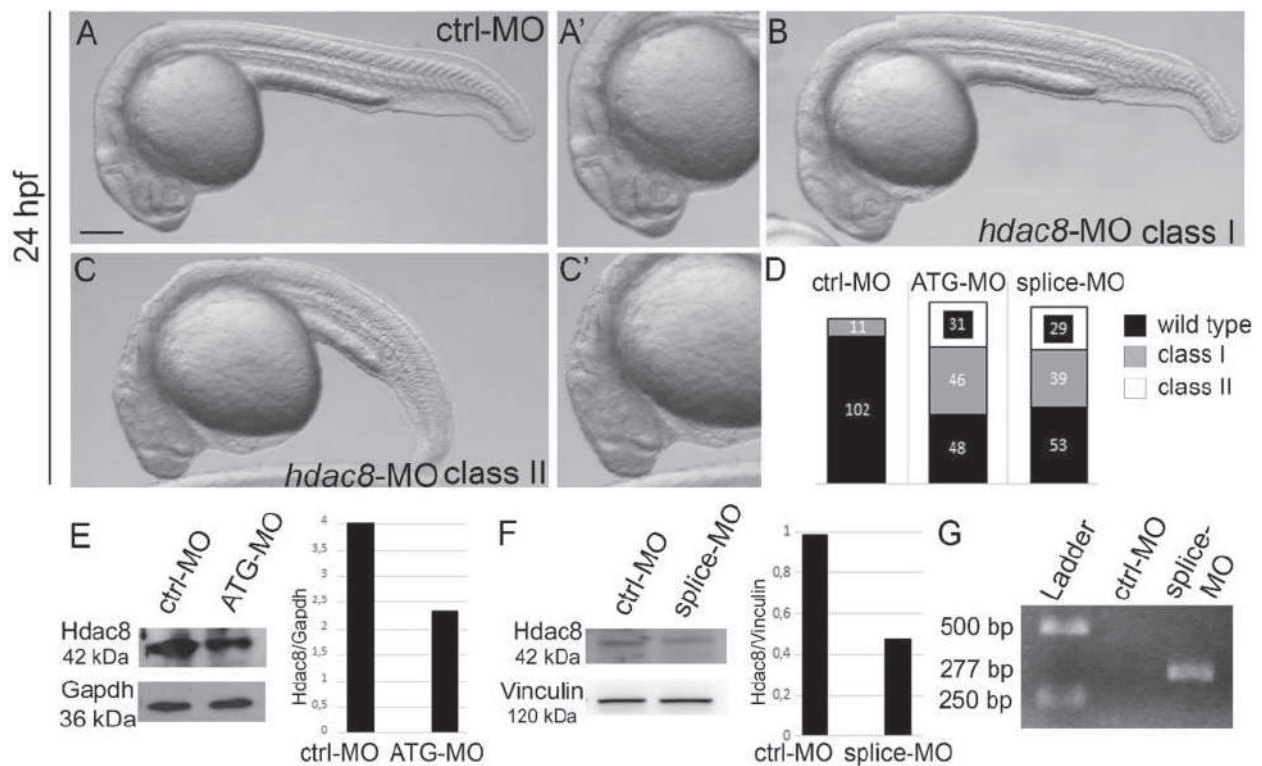


Figure 6. Phenotypical analysis of embryos with *hdac8* loss of function. (A–D) Phenotypical analysis of embryos at 24 hpf microinjected with *hdac8*-MO. (B and C) compared to control embryos (A). (A', C') higher magnification of the cephalic region of the embryo in A and C. (D) Quantification of embryos microinjected with *hdac8*-MO presenting phenotypes with different degree of severity classified as: class I mild phenotype and class II severe phenotype. (E and F) Western blot analyses showed reduced levels of Hdac8 (42 kDa) in the 24 hpf ATG-*hdac8*-MO injected embryos compared to controls at the same developmental stage (E) and in splice-*hdac8*-MO injected embryos compared to controls at the same developmental stage (F). Gapdh (36 kDa) housekeeping in (E) and Vinculin (120 kDa) in (F). (G) RT-PCR performed on control and splice-*hdac8*-MO injected embryos at 24 hpf. RT-PCR primers were designed in exon1 and intron1. The amplification product was 277 bp and comprehended the intron1 in splice-*hdac8*-MO injected embryos, while in ctrl-MO there was no amplification as the intron1 was removed. Scale bars indicate 100 µm.

(eye size, structure of the CNS) and in the formation of the tail (curved tail). Similar morphological phenotypes were obtained with the injection of the two different morpholinos directed against *hdac8*. These defects were used as benchmark to classify *hdac8*-MO into two phenotypic classes (class I mild phenotype and class II severe phenotype) (Fig. 6A–C). The distribution of the phenotypic classes was comparable between the ATG- and splice-*hdac8*-MOs, strongly suggesting that the morphological defects were caused by *hdac8* loss of function (Fig. 6D). To further validate the *hdac8*-MO efficiency, we analyzed Hdac8 protein levels in 24 hpf embryos injected with ATG- or splice-*hdac8*-MOs. Quantification analyses indicated that, at this concentration, the efficiency of Hdac8 reduction was ~50% (Fig. 6E–F). Since splice-*hdac8*-MO was designed against the *hdac8* exon1–intron1 junction, the retention of intron1 in morphant embryos was verified by PCR technique (Fig. 6G).

CNS malformations are caused by augmented apoptosis rescued by WNT pathway activation

The abnormal development of cephalic CNS was associated with the presence of apoptotic/necrotic tissues. Hence, TUNEL assays were conducted in *hdac8*-loss-of-function embryos at 24 hpf for evaluating rate of programmed cell death. Analysis showed increased apoptosis at the level of the midbrain, hind-brain optic vesicles and spinal cord in embryos injected with

hdac8-MO compared to the control embryos (Fig. 7A–B). As we have previously shown in zebrafish models of cohesinopathies (13,14) that augmented apoptosis was caused by altered canonical WNT pathway, *hdac8*-loss-of-function embryos were treated with lithium chloride (LiCl) for activating the WNT pathway. Following treatment with LiCl, TUNEL assay showed significantly reduced levels of apoptosis compared to control embryos (83.3%; N = 42; Fig. 7C). Moreover, injecting an *in vitro* synthesized zebrafish *hdac8*-mRNA a rescue of the apoptotic phenotype caused by the splice-*hdac8*-MO was observed, confirming the role for *hdac8* in preventing apoptosis (Fig. 7D). For these experiments, the splice-*hdac8*-MO was utilized for avoiding the possible direct impact of the ATG-*hdac8*-MO against the injected *hdac8*-mRNA.

The efficacy and specificity of the *hdac8* loss of function were extensively tested with the two *hdac8* morpholinos as shown in Fig. 8. Increased apoptosis was obtained with the injection of the ATG or splice-*hdac8*-MO (Fig. 8B–C) in comparison to controls (A); the levels of apoptotic cells were increased in class II embryos with more severe phenotype than class I (Fig. 8B'–C'). Moreover, to address a synergistic effect of the two morpholinos, we injected subcritical doses of ATG-*hdac8*-MO (0,5 pmol/embryo) or splice-*hdac8*-MO (0,5 pmol/embryo) that singularly did not cause any effects on cell death. When co-injected with subcritical doses of each MO, the typical apoptotic phenotype previously observed by means of full doses injections was found (Fig. 8D).

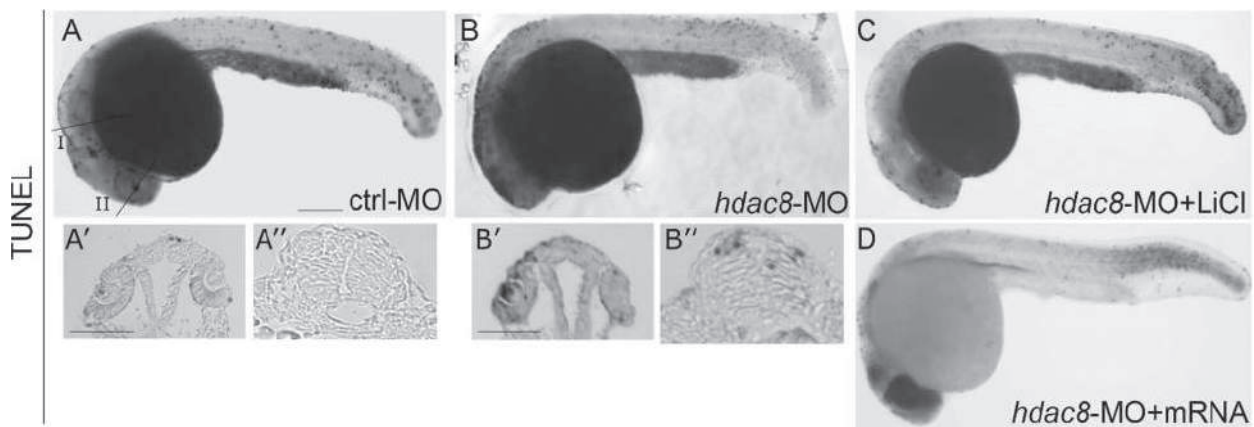


Figure 7. Apoptosis is increased in *hdac8*-MO-injected embryos and rescued by LiCl treatment or *hdac8*-mRNA injection. (A–C) Analysis of the apoptotic cells by visual TUNEL staining in embryos at 24 hpf microinjected with *hdac8*-MO (B) compared to control embryos (A). Dying cells were present in particular at the level of the CNS (arrows in brain and spinal cord) and in optic vesicles as shown by transverse histological sections carried out at the level of the black line (I and II) in A and B (A^I, A^{II}, B^I, B^{II}). (C) Reduced apoptosis in *hdac8*-MO injected embryos upon LiCl treatment. (D) Reduced apoptosis was also observed in embryos co-injected with splice-*hdac8*-MO and *hdac8*/mRNA. Scale bar indicates 100 μ m.

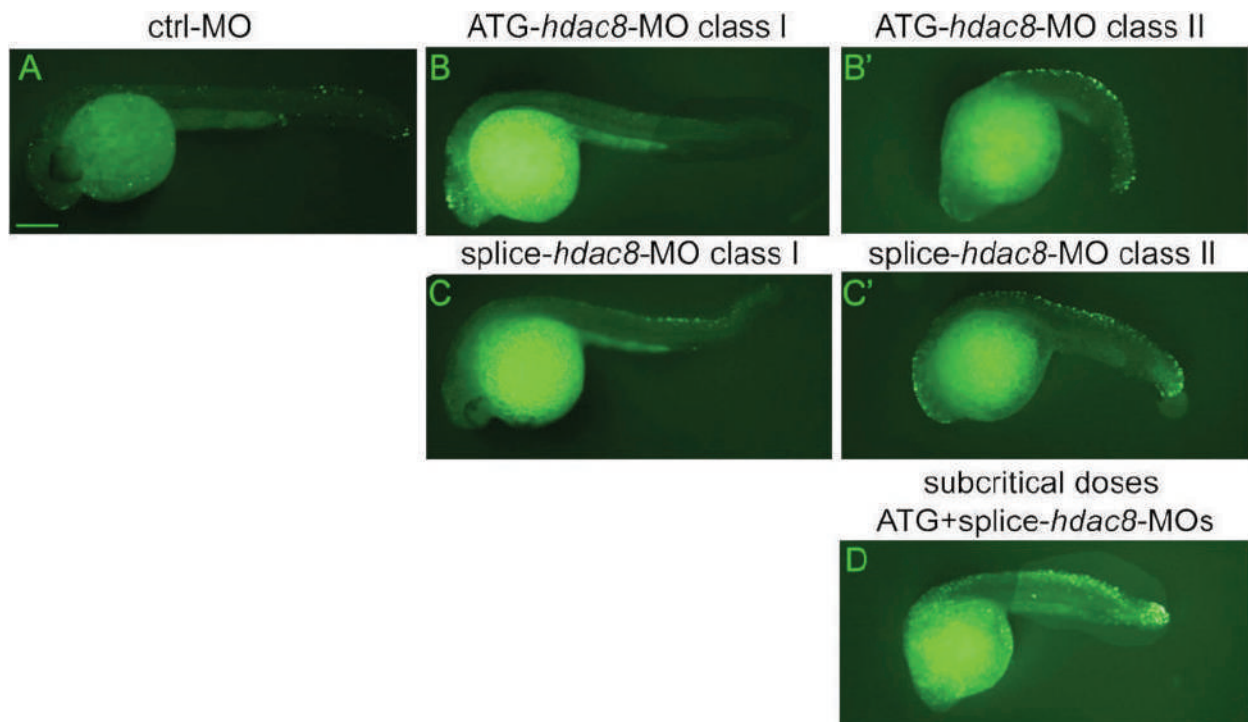


Figure 8. Specificity of the apoptotic phenotype observed following *hdac8* haploinsufficiency. The increased apoptosis was specifically due to the *hdac8* haploinsufficiency as it was obtained by injecting of the two different ATG and splice-*hdac8*-MO. (A–C) Specificity of the apoptotic phenotype following *hdac8* loss of function. The increased apoptotic levels were present in both ATG- and splice-*hdac8*-MO-injected embryos (B and C) in comparison to controls (A). Fluorescent TUNEL staining in embryos injected with different morpholinos confirmed the specificity of the phenotype. The class II embryos (B'–C') presented more apoptotic cells than embryos of class I (B and C). (D) Injection of subcritical doses of ATG- and splice-*hdac8*-MO that singularly did not generate apoptosis demonstrated a synergistic effect on apoptotic levels. SC, spinal cord; di, diencephalon; h, hindbrain; n, notocord. Scale bar indicates 100 μ m.

Discussion

Regulation of neuronal cell death is a fundamental process during both embryonic and adult life (19). During embryonic development, neurons are produced in excess number probably to ensure an adequate number of nerve cells at birth (20). Increased apoptosis during brain development has been associated to abnormal morphology and to adult behavioral abnormalities

(21). In the present study, inhibition of HDAC8 enzymatic activity leads to an excessive apoptosis both in murine NSCs and in the developing vertebrate brain. HDAC8 is a histone deacetylase known to act on SMC3 availability; hence, it is considered a player in the cohesin complex (12). Indeed, deacetylation of SMC3 is a critical step for protein recycling in cells. Cohesins and condensins are protein complexes acting prominently as

regulators of cell division, controlling deoxyribonucleic acid (DNA) content separation in daughter cells. Intriguingly, germ line mutations in both complexes are associated with human conditions affecting brain development. Biallelic mutations in condensin components *NCAPD2*, *NCAPH*, or *NCAPD3* cause microcephaly in humans (22). Dominant autosomal or X-linked mutations in cohesin complex genes cause CdLS, a congenital multiorgan syndrome that presents microcephaly and autistic self-aggressive behaviors (9). Previous studies on models of CdLS have reported increased cell death in the developing brain (13,14,23) associated to an impaired activation of the canonical WNT pathway or mitotic imbalance in the *rad21* model, in which molecular analyses have shown both by array and RNA sequencing deregulation of the WNT pathway (24,25). Canonical WNT pathway is mediated by activation of β -catenin, reduced in CdLS models, that translocates in the cell nucleus where it binds to DNA for gene expression regulation (26,27). Among known targets, Cyclin D1 (*CCND1*) is extensively described (28). Notably, *CCND1* is known to play a pivotal role during neurogenesis. Indeed, it has been shown that overexpression of the cyclin-dependent kinase 4 (*cdk4*)–cyclinD1 complex, positive regulators of cell cycle progression, induces NSCs' expansion (29). Moreover, several studies indicated that shortening of NSCs' cell cycle in embryonic and adult brain is sufficient for inhibiting neuronal differentiation (30,31). Hence, we sought to evaluate a model of CdLS NSCs. We inhibited HDAC8 using PCI34051, a chemical compound known to specifically act on HDAC8 deacetylase activity (12) in proliferating and differentiating murine NSCs. Our results clearly showed that upon HDAC8 inhibition NSCs reduce their capability of proliferating, confirming recent findings shown in cell lines (32). Likely, this is because of the observed increased apoptosis and it does not translate into an augmented differentiation as expected in physiological condition in smooth muscle (33) and brain (34). It was already demonstrated, in cellular model of glioblastomas, that the knockdown of another cohesin, *SMC1A*, led to the significant decrease in proliferation of U251 and U87MG cells (35). These results are on line with our *in vitro* analysis of the role of HDAC8 in NSCs. Importantly, we found a significant reduction in cells positive for the neuronal marker β -tubulin III, indicating that their neurogenic differentiating capabilities are hampered. Importantly, it has been recently shown that retinoic pathway response is impaired in CdLS patients fibroblasts, suggesting a weaker activation following exposure to a master player in neuronal differentiation (36). A neuronal reduction in CdLS patients could explain part of the behavioral and morphological features often reported after birth [as reviewed in (37,38)]. Hence, a detailed analysis in mammals should be conducted for better dissecting this possibility. To note, a consistently high expression of CdLS–cohesins in the developing mouse embryos and human adult CNS, especially in hindbrain and hindbrain-derived structures (39), notwithstanding the non-proliferative characteristics of such organs, has been recently reported. In the present study, *Danio rerio* models of *hdac8* deficiency obtained by morpholino antisense injections confirmed an increased apoptosis in the developing CNS associated with altered canonical WNT pathway. Molecular and morphological alterations could be rescued upon chemical activation by LiCl treatment as previously shown in other CdLS models (13).

In conclusion, we report an association between HDAC8 inhibition—model of CdLS—and increased cell death in the developing neural tissues, both *in vitro* and *in vivo* with a consequent reduction in neuronal differentiation capabilities, which could be involved in the severe mental retardation observed in CdLS.

Materials and Methods

Neural stem cells

NSCs obtained from SVZ of 4 months old C57 BL6 male mice were used. Cells were cultivated in a medium containing epidermal growth factor (EGF) and fibroblast growth factor (FGF) (40–42). Three different cultures from three mice were used for the experiments.

PCI34051 treatment

Cells were firstly grown in a large culture flask and then plated in a 12 wells tissue culture plate at the concentration of 10 000 cell/cm². Experiments were performed in triplicate for each culture. For proliferating cells experiments, cultures were treated either with PCI34051 25 μ M, a known HDAC8 inhibitor (12), or with DMSO 1:1000, a concentration that does not alter NSCs' properties, such as proliferation and differentiation. After 5 days of culture, spheres were harvested and mechanically dissociated to single cells and counted. The fold change was determined dividing the total number of cells by the initial number of plated cells. Differentiation was achieved by plating cells in presence of adhesion molecules Cultrex (Tema Ricerca, Italy) and in absence of growth factors. In a 48 well plate, round sterile coverslip of the diameter of 1 cm was inserted. Wells were coated with 150 μ l of Cultrex for 1 h and 40 000 cells were loaded with 500 μ l of medium containing FGF but not EGF (40–42) for 2 days. Following growth factor removal, treatment with HDAC8 inhibitor was started. Two different time points (from day 3 to day 7 and from day 5 to day 7) were used. As control, treated cells with DMSO 1:1000 for days 3 to 7 were used. At the end of the treatment, the medium was removed, the cells washed once with Phosphate-Buffered Saline (PBS) and fixed with 4% paraformaldehyde for 10 min. Cells were then washed once with PBS and either used for immunocytochemistry or stored at 4°C. Experiments were run in duplicates.

Silencing NSCs

A 48 multiwell plate was coated with laminin (Synthetic Laminin Peptide, Sigma SCR127, Darmstadt, Germany) using a concentration of 150 μ g/ml as suggested by the supplier. Two siRNAs (Qiagen, Germantown, MD, USA) expected to anneal different regions of the HDAC8 transcript (Flexitube siRNA 5 nmol cat nr SI01063895 and catalogue number SI01063902) were used. As negative control AllStars Negative Control siRNA (cat nr 1027280) with no homology to any known mammalian genes and minimal non-specific effects was selected. HiPerFect Transfection Reagent (Qiagen) was used for siRNAs delivery. Four different cultures of NSCs were used, and experiments were run in triplicates. We first plated dissociated cells (10 000 cells per well) on laminin-coated wells as a monolayer in 500 μ l of proliferative medium (PM) for 1 day. The following day, incubation medium (with siRNAs and Transfection Reagent prepared following the manufacturer instruction) was added drop-wise onto the attached cells that were incubated under their normal growth conditions for 3 h before adding the PM medium. The medium was changed after 24 h and cells were cultured for 2–3 days. The cells were then harvested, dissociated and counted. siRNAs concentrations were selected in pilot studies, choosing 20 nM as experimental concentration. For analyses of *Hdac8* silencing in differentiating NSCs, three different cultures were used.

Immunostaining of differentiated NSC

Differentiation capabilities were assayed by means of immunostaining. For this purpose, antibodies against glial fibrillary acidic protein (GFAP; 1:250, Immunological Sciences AB-10635) and β -tubulin III (1:250, Immunological Sciences AB-10288) were used. Briefly, fixed cells were permeabilized with 0.1% Triton-X in PBS for 10 min at room temperature, then the primary antibodies were added overnight at 4°C in PBS with 10% normal goat serum NGS. Secondary antibodies conjugated with fluorophores were used: Alexa-fluor 488 (Goat anti mouse Immunological Sciences IS20010) and Alexa-fluor 555 (Goat anti rabbit Immunological Sciences IS20012). Nuclei were stained with 4', 6-Diamidino-2'-phenylindole dihydrochloride (DAPI) 300 nM (43). Images were acquired using a Leica SP2 microscope, Buccinasco, Milan, Italy with Helium/Neon and Argon/Krypton lasers. The number of positive cells was counted and compared within treatments. Experiments were repeated twice. A minimum of 1400 cells for each sample and for each treatment were counted.

Apoptosis assay

Apoptosis in NSCs was quantified using a Caspase-3/ CPP32 Colorimetric Assay (BioVision, Milpitas, CA, USA) following manufacturer's protocol. Briefly, NSCs were harvested after 5 days of culture, resuspended in chilled lysis buffer and centrifuged and supernatant (representing cytosolic extract) was used. Following protein concentration measurement, spectrophotometric detection of the chromophore p-nitroaniline (pNA) after cleavage from the labeled substrate DEVD-pNA allowed for cell death assessment. Samples were run as experimental triplicates and technical duplicates.

Animals

Breeding wild-type fish (zebrafish, *D. rerio*) of the AB strain were maintained at 28°C on a 14 h light/10 h dark cycle. Embryos were collected by natural spawning, staged according to Kimmel and colleagues (44) and raised at 28°C in fish water (Instant Ocean, Blacksburg, VA, USA, 0.1% methylene blue) in Petri dishes, according to established techniques. Zebrafish embryos were raised and maintained under standard conditions and national guidelines

(Italian decree 4 March 2014, n. 26). All experimental procedures were approved by Institutional Animal Care and Use Committee, N. OPBA_93_2017. Embryonic ages are expressed in hpf and dpf.

LiCl was added to fish water for 30 min at the 10–12 somite stages at a concentration of 0.3 M at 28°C as previously described (13). Treated embryos were then washed three times with water and allowed to develop to 24 hpf.

Reverse transcription-PCR assays

Total RNA from 12 samples (an average of 30 embryos per sample) was extracted with the TOTALLY RNA isolation kit (Ambion, Life Technologies, Paisley UK), treated with RQ1 RNase-Free DNase (Promega Madison WI, USA) and oligo(dT)-reverse transcribed using SuperScript II RT (Invitrogen, Carlsbad, CA, USA), according to manufacturers' instructions. PCR products were loaded and resolved onto 1% agarose gels. The β -actin expression was tested in parallel with the gene of interest as a housekeeping gene control for the complementary DNA loaded.

The following primers were used:

hdac8pr_sense 5'-ACATGAGGGTCGTGAAGCCT-3'
hdac8pr_antisense 5'-ACCGCGTCATTACATAACA-3'
hdac8fl_sense 5'-ATGAGTGAAAAAGCGACAG-3'
hdac8fl_antisense 5'-CGATCCTAAACTACATTCTTC-3'
hdac8E1_sense 5'-GTCCAAAGTCAGCAGACT-3'
hdac8I2_antisense 5'-GTGAGATGAACTGCACTCT-3'

In situ hybridization and histological analysis

WISH experiments were carried out as described by Thisse and colleagues (45). For each experiment a minimum of 30 controls and MO-injected embryos were analyzed. *hdac8* probe was cloned using RT-PCR primers. For histological sections, stained embryos were refixed in 4% PFA Paraformaldehyde, dehydrated and stored in methanol, wax embedded and sectioned (5 μ m). Images of embryos and sections were acquired using a microscope equipped with digital camera with LAS Leica Imaging software (Leica, Wetzlar, Germany). Images were processed using Adobe Photoshop software and, when necessary, different focal planes of the same image have been taken separately and later merged in a single image.

TUNEL staining

For (Terminal deoxynucleotidyl transferase dUTP nick end labeling) assay, a minimum of 24 embryos (per experimental group) were fixed in 4% PFA for 2 h at room temperature. Embryos were washed with methanol at –20°C and then twice with PBC Phosphate-Buffered Saline with Citrate (0.001% Triton X-100; 0.1% sodium citrate in PBS) for 10 min. Staining for apoptotic cells was performed using the AP-*In situ* Cell Death Detection Kit (Roche Diagnostics, Penzberg, Germany) carefully leaving labeling reagents to react for the same length of time for all experiments. Embryos were incubated at 37°C for 1 h and fluorescent apoptotic cells were detected under a fluorescent microscope (Leica). For the visual staining, embryos were then washed, stained and mounted for microscopic imaging.

Injections

To repress *hdac8* mRNA translations, two morpholinos were synthesized (Gene Tools LLC) targeting *hdac8*-ATG and exon1-intron1 junction (splice-*hdac8*-MO) (46),

ATG-*hdac8*-MO: 5'-CATTACTGTGCGTTTTTCTACTCAT-3'

splice-*hdac8*-MO: 5'-TGCAGAGTGCAGTTCATCTCACCG-3',

and used at the concentration of 1 pmole per embryo in 1x Danieau buffer (pH 7.6). A standard control morpholino oligonucleotide (ctrl-MO) was injected in parallel (47). When co-injected, ATG- and splice-*hdac8*-MOs were used at subcritical doses of 0.5 pmole per embryo in 1x Danieau buffer (pH 7.6). In all experiments, *hdac8*-MO-injected embryos were compared to embryos injected with the same amount of ctrl-MO at the same developmental stage. For the *in vivo* test of the specificity of morpholino-mediated knockdown, the rescue of morphants phenotype was evaluated by co-injecting zebrafish *hdac8*-mRNA at the concentration of 500 pg per embryo.

Western blot

Fish embryos (minimum 30 per experimental group) were lysated in RIPA buffer (5 μ l for each embryo) and homogenized.

Samples were boiled for 10 min at 95°C. A total of 20 µl of protein sample was size-fractionated by gel Pre-cast (Invitrogen) and transferred with iBlot (Invitrogen). The nitrocellulose membranes were blocked with 5% non-fat dry milk in PBST (PBS containing 0.1% Tween 20) for 30 min at room temperature and subsequently incubated with the primary antibody: rabbit anti-Hdac8 [1:1000, HDAC8 (H-145) sc-11405, Santa Cruz Biotechnology, Santa Cruz, CA, USA and mouse anti-GAPDH (1:2500, Developmental Studies Hybridoma bank)] and mouse anti-Vinculin (1:6000, Sigma), diluted in 4% milk/PBST over night at 4°C. Horseradish peroxidase-conjugated secondary antibody (Sigma Aldrich, St Louis MO, USA) was used for 1 h at room temperature. The antigen signal was detected with the ECL chemiluminescence detection system (Amersham, Piscataway, NJ, USA) as specified by the manufacturer.

Data analysis

Proliferation statistical analysis was performed using Student's t-test. NSC immunostaining analysis was performed using the one-way analysis of variance followed by Bonferroni's multiple comparison test. Apoptosis assay was analyzed using student's t-test. $P \leq 0.05$ was set as statistically significant. For graphs, Graphpad Prism software was used; for figures, Adobe Photoshop was used.

Acknowledgements

The authors are grateful to the Italian National Association of Volunteers Cornelia de Lange for support and inspiration. The authors want to express their deepest gratitude to Dr Julia Horsfield for manuscript commenting.

Conflict of Interest statement. None declared.

Funding

Fondazione Cariplo (2015-0783 to V.M.); Dipartimento DISS, Linea B, Università degli Studi di Milano (to V.M.); Dipartimento BIOMETRA, Linea B, Università degli Studi di Milano (to A.P.); Fondazione Mariani (Como, Italy) (to A.S.); Molecular and Translational Science-Università degli Studi di Milano scholarship (to P.G.).

References

- Ribe, E.M., Serrano-Saiz, E., Akpan, N. and Troy, C.M. (2008) Mechanisms of neuronal death in disease: defining the models and the players. *Biochem. J.*, **415**, 165–182.
- Martin, L.J. (2001) Neuronal cell death in nervous system development, disease, and injury (Review). *Int. J. Mol. Med.*, **7**, 455–478.
- Pfisterer, U. and Khodosevich, K. (2017) Neuronal survival in the brain: neuron type-specific mechanisms. *Cell Death Dis.*, **8**, e2643.
- Temple, S. (2001) The development of neural stem cells. *Nature*, **414**, 112–117.
- Gage, F.H. (2000) Mammalian neural stem cells. *Science*, **287**, 1433–1438.
- Xu, W., Lakshman, N. and Morshead, C.M. (2017) Building a central nervous system: the neural stem cell lineage revealed. *Neurogenesis (Austin)*, **4**, e1300037.
- Daniela, F., Vescovi, A.L. and Bottai, D. (2007) The stem cells as a potential treatment for neurodegeneration. *Methods Mol. Biol.*, **399**, 199–213.
- Gaspar-Maia, A., Alajem, A., Meshorer, E. and Ramalho-Santos, M. (2011) Open chromatin in pluripotency and reprogramming. *Nat. Rev. Mol. Cell Biol.*, **12**, 36–47.
- Deardorff, M.A., Noon, S.E. and Krantz, I.D. (1993) Cornelia de Lange syndrome. In *Gene Reviews*, University of Washington: Seattle (WA).
- Hagstrom, K.A. and Meyer, B.J. (2003) Condensin and cohesin: more than chromosome compactor and glue. *Nat. Rev. Genet.*, **4**, 520–534.
- Bjornsson, H.T. (2015) The Mendelian disorders of the epigenetic machinery. *Genome Res.*, **25**, 1473–1481.
- Deardorff, M.A., Bando, M., Nakato, R., Watrin, E., Itoh, T., Minamino, M., Saitoh, K., Komata, M., Katou, Y., Clark, D. et al. (2012) HDAC8 mutations in Cornelia de Lange syndrome affect the cohesin acetylation cycle. *Nature*, **489**, 313–317.
- Pistocchi, A., Fazio, G., Cereda, A., Ferrari, L., Bettini, L.R., Messina, G., Cotelli, F., Biondi, A., Selicorni, A. and Massa, V. (2013) Cornelia de Lange syndrome: NIPBL haploinsufficiency downregulates canonical Wnt pathway in zebrafish embryos and patients fibroblasts. *Cell Death Dis.*, **4**, e866.
- Fazio, G., Gaston-Massuet, C., Bettini, L.R., Graziola, F., Scagliotti, V., Cereda, A., Ferrari, L., Mazzola, M., Cazzaniga, G., Giordano, A. et al. (2016) Cyclin D1 down-regulation and increased apoptosis are common features of cohesinopathies. *J. Cell. Physiol.*, **231**, 613–622.
- Yan, W., Liu, S., Xu, E., Zhang, J., Zhang, Y., Chen, X. and Chen, X. (2013) Histone deacetylase inhibitors suppress mutant p53 transcription via histone deacetylase 8. *Oncogene*, doi: [10.1038/onc.2012.81](https://doi.org/10.1038/onc.2012.81).
- Qi, J., Singh, S., Hua, W.K., Cai, Q., Chao, S.W., Li, L., Liu, H., Ho, Y., McDonald, T., Lin, A., et al. (2015) HDAC8 inhibition specifically targets inv(16) acute myeloid leukemic stem cells by restoring p53 acetylation. *Cell Stem Cell*, doi: [10.1016/j.stem.2015.08.004](https://doi.org/10.1016/j.stem.2015.08.004).
- Wu, J., Du, C., Lv, Z., Ding, C., Cheng, J., Xie, H., Zhou, L. and Zheng, S. (2013) The up-regulation of histone deacetylase 8 promotes proliferation and inhibits apoptosis in hepatocellular carcinoma. *Dig. Dis. Sci.*, doi: [10.1007/s10620-013-2867-7](https://doi.org/10.1007/s10620-013-2867-7).
- Hua, W.K., Qi, J., Cai, Q., Carnahan, E., Ayala Ramirez, M., Li, L., Marcucci, G. and Kuo, Y.H. (2017) HDAC8 regulates long-term hematopoietic stem-cell maintenance under stress by modulating p53 activity. *Blood*, doi: [10.1182/blood-2017-03-771386](https://doi.org/10.1182/blood-2017-03-771386).
- Hutchins, J.B. and Barger, S.W. (1998) Why neurons die: cell death in the nervous system. *Anat. Rec.*, **253**, 79–90.
- Dekkers, M.P.J., Nikolettou, V. and Barde, Y.A. (2013) Death of developing neurons: new insights and implications for connectivity. *J. Cell Biol.*, **203**, 385–393.
- Broad, K.D., Curley, J.P. and Keverne, E.B. (2009) Increased apoptosis during neonatal brain development underlies the adult behavioral deficits seen in mice lacking a functional paternally expressed gene 3 (Peg3). *Dev. Neurobiol.*, **69**, 314–325.
- Martin, C.A., Murray, J.E., Carroll, P., Leitch, A., Mackenzie, K.J., Halachev, M., Fetit, A.E., Keith, C., Bicknell, L.S., Fluteau, A. et al. (2016) Mutations in genes encoding condensin complex proteins cause microcephaly through decatenation failure at mitosis. *Genes Dev.*, **30**, 2158–2172.
- Horsfield, J.A., Anagnostou, S.H., Hu, J.K., Cho, K.H., Geisler, R., Lieschke, G., Crosier, K.E. and Crosier, P.S. (2007) Cohesin-independent regulation of Runx genes. *Development*, **134**, 2639–2649.

24. Rhodes, J.M., Bentley, F.K., Print, C.G., Dorsett, D., Misulovin, Z., Dickinson, E.J., Crosier, K.E., Crosier, P.S. and Horsfield, J.A. (2010) Positive regulation of c-Myc by cohesin is direct, and evolutionarily conserved. *Dev. Biol.*, doi: [10.1016/j.ydbio.2010.05.493](https://doi.org/10.1016/j.ydbio.2010.05.493).
25. Schuster, K., Leeke, B., Meier, M., Wang, Y., Newman, T., Burgess, S. and Horsfield, J.A. (2015) A neural crest origin for cohesinopathy heart defects. *Hum. Mol. Genet.*, doi: [10.1093/hmg/ddv402](https://doi.org/10.1093/hmg/ddv402).
26. Tortelote, G.G., Reis, R.R., de Almeida Mendes, F. and Abreu, J.G. (2017) Complexity of the Wnt/ β -catenin pathway: searching for an activation model. *Cell. Signal.*, **40**, 30–43.
27. Barker, N., Morin, P.J. and Clevers, H. (2000) The yin-yang of TCF/ β -catenin signaling. *Adv. Cancer Res.*, **77**, 1–24.
28. Shtutman, M., Zhurinsky, J., Simcha, I., Albanese, C., D'Amico, M., Pestell, R. and Ben-Ze'ev, A. (1999) The cyclin D1 gene is a target of the β -catenin/LEF-1 pathway. *Proc. Natl. Acad. Sci. U. S. A.*, **96**, 5522–5527.
29. Lange, C., Huttner, W.B. and Calegari, F. (2009) Cdk4/CyclinD1 overexpression in neural stem cells shortens G1, delays neurogenesis, and promotes the generation and expansion of basal progenitors. *Cell Stem Cell*, **5**, 320–331.
30. Salomoni, P. and Calegari, F. (2010) Cell cycle control of mammalian neural stem cells: putting a speed limit on G1. *Trends Cell Biol.*, **20**, 233–243.
31. Artegiani, B., Lange, C. and Calegari, F. (2012) Expansion of embryonic and adult neural stem cells by in utero electroporation or viral stereotaxic injection. *J. Vis. Exp.*, doi: [10.3791/4093](https://doi.org/10.3791/4093).
32. Dasgupta, T., Antony, J., Braithwaite, A.W. and Horsfield, J.A. (2016) HDAC8 inhibition blocks SMC3 deacetylation and delays cell cycle progression without affecting cohesin-dependent transcription in MCF7 cancer cells. *J. Biol. Chem.*, doi: [10.1074/jbc.M115.704627](https://doi.org/10.1074/jbc.M115.704627).
33. Waltregny, D., De Leval, L., Glénisson, W., Ly Tran, S., North, B.J., Bellahcène, A., Weidle, U., Verdin, E. and Castronovo, V. (2004) Expression of histone deacetylase 8, a class I histone deacetylase, is restricted to cells showing smooth muscle differentiation in normal human tissues. *Am. J. Pathol.*, **165**, 553–564.
34. Murko, C., Lagger, S., Steiner, M., Seiser, C., Schoefer, C. and Pusch, O. (2010) Expression of class I histone deacetylases during chick and mouse development. *Int. J. Dev. Biol.*, **54**, 1525–1535.
35. Yang, Y., Zhang, Z., Wang, R., Ma, W., Wei, J. and Li, G. (2013) siRNA-mediated knockdown of SMC1A expression suppresses the proliferation of glioblastoma cells. *Mol. Cell. Biochem.*, doi: [10.1007/s11010-013-1704-9](https://doi.org/10.1007/s11010-013-1704-9).
36. Fazio, G., Bettini, L.R., Rigamonti, S., Meta, D., Biondi, A., Cazzaniga, G., Selicorni, A. and Massa, V. (2017) Impairment of retinoic acid signaling in Cornelia de Lange syndrome fibroblasts. *Birth Defects Res.*, **109**, 1268–1276.
37. Avagliano, L., Grazioli, P., Mariani, M., Bulfamante, G.P., Selicorni, A. and Massa, V. (2017) Integrating molecular and structural findings: Wnt as a possible actor in shaping cognitive impairment in Cornelia de Lange syndrome. *Orphanet J. Rare Dis.*, **12**.
38. Avagliano, L., Bulfamante, G.P. and Massa, V. (2017) Cornelia de Lange syndrome: to diagnose or not to diagnose in utero? *Birth Defects Res.*, **109**, 771–777.
39. Bettini, L.R., Graziola, F., Fazio, G., Grazioli, P., Scagliotti, V., Pasquini, M., Cazzaniga, G., Biondi, A., Larizza, L., Selicorni, A., Gaston-Massuet, C. and Massa, V. (2018) Rings and bricks: expression of cohesin components is dynamic during development and adult life. *Int. J. Mol. Sci.*, **19**.
40. Gelain, F., Bottai, D., Vescovi, A. and Zhang, S. (2006) Designer self-assembling peptide nanofiber scaffolds for adult mouse neural stem cell 3-dimensional cultures. *PLoS One*, **1**, e119.
41. Henry, G.R., Heise, A., Bottai, D., Formenti, A., Gorio, A., Di Giulio, A.M. and Koning, C.E. (2008) Acrylate end-capped poly(ester-carbonate) and poly(ether-ester)s for polymer-on-multielectrode array devices: synthesis, photocuring, and biocompatibility. *Biomacromolecules*, **9**, 867–878.
42. Adami, R., Pagano, J., Colombo, M., Platonova, N., Recchia, D., Chiaramonte, R., Bottinelli, R., Canepari, M. and Bottai, D. (2018) Reduction of movement in neurological diseases: effects on neural stem cells characteristics. *Front. Neurosci.*, doi: [10.3389/fnins.2018.00336](https://doi.org/10.3389/fnins.2018.00336).
43. Bottai, D., Scesa, G., Cigognini, D., Adami, R., Nicora, E., Abrignani, S., Di Giulio, A.M. and Gorio, A. (2014) Third trimester NG2-positive amniotic fluid cells are effective in improving repair in spinal cord injury. *Exp. Neurol.*, doi: [10.1016/j.expneurol.2014.01.015](https://doi.org/10.1016/j.expneurol.2014.01.015).
44. Kimmel, C.B., Ballard, W.W., Kimmel, S.R., Ullmann, B. and Schilling, T.F. (1995) Stages of embryonic development of the zebrafish. *Dev. Dyn.*, **203**, 253–310.
45. Thisse, C., Thisse, B., Schilling, T.F. and Postlethwait, J.H. (1993) Structure of the zebrafish *snail1* gene and its expression in wild-type, spadetail and no tail mutant embryos. *Development*, **119**, 1203–1215.
46. Ferrari, L., Bragato, C., Brioschi, L., Spreafico, M., Esposito, S., Pezzotta, A., Pizzetti, F., Moreno-Fortuny, A., Bellipanni, G., Giordano, A. et al. (2018) HDAC8 regulates canonical Wnt pathway to promote differentiation in skeletal muscles. *J. Cell. Physiol.*, **1**.
47. Nasevicius, A. and Ekker, S.C. (2000) Effective targeted gene 'knockdown' in zebrafish. *Nat. Genet.*, **26**, 216–220.

Acknowledgments